Scattering of time-harmonic acoustic waves:
Helmholtz equation, boundary integral equations and BEM

Lecture notes for the "Advanced numerical methods for PDEs" class

Andrea Moiola

Department of Mathematics, University of Pavia

`andrea.moiola@unipv.it`

`https://euler.unipv.it/moiola/T/MNAPDE2025/MNAPDE2025.html`

February 24, 2025

This is a preliminary version of the notes.
Please let me know if you find any error or have any suggestion.

The main character in this course is the **Helmholtz equation** (also known as "reduced wave equation"), which is the following partial differential equation (PDE):

$$\Delta u + k^2 u = 0. \tag{1}$$

Here $\Delta = \sum_{j=1}^{n} \partial_{x_j}^2$ is the Laplace operator in n variables for $n \in \{1, 2, 3\}$, $k > 0$ is a real parameter called wavenumber, and u is the unknown of the equation, a scalar field defined on a subset of $\mathbb{R}^n$. We will mostly consider the two-dimensional case $n = 2$.

In the following, we first derive the Helmholtz equation from several physical phenomena, showing that it can be used to model different kinds of linear wave problems. Then we show some simple special solutions of the equation. We describe some boundary value problems (BVPs) and focus on one of them, the exterior Dirichlet problem (EDP). We show how to reformulate this as a boundary integral equation (BIE), introduce a numerical method (the boundary element method, BEM) to approximate its solution, and explain how to implement it. We also use Fredholm theory to study some properties of the BIE and the BEM, in particular their well-posedness, sketch some alternative BIEs for the same BVP, and study some related problems.

At the end of the course you should be able to reproduce all the figures present in these notes with Matlab or a similar language.

In the first few sections the approach will be more "physical" than "mathematical", so we will not make precise assumptions and will gloss over some issues such as the regularity of the objects involved or the admissibility of some operations.

All the results presented here are well-known, but scattered over several books and papers. At the end of this document (Appendix G) a few useful references are listed; they are the main sources used in the preparation of these notes (see also those mentioned in Remark 5.29). A few other references, which are relevant for specific results or because they are the original sources, are mentioned (with clickable links) in footnotes.

1 WHY IS THE HELMHOLTZ EQUATION RELEVANT?

1.1 ACOUSTICS

Sound waves are mechanical vibrations propagating in a fluid, which could be either a gas or a liquid. In this section we introduce the basic equations that model them. A more complete introduction can be found in [CJ77, §6] and [BK00, §3]. Being able to model, and thus to control, sound propagation is important for numerous industrial and medical applications: not only for the design of concert halls, musical instruments, microphones and loudspeakers, but also for noise and vibration mitigation (e.g. in cars and aircraft), medical ultrasound imaging, non-invasive therapy such as high-intensity focused ultrasound surgery (HIFU), offshore oil exploration, underwater communication (sonar), bioacoustics, nondestructive testing, sensors. . .

We denote by $\rho(\mathbf{x}, t)$ the **density**, by $p(\mathbf{x}, t)$ the **pressure** and by $\mathbf{v}(\mathbf{x}, t)$ the **velocity** of the fluid in a point $\mathbf{x} \in \mathbb{R}^n$ at time $t \in \mathbb{R}$. We denote by ∇, div (or $\nabla\cdot$) and Δ the gradient, the divergence and the Laplacian in the space coordinate $\mathbf{x}$ only (i.e. without derivatives in t). Conservation of mass gives the **continuity equation**

$$\frac{\partial \rho}{\partial t} + \operatorname{div}(\rho \mathbf{v}) = 0, \tag{2}$$

and conservation of momentum gives **Euler's equation**

$$\frac{\partial \mathbf{v}}{\partial t} + (\mathbf{v} \cdot \nabla)\mathbf{v} + \frac{1}{\rho}\nabla p = \mathbf{0} \tag{3}$$

where $[(\mathbf{v}\cdot\nabla)\mathbf{v}]_j = \sum_{m=1}^n v_m \partial_{x_m} v_j$. See Remark 1.8 for a derivation of (2)–(3). Both PDEs are non-linear as they contain quadratic terms (products of ρ and $\mathbf{v}$ or $\mathbf{v}$ and its derivatives). We assume that all three quantities considered are small perturbations of the constant[1] static values:

$$\rho(\mathbf{x}, t) = \rho_0 + \rho_\approx(\mathbf{x}, t), \quad p(\mathbf{x}, t) = p_0 + p_\approx(\mathbf{x}, t), \quad \mathbf{v}(\mathbf{x}, t) = \mathbf{v}_0 + \mathbf{v}_\approx(\mathbf{x}, t) \quad \text{and that} \quad \mathbf{v}_0 = \mathbf{0}.$$

$p_\approx$ is called **acoustic pressure** or **excess pressure**. Linearising both equations around the static values (using $\frac{1}{\rho} = \frac{1}{\rho_0(1+\frac{\rho_\approx}{\rho_0})} \approx \frac{1}{\rho_0}(1 - \frac{\rho_\approx}{\rho_0})$) we obtain

$$\frac{\partial \rho_\approx}{\partial t} + \rho_0 \operatorname{div}(\mathbf{v}_\approx) = 0 \quad \text{and} \quad \frac{\partial \mathbf{v}_\approx}{\partial t} + \frac{1}{\rho_0}\nabla p_\approx = \mathbf{0}. \tag{4}$$

The pressure is an increasing function of the density $p = f(\rho)$ with $p_0 = f(\rho_0)$. Linearising this relation and denoting $c^2 := \frac{\partial f}{\partial \rho}(\rho_0)$ we have $p_0 + p_\approx = f(\rho_0 + \rho_\approx) \approx f(\rho_0) + c^2\rho_\approx$, thus $p_\approx = c^2\rho_\approx$. (We can call the equations (4) together with $p_\approx = c^2\rho_\approx$ the "first-order acoustic wave equation system".) Using this relation in the two linearised PDEs (4) we obtain that the pressure satisfies the **wave equation**:

$$\frac{1}{c^2}\frac{\partial^2 p_\approx}{\partial t^2} - \Delta p_\approx = 0.$$

(Here we use that the divergence of the gradient is the Laplacian, $\Delta u = \operatorname{div}\nabla u$.) Since $\rho_\approx = \frac{1}{c^2}p_\approx$, also $\rho_\approx$ satisfies the same equation.

The wave equation has been obtained from the linearisation of two "conservation laws" (for mass and momentum) and a "constitutive relation" (relating p and ρ).

In this derivation we have neglected the effect of the non-linear advection term $(\mathbf{v}\cdot\nabla)\mathbf{v}$ and, implicitly, those of fluid viscosity and gravity. A brief discussion of the validity of these assumptions is in [BK00, p. 41]. Moreover, $|p_\approx| \ll p_0$ is true for typical sounds in air: e.g. acoustic pain threshold is between 63 and 200 Pa, while ambient pressure is $p_0 \approx 101\,325$ Pa, so $|p_\approx|/p_0 \approx 6 \times 10^{-4}$—$2 \times 10^{-3}$.

Exercise 1.1: (Acoustic velocity).

- Show that the velocity $\mathbf{v}_\approx$ satisfies the vector wave equation $\frac{1}{c^2}\frac{\partial^2 \mathbf{v}_\approx}{\partial t^2} - \nabla \operatorname{div}\mathbf{v}_\approx = \mathbf{0}$.

- Fix $n = 3$. Prove that for all vector fields $\mathbf{F} \in C^2(\mathbb{R}^3)^3$ the following vector calculus identity holds

$$\nabla \operatorname{div}\mathbf{F} = \mathbf{\Delta}\mathbf{F} + \operatorname{curl}\operatorname{curl}\mathbf{F}. \tag{5}$$

Here $\mathbf{\Delta}$ is the vector Laplacian (defined componentwise) and $\operatorname{curl}\mathbf{F} = \nabla \times \mathbf{F} = \left(\frac{\partial F_3}{\partial x_2} - \frac{\partial F_2}{\partial x_3}, \frac{\partial F_1}{\partial x_3} - \frac{\partial F_3}{\partial x_1}, \frac{\partial F_2}{\partial x_1} - \frac{\partial F_1}{\partial x_2}\right)$ is the usual curl operator.

---

[1] In some applications, the static (time-independent) background quantities ρ_0, p_0 and $\mathbf{v}_0$ are not constant in space. E.g. in ocean acoustics the background density and pressure typically depend on salinity and depth; in the modelling of airplane noise the velocity of the fluid is non-zero and variable. This leads to the presence of extra terms in the linearised differential equations; see also Remark 1.15.

- Deduce that if $\mathbf{v}_{\approx}$ is irrotational, i.e. curl-free $(\operatorname{curl} \mathbf{v}_{\approx} = \mathbf{0})$, then each Cartesian component $v_{\approx,1}, v_{\approx,2}, v_{\approx,3}$ is solution of the scalar wave equation: $\frac{1}{c^2}\frac{\partial^2 v_{\approx,j}}{\partial t^2} - \Delta v_{\approx,j} = 0$, $j = 1, 2, 3$.

- Show that if $\mathbf{v}_{\approx}$ is irrotational at some given time t_0, then it remains irrotational for all $t > t_0$.

Exercise 1.2: (Velocity potential). Assume that, at some initial time $t = t_0$, the velocity $\mathbf{v}_{\approx}(\mathbf{x}, t_0)$ is gradient of a (time-independent) scalar field $\frac{1}{\rho_0}\phi_0(\mathbf{x})$. Show that the scalar field $\phi(\mathbf{x}, t) := \phi_0(\mathbf{x}) - \int_{t_0}^t p_{\approx}(\mathbf{x}, s)\,\mathrm{d}s$, called **velocity potential**, satisfies $-\frac{\partial \phi}{\partial t} = p_{\approx}$ and $\frac{1}{\rho_0}\nabla\phi = \mathbf{v}_{\approx}$. Show that the velocity potential satisfies the wave equation $\frac{1}{c^2}\frac{\partial^2 \phi}{\partial t^2} - \Delta\phi = 0$.

We have seen that several quantities (the acoustic pressure $p_{\approx}$, the density $\rho_{\approx}$, and, under suitable assumptions, the velocity potential ϕ and the components of the velocity $v_{\approx,j}$) satisfy the same wave equation, so we write it for a general scalar field U:
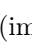
$$\boxed{\frac{1}{c^2}\frac{\partial^2 U}{\partial t^2} - \Delta U = 0.} \tag{6}$$

This is the prototype of second-order, linear, hyperbolic PDEs.

Exercise 1.3: (Time-domain plane waves). Show that for any smooth function $F : \mathbb{R} \to \mathbb{R}$ and any unit vector $\mathbf{d} \in \mathbb{R}^n$, $|\mathbf{d}| = 1$, the field $U(\mathbf{x}, t) = \boxed{F(\mathbf{x} \cdot \mathbf{d} - ct)}$ is a solution of the wave equation (6).

Exercise 1.4: (Time-domain spherical waves). Show that for any smooth function $F : \mathbb{R} \to \mathbb{R}$, the field $U(\mathbf{x}, t) = \frac{F(|\mathbf{x}| - ct)}{|\mathbf{x}|}$ is a solution of the wave equation for $\mathbf{x} \in \mathbb{R}^3 \setminus \{0\}$, $t \in \mathbb{R}$.
   Recall the expression of the Laplace operator in spherical coordinates [DLMF, eq. 1.5.17].

Exercise 1.3 shows that any wave profile (imagine F as a pulse, e.g. ⌁) move across space–time with speed c, which is thus called **wave speed**.[2] Indeed, $c = \sqrt{\frac{p_{\approx}}{\rho_{\approx}}}$ and the square root of the ratio between a pressure and a mass density has the dimension of a velocity (i.e. $\sqrt{\frac{kg\,m^{-1}s^{-2}}{kg\,m^{-3}}} = \frac{m}{s}$). Exercise 1.4 shows that in 3D any wave profile can move radially away from the origin; in this case the profile decreases proportionally to the distance $|\mathbf{x}|$ from the origin as it spreads over a wider spherical surface.

Exercise 1.5: (Damped wave equation). The **damped wave equation** (or equation of telegraphy, see [CJ77, §9]) with damping parameter $\gamma > 0$ is

$$\frac{1}{c^2}\frac{\partial^2 U}{\partial t^2} + \frac{\gamma}{c^2}\frac{\partial U}{\partial t} - \Delta U = 0. \tag{7}$$

Assume that γ is small so that γ^2 can be neglected. Show that wave profiles are damped in time with rate $\frac{\gamma}{2}$ while they propagate: for any smooth function $F : \mathbb{R} \to \mathbb{R}$ and any unit vector $\mathbf{d} \in \mathbb{R}^n$, $|\mathbf{d}| = 1$ the field $U(\mathbf{x}, t) = F(\mathbf{x} \cdot \mathbf{d} - ct)\mathrm{e}^{-\frac{\gamma}{2}t}$ is a solution of the damped wave equation (7) up to a factor $-\frac{\gamma^2}{4c^2}U \approx 0$.
   Conversely, show that if U is solution of the damped wave equation (7), then $W(\mathbf{x}, t) := \mathrm{e}^{\frac{\gamma}{2}t}U(\mathbf{x}, t)$ is solution of the wave equation (6) up to a factor $\frac{\gamma^2}{4c^2}W \approx 0$.
   You can find an interactive animation of the damped wave equation on a rectangle (your browser) with sound-soft boundary conditions (§1.1.1) on https://apps.amandaghassaei.com/MassSpringShader/

Remark 1.6: (Measuring sound). The **acoustic intensity** $\mathbf{I} := p_{\approx}\mathbf{v}_{\approx}$ is the flux of energy per unit area carried by a sound wave; see [BK00, eq. (3.25)] for a derivation. The **sound power** through a surface S with unit normal $\mathbf{n}$ is $\int_S \mathbf{I} \cdot \mathbf{n}\,\mathrm{d}S$ and is measured in watt. Integrating also in time we obtain the energy carried by the acoustic wave. The intensity $\mathbf{I}$ is proportional to $p_{\approx}^2$, see Exercise 1.7.
   Since the human ear has a logarithmic sensitivity, the strength of sound waves is usually measured by the **sound pressure level** $\mathrm{SPL} := 20\log_{10}(p_{\approx}/p_{\mathrm{ref}})$. The SPL unit of measure is the **decibel** (dB, or $\mathrm{dB_{SPL}}$). Here p_{ref} is a reference pressure level: for sound in air this is conventionally taken as $p_{\mathrm{ref}} = 2 \cdot 10^{-5}$ Pa, roughly the human hearing threshold (at appropriate frequencies). With this definition, if the intensity magnitude $|\mathbf{I}| \sim p_{\approx}^2$

---

[2] Thermodynamics states that sound waves are adiabatic, i.e. there is no heat loss, and that $p = a\rho^{\gamma}$, where a is a proportionality constant and $\gamma = 1.4$ for air (or for a diatomic ideal gas), see [BK00, p. 39 and §7.2, (7.33)]. Indeed, taking air pressure $p_0 = 1\mathrm{atm} \approx 101\,325 N/m^2$ and air density $\rho_0 \approx 1.225 kg/m^3$ we have $c = \sqrt{\frac{\partial p}{\partial \rho}(\rho_0)} = \sqrt{\gamma a\rho_0^{\gamma-1}} = \sqrt{\gamma p_0/\rho_0} \approx 340 m/s$, which is the speed of sound in air.

(the power output) of a signal is 10 times higher than that of another signal, then the SPL of the first one is 10 dB higher than the SPL of the second:

$$p_1^2 \sim |\mathbf{I}_1| = 10|\mathbf{I}_2| \sim p_2^2, \qquad \mathrm{SPL}_1 = 20\log\frac{p_1}{p_{\mathrm{ref}}} = 20\log\frac{\sqrt{10}\,p_2}{p_{\mathrm{ref}}} = \mathrm{SPL}_2 + 20\log_{10}\sqrt{10} = \mathrm{SPL}_2 + 10.$$

A sound below 0 dB is inaudible, while $130 - 140$ dB is the pain threshold and sounds at this SPL can lead to permanent hearing damage: these two thresholds roughly correspond to the pressures $2 \cdot 10^{-5}$ Pa and 63–200 Pa, and to the power output 10^{-12} W and 10–100 W.

Exercise 1.7: (Plane wave intensity). Let the acoustic pressure field be a plane wave $p_\approx(\mathbf{x},\cdot) = F(\mathbf{x}\cdot\mathbf{n} - ct)$ as in Exercise 1.3. Using the linearised equations (4), compute the acoustic velocity $\mathbf{v}_\approx$ and show that the acoustic intensity is $\mathbf{I} = \frac{p_\approx^2 \mathbf{d}}{\rho_0 c}$.

Remark 1.8: (Derivation of the continuity and the Euler equations). Let $\psi(\mathbf{x},t)$ be the density of some quantity and $q(\mathbf{x},t)$ its source rate. This means that $\int_D \psi(\mathbf{x},t)\,\mathrm{d}\mathbf{x}$ is the total quantity in a smooth open region $D \subset \mathbb{R}^n$ at a given time t, and $\int_D q(\mathbf{x},t)\,\mathrm{d}\mathbf{x}$ is its net production per unit of time. If the quantity is transported by a fluid with velocity $\mathbf{v}$, its net flow through the boundary of D is $\oint_{\partial D} \psi(\mathbf{x},t)\mathbf{v}(\mathbf{x},t)\cdot\mathbf{n}(\mathbf{x})\,\mathrm{d}S(\mathbf{x})$, $\mathbf{n}$ being the outward unit normal on ∂D. The variation of the total quantity in D is equal to the sum of the amount generated by the source q and the amount flowing through the boundary:

$$\frac{\partial}{\partial t}\int_D \psi(\mathbf{x},t)\,\mathrm{d}\mathbf{x} = \int_D q(\mathbf{x},t)\,\mathrm{d}\mathbf{x} - \oint_{\partial D}\psi(\mathbf{x},t)\mathbf{v}(\mathbf{x},t)\cdot\mathbf{n}(\mathbf{x})\,\mathrm{d}S(\mathbf{x}) = \int_D\Big(q(\mathbf{x},t) - \mathrm{div}\,\big(\psi(\mathbf{x},t)\mathbf{v}(\mathbf{x},t)\big)\Big)\,\mathrm{d}\mathbf{x},$$

thanks to the divergence theorem. Moving the time derivative under the integral sign, since the region D is arbitrary, we obtain that the quantity satisfies the conservation law

$$\frac{\partial\psi}{\partial t} + \mathrm{div}(\psi\mathbf{v}) = q. \tag{8}$$

The conservation of mass is modelled choosing $\psi = \rho$ and $q = 0$ in (8) (since mass is not created nor destroyed), which gives immediately the continuity equation (2). The momentum density is $\rho\mathbf{v}$: the conservation of its jth component $\psi = \rho v_j$ gives

$$\frac{\partial(\rho v_j)}{\partial t} + \mathrm{div}(\rho v_j \mathbf{v}) = F_j, \qquad j = 1,\dots,n,$$

where F_j is the jth component of the external force density acting on the fluid. This is a version of Newton's second law for continua: a force causes a variation of momentum. Using the product rule for the divergence we obtain

$$F_j = \frac{\partial(\rho v_j)}{\partial t} + \mathrm{div}(\rho v_j\mathbf{v}) = v_j\Big(\underbrace{\frac{\partial\rho}{\partial t} + \mathrm{div}(\rho\mathbf{v})}_{=0,\ (2)}\Big) + \rho\Big(\frac{\partial v_j}{\partial t} + \mathbf{v}\cdot\nabla v_j\Big), \qquad j = 1,\dots,n.$$

In the case of our interest, the force density is due to the fluid pressure: $\mathbf{F} = -\nabla p$. Using this in the formula above and dividing by the density ρ we obtain Euler's equation (3).

1.1.1 BOUNDARY CONDITIONS AND SOURCE TERM

When the acoustic waves hits an obstacle $D \subset \mathbb{R}^n$ through which it cannot propagate, on the interface between the obstacle and the fluid some boundary conditions have to be imposed. Depending on the nature of the obstacle and of the fluid, different conditions can be imposed.

- If the obstacle is "**sound-soft**" then the acoustic pressure on its boundary vanishes, i.e. $p_\approx = 0$.

- If the obstacle is "**sound-hard**" then the normal velocity on the boundary vanishes, i.e. $\mathbf{v}_\approx \cdot \mathbf{n} = 0$, where $\mathbf{n}$ is the unit normal vector on the boundary of D.

  Both sound-soft and sound-hard boundary conditions reflect all the energy carried by the wave (§4.1, Exercise 4.18).

- A simple way to model a more realistic boundary condition is to impose that the normal velocity is proportional to the pressure: $\mathbf{v}_\approx \cdot \mathbf{n} = \frac{\vartheta}{c\rho_0}p_\approx$ for some $\vartheta > 0$ that represents how easily the obstacle yields to the acoustic pressure. Here we have assumed that $\mathbf{n}$ points outwards of the domain where the wave propagates and into the obstacle D. We have divided by $c\rho_0$ to ensure that ϑ is dimensionless (check this fact). Deriving this relations and using the linearised Euler's equation (4), we obtain a relation involving $p_\approx$ only: $\mathbf{n}\cdot\nabla p_\approx + \frac{\vartheta}{c}\frac{\partial p_\approx}{\partial t} = 0$. This is called "**impedance**" boundary condition.

- If the obstacle is made of a different fluid, then instead of imposing boundary conditions we consider two copies of the wave equations in the two fluids, with different values of c. The two equations are coupled by suitable **transmission conditions**, i.e. by imposing the continuity of the pressure and the normal displacement across the interface (see [Martin06, §1.3.3] and §7.1.1 below).

  If the obstacle is an elastic solid, acoustic waves in the fluid generates elastic waves in the solid and vice versa. This is modelled by coupling the acoustic wave equation (6) with the (more complicated) elastodynamic wave equation, whose unknown is the point displacement, through appropriate transmission conditions, [Ihlenburg98, §1.3]. We briefly describe the equations of elastodynamics in §1.4.

In "aeroacoustics", sound is generated by fluid turbulence, thus the source of acoustic disturbance is distributed in the bulk of the fluid. This is modelled by the **inhomogeneous wave equation**:

$$\frac{1}{c^2}\frac{\partial^2 U}{\partial t^2} - \Delta U = F, \tag{9}$$

where $F(\mathbf{x}, t)$ is the source term. Vice versa, in "vibroacoustics" the sound is generated by vibrating structures immersed in the acoustic fluid. In this case the source of disturbance is imposed as a boundary condition, justifying the interest in the homogeneous wave equation (6). For an extensive physical description of sound generation see [Heller13]; in particular, see Ch. 7 for sound produced by vibrations of solid objects and Ch. 14 for sound produced by turbulence.

1.2 Time-harmonic waves

A **time-harmonic** function is a scalar field with sinusoidal time dependence, in the form[3]

$$\boxed{U(\mathbf{x}, t) = \Re\{u(\mathbf{x})e^{-i\omega t}\}} = \Re\{u(\mathbf{x})\}\cos\omega t + \Im\{u(\mathbf{x})\}\sin\omega t \tag{10}$$

for an **angular frequency** $\omega > 0$ and a complex-valued field u which depends on the position in space $\mathbf{x}$ but not on the time variable t. (Here $\Re\{\cdot\}$ and $\Im\{\cdot\}$ denote real and imaginary parts, and i is the imaginary unit.) A sound wave in the form (10) is a "pure tone" or a "monocromatic wave".

By taking the Laplacian and the second time-derivative of (10) we obtain that

$$\frac{1}{c^2}\frac{\partial^2 U}{\partial t^2}(\mathbf{x}, t) - \Delta U(\mathbf{x}, t) = \Re\Big\{\Big(-\frac{\omega^2}{c^2}u - \Delta u\Big)e^{-i\omega t}\Big\}$$

and the following crucial fact.

> If $U(\mathbf{x}, t)$ is a time-harmonic (10) solution of the wave equation (6),
> then $u(\mathbf{x})$ is solution of the Helmholtz equation $\Delta u + k^2 u = 0$ with **wavenumber** $k := \omega/c > 0$.

This is **the main reason for the interest in the Helmholtz equation: it describes all time-harmonic solutions of the wave equation**. Any solution of the Helmholtz equation has to be interpreted via (10): multiplying by $e^{-i\omega t}$ and taking the real part we obtain a "physical" field depending on space and time.

The angular frequency ω is measured in radians per second and is proportional to the time frequency f, which is measured in Hertz ($1\text{Hz} = 1s^{-1}$), with the relation $\omega = 2\pi f$. For brevity, in the following we simply use the word "frequency" for ω. The higher the frequency ω and the wavenumber k, the more oscillatory are the solutions of the Helmholtz equation. Sounds that are audible by humans correspond to values of f ranging approximately between 20Hz and $20\,000$Hz.

Another important acoustic quantity is the **wavelength** $\boxed{\lambda := \frac{2\pi}{k}}$. From $k = \frac{\omega}{c}$ and $\omega = 2\pi f$, we have $\lambda = \frac{c}{f}$, thus the wavelengths of audible sounds in the atmosphere range between $17mm$ and $17m$. The wavelength is a characteristic length associated to the Helmholtz operator $\Delta + k^2$: as we will see in §2.2, λ is the spatial period of some important periodic Helmholtz solutions.

Sound-soft conditions translate to Dirichlet boundary conditions $u = 0$, sound-hard to Neumann $\mathbf{n} \cdot \nabla u = 0$, and impedance to Robin $\mathbf{n} \cdot \nabla u - ik\vartheta u = 0$. Note that the coefficient in the impedance condition is imaginary and that $k\vartheta > 0$. A time-harmonic wave propagating in two adjacent regions filled with different fluids (e.g. the atmosphere above the sea) is modelled by two copies of the Helmholtz equation with different values of k coupled by "transmission conditions", see §7.1.1. [4]

---

[3]Unfortunately, several references use the opposite convention $U(\mathbf{x}, t) = \Re\{u(\mathbf{x})e^{i\omega t}\}$, with a different sign at the exponent. This causes changes in the signs and conjugation in all formulas in the following.

[4]If a region Ω_{abs} contains a strongly absorbing medium (see Exercise 1.14), one can approximate the waves propagating in its complement by imposing impedance conditions on $\partial\Omega_{\text{abs}}$. For a justification of this fact and the derivation of more accurate generalised impedance boundary conditions, see [Haddar, Joly, Nguyen, Generalized impedance boundary conditions for scattering by strongly absorbing obstacles: the scalar case, M3AS 2005].

At low frequencies, i.e. for small values of k, the Helmholtz equation is a regular perturbation of the Laplace equation $\Delta u = 0$. Indeed, the two PDEs share many properties, and the same analytical and numerical techniques apply to both. However, at medium and high frequencies, i.e. for larger values of k, time-harmonic problems become much more challenging and interesting: the standard "elliptic" techniques do not apply and we have to resort to more advanced analytical tools and numerical methods. Whether a given $k > 0$ is to be considered a large or a small wavenumber usually depends on the ratio between a characteristic length L of the domain of interest and the wavelength λ: if $\frac{L}{\lambda} \gg 1$ the domain "contains" many wavelengths and we have a high-frequency problem.

Exercise 1.9: (Amplitude and phase). Show that a time-harmonic function $U(\mathbf{x}, t)$ as in (10) (not necessarily solution of any PDE) can be written in terms of an **amplitude** function $A(\mathbf{x}) \geq 0$ and a (real) **phase** function $\phi(\mathbf{x})$ as
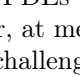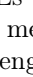
$$U(\mathbf{x}, t) = A(\mathbf{x}) \cos\big(\omega(t - \phi(\mathbf{x}))\big).$$

Express A and ϕ in terms of u and vice versa.

At the point $\mathbf{x}$, the wave U oscillates between the values $-A(\mathbf{x})$ and $A(\mathbf{x})$. Different points $\mathbf{x}_1$ and $\mathbf{x}_2$ reach the maximum periodically at different times dictated by ϕ: show that they are synchronised if and only of $\phi(\mathbf{x}_1) - \phi(\mathbf{x}_2)$ is an integer multiple of $\frac{2\pi}{\omega}$.

Exercise 1.10: (Inhomogeneous wave and Helmholtz equations). Let U be time-harmonic as in (10) and be a solution of the inhomogeneous wave equation (9) with $F(\mathbf{x}, t) = \Re\{f(\mathbf{x})e^{-i\omega t}\}$. Show that u satisfies the inhomogeneous Helmholtz equation $-\Delta u - k^2 u = f$.

Exercise 1.11: (Time reversal). Show that complex conjugation of Helmholtz solutions "reverses time": if U is the space–time wave solution associated to the Helmholtz solution u, then the space–time wave solution W associated to $\overline{u} = \Re u - i\Im u$ satisfies $W(\mathbf{x}, t) = U(\mathbf{x}, -t)$.

Exercise 1.12: (Helmholtz solutions oscillate around 0). Show that if u is a Helmholtz solution defined on an open set and $\mathbf{x}_*$ is an interior local maximum (minimum, respectively) of its real part, then $\Re u(\mathbf{x}_*) \geq 0$ ($\Re u(\mathbf{x}_*) \leq 0$, respectively). This means that $\Re u$ can look like ⤳〰〰〰⤳ but not like ⤳〰〰⤳.

Exercise 1.13: (Time-harmonic loop). Verify that for every time-harmonic U as in (10)

$$U(\mathbf{x}, 0) = \Re\{u(\mathbf{x})\}, \quad U\Big(\mathbf{x}, \frac{\pi}{2\omega}\Big) = \Im\{u(\mathbf{x})\}, \quad U\Big(\mathbf{x}, \frac{\pi}{\omega}\Big) = -\Re\{u(\mathbf{x})\}, \quad U\Big(\mathbf{x}, \frac{3\pi}{2\omega}\Big) = -\Im\{u(\mathbf{x})\}.$$

This means that when the wave U has value equal to the real part of u, it will shift towards a value equal to the imaginary part of u. We will use this to determine direction a time-harmonic wave u is moving, from the comparison of his real and imaginary part.

Exercise 1.14: (Helmholtz equation with complex wavenumber). Show that if U is a time-harmonic solution of the damped wave equation (7) then it is solution of the Helmholtz equation with complex wavenumber k, such that $k^2 = \omega(\omega + i\gamma)/c^2$. (We always choose the root k with $\Re k > 0$ and $\Im k \geq 0$).

This shows that the solutions of the Helmholtz equation with complex wavenumber k can be understood as waves that are attenuated while they propagate, i.e. they are absorbed by the medium through which they propagate. The larger the imaginary part of the wavenumber, the stronger the damping. A negative imaginary part of k corresponds to $\gamma < 0$ in (7) and to waves increasing in time, which is an unphysical situation.

Remark 1.15: (Waves in heterogeneous media). We have assumed that the medium through which the wave propagates is uniform. In the more general case of an acoustic wave propagating through heterogeneous materials, both the sound speed c and the static density ρ_0 depend on the position $\mathbf{x}$. In this case, one obtains the wave equation $\frac{1}{\rho_0(\mathbf{x})c^2(\mathbf{x})}\frac{\partial^2 p_\approx}{\partial t^2} - \mathrm{div}(\frac{1}{\rho_0(\mathbf{x})}\nabla p_\approx) = 0$. Assuming time-harmonic behaviour (10) for $U = p_\approx$ we have the Helmholtz equation with variable coefficients (also called Bergmann equation, [Martin06, eq. (1.27)]):

$$\mathrm{div}\left(\frac{1}{\rho_0(\mathbf{x})}\nabla u(\mathbf{x})\right) + \frac{\omega^2}{\rho_0(\mathbf{x})c^2(\mathbf{x})}u(\mathbf{x}) = 0. \tag{11}$$

When a wave passes through materials with variable acoustic properties ρ_0 and c, it deviates from a straight propagation path: this phenomenon is called **refraction**.

In the following sections we do not consider this more general problem and we stick to the constant-coefficients case. Then in §7 we return to (11), assuming constant ρ_0 and variable c. See also [CK2, §8] and [Martin06, §1.3.4] for more details on time-harmonic wave problems in heterogeneous media.

Remark 1.16: (Is the Helmholtz equation elliptic?). According to the standard classification of second-order linear PDEs, Helmholtz equation is clearly elliptic: its principal part (the second order term) is simply the Laplacian (see [Brezis11, Ch. 9, eq. (36)], [McLean00, eq. (4.7)]). Indeed it shares many properties with Laplace equation, e.g. "elliptic regularity" (all solutions are C^∞ in their domain). But often the word "elliptic" is used to denote problems that satisfy the assumptions of Lax–Milgram theorem. We will see that the typical variational forms of Helmholtz BVPs do not satisfy this requirement, so under this respect the equation is not elliptic. Indeed, it does not satisfy some other typical properties of elliptic PDEs, such as the maximum principle; moreover it is closely related to the wave equation, which is the prototypical hyperbolic equation.

Remark 1.17: (Helmholtz equation = wave equation + Fourier transform). Fourier analysis tells us that any "reasonable" (e.g. square-integrable) time-dependent field U can be written as a continuous linear combination of time-harmonic fields $e^{i\omega t}\widehat{U}(\mathbf{x},\omega)$ with different frequencies $\omega \in \mathbb{R}$, where $\widehat{U}$ is its Fourier transform (in time):

$$U(\mathbf{x},t) = \frac{1}{\sqrt{2\pi}}\int_{\mathbb{R}} e^{i\omega t}\widehat{U}(\mathbf{x},\omega)\,d\omega \qquad \text{with} \qquad \widehat{U}(\mathbf{x},\omega) = \frac{1}{\sqrt{2\pi}}\int_{\mathbb{R}} e^{-i\omega t}U(\mathbf{x},t)\,dt.$$

Reasoning as above, we can verify that, if U is solution of the wave equation with wave speed c, then its Fourier transform $\widehat{U}$ evaluated at a given frequency ω, i.e. $u(\mathbf{x}) = \widehat{U}(\mathbf{x},\omega)$, is solution of the Helmholtz equation with wavenumber $k = \omega/c$. Thus any solution of the wave equation is a linear combination of infinitely many solutions of the Helmholtz equation at different wavenumbers. (Roughly speaking, this is how human ears process sound: different parts of the ear receive and transmit to the brain different frequencies.) Numerically, often one approximates a wave equation solution by solving several Helmholtz problems. This is an important reason for studying the Helmholtz equation, even if we were not interested in problems at a fixed frequency.

When we study U and the wave equation we say that we work "in time domain"; when we study $\widehat{U}$ or u and the Helmholtz equation we say that we work "in frequency domain".

1.3 ELECTROMAGNETISM

Although the Helmholtz equation is usually associated to acoustic waves, it is important also in the modelling of other kinds of linear waves, e.g. electromagnetic ones. In this section and in the next one we fix $n = 3$, i.e. we consider 3D problems. Electromagnetic waves in a homogeneous material, in the absence of charges, are described by the **Maxwell's equations**:

$$\operatorname{curl}\mathcal{E}(\mathbf{x},t) + \mu\frac{\partial\mathcal{H}}{\partial t}(\mathbf{x},t) = \mathbf{0}, \qquad \operatorname{curl}\mathcal{H}(\mathbf{x},t) - \epsilon\frac{\partial\mathcal{E}}{\partial t}(\mathbf{x},t) - \sigma\mathcal{E}(\mathbf{x},t) = \mathbf{0}, \tag{12}$$

where $\mathcal{E}$ is the electric field, $\mathcal{H}$ the magnetic field, ϵ the electric permittivity, μ the magnetic permeability, and σ the conductivity. The parameters ϵ, μ and σ represent the properties of the material through which the wave propagates. As we consider a homogeneous, isotropic medium, ϵ and μ are positive constants, σ is a non-negative constant (0 in a dielectric, i.e. a perfect insulator, and positive in a conducting medium). The first equation is called Faraday law, the second one Ampère law.

If both the electric and the magnetic field are time-harmonic, i.e. $\mathcal{E}(\mathbf{x},t) = \Re\{\mathbf{E}(\mathbf{x})e^{-i\omega t}\}$ and $\mathcal{H}(\mathbf{x},t) = \Re\{\mathbf{H}(\mathbf{x})e^{-i\omega t}\}$ for some $\omega > 0$, then the time-independent fields $\mathbf{E}$ and $\mathbf{H}$ satisfy the **time-harmonic Maxwell's equations**:

$$\operatorname{curl}\mathbf{E}(\mathbf{x}) - i\omega\mu\mathbf{H}(\mathbf{x}) = \mathbf{0}, \qquad \operatorname{curl}\mathbf{H}(\mathbf{x}) + i\omega\epsilon\mathbf{E}(\mathbf{x}) - \sigma\mathbf{E}(\mathbf{x}) = \mathbf{0}. \tag{13}$$

These are two vector-valued PDEs with two vector fields as unknowns. Eliminating $\mathbf{H}$, we obtain the **second-order time-harmonic Maxwell's equations** for the electric field:

$$\operatorname{curl}\operatorname{curl}\mathbf{E} - k^2\mathbf{E} = \mathbf{0} \qquad \text{with} \quad k^2 = \omega^2\epsilon\mu + i\omega\sigma\mu. \tag{14}$$

Since $\operatorname{div}\operatorname{curl}\mathbf{v} = 0$ for any vector field $\mathbf{v}$, any solution of (14) is divergence-free (solenoidal). Then the expansion (5) ($\operatorname{curl}\operatorname{curl} = \nabla\operatorname{div} - \boldsymbol{\Delta}$) implies that each component of the solution of the second-order Maxwell's equations (14) is solution of the Helmholtz equation with (possibly complex, if $\sigma > 0$) wavenumber k:

$$\Delta E_j + k^2 E_j = 0 \qquad \text{for} \quad j = 1,2,3. \tag{15}$$

The speed of propagation of electromagnetic waves (e.g. of light) is $c = \frac{1}{\sqrt{\epsilon\mu}} > 0$ and the damping factor (as in Exercise 1.14) is $\gamma = \Im\{k^2\}\frac{c^2}{\omega} = \frac{\sigma}{\epsilon} \geq 0$.

As any other PDE, time-harmonic Maxwell's equations are complemented by boundary conditions. When the domain under consideration is surrounded by a metal, through which the electric field does not penetrate, then typically one imposes the "**perfect electric conductor**" (PEC) boundary conditions, which impose that the *tangential* component of the electric field vanishes. In formulas this is $\mathbf{E} \times \mathbf{n} = \mathbf{0}$, where $\times$ denote the vector product and $\mathbf{n}$ is the unit normal vector on the boundary. In terms of the magnetic field, the PEC boundary conditions correspond to the vanishing of the *normal* component: $\mathbf{H} \cdot \mathbf{n} = 0$. This is easy to verify for a plane boundary, e.g. $\Pi = \{x_1 = 0\}$: in this case $\mathbf{E} \times \mathbf{n} = \mathbf{E} \times (1, 0, 0) = (0, E_3, -E_2)$ so $E_2 = E_3 = 0$ on the whole plane Π, and $\mathbf{H} \cdot \mathbf{n} = \frac{1}{\mathrm{i}\omega\mu} \operatorname{curl} \mathbf{E} \cdot (1, 0, 0) = \frac{1}{\mathrm{i}\omega\mu}(\frac{\partial E_3}{\partial x_2} - \frac{\partial E_2}{\partial x_3}) = 0$.

We also often encounter **impedance** (or Leontovich) **boundary conditions**: $\mathbf{H} - \vartheta(\mathbf{n} \times \mathbf{E}) \times \mathbf{n} = \frac{1}{\mathrm{i}k}\mathbf{g}$, or equivalently $\mu^{-1} \operatorname{curl} \mathbf{E} \times \mathbf{n} - \mathrm{i}k\vartheta(\mathbf{n} \times \mathbf{E}) \times \mathbf{n} = \mathbf{g}$, for a parameter ϑ with $\Re\vartheta > 0$ and a boundary source term $\mathbf{g}$. Here $(\mathbf{n} \times \mathbf{E}) \times \mathbf{n} = \mathbf{E} - (\mathbf{E} \cdot \mathbf{n})\mathbf{n}$ is the tangential component of $\mathbf{E}$. Impedance conditions can be used to model an "imperfect conductor": if the complement of the domain of interest is a metal with large (but finite) conductivity σ, then the electromagnetic field decays exponentially in it (skin effect); impedance conditions approximate the relation between $\mathbf{E}$ and $\mathbf{H}$ on the surface without the need of knowing the evanescent fields in the conductor. In this case the parameter ϑ is complex and can be computed[5] from the material parameters $\epsilon_c, \mu_c, \sigma_c$ of the conductor as $\vartheta = \sqrt{\frac{\epsilon_c + \mathrm{i}\sigma_c/\omega}{\mu_c}}$; $\zeta = 1/\vartheta$ is called "surface impedance".

Exercise 1.18: (Maxwell-vs-Helmholtz). Complete the proof of the following statement. For $k \in \mathbb{C}$, $k \neq 0$, a vector field $\mathbf{v}$ is solution of $\operatorname{curl}\operatorname{curl}\mathbf{v} - k^2\mathbf{v} = \mathbf{0}$ if and only if it is divergence-free and each of its three components is solution of the Helmholtz equation $\Delta v_j + k^2 v_j = 0$, $j = 1, 2, 3$.

Exercise 1.19: (Alternative derivation). We have shown that the components of the time-harmonic solutions of the Maxwell's equations (12) are Helmholtz solutions. Show again the same fact performing the same operations in different order. First eliminate $\mathcal{H}$ from (12) obtaining second-order Maxwell's equations in time-domain. Then verify that each component of $\mathcal{E}$ satisfies the wave equation (6). Finally assume that $\mathcal{E}$ is time-harmonic.

Remark 1.20: (Current density). Often the conductivity term $\sigma\mathcal{E}(\mathbf{x}, t)$ in the time-domain Maxwell's equation is modelled as a *given* current density $\mathcal{J}(\mathbf{x}, t)$ and treated as a datum. If this is assumed to be time-harmonic $\mathcal{J}(\mathbf{x}, t) = \Re\{\mathbf{J}(\mathbf{x})e^{-\mathrm{i}\omega t}\}$ we obtain the inhomogeneous time-harmonic Ampère law $\operatorname{curl}\mathbf{H} + \mathrm{i}\omega\epsilon\mathbf{E} = \mathbf{J}$ and the second-order equation $\operatorname{curl}\frac{1}{\mu}\operatorname{curl}\mathbf{E} - \omega^2\epsilon\mathbf{E} = \mathrm{i}\omega\mathbf{J}$. In absence of charges, the current density is divergence free: $\operatorname{div}\mathbf{J} = 0$ (more generally we would have the continuity equation $\operatorname{div}\mathbf{J} = -\frac{\partial\rho}{\partial t}$, where ρ is the charge density), so the component of the electric field satisfy the inhomogeneous Helmholtz equation $\Delta E_j + k^2 E_j = -\mathrm{i}\omega\mu J_j$.

Remark 1.21: (1 Maxwell PDE $\Rightarrow$ 3 Helmholtz PDEs, 1 Maxwell BVP $\not\Rightarrow$ 3 Helmholtz BVPs). We have seen that time-harmonic Maxwell solutions are componentwise Helmholtz solutions. However, in general one cannot reduce the solution of a boundary value problem for the Maxwell's equations (14) to three independent Helmholtz problems for E_1, E_2, E_3, because the boundary conditions required are different.

For instance, when we impose PEC boundary conditions, only the tangential component of the electric field vanishes. This is equivalent to the imposition of two scalar boundary conditions (e.g. on two Cartesian components if the domain is a cube) for three unknown scalar fields and three scalar PDEs (Helmholtz); the boundary value problem is closed by the condition $\operatorname{div}\mathbf{E} = 0$ which intertwines the three components. Being able to solve/approximate Helmholtz BVPs is not enough to solve/approximate Maxwell BVPs.

We see in the next remark that the decoupling of the scalar components and the reduction of Maxwell's problems to Helmholtz ones can be performed when symmetries are present.

Remark 1.22: (TE and TM modes). ([Nédélec01, p. 5], [CJ77, §86], [BK00, §6.8].) The Helmholtz equation is important in dimensional reductions of the Maxwell's equations. Maxwell's equations simplify when we assume that the dependence on one of the Cartesian variables of all components of the fields is a given complex exponential, i.e.

$$\mathbf{E}(x_1, x_2, x_3) = \widetilde{\mathbf{E}}(x_1, x_2)e^{\mathrm{i}\eta x_3}, \qquad \mathbf{H}(x_1, x_2, x_3) = \widetilde{\mathbf{H}}(x_1, x_2)e^{\mathrm{i}\eta x_3}, \qquad \eta > 0. \tag{16}$$

If the pair $(\mathbf{E}, \mathbf{H})$ satisfies the Maxwell equations (13), from (15) we see that each component of $\widetilde{\mathbf{E}}$ and $\widetilde{\mathbf{H}}$ satisfies $\Delta\widetilde{E}_j + (k^2 - \eta^2)\widetilde{E}_j = 0$ and $\Delta\widetilde{H}_j + (k^2 - \eta^2)\widetilde{H}_j = 0$. Note that this is a two-dimensional Laplacian.

This is relevant when we consider the propagation of waves through very long objects such as optical fibres. For a field in the form (16), the curl becomes

$$\operatorname{curl}\mathbf{H} = e^{\mathrm{i}\eta x_3}\Big(\frac{\partial\widetilde{H}_3}{\partial x_2} - \mathrm{i}\eta\widetilde{H}_2, \ \mathrm{i}\eta\widetilde{H}_1 - \frac{\partial\widetilde{H}_3}{\partial x_1}, \ \frac{\partial\widetilde{H}_2}{\partial x_1} - \frac{\partial\widetilde{H}_1}{\partial x_2}\Big).$$

---

[5]See [Senior, Impedance boundary conditions for imperfectly conducting surfaces, 1960, eq. (25)–(26)] for a flat interface.

Maxwell's equations (13) (with $\sigma = 0$) become

$$\frac{\partial \widetilde{E}_3}{\partial x_2} - \mathrm{i}\eta \widetilde{E}_2 - \mathrm{i}\omega\mu \widetilde{H}_1 = 0, \qquad \frac{\partial \widetilde{H}_3}{\partial x_2} - \mathrm{i}\eta \widetilde{H}_2 + \mathrm{i}\omega\epsilon \widetilde{E}_1 = 0,$$

$$\mathrm{i}\eta \widetilde{E}_1 - \frac{\partial \widetilde{E}_3}{\partial x_1} - \mathrm{i}\omega\mu \widetilde{H}_2 = 0, \qquad \mathrm{i}\eta \widetilde{H}_1 - \frac{\partial \widetilde{H}_3}{\partial x_1} + \mathrm{i}\omega\epsilon \widetilde{E}_2 = 0,$$

$$\frac{\partial \widetilde{E}_2}{\partial x_1} - \frac{\partial \widetilde{E}_1}{\partial x_2} - \mathrm{i}\omega\mu \widetilde{H}_3 = 0, \qquad \frac{\partial \widetilde{H}_2}{\partial x_1} - \frac{\partial \widetilde{H}_1}{\partial x_2} + \mathrm{i}\omega\epsilon \widetilde{E}_3 = 0.$$

If $\widetilde{E}_3 = 0$, assuming $\eta \neq k$ (recall that $k = \omega\sqrt{\epsilon\mu}$ from (14)), with some manipulation one can see that all other field components can be computed from $\widetilde{H}_3$:

$$\widetilde{E}_1 = -\Big(\mathrm{i}\omega\epsilon - \frac{\mathrm{i}\eta^2}{\omega\mu}\Big)^{-1} \frac{\partial \widetilde{H}_3}{\partial x_2}, \qquad \widetilde{E}_2 = \Big(\mathrm{i}\omega\epsilon - \frac{\mathrm{i}\eta^2}{\omega\mu}\Big)^{-1} \frac{\partial \widetilde{H}_3}{\partial x_1}, \qquad \widetilde{H}_1 = -\frac{\eta}{\omega\mu}\widetilde{E}_2, \qquad \widetilde{H}_2 = \frac{\eta}{\omega\mu}\widetilde{E}_1. \quad (17)$$

In particular, $(\widetilde{H}_1, \widetilde{H}_2) = \frac{\mathrm{i}\eta}{k^2 - \eta^2}\nabla \widetilde{H}_3$. These solutions are called "**transverse-electric (TE) modes**", since $E_3 = \widetilde{E}_3 = 0$ means that the electric field is perpendicular to the x_3 axis, along which the wave propagates. Similarly, the "**transverse-magnetic (TM) modes**" are solutions with $\widetilde{H}_3 = 0$ and all their components can be computed from $\widetilde{E}_3$. All Maxwell solutions in the form (16) with $\eta \neq k$ are sum of a TE and a TM mode, so they can computed by solving two Helmholtz problems with wavenumber $\sqrt{k^2 - \eta^2}$ for $\widetilde{H}_3$ and $\widetilde{E}_3$.

Now assume that we want to compute the solutions of Maxwell's equation in an infinite cylinder $\Omega \times \mathbb{R} = \{\mathbf{x} = (x_1, x_2, x_3) \in \mathbb{R}^3 : (x_1, x_2) \in \Omega, x_3 \in \mathbb{R}\}$, where $\Omega \subset \mathbb{R}^2$ is bounded, and PEC boundary conditions are imposed on $\partial\Omega \times \mathbb{R}$. A TE mode satisfies the PEC conditions $\widetilde{\mathbf{H}} \cdot \mathbf{n} = 0$ if the Neumann condition $\mathbf{n} \cdot \nabla \widetilde{H}_3 = 0$ holds (recall (17)), while a TM mode has to satisfy the Dirichlet one $\widetilde{E}_3 = 0$. Thus there exists an electromagnetic wave propagating through the (closed) **waveguide** $\Omega \times \mathbb{R}$ with wavenumber η in the x_3 direction only if the 2D Helmholtz problem admits a non-trivial solution. This is the same as saying that $\omega^2\epsilon\mu - \eta^2 = k^2 - \eta^2$ is either a Dirichlet (TM) or a Neumann (TE) eigenvalue for the 2D Laplacian in Ω (we will describe Laplace eigenvalues in §4.2).

Thanks to symmetry, 3D Maxwell's problems have been reduced to 2D Helmholtz ones. We will encounter a similar situation in Remark 4.33.

Exercise 1.23: (TEM modes). Assume that the (non-trivial) pair $(\mathbf{E}, \mathbf{H})$ is a "TEM mode", which means that it is simultaneously a TE and a TM mode: it is in the form (16) with $\widetilde{E}_3 = \widetilde{H}_3 = 0$. Show the following facts.

- $\eta^2 = \omega^2\epsilon\mu$, i.e. $\eta = k$: the wavenumber in the x_3 direction coincide with the free-space wavenumber (recall that (17) holds in the opposite case $\eta \neq k$ as it follows from a division by $k^2 - \eta^2$).
- $\mathbf{H} = \sqrt{\epsilon/\mu}\,\mathbf{e}_3 \times \mathbf{E}$, where $\mathbf{e}_3 = (0, 0, 1)$. This means that $\mathbf{E}$ and $\mathbf{H}$ are orthogonal vectors in the $x_1 x_2$-plane.
- If ϕ is a 2D harmonic function ($\Delta\phi = 0$), then $\mathbf{E} = \nabla\phi(x_1, x_2)\mathrm{e}^{\mathrm{i}kx_3}$ and $\mathbf{H} = \sqrt{\epsilon/\mu}\,\mathbf{e}_3 \times \mathbf{E}$ constitute a TEM mode.
- Linear polynomials are the simplest harmonic functions: write the corresponding TEM modes.
- If the domain $\Omega \subset \mathbb{R}^2$ is simply connected then there is no non-trivial TEM mode with PEC conditions propagating through $\Omega \times \mathbb{R}$. (This is a main motivation for the use of coaxial cables.)

The Helmholtz equation is used in place of the Maxwell's equations when the effects of the wave polarisation (the direction in which the field points) are neglected. This is often done, for example, in the Fresnel, Fraunhofer and Kirchhoff descriptions of light diffraction by apertures.

Remark 1.24: (Reality is more complicated than this!). The setting considered in this section is a special case of much more general ones, which are needed in many applications. If different materials are present in the region considered, or the properties of the material vary in space, then ϵ, μ, σ are function of position. In this case, for instance, to obtain (14) we cannot simply move μ to the second term and find componentwise solution of the Helmholtz equation, but we obtain some more general elliptic equations. If the material is anisotropic, then the coefficients are modelled by symmetric positive definite matrices (semi-definite in case of σ). Since the polarisation of a material given an impinging electromagnetic field is not immediate, the multiplications $\epsilon\mathcal{E}$ and $\mu\mathcal{H}$ in (12) are more precisely modelled as convolutions in time between $\mathcal{E}/\mathcal{H}$ and suitable kernels; however in frequency-domain these give rise to standard products $\epsilon(\omega)\mathbf{E}$ and $\mu(\omega)\mathbf{H}$ where now the coefficients depends on the frequency ω. In some materials and regimes (e.g. in lasers) the coefficients ϵ and μ need to be modelled as non-linear operators acting on $\mathbf{E}$ and $\mathbf{H}$: this is the field of non-linear optics.

1.4 ELASTODYNAMICS

Mechanical vibrations propagating in solids have more complicated behaviour than those in fluids, as two different types of waves can be present. The relevant PDEs are similar to the wave and the Helmholtz equations, with some complications due to the fact that the unknown is a vector field and the differential operator (in the space variable $\mathbf{x}$) is not as simple as the Laplacian. The **Navier's equations** are the system of PDEs that describes small-amplitude vibrations in (homogeneous, isotropic) solid objects:

$$\rho \frac{\partial^2 \mathbf{U}}{\partial t^2} = (\lambda + 2\mu)\nabla \operatorname{div} \mathbf{U} - \mu \operatorname{curl} \operatorname{curl} \mathbf{U} + \mathbf{F}.$$

Here $\mathbf{U}(\mathbf{x}, t)$ is the **displacement** vector field, describing the position of a material point of the object with respect to the rest position; $\mathbf{F}$ are the forces per unit of volume (e.g. gravity forces); the positive parameters λ and μ are the **Lamé constants**[6], describing the elastic properties of the material; and $\rho > 0$ is the mass density of the medium at rest. These are the main equation of "linear elastodynamics", while "elastostatics" studies the equilibrium case where $\mathbf{U}$ is independent of time (e.g. it studies small deformations of an object under a static load). In absence of external forces acting in the volume of the body ($\mathbf{F} = \mathbf{0}$), and if the waves are time-harmonic with angular frequency ω (i.e. (10) holds for each component of $\mathbf{U}$), the Navier's equations become

$$(\lambda + 2\mu)\nabla \operatorname{div} \mathbf{u} - \mu \operatorname{curl} \operatorname{curl} \mathbf{u} + \omega^2 \rho \, \mathbf{u} = \mathbf{0}. \tag{18}$$

We define the wavenumber of pressure (longitudinal) and shear (transverse) waves, respectively, as:

$$k_P := \omega \sqrt{\frac{\rho}{\lambda + 2\mu}}, \qquad k_S := \omega \sqrt{\frac{\rho}{\mu}}.$$

We define the scalar and vector potential, respectively, as

$$\chi := -\frac{\lambda + 2\mu}{\omega^2 \rho} \operatorname{div} \mathbf{u} = -\frac{\operatorname{div} \mathbf{u}}{k_P^2}, \qquad \boldsymbol{\psi} := \frac{\mu}{\omega^2 \rho} \operatorname{curl} \mathbf{u} = \frac{\operatorname{curl} \mathbf{u}}{k_S^2}. \tag{19}$$

The fields $\chi, \boldsymbol{\psi}$ are called "Lamé potentials". From (18), we can use these potentials to represent $\mathbf{u}$:

$$\mathbf{u} = -\frac{\lambda + 2\mu}{\omega^2 \rho} \nabla \operatorname{div} \mathbf{u} + \frac{\mu}{\omega^2 \rho} \operatorname{curl} \operatorname{curl} \mathbf{u} = \nabla \chi + \operatorname{curl} \boldsymbol{\psi}, \tag{20}$$

which is a "Helmholtz decomposition" of the displacement field. With some manipulation we obtain

$$\Delta \chi + k_P^2 \chi \overset{(19), \Delta = \operatorname{div} \nabla}{=} -\operatorname{div} \nabla \frac{\operatorname{div} \mathbf{u}}{k_P^2} - \operatorname{div} \mathbf{u} \overset{(18)}{=} -\frac{1}{k_P^2} \operatorname{div} \left(\frac{\mu}{\lambda + 2\mu} \operatorname{curl} \operatorname{curl} \mathbf{u} - k_P^2 \mathbf{u} \right) - \operatorname{div} \mathbf{u} \overset{\operatorname{div} \operatorname{curl} = 0}{=} 0,$$

$$\operatorname{curl} \operatorname{curl} \boldsymbol{\psi} - k_S^2 \boldsymbol{\psi} \overset{(19)}{=} \operatorname{curl} \operatorname{curl} \frac{\operatorname{curl} \mathbf{u}}{k_S^2} - \operatorname{curl} \mathbf{u} \overset{(18)}{=} \frac{1}{k_S^2} \operatorname{curl} \left(\frac{\lambda + 2\mu}{\mu} \nabla \operatorname{div} \mathbf{u} + k_S^2 \mathbf{u} \right) - \operatorname{curl} \mathbf{u} \overset{\operatorname{curl} \nabla = \mathbf{0}}{=} \mathbf{0}.$$

This means that the scalar and vector potentials satisfy Helmholtz and Maxwell's equations, respectively.

The decomposition (20) shows that any solution $\mathbf{u}$ of Navier's equations (18) is sum of two terms. The first one is a curl-free, longitudinal, time-harmonic wave propagating at speed $c_P = \frac{\omega}{k_P} = \sqrt{\frac{\lambda + 2\mu}{\rho}}$; this is called **pressure wave** (P-wave). The second one is a divergence-free, transverse, time-harmonic wave propagating at (lower) speed $c_S = \frac{\omega}{k_S} = \sqrt{\frac{\mu}{\rho}}$; this is called **shear wave** (S-wave). In seismology, P-waves and S-waves are called primary and secondary waves, respectively, because after an earthquake they reach a give point the surface in this order, due to their different speeds.

In particular, all time-harmonic elastic waves can be 'assembled' from solutions of two copies of the Helmholtz equation with different wavenumbers. In some applications, such as seismic imaging for oil retrieval, Navier's equations are sometimes approximated by the scalar Helmholtz equation, neglecting shear waves.

The limit $\mu \to 0$ corresponds to a fluid material, elasticity reduces to acoustics and shear waves disappear: Navier's equations tend to $\nabla \operatorname{div} \mathbf{u} + k_P^2 \mathbf{u} = \mathbf{0}$, which is the equation satisfied by the acoustic displacement and the acoustic velocity.

---

[6]Sometimes these equations are written in terms of the Poisson ratio ν and Young's modulus E, which are other relevant material parameters related to the Lamé constants by the relations $\lambda = \frac{E\nu}{(1+\nu)(1-2\nu)}$ and $\mu = \frac{E}{2(1+\nu)}$. Vice versa, $\nu = \frac{\lambda}{2(\lambda + \mu)}$ and $E = \frac{\mu(3\lambda + 2\mu)}{\lambda + \mu}$. The "shear modulus" μ is also denoted G.

The Dirichlet boundary condition for the Navier's equations consists in imposing a given displacement on the boundary: $\mathbf{u} = \mathbf{g}$. The Neumann boundary condition requires the **traction** operator $\mathbf{T}(\mathbf{u}) := 2\mu\frac{\partial \mathbf{u}}{\partial \mathbf{n}} + \lambda\mathbf{n}\operatorname{div}\mathbf{u} + \mu\mathbf{n} \times \operatorname{curl}\mathbf{u}$, with $\mathbf{n}$ the outward-pointing unit normal; setting $\mathbf{T}(\mathbf{u}) = \mathbf{g}$ on the boundary corresponds to imposing the action of a force on the surface of the body.

When an elastic solid is in contact with a fluid, elastic vibrations in the solid generate acoustic waves in the fluid, and vice versa. The simulation of this interaction is important for noise mitigation in vehicles and aircraft. On the boundary between the fluid and the solid domain, one has to impose "transmission conditions", to ensure the continuity of pressure and particle displacement (in formulas: $p\mathbf{n} = -\mathbf{T}(\mathbf{u})$ and $\mathbf{n} \cdot \nabla p = \omega^2\rho\,\mathbf{u} \cdot \mathbf{n}$, where p is the fluid pressure), see [Ihlenburg98, §1.3]. This is sometimes called "strong coupling". If the pressure forces of the fluid on the solid are negligible, then one can impose a "weak coupling": first compute the elastic vibrations of the solid and use them as input for the computation of the acoustic field.

Elastic and acoustic waves interact with one another also in porous materials (e.g. soil, rocks, biological tissues, foam sound absorbers, . . .), i.e. solid materials containing pores, which are spaces filled by a fluid (water, oil, air, . . .). The theory of "poroelasticity", first developed by Biot, describes the mechanical vibrations of porous media and arises from the interaction between elastic waves in the solid structure and acoustic waves in the fluid component.

All properties mentioned here have an analogue in time-domain, as opposed to frequency-domain.

More information can be found e.g. in [BK00, §5] and [Ihlenburg98, §1.2].

Remark 1.25: (Navier's equations with strain and stress tensors). We give some more notation and write Navier's equations in different equivalent forms to help relate other references to this section. Using identity (5), equation (18) can also be written as

$$(\lambda + \mu)\nabla\operatorname{div}\mathbf{u} + \mu\boldsymbol{\Delta}\mathbf{u} + \omega^2\rho\mathbf{u} = \mathbf{0}.$$

We denote by $\underline{\underline{\mathbf{D}}}\mathbf{v}$ the Jacobian of the vector field $\mathbf{v}$, by $\underline{\underline{\mathbf{D}}}^S\mathbf{v} := \frac{1}{2}(\underline{\underline{\mathbf{D}}}\mathbf{v} + \underline{\underline{\mathbf{D}}}^\top\mathbf{v})$ the symmetric gradient, by $\mathbf{div}$ the (row-wise) vector divergence of matrix fields, and by $\underline{\underline{\mathrm{Id}}}$ the 3×3 identity matrix. The symmetric gradient of the displacement $\underline{\underline{\mathbf{D}}}^S(\mathbf{u})$ is called "Cauchy strain tensor" and often denoted $\underline{\underline{\varepsilon}}$: it is a matrix field measuring the deformation of the solid body. Using the identity $2\,\mathbf{div}\,\underline{\underline{\mathbf{D}}}^S = \nabla\operatorname{div} + \boldsymbol{\Delta} = 2\nabla\operatorname{div} - \operatorname{curl}\operatorname{curl}$, equation (18) can be written in the form

$$\mathbf{div}\,\underline{\underline{\sigma}} + \omega^2\rho\mathbf{u} = \mathbf{0}, \qquad \text{where} \quad \underline{\underline{\sigma}} := 2\mu\,\underline{\underline{\mathbf{D}}}^S\mathbf{u} + \lambda\,(\operatorname{div}\mathbf{u})\underline{\underline{\mathrm{Id}}} = 2\mu\,\underline{\underline{\varepsilon}} + \lambda\operatorname{Tr}(\underline{\underline{\varepsilon}})\underline{\underline{\mathrm{Id}}}$$

is called "Cauchy stress tensor". Then the traction operator on the boundary can be written as $\mathbf{T}(\mathbf{u}) = \underline{\underline{\sigma}}\mathbf{n}$ (the matrix–vector product between the stress tensor and the unit normal to the boundary). The elastic wave equations for more general anisotropic linear materials are still written in the form $\mathbf{div}\,\underline{\underline{\sigma}} + \omega^2\rho\mathbf{u} = \mathbf{0}$ but the strain and stress tensors are related by the more general relation $\underline{\underline{\sigma}} = \mathsf{C}\underline{\underline{\varepsilon}}$, where C is the fourth-order "stiffness tensor".

Exercise 1.26: (Somigliana potential). Show that, if the smooth vector field $\mathbf{g}$ satisfies the iterated Helmholtz equation $(\Delta + k_S^2)(\Delta + k_P^2)\mathbf{g} = \mathbf{0}$, then $\mathbf{u} := (2 - \frac{\lambda}{\lambda+\mu})(\Delta + k_P^2)\mathbf{g} - \nabla\operatorname{div}\mathbf{g}$ is a solution of Navier's equation (18).

Hint: the expression of Navier's equations using the vector Laplacian as in Remark 1.25 and the vector calculus identities in Appendix A might help.
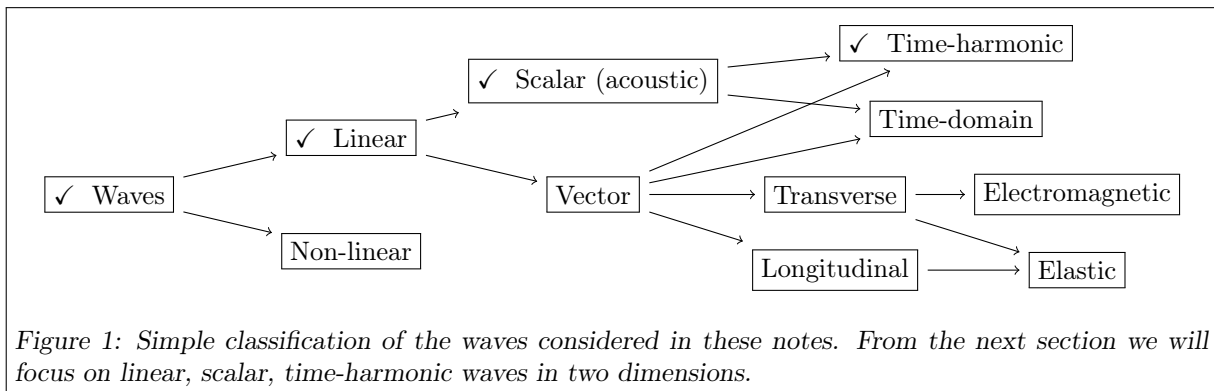

Figure 1: *Simple classification of the waves considered in these notes. From the next section we will focus on linear, scalar, time-harmonic waves in two dimensions.*

1.5 OTHER TIME-HARMONIC WAVES

We mention a few other examples of oscillatory phenomena where the Helmholtz equation plays a role.

Remark 1.27: (Membrane vibrations [CJ77, Ch. 7]). The small-amplitude vibrations of a membrane are described by the scalar wave equation (6) in two variables and, in the time-harmonic case, by the Helmholtz equation. This model is accurate under the assumptions that the rest position is flat, the displacement is small and vertical (so the vertical component of the displacement is the unknown, the horizontal components are zero), the membrane is perfectly flexible and elastic, in particular it does not resist to bending, and tension forces act only tangentially to the membrane. Typical examples are drums, loudspeakers, microphones and our own eardrums.

Remark 1.28: (Helmholtz equation for water waves). The most obvious kind of waves we encounter in nature are **water waves**, such as those we find at the sea. Their prediction is relevant to design harbours, breakwaters, oil rigs, and ships. The disturbances to the free surface of a fluid are called **gravity waves**, as gravity is the main restoring force (with also surface tension playing a role) that balances the fluid inertia and generates the waves. Usually, water waves are modelled by non-linear equations, [BK00, §8]. However, in some situations linear approximations are applicable, [BK00, §4], [Martin06, §1.6].

Let $\mathbf{v} = \mathbf{v}(\mathbf{x}, t)$ be the velocity field of a fluid, which we assume to be homogeneous, incompressible $(\operatorname{div} \mathbf{v} = 0)$, and in irrotational $(\operatorname{curl} \mathbf{v} = \mathbf{0})$, time-harmonic motion. Then, there is a velocity potential Φ such that $\mathbf{v}(\mathbf{x}, t) = \nabla \Phi(\mathbf{x}, t)$ and $\Phi(\mathbf{x}, t) = \Re\{\phi(\mathbf{x}) e^{-i\omega t}\}$, with $\Delta \phi = 0$. Let $x_3 = 0$ be the undisturbed free surface, and $x_3 = -h(x_1, x_2) < 0$ be the sea bottom topography.

Let $k = k(h(x_1, x_2))$ be the positive root of the dispersion relation $gk \tanh(kh) = \omega^2$ (with g the gravity acceleration). Assume the "mild-slope approximation" $|\nabla h| \ll kh$. Prescribing the x_3 dependence of the potential as $\phi(\mathbf{x}) \approx \frac{g}{i\omega} \frac{\cosh(k(x_3+h))}{\cosh(kh)} \psi(x_1, x_2)$, we obtain the **mild-slope, or Berkhoff, equation**[7]:

$$\operatorname{div}(w \nabla \psi) + k^2 w \psi = 0 \qquad \text{with} \qquad w = \frac{\tanh(kh)}{2k}\left(1 + \frac{2kh}{\sinh(2kh)}\right).$$

Here the divergence and the gradient are in the horizontal (x_1, x_2) variable only. This is a variable-coefficient Helmholtz equation in the unknown ψ.

If, instead of the mild-slope assumption, the horizontal wavelength is much longer than the fluid depth, we obtain an important system on non-linear hyperbolic PDEs called **shallow water equations**, [BK00, §4.7, §8.1]. These equations are used to model waves in harbours and beaches, tsunamis, floodings,... If we further assume that the wave speed is small and the wave height η is much smaller than the water depth h, we obtain the **linear shallow water equations**, which in time-harmonic regime are again a variable-coefficient Helmholtz equation: $g \operatorname{div}(h \nabla \eta) + \omega^2 \eta = 0$, [BK00, eq. (4.84)].

Typically, Neumann boundary conditions are imposed on rigid obstacles, while more complicated ones have to be imposed on floating objects, [Martin06, §1.6].

Exercise 1.29: (Helmholtz equation and Kirchhoff–Love plates). In mechanical engineering, flat, thin, elastic structures are called "plates" and often modelled by Kirchhoff–Love theory. The flat three-dimensional object is represented by a domain in $\mathbb{R}^2$. In the "pure bending" time-harmonic case, the plate displacement in the direction perpendicular to the plate satisfies the fourth-order equation $-\Delta^2 u + k^4 u = 0$, where $\Delta^2 = \Delta\Delta$ is the bi-Laplacian operator.[8]

- Show that solutions of the Helmholtz equation $\Delta u + k^2 u = 0$ and of the reaction–diffusion equation $\Delta u - k^2 u = 0$ solve also the fourth-order equation.

- Let u be a smooth solution of $-\Delta^2 u + k^4 u = 0$. Define two fields $w_\pm := \Delta u \pm k^2 u$. Show that they satisfy $\Delta w_\pm \mp k^2 w_\pm = 0$ and that $u = \frac{1}{2k^2}(w_+ - w_-)$.

  This means that all time-harmonic Kirchhoff–Love solutions can be written as sums of oscillatory and boundary-layer components, that are solution of Helmholtz and reaction–diffusion equations, respectively.

---

[7][Chamberlain, Wave scattering over uneven depth using the mild-slope equation, Wave Motion, 1993]

[8]See [Bourgeois, Hazard, On well-posedness of scattering problems in a Kirchhoff–Love infinite plate, SIAM 2020] for a description of scattering problems for the plate model analogous to the acoustic scattering problem in §4.

2 PARTICULAR SOLUTIONS OF THE HELMHOLTZ EQUATION

We now focus on the construction of some simple analytical solutions of the Helmholtz equation $\Delta u + k^2 u = 0$ in 2D and we study some of their qualitative properties. This is useful to understand some typical features of all Helmholtz solutions. Moreover, in the next sections we will use some of these functions to study some boundary value problems and to construct integral operators.

Plots and time-harmonic animations are available on the course webpage[9]; see also the links provided there to the pages of R. Hogan and D.A. Russell.

2.1 THE ONE-DIMENSIONAL CASE

We begin with the simpler case of one space dimension ($n = 1$). In this case, the Helmholtz equation reduces to the ordinary differential equation: $u'' + k^2 u = 0$. All solutions are in the form

$$u(x) = c_1 \cos(kx) + c_2 \sin(kx) \qquad \text{for some } c_1, c_2 \in \mathbb{C}.$$

Equivalently

$$u(x) = C_1 e^{ikx} + C_2 e^{-ikx} \qquad \text{for some } C_1, C_2 \in \mathbb{C}.$$

All 1D Helmholtz solutions are periodic with period $\lambda = \frac{2\pi}{k}$.

Let us fix $c = 1$, so $\omega = kc = k$. When we expand the time-dependence of the corresponding solutions (10) of the wave equation, we see that $u(x) = e^{ikx}$ corresponds to $U(x, t) = \Re\{e^{ikx - ikt}\} = \cos(k(x - t))$, which is a wave propagating to the right. On the other hand, $u(x) = \cos(kx)$ corresponds to $U(x, t) = \Re\{\cos(kx)e^{-ikt}\} = \cos(kx)\cos(kt)$, which oscillates in time but maintains the same space profile and does not propagate. See Figure 2 and the animations[9].

Figure 2: Panel 1: the real and the imaginary part of the one-dimensional propagative wave $u(x) = e^{ikx}$ over the interval $(-1, 1)$, with $k = 10$.
Panel 2: the real part of the corresponding solution of the wave equation $U(x, t) = \Re\{e^{ikx}e^{-i\omega t}\}$, plotted as function of x (horizontal axis) and t (vertical axis). Here we are taking $\omega = k$ and $c = 1$. The wave propagates towards the right endpoint of the space interval.
Panels 3 and 4: the same plots for the stationary wave $u(x) = \cos(kx) = \frac{1}{2}(e^{ikx} + e^{-ikx})$. The waves oscillates in time but does not propagate: the peaks (yellow parts) appear at the same locations in space.

2.2 PLANE WAVES

We have seen in Exercise 1.3 that the space–time field $U(\mathbf{x}, t) = F(\mathbf{x} \cdot \mathbf{d} - ct)$, propagating in the direction of $\mathbf{d}$ at speed c, is solution of the wave equation (here $\mathbf{d} \in \mathbb{R}^2$ is a unit vector and F a smooth real function). To have a Helmholtz solution, we want U to be time-harmonic, i.e. $U(\mathbf{x}, t) = \Re\{u(\mathbf{x})e^{-i\omega t}\}$. A simple way to reconcile these two expressions is to choose $F(z) = \Re\{e^{ikz}\}$ so that $U(\mathbf{x}, t) = \Re\{e^{i(k\mathbf{x} \cdot \mathbf{d} - \omega t)}\} = \cos(k\mathbf{x} \cdot \mathbf{d} - \omega t)$ (recalling that $\omega = kc$) and

$$u(\mathbf{x}) = \boxed{e^{ik\mathbf{x} \cdot \mathbf{d}}} = \cos(k\mathbf{x} \cdot \mathbf{d}) + i\sin(k\mathbf{x} \cdot \mathbf{d}).$$

This is a time-harmonic **propagative plane wave**, which propagates in the direction $\mathbf{d}$. Plane waves are the simplest solutions of the Helmholtz equation.

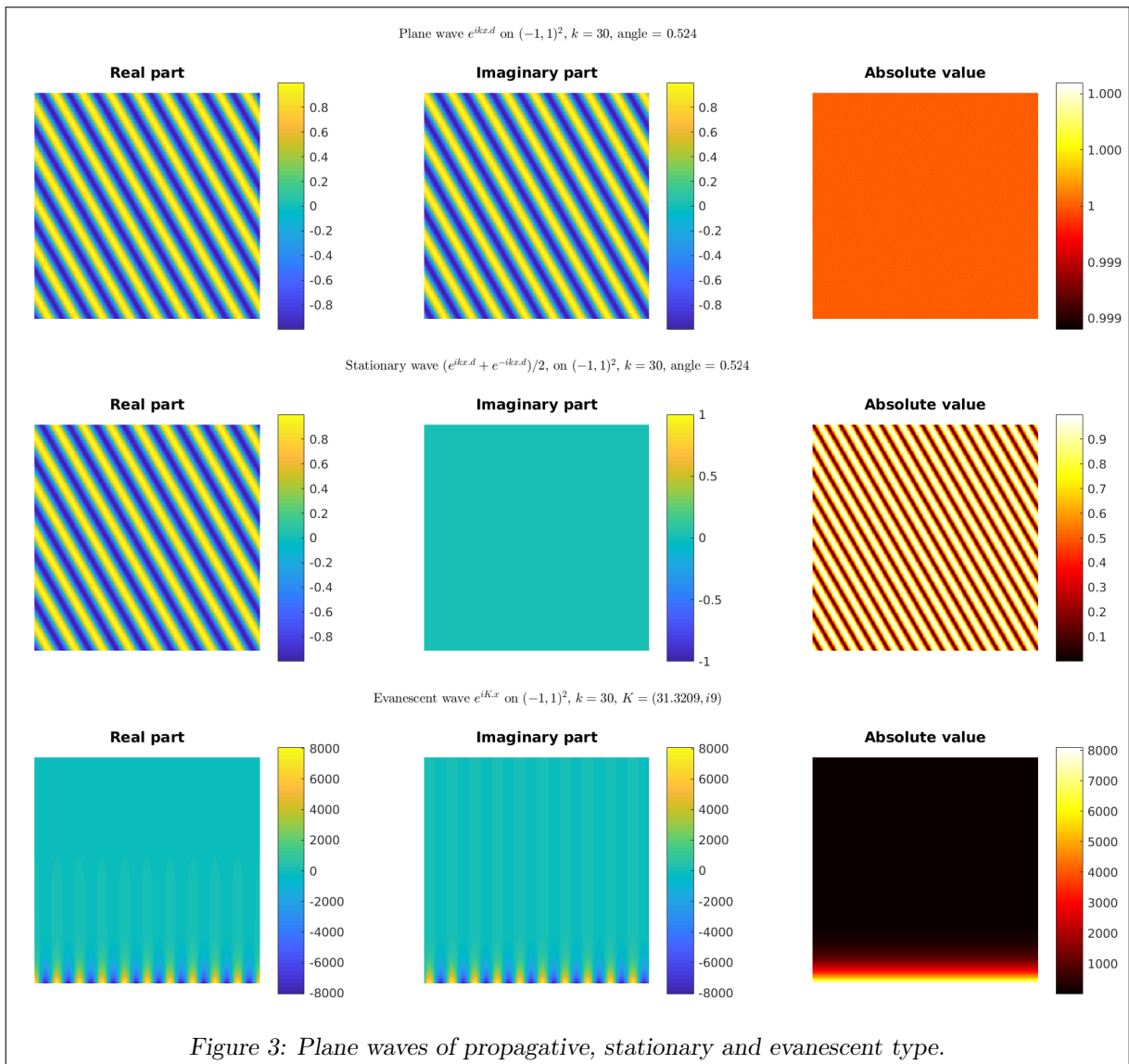[9]https://mate.unipv.it/moiola/T/MNAPDEanim/MNAPDEanim.html

Another way to obtain plane waves is to look for Helmholtz solutions that are independent of one of the Cartesian variables. If $u(x_1, x_2) = \tilde{u}(x_1)$, then $\tilde{u}$ has to satisfy $\tilde{u}'' + k^2 \tilde{u} = 0$, so $\tilde{u}(x_1) = c_1 \cos(kx_1) + c_2 \sin(kx_2)$ for some $c_1, c_2 \in \mathbb{C}$. Propagative plane waves correspond to the choice $c_1 = 1$, $c_2 = \mathrm{i}$.

Plane waves have constant **amplitude** $|u(\mathbf{x})|$ and are constant on the lines perpendicular to $\mathbf{d}$. Their complex argument $\arg(u(\mathbf{x})) = k\mathbf{x} \cdot \mathbf{d}$ in a point $\mathbf{x}$ is called **phase**. Plane waves are periodic in the direction $\mathbf{d}$ with period equal to the wavelength $\lambda = \frac{2\pi}{k}$: the wavelength is precisely the distance between two consecutive peaks of a plane wave. A translation along a vector $\mathbf{v}$ corresponds to a multiplication by a complex factor of absolute value 1, i.e. it is a phase shift: $u(\mathbf{x} + \mathbf{v}) = \mathrm{e}^{\mathrm{i}k(\mathbf{x}+\mathbf{v})\cdot\mathbf{d}} = \mathrm{e}^{\mathrm{i}k\mathbf{v}\cdot\mathbf{d}}u(\mathbf{x})$.

The sum and the difference of two plane waves with opposite directions are called **stationary**, or **standing**, plane waves:

$$\mathrm{e}^{\mathrm{i}k\mathbf{x}\cdot\mathbf{d}} + \mathrm{e}^{-\mathrm{i}k\mathbf{x}\cdot\mathbf{d}} = 2\cos(k\mathbf{x}\cdot\mathbf{d}), \qquad \mathrm{e}^{\mathrm{i}k\mathbf{x}\cdot\mathbf{d}} - \mathrm{e}^{-\mathrm{i}k\mathbf{x}\cdot\mathbf{d}} = 2\mathrm{i}\sin(k\mathbf{x}\cdot\mathbf{d}).$$

As in the one-dimensional case of §2.1, the reason why these are called stationary while $\mathrm{e}^{\mathrm{i}k\mathbf{x}\cdot\mathbf{d}}$ is called propagative is clear if one looks at the evolution in time of the corresponding time-domain wave $U(\mathbf{x}, t) = \Re\{u(\mathbf{x})\mathrm{e}^{-\mathrm{i}\omega t}\}$; see Figure 3 and the animations[9, 10].

Figure 3: *Plane waves of propagative, stationary and evanescent type.*

---

[10]In one of the animations available online you can observe a sketch of the motion of the fluid particles subject to a time-harmonic propagative plane wave: each particle oscillates back and forth harmonically around a fixed position, and never moves far, even if the wave propagates over the whole space. This happens for all solutions of the Helmholtz and the wave equations: pressure, energy and momentum are transported while matter oscillates but does not move away. The basic principle of sound as propagation of pressure variations was already understood by Aristotle, see [Heller13, p. 3].

Exercise 2.1: (Conjugate of a plane wave). Show that the complex-conjugate of a plane wave is a plane wave propagating in the opposite direction, in accordance with Exercise 1.11.

Exercise 2.2: (Periodicity of sum of plane wave). Show that a linear combination of two propagative plane waves with directions the unit vectors $\mathbf{d}$ and $\mathbf{p}$, with $\mathbf{d} \neq \pm\mathbf{p}$, is periodic both in the direction of the bisectrix $\mathbf{b} = \mathbf{d} + \mathbf{p}$ and in the direction of its orthogonal $\mathbf{b}^{\perp} = \mathbf{d} - \mathbf{p}$. Show that the period of the linear combination in these two directions is $\frac{\lambda}{\cos(\alpha/2)}$ and $\frac{\lambda}{\sin(\alpha/2)}$, respectively, where α is the angle between $\mathbf{d}$ and $\mathbf{p}$.

Exercise 2.3: (Vector plane waves). Show that the vector plane wave $\mathbf{E}(\mathbf{x}) = \mathbf{A}e^{ik\mathbf{x}\cdot\mathbf{d}}$ is solution of Maxwell's equations $\operatorname{curl}\operatorname{curl}\mathbf{E} - k^2\mathbf{E} = \mathbf{0}$ in $\mathbb{R}^3$ if and only if $\mathbf{d}\cdot\mathbf{d} = 1$ and $\mathbf{d}\cdot\mathbf{A} = 0$. This means that the amplitude vector is orthogonal to the propagation direction, i.e. electromagnetic plane waves are transverse waves. The formula $\mathbf{u}\times(\mathbf{v}\times\mathbf{w}) = \mathbf{v}(\mathbf{u}\cdot\mathbf{w}) - \mathbf{w}(\mathbf{u}\cdot\mathbf{v})$ might help. Show that the corresponding magnetic field $\mathbf{H}$ is perpendicular to both $\mathbf{E}$ and $\mathbf{A}$ and that $\sqrt{\mu}|\mathbf{H}| = \sqrt{\epsilon}|\mathbf{E}|$.

Show that Navier's equations (18) support both transverse plane waves $\mathbf{A}e^{ik_S\mathbf{x}\cdot\mathbf{d}}$, with $\mathbf{d}\cdot\mathbf{A} = 0$, and longitudinal ones $\mathbf{d}e^{ik_P\mathbf{x}\cdot\mathbf{d}}$. Longitudinal elastic waves are faster and have longer wavelengths than transverse ones.

Here $\mathbf{A} \in \mathbb{C}^3$. If $\Re\mathbf{A}$ and $\Im\mathbf{A}$ are parallel to one another, then the plane wave $\mathbf{u}(\mathbf{x}) = \mathbf{A}e^{ik\mathbf{x}\cdot\mathbf{d}}$ is said to have linear polarisation. If $\Re\mathbf{A}$ and $\Im\mathbf{A}$ are perpendicular to one another and $|\Re\mathbf{A}| = |\Im\mathbf{A}|$ (so that $\Im\mathbf{A} = \pm\Re\mathbf{A}\times\mathbf{d}$), then the polarisation is circular. In all other cases the polarisation is called elliptical. To understand the meaning of these names, draw the graph of $t \mapsto \mathbf{U}(\mathbf{x},t) = \Re\{\mathbf{u}(\mathbf{x})e^{-i\omega t}\}$ in the plane perpendicular to $\mathbf{d}$, for a given $\mathbf{x}$. See also [BK00, §6.5].

Figure 4: *The deformation of an elastic medium perturbed by plane waves. Left: the unperturbed medium. Centre: a longitudinal plane wave $\mathbf{d}e^{ik\mathbf{x}\cdot\mathbf{d}}$. Right: a transverse plane wave $\mathbf{A}e^{ik\mathbf{x}\cdot\mathbf{d}}$ with $\mathbf{A}\cdot\mathbf{d} = 0$. In this example the wave propagates horizontally ($\mathbf{d} = (1,0,0)$) and $\mathbf{A} = (0,0,1)$. See §1.4 and Exercise 2.3. Acoustic waves are longitudinal waves, since fluids cannot support transverse waves.*
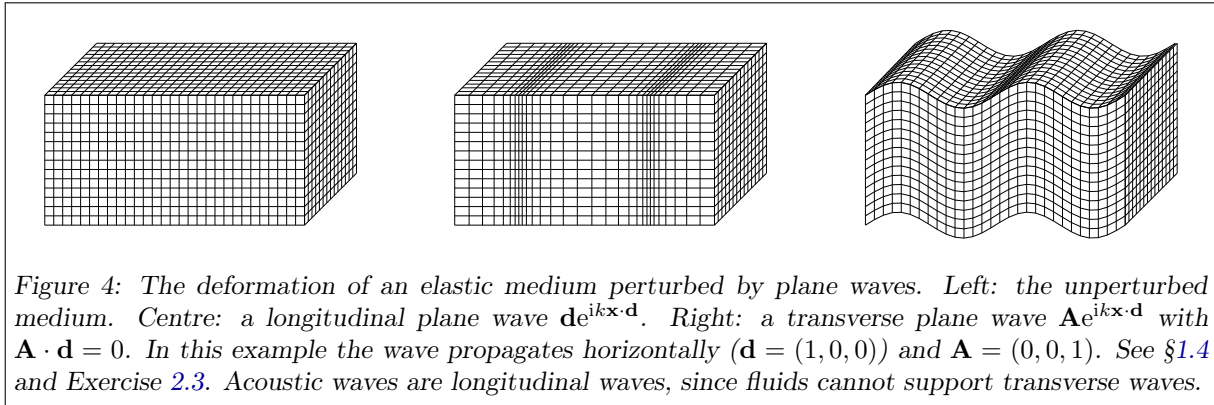
2.2.1 EVANESCENT PLANE WAVES

Propagative and stationary waves are not the only solutions of the Helmholtz equation that are "separable" in Cartesian coordinates (i.e. that can be written as $u(\mathbf{x}) = u_1(x_1)u_2(x_2)$). If we look for functions in the form $u(\mathbf{x}) = e^{i\mathbf{k}\cdot\mathbf{x}} = e^{i(k_1x_1+k_2x_2)}$ satisfying $\Delta u + k^2 u = 0$, we see that we need a "wavevector" $\mathbf{k} \in \mathbb{C}^2$ with $\mathbf{k}\cdot\mathbf{k} = k_1^2 + k_2^2 = k^2$. If both k_1 and k_2 are real then we obtain again the plane waves. If at least one of the two is not real then we have a new kind of waves, called evanescent (plane) waves. Expanding $\mathbf{k} = \mathbf{k}_R + i\mathbf{k}_I$ with $\mathbf{k}_R, \mathbf{k}_I \in \mathbb{R}^2$, we have $\boxed{u(\mathbf{x}) = e^{i\mathbf{k}\cdot\mathbf{x}} = e^{i\mathbf{k}_R\cdot\mathbf{x}}e^{-\mathbf{k}_I\cdot\mathbf{x}}}$: this field oscillates in the direction $\mathbf{k}_R$ with wavenumber $|\mathbf{k}_R| \geq k$ and decays exponentially in the orthogonal direction $\mathbf{k}_I$ ($|u(\mathbf{x})| = e^{-\mathbf{k}_I\cdot\mathbf{x}}$). The orthogonality of $\mathbf{k}_R$ and $\mathbf{k}_I$ is a consequence of $\mathbf{k}\cdot\mathbf{k} \in \mathbb{R}$. See Figure 3 for a representation.

Evanescent (non-plane) waves typically appear at the interface between different materials or near boundaries; important examples in elasticity are Rayleigh waves, which include the surface waves generated by earthquakes.

Exercise 2.4: (Evanescent plane wave computations). Verify the statements made in the paragraph.

Exercise 2.5: (Complex parametrisation of plane waves). Show that all 2D plane waves, either propagative or evanescent, can be written in the form $e^{ik(x_1\cos\theta+x_2\sin\theta)} = e^{\frac{k}{2}(i(\nu+\frac{1}{\nu})x_1+(\nu-\frac{1}{\nu})x_2)}$, parametrised by $0 \neq \nu \in \mathbb{C}$ or $\theta \in \mathbb{C}$, with $\nu = e^{i\theta}$.

2.3 CIRCULAR WAVES AND BESSEL FUNCTIONS

We have seen Helmholtz solutions that are separable in Cartesian coordinates, we now look for those that are separable in the polar coordinates (r, θ), where $(x_1, x_2) = (r\cos\theta, r\sin\theta)$. The 2D Laplacian in polar

coordinates reads

$$\Delta u = \frac{1}{r}\frac{\partial}{\partial r}\left(r\frac{\partial u}{\partial r}\right) + \frac{1}{r^2}\frac{\partial^2 u}{\partial\theta^2} = \frac{\partial^2 u}{\partial r^2} + \frac{1}{r}\frac{\partial u}{\partial r} + \frac{1}{r^2}\frac{\partial^2 u}{\partial\theta^2}. \tag{21}$$

If we have a separable Helmholtz solution $u(\mathbf{x}) = f(r)g(\theta)$, the functions f, g have to satisfy

$$f''(r)g(\theta) + \frac{1}{r}f'(r)g(\theta) + \frac{1}{r^2}f(r)g''(\theta) + k^2 f(r)g(\theta) = \Delta u + k^2 u = 0.$$

The angular component g has to be periodic of period 2π, so we take the circular harmonic $g(\theta) = e^{i\ell\theta}$, for $\ell \in \mathbb{Z}$. Then $g''(\theta) = -\ell^2 g(\theta)$, so we can cancel g from the expression above, multiply by r^2, and obtain that f satisfies

$$r^2 f''(r) + r f'(r) + (r^2 k^2 - \ell^2)f(r) = 0. \tag{22}$$

For $k = 1$, this is called **Bessel differential equation**: it is a linear, second-order ODE with variable coefficients, it depends on the index ℓ and degenerates at $r = 0$. Two linearly independent real-valued solutions are the **Bessel functions of the first kind** and order ℓ, denoted $\boxed{J_\ell(r)}$, and the **Bessel function of the second kind** (or Neumann functions) and order ℓ, denoted $\boxed{Y_\ell(r)}$. Explicit expressions (e.g. as power series or integral representations), plenty of useful formulas and graphs can be found online on the "NIST Digital Library of Mathematical Functions" [DLMF]. See also Appendix B.
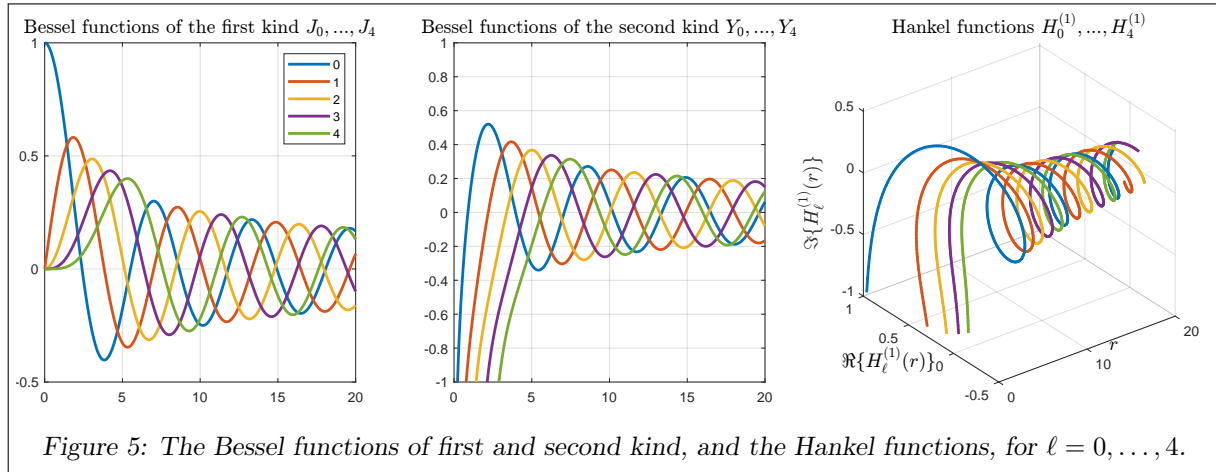
Figure 5: The Bessel functions of first and second kind, and the Hankel functions, for $\ell = 0, \ldots, 4$.

The Bessel functions of the first and second kind for $\ell = 0, \ldots, 4$ are plotted in Figure 5. We see that both families of functions oscillate around 0 and decay slowly for $r \to \infty$. The distance between two successive zeros of either J_ℓ or Y_ℓ is slightly shorter than π for $\ell = 0$ and slightly longer than π for $\ell \neq 0$. The main difference is that the $J_\ell(r)$s are smooth over $\mathbb{R}$, while the $Y_\ell(r)$s have a singularity at $r = 0$; the higher ℓ the stronger the singularity. Useful formulas are $J_{-\ell}(r) = (-1)^\ell J_\ell(r)$ and $Y_{-\ell}(r) = (-1)^\ell Y_\ell(r)$.

The **Hankel functions** (sometimes called Bessel functions of the third kind) are the complex-valued linear combinations

$$\boxed{H_\ell^{(1)}(r)} := J_\ell(r) + iY_\ell(r), \qquad \boxed{H_\ell^{(2)}(r)} := J_\ell(r) - iY_\ell(r) = \overline{H_\ell^{(1)}(r)}. \tag{23}$$

The right panel of Figure 5 shows the first few Hankel functions: the argument r is one of the axis, the real and the imaginary parts of $H_\ell^{(1)}(r)$ are on the other two axes. An important property of the Hankel functions is that the magnitude $r \mapsto |H_\ell^{(1)}(r)|$ is a monotonically decreasing function ($|H_\ell^{(1)}(r)| \approx \sqrt{2/(\pi r)}$ for large r). For increasing r the complex number $H_\ell^{(1)}(r)$ spirals clockwise towards the origin.

Bessel and Hankel functions can be used in Matlab with the commands `besselj`, `bessely` and `besselh`.

Exercise 2.6: (Bessel equation). Verify that if f_1 is solution of (22) for $k = 1$, then, for any $k > 0$, $f_k(r) := f_1(kr)$ solves (22).

Exercise 2.7: (Bessel function asymptotics). Compare numerically the plots of the Bessel functions against the asymptotics for small and large (positive) arguments (from [DLMF, §10.7]):

$$J_\ell(z) \sim \frac{z^\ell}{\ell!\, 2^\ell} \quad \ell \in \mathbb{N}_0, \qquad Y_0(z) \sim \frac{2}{\pi}\log z, \qquad Y_\ell(z) \sim -\frac{(\ell-1)!\, 2^\ell}{\pi z^\ell} \quad \ell \in \mathbb{N}, \qquad z \to 0,$$

$$J_\ell(z) \sim \sqrt{\frac{2}{\pi z}}\cos\left(z - \frac{\ell\pi}{2} - \frac{\pi}{4}\right), \qquad Y_\ell(z) \sim \sqrt{\frac{2}{\pi z}}\sin\left(z - \frac{\ell\pi}{2} - \frac{\pi}{4}\right) \quad \ell \in \mathbb{N}_0, \qquad z \to \infty. \tag{24}$$

Figure 6: *The Fourier–Bessel function* $J_3(kr)\mathrm{e}^{\mathrm{i}3\theta}$, *the Fourier–Hankel function* $H_5^{(1)}(kr)\mathrm{e}^{\mathrm{i}5\theta}$, *and the sum of two Fourier–Hankel functions with opposite indices* $H_5^{(1)}(kr)\mathrm{e}^{\mathrm{i}5\theta} + H_{-5}^{(1)}(kr)\mathrm{e}^{-\mathrm{i}5\theta}$. *Since the Hankel functions are unbounded at the origin, the field has been truncated in the region where its absolute value is larger than 2.*
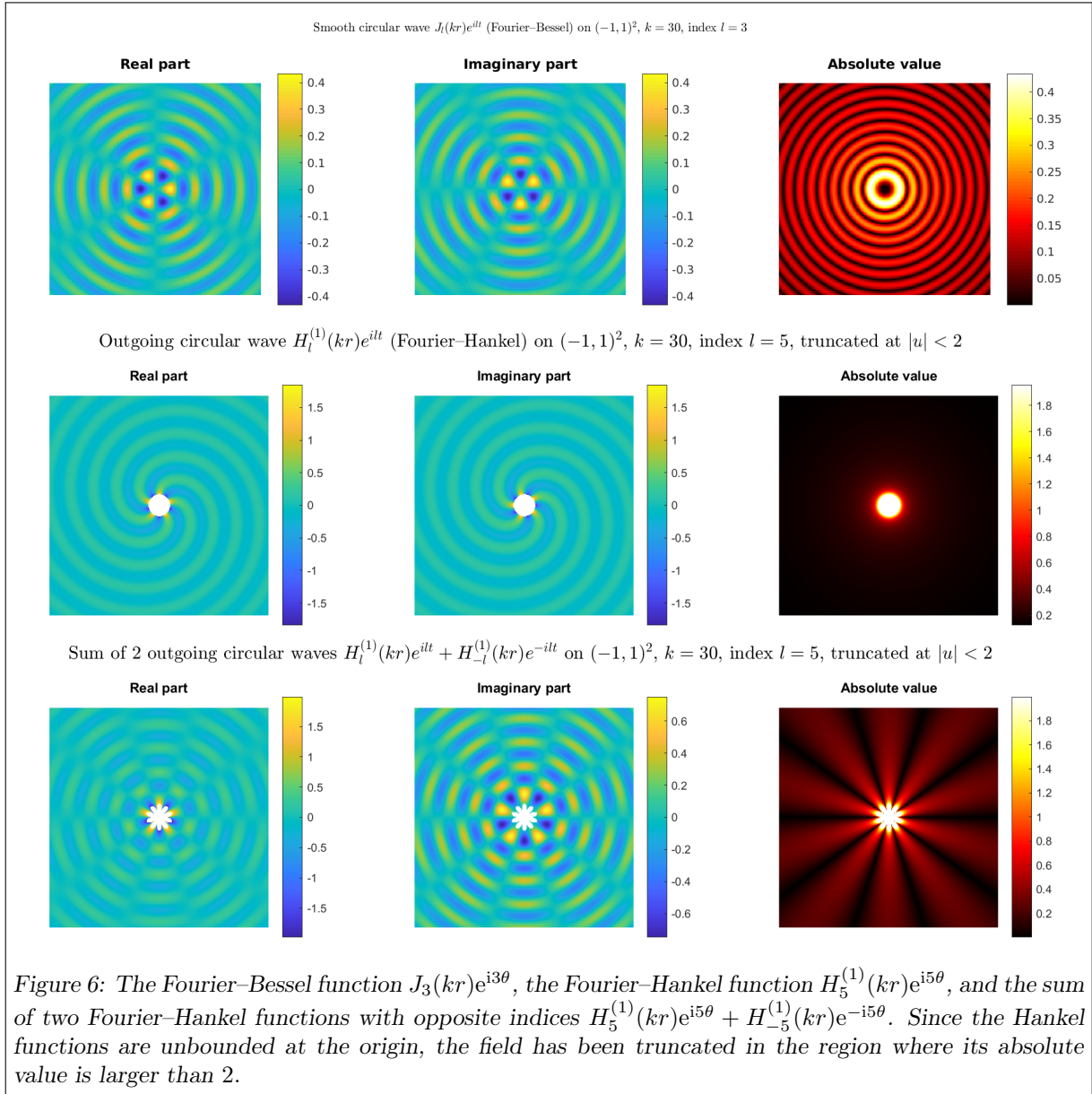
From what we have said, we deduce that for any $\ell \in \mathbb{Z}$ the two fields

$$\boxed{J_\ell(kr)\mathrm{e}^{\mathrm{i}\ell\theta}, \qquad Y_\ell(kr)\mathrm{e}^{\mathrm{i}\ell\theta}}$$

and their linear combinations are the solutions of the Helmholtz equations that are separable in polar coordinates. They are called **circular waves** or **Fourier–Bessel** functions. Of all the elements of the 2-dimensional space $\mathrm{span}\{J_\ell(kr)\mathrm{e}^{\mathrm{i}\ell\theta}, Y_\ell(kr)\mathrm{e}^{\mathrm{i}\ell\theta}\}$, only $J_\ell(kr)\mathrm{e}^{\mathrm{i}\ell\theta}$ is defined in the whole of $\mathbb{R}^2$, while all the others are defined in the punctured plane $\mathbb{R}^2 \setminus \{0\}$. They are all of class C^∞ in their domain of definition. From the angular dependence, we see that all these function are invariant under rotations of an angle multiple of $2\pi/|\ell|$; a rotation by an angle α corresponds to a multiplication by a complex factor $\mathrm{e}^{\mathrm{i}\ell\alpha}$.

Special circular waves are the **Fourier–Hankel** functions, namely

$$\boxed{H_\ell^{(1)}(kr)\mathrm{e}^{\mathrm{i}\ell\theta}} = J_\ell(kr)\mathrm{e}^{\mathrm{i}\ell\theta} + \mathrm{i}Y_\ell(kr)\mathrm{e}^{\mathrm{i}\ell\theta}, \qquad \boxed{H_\ell^{(2)}(kr)\mathrm{e}^{\mathrm{i}\ell\theta}} = J_\ell(kr)\mathrm{e}^{\mathrm{i}\ell\theta} - \mathrm{i}Y_\ell(kr)\mathrm{e}^{\mathrm{i}\ell\theta}, \qquad \ell \in \mathbb{Z}.$$

We will see soon why the the Fourier–Hankel functions $H_\ell^{(1)}(kr)\mathrm{e}^{\mathrm{i}\ell\theta}$ are important for problems posed in unbounded domains. The Fourier–Bessel $J_\ell(kr)\mathrm{e}^{\mathrm{i}\ell\theta}$ and the Fourier–Hankel $H_\ell^{(1)}(kr)\mathrm{e}^{\mathrm{i}\ell\theta}$ functions are called "regular cylindrical wavefunctions" and "outgoing cylindrical wavefunctions" in [Martin06, Def. 2.13].

Plotting the time evolution (10) of these fields, one notes that the Fourier–Bessel functions $J_\ell(kr)\mathrm{e}^{\mathrm{i}\ell\theta}$ and $Y_\ell(kr)\mathrm{e}^{\mathrm{i}\ell\theta}$ rotate around the origin (anticlockwise if $\ell > 0$, clockwise if $\ell < 0$) and do not propagate in the radial direction. The Fourier–Hankel functions $H_\ell^{(1)}(kr)\mathrm{e}^{\mathrm{i}\ell\theta}$ rotate and move towards infinity, while

the $H_\ell^{(2)}(kr)e^{i\ell\theta}$ towards the origin. This can be seen in the animations on the course webpage[9]. Figure 6 shows some circular waves.

Exercise 2.8: (Singular circular waves are not in H^1). Show that the Fourier–Bessel functions $Y_\ell(kr)e^{i\ell\theta}$ and all the Fourier–Hankel functions do not belong to $H^1(\Omega)$, for any domain Ω containing the origin $\mathbf{0}$, because of the singularity at that point.

Use the small-argument asymptotics (24), the derivative formula $Y_\ell' = \frac{1}{2}(Y_{\ell-1} - Y_{\ell+1})$ [DLMF, eq. 10.6.1], and recall how to compute gradients and integrals in polar coordinates.

Remark 2.9: (Plane waves as Fourier–Hankel functions "at infinity"). A Fourier–Hankel function centred at a point $\mathbf{x}_0$ with $|\mathbf{x}_0| \gg 1$, restricted to a region close to the origin, looks like a plane wave. In the limit $|\mathbf{x}_0| \to \infty$, scaling the Fourier–Hankel function appropriately, we see that it converges to a plane wave with propagation direction $\mathbf{d} = -\frac{\mathbf{x}_0}{|\mathbf{x}_0|}$. So we can think at a plane wave as a Fourier–Hankel function "centred at infinity". See Figure 7.

We use the large-argument asymptotics (24) from [DLMF, eq. 10.7.8], which gives $H_0^{(1)}(z) \sim \sqrt{\frac{2}{\pi z}}e^{i(z-\frac{\pi}{4})}$ for $0 < z \to \infty$. So $cH_0^{(1)}(k|\mathbf{x} - \mathbf{x}_0|) \sim e^{ik|\mathbf{x}-\mathbf{x}_0|}$ for, say, $|\mathbf{x}| < 1 \ll \mathbf{x}_0$ and a scaling factor $c = e^{i\frac{\pi}{4}}\sqrt{\frac{\pi}{2}k|\mathbf{x}_0|}$, which takes into account the Hankel function's radial decay. Take for simplicity $\mathbf{x}_0 = R\widehat{\mathbf{x}}_0 = (R, 0)$ with $R \gg 1$ and $\widehat{\mathbf{x}}_0 = (1, 0)$, then

$$cH_0^{(1)}(k|\mathbf{x} - \mathbf{x}_0|) \sim e^{ik|\mathbf{x}-\mathbf{x}_0|} = e^{ik\sqrt{(x_1-R)^2+x_2^2}} = e^{ikR\sqrt{1-\frac{2}{R}x_1+\frac{|\mathbf{x}|^2}{R^2}}} = e^{ikR(1-\frac{1}{R}x_1+\mathcal{O}(R^{-2}))} \sim e^{ikR}e^{-ik\mathbf{x}\cdot\widehat{\mathbf{x}}_0}.$$

Figure 7: *The real part of the Hankel functions $H_0^{(1)}(k|\mathbf{x} - \mathbf{x}_0|)$ on the unit disc B_1 for $k = 20$ and increasing values of $|\mathbf{x}_0|$. Last plot: the plane wave with direction $\mathbf{d} = (0, -1)$. See Remark 2.9.*
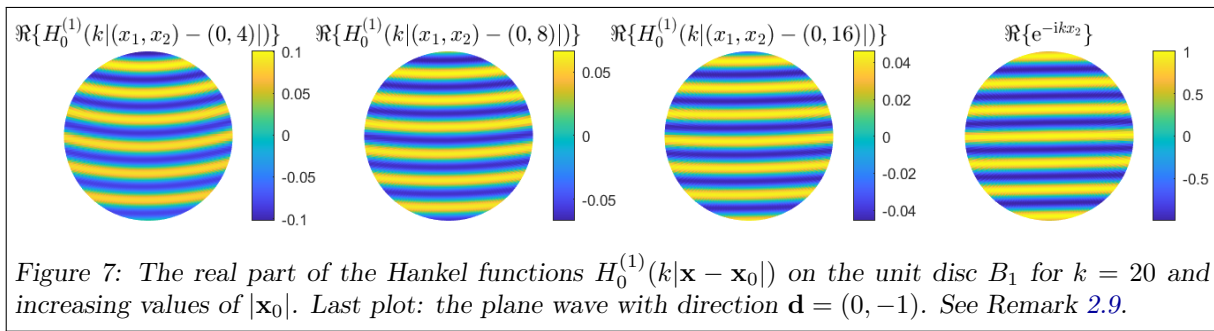
Remark 2.10: (Special Helmholtz solutions in 3D). Plane waves in $\mathbb{R}^3$ are defined exactly as in 2D.

The 3D analogous of circular waves are called **spherical waves**. In their expression, Bessel and Hankel functions are substituted by the similar **spherical Bessel functions** and **spherical Hankel functions**, denoted $j_\ell, y_\ell, h_\ell^{(1)}, h_\ell^{(2)}$. The angular component $e^{i\ell\theta}$ is substituted by the **spherical harmonics** Y_ℓ^m, which are smooth functions defined on the unit sphere and indexed by two indices ℓ and m. All these functions are described in details in e.g. [Nédélec01, §2.4, 2.6], [CK2, §2.3, 2.4] and [DLMF, §10.47–60, §14.30].

In 3D, there are also **cylindrical waves** in the form $J_\ell(k_1\rho)e^{i\ell\theta}e^{ik_2z}$, where (ρ, θ, z) is a system of cylindrical coordinates and $k_1^2 + k_2^2 = k^2$ (J_ℓ can be replaced by Y_ℓ, $H_\ell^{(1)}$ or $H_\ell^{(2)}$). More in general, for any solution w of the Helmholtz equation with wavenumber k_1 in $\mathbb{R}^2$, $w(x_1, x_2)e^{i\sqrt{k^2-k_1^2}x_3}$ is a Helmholtz solution in $\mathbb{R}^3$.

2.4 OTHER REMARKS ON THE HELMHOLTZ EQUATION

Exercise 2.11: (Jacobi–Anger formula). From the expansion $e^{\frac{1}{2}z(t+t^{-1})} = \sum_{\ell\in\mathbb{Z}} t^\ell J_\ell(z)$, valid for $z \in \mathbb{C}$, $0 \neq t \in \mathbb{C}$ (see [DLMF, eq. 10.12.1]), derive the following forms of the "Jacobi–Anger formula":

$$e^{iz\cos\alpha} = \sum_{\ell\in\mathbb{Z}} i^\ell J_\ell(z)e^{i\ell\alpha} \qquad z, \alpha \in \mathbb{C},$$

$$e^{ik\mathbf{x}\cdot\mathbf{d}} = \sum_{\ell\in\mathbb{Z}} i^\ell e^{-i\ell\varphi} J_\ell(kr)e^{i\ell\theta} \qquad \mathbf{x} = (r\cos\theta, r\sin\theta) \in \mathbb{R}^2, \quad \mathbf{d} = (\cos\varphi, \sin\varphi) \in \mathbb{R}^2, \quad |\mathbf{d}| = 1. \tag{25}$$

This means that the plane wave with propagation direction $\mathbf{d}$ is a linear combination of smooth circular waves.[11]

---

[11]See the animation `https://www.acs.psu.edu/drussell/Demos/PartialWaveExpansion/PlaneWaveExpansion.html`

Remark 2.12: (Herglotz functions). For $g \in L^2(0, 2\pi)$, the field

$$u(\mathbf{x}) = \int_0^{2\pi} g(\varphi) e^{ik(x_1 \cos \varphi + x_2 \sin \varphi)} \, d\varphi \in C^\infty(\mathbb{R}^2)$$

is called **Herglotz function** with kernel g. It can be thought as a continuous linear combination of plane waves with different directions $(\cos \varphi, \sin \varphi)$ weighted by $g(\varphi)$. Some interesting cases are the following.

- When g approximates a Dirac δ function centred at $\varphi_\star$ then u approximates the plane wave with direction $\mathbf{d} = (\cos \varphi_\star, \sin \varphi_\star)$.

- When g is constant in a small interval of $(0, 2\pi)$ and 0 otherwise, then u approximates a plane wave in a strip of the plane and decays away from it. In some applications this is more realistic than a plane wave, which has an infinite propagating front. You can see the plot of such a Herglotz function in Figure 8.

- When g is a circular harmonic $g(\varphi) = e^{i\ell\varphi}$ we obtain a Fourier–Bessel function $u(\mathbf{x}) = (2\pi i^\ell) J_\ell(kr) e^{i\ell\theta}$.

  (Prove this fact using the Jacobi–Anger formula (25) and the $L^2(0, 2\pi)$-orthogonality of circular harmonics.)

  This is a sort of vice versa of (25): a smooth circular wave is a (continuous) superposition of plane waves.

If u is a Herglotz function with kernel g, its translate $\widetilde{u}(\mathbf{x}) = u(\mathbf{x} + \mathbf{c})$ is also a Herglotz function with kernel $\widetilde{g}(\varphi) = e^{ik(c_1 \cos \varphi + c_2 \sin \varphi)} g(\varphi)$.

Plot with Matlab some Herglotz functions with different kernels.

Herglotz function on $(-1, 1)^2$, $k = 30$, constant kernel supported on $(0, 0.524)$

Real part   **Imaginary part**   **Absolute value**
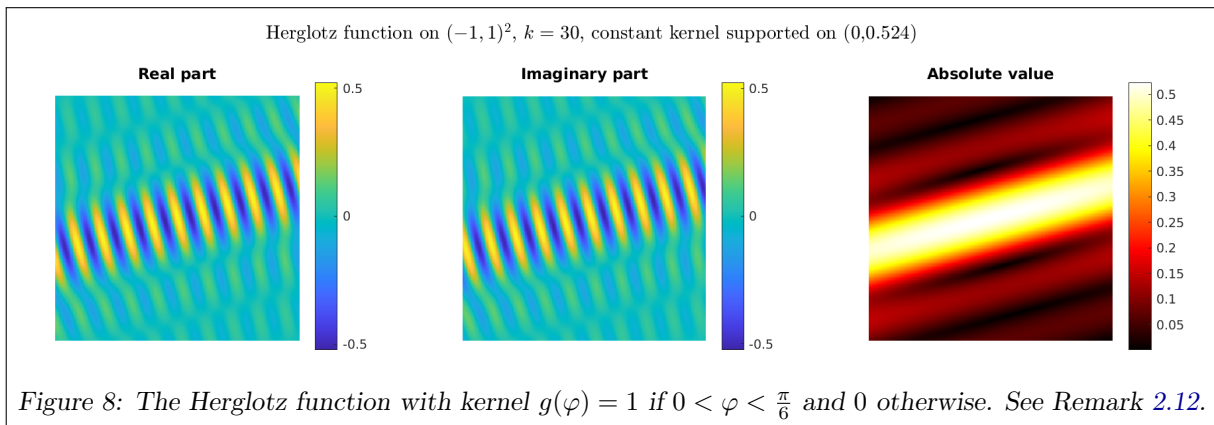
Figure 8: The Herglotz function with kernel $g(\varphi) = 1$ if $0 < \varphi < \frac{\pi}{6}$ and 0 otherwise. See Remark 2.12.

Exercise 2.13: (PDEs for phase and amplitude). Let c, ω be positive constants. Assume that the real-valued phase function ϕ satisfies the non-linear **eikonal equation** $|\nabla \phi| = c^{-1}$ and that the complex-valued amplitude A satisfies the complex, ϕ-dependent, **diffusion–advection–reaction** equation $\Delta A + i\omega(2\nabla\phi \cdot \nabla A + A\Delta\phi) = 0$. Differently from Exercise 1.9 here we allow A to take complex values.

This can be interpreted as saying that ϕ varies at constant given rate, in a direction that is not known a priori, and that A is transported in the direction of variation of ϕ and it spreads. For large frequencies $\omega \gg 1$, we can approximate A with the solution $\widetilde{A}$ of the (first-order) **advection–reaction** equation $2\nabla\phi \cdot \nabla\widetilde{A} + \widetilde{A}\Delta\phi = 0$, which is a singular perturbation of the previous one; the absence of the diffusion term prevents the "spreading" of $\widetilde{A}$.

- Prove that $u(\mathbf{x}) = A(\mathbf{x}) e^{i\omega\phi(\mathbf{x})}$ solves the Helmholtz equation (with $k = \frac{\omega}{c}$).

- Show that some affine ϕ and any constant A satisfy these equations and lead to plane waves.

- Show that $\phi(\mathbf{x}) = |\mathbf{x}|$ and $A(\mathbf{x}) = H_0^{(1)}(k|\mathbf{x}|) e^{-ik|\mathbf{x}|}$ satisfy the eikonal equation and the diffusion–advection–reaction equation in $\mathbb{R}^2 \setminus \{\mathbf{0}\}$, respectively (with $c = 1$ and $k = \omega$). (Use the Bessel differential equation (22).) Verify numerically that A does not oscillate.

Often one chooses a given curve Γ as a "wavefront" and imposes the boundary condition $\phi = 0$ for the phase on Γ. Solving first the eikonal equation and then the advection–reaction PDEs corresponds to "advancing" the wavefront according to Huygens principle, and is independent of ω: whatever method is used, the cost of this procedure is frequency-independent, thus convenient for high-frequency problems. As in the examples above, A and ϕ are non-oscillatory. The solutions of the eikonal equation have to be understood in a special weak sense (called "viscosity solution"). Not all Helmholtz solutions can be written in this form; often u is a sum of waves $u = \sum_j A_j e^{i\omega\phi_j}$, each of them with well-defined phase and amplitude. [12]

---

[12]More details and numerical methods to approximate ϕ (such as ray tracing, fast-marching, and a pseudo-time stepping scheme) are described in [Runborg12, §4]. For a wider survey of formulations and numerical methods related to the eikonal equation, see [Runborg, Mathematical models and numerical methods for high frequency waves, CICP 2007].

Exercise 2.14: (Helmholtz and Schrödinger equations). Let u be a Helmholtz solution defined on a domain in the xy-plane. Fix a number $k_0 > 0$.

- Assume that $u(x,y) = \mathrm{e}^{\mathrm{i}k_0 y}\psi(x,y)$, where the "envelope" ψ is a field that varies slowly in the variable y, more precisely that $|\frac{\partial^2 \psi}{\partial y^2}| \ll |k\frac{\partial \psi}{\partial y}|$. Show that ψ approximately satisfies the Schrödinger equation

$$2\mathrm{i}k_0 \frac{\partial \psi}{\partial y} + \frac{\partial^2 \psi}{\partial x^2} + (k^2 - k_0^2)\psi = 0.$$

- Now assume that u can be written in polar coordinates as $u(r,\theta) = H_0^{(1)}(k_0 r)\Psi(r,\theta)$ where Ψ varies slowly in the radial variable: $|\frac{\partial^2 \Psi}{\partial r^2}| \ll |k\frac{\partial \Psi}{\partial r}|$. Using the approximation (24) for $k_0 r \gg 1$, show that Ψ approximately satisfies the Schrödinger equation with (r,θ) in place of (x,y).

This equation is used to model waves propagating in directions close to a leading one (either the y direction or the radial one). This regime is called "paraxial approximation". We factored out the leading term (either a plane or a circular wave), and showed that the if the remainder behaves smoothly in the dominant direction, then we can approximate it with a PDE that is first-order in this variable (y or r).

This PDE is also called "parabolic wave equation" and has the same mathematical form of the linear Schrödinger equation used in quantum mechanics, where the variable y is the time variable.

A completely different relation between Helmholtz and Schrödinger equations is explained in [Runborg12, §1.2]: the Helmholtz equation can be used to model stationary states of particles in quantum mechanics. This is the motivation for a considerable part of the research done on the Helmholtz equation.

Exercise 2.15: (The Helmholtz Poynting vector). The Poynting vector $\mathbf{S} := \Re\{\mathbf{E} \times \overline{\mathbf{H}}\}$ (often defined with a multiplicative constant) denotes the direction in which the energy of a time-harmonic electromagnetic field $(\mathbf{E}, \mathbf{H})$ flows. Note the conjugation on $\mathbf{H}$.

- Compute the Poynting vector of the plane wave in Exercise 2.3 (you first need to compute $\mathbf{H}$).
- Show that the Poynting vector of a TE and a TM mode ((16) with $\widetilde{E}_3 = 0$ and $\widetilde{H}_3 = 0$, respectively) are

$$\mathbf{S}_{\mathrm{TE}} = \Re\Big\{ \frac{\mathrm{i}\omega\mu}{\eta^2 - \omega^2\epsilon\mu}\overline{\widetilde{H}_3}\nabla\widetilde{H}_3 + \frac{\eta}{\omega\mu}(|\widetilde{E}_1|^2 - |\widetilde{E}_2|^2)\hat{\mathbf{e}}_3 \Big\},$$

$$\mathbf{S}_{\mathrm{TM}} = \Re\Big\{ \frac{\mathrm{i}\omega\epsilon}{\omega^2\epsilon\mu - \eta^2}\widetilde{E}_3\nabla\overline{\widetilde{E}_3} + \frac{\omega\epsilon\eta}{(\eta^2 - \omega\epsilon\mu)^2}|\nabla\widetilde{E}_3|^2\hat{\mathbf{e}}_3 \Big\}.$$

Show that if $\eta = 0$ then $\mathbf{S}_{\mathrm{TE}} = \Im\{\frac{1}{\omega\epsilon}\overline{\widetilde{H}_3}\nabla\widetilde{H}_3\}$ and $\mathbf{S}_{\mathrm{TM}} = \Im\{\frac{1}{\omega\mu}\overline{\widetilde{E}_3}\nabla\widetilde{E}_3\}$ lie in the $x_1 x_2$-plane.

Recalling that $\widetilde{H}_3$ and $\widetilde{E}_3$ are Helmholtz solutions in two dimensions, this suggests to define the Poynting vector for a 2D Helmholtz solution u as

$$\mathbf{S} = \mathbf{S}(u) := \Im\Big\{\frac{1}{k}\overline{u}\nabla u\Big\} = \Im\Big\{-\frac{1}{k}u\nabla\overline{u}\Big\} = \Re\Big\{\frac{1}{\mathrm{i}k}\overline{u}\nabla u\Big\}. \tag{26}$$

Verify the following facts.

- The Poynting vector is reversed by conjugation: $\mathbf{S}(\overline{u}) = -\mathbf{S}(u)$ (recall Exercise 1.11).
- If u is Helmholtz solution, its Poynting vector is solenoidal: $\operatorname{div}\mathbf{S} = 0$.
- If u is a complex multiple of a real field, i.e. a standing wave, then $\mathbf{S} = \mathbf{0}$.
- The Poynting vector of a propagating or evanescent plane wave identifies the propagation direction: $\mathbf{S}(\mathrm{e}^{\mathrm{i}k\mathbf{x}\cdot\mathbf{d}}) = \mathbf{d}$ and $\mathbf{S}(\mathrm{e}^{\mathrm{i}\mathbf{k}_R\cdot\mathbf{x}}\mathrm{e}^{-\mathbf{k}_I\cdot\mathbf{x}}) = \frac{\mathrm{e}^{-2\mathbf{k}_I\cdot\mathbf{x}}}{k}\mathbf{k}_R$.
- For a field written in polar coordinates as $u(\mathbf{x}) = f(r)g(\theta)$, we have $\nabla u = f'g\hat{\mathbf{r}} + \frac{1}{r}fg'\hat{\boldsymbol{\theta}}$, so that $\mathbf{S} = \frac{1}{k}\Im\{f'\overline{f}|g|^2\hat{\mathbf{r}} + \frac{1}{r}|f|^2 g'\overline{g}\hat{\boldsymbol{\theta}}\}$.
-
$$\mathbf{S}\big(\mathrm{e}^{\mathrm{i}\ell\theta}J_\ell(kr)\big) = \frac{\ell}{kr}|J_\ell(kr)|^2\hat{\boldsymbol{\theta}}, \qquad \mathbf{S}\big(\mathrm{e}^{\mathrm{i}\ell\theta}H_\ell^{(1)}(kr)\big) = \frac{\ell}{kr}|H_\ell^{(1)}(kr)|^2\hat{\boldsymbol{\theta}} + \frac{2}{\pi kr}\hat{\mathbf{r}}.$$

This is consistent with the fact that smooth Fourier–Bessel functions rotate around the origin (anticlockwise for $\ell > 0$ and clockwise for $\ell < 0$) and do not propagates radially, while Fourier–Hankel functions rotate and simultaneously propagate outwards.

Hint: use the Wronskian identity $J_\ell(z)Y_\ell'(z) - Y_\ell(z)J_\ell'(z) = \frac{2}{\pi z}$ ([DLMF, eq. 10.5.2]).

Compare the results with the animations on the webpage[9].

3 ANALYTICAL TOOLS

We introduce a few mathematical tools that will be useful in the following. Much more detail on the content of this section can be found e.g. in the first part of [SBH19] and in [McLean00].

3.1 LIPSCHITZ DOMAINS

We say that an open set $\Omega \subset \mathbb{R}^2$ with bounded boundary is Lipschitz if (1) there is a finite family of open sets $\{W_j\}_{j=1,\dots,J}$ that cover $\partial\Omega$ (i.e. $\partial\Omega \subset \bigcup_{j=1,\dots,J} W_j$), (2) there is a family of rotated Lipschitz hypographs $\{\Omega_j\}_{j=1,\dots,J}$ (i.e. $\Omega_j = \{(x_1', x_2') : x_2' < f_j(x_1')\}$, where (x_1', x_2') is a system of rotated Cartesian coordinates in $\mathbb{R}^2$ and f_j is a Lipschitz function), and (3) $W_j \cap \Omega = W_j \cap \Omega_j$.

Intuitively, for each $\mathbf{x} \in \partial\Omega$, there is a neighbourhood where the boundary can be represented as the graph of a Lipschitz function, and Ω lies only on one side of $\partial\Omega$. Smooth domains, convex domains, and polygons are Lipschitz. Domains with cusps (such as $\{0 < \sqrt{x_2} < x_1 < 1\}$) or cracks (such as $\{|\mathbf{x}| < 1, x_2 \neq 0\}$) are not allowed.

We also say that Ω is of class C^m, $m = 0, 1, \dots, \infty$, if the functions f_j are of class C^m.

An important property of Lipschitz domains is that the unit normal vector field $\mathbf{n}$ is defined almost everywhere on their boundary (a.e. with respect to the 1-dimensional measure). E.g. on a polygon the unit normal is defined everywhere except that at corners.

3.2 FUNCTION SPACES ON LIPSCHITZ DOMAINS

To study boundary value problems we need some function spaces. Let $\Omega \subset \mathbb{R}^2$ be an open, Lipschitz set. We denote by $\boxed{\mathscr{D}(\Omega)}$ the space of the "test functions": complex-valued C^∞ functions defined on Ω whose support is compactly contained in Ω.

We denote by $\boxed{L^2(\Omega)}$ the usual Lebesgue space of complex-valued, square-integrable functions. This is a Hilbert space with inner product $(v, w)_{L^2(\Omega)} = \int_\Omega v\overline{w}\, \mathrm{d}\mathbf{x}$ and norm $\|v\|_{L^2(\Omega)}^2 = \int_\Omega |v|^2\, \mathrm{d}\mathbf{x}$. Since we are dealing with complex-valued functions, the inner product is a sesquilinear form (with a complex conjugation on the second entry) and the norm requires the use of the absolute value of the argument.

Definition 3.1: $\big(H^1(\Omega)$ **and** $H_0^1(\Omega)\big)$**.** The Sobolev space $\boxed{H^1(\Omega)}$ is space of complex-valued $L^2(\Omega)$ functions, whose first (distributional) partial derivatives are in $L^2(\Omega)$. It is provided with the following seminorm, norm, and inner product:

$$|v|_{H^1(\Omega)}^2 := \|\nabla v\|_{L^2(\Omega)^2}^2 = \left\|\frac{\partial v}{\partial x_1}\right\|_{L^2(\Omega)}^2 + \left\|\frac{\partial v}{\partial x_2}\right\|_{L^2(\Omega)}^2, \qquad \|v\|_{H^1(\Omega)}^2 := |v|_{H^1(\Omega)}^2 + \|v\|_{L^2(\Omega)}^2,$$

$$(v, w)_{H^1(\Omega)} := \left(\frac{\partial v}{\partial x_1}, \frac{\partial w}{\partial x_1}\right)_{L^2(\Omega)} + \left(\frac{\partial v}{\partial x_2}, \frac{\partial w}{\partial x_2}\right)_{L^2(\Omega)} + (v, w)_{L^2(\Omega)} = \int_\Omega (\nabla v \cdot \nabla \overline{w} + v\overline{w})\, \mathrm{d}\mathbf{x}.$$

The space $\boxed{H_0^1(\Omega)}$ is the subspace of $H^1(\Omega)$ of the elements that can be approximated in $H^1(\Omega)$ norm by a sequence of elements of $\mathscr{D}(\Omega)$.

Remark 3.2: (Distributional derivatives). When we say that a partial derivative "in the sense of distributions" $\frac{\partial v}{\partial x_1}$ of an $L^2(\Omega)$ function is in $L^2(\Omega)$, we mean that there is a function $w \in L^2(\Omega)$ such that $\int_\Omega v \frac{\partial \varphi}{\partial x_1} = -\int_\Omega w\varphi$ for all $\varphi \in \mathscr{D}(\Omega)$.

We define also the subspace of $H^1(\Omega)$ of the functions with square-integrable (distributional) Laplacian:

$\boxed{H^1(\Omega; \Delta)} = \{v \in H^1(\Omega) : \Delta v \in L^2(\Omega)\}.$

Finally, we say that $u \in \boxed{H_{\mathrm{loc}}^1(\Omega)}$ if the restriction of u to any bounded open subset D of Ω belongs to $H^1(D)$, [Sayas06, p. 12]. If Ω is bounded, then $H_{\mathrm{loc}}^1(\Omega) = H^1(\Omega)$, while if Ω is unbounded then the "local space" $H_{\mathrm{loc}}^1(\Omega)$ includes functions that do not decay at infinity. For instance, all plane and circular waves belong to $H_{\mathrm{loc}}^1(\Omega) \setminus H^1(\Omega)$ if Ω is the complement of a bounded set (which must contain the origin, if the circular waves are the singular ones). We haven't defined a norm on $H_{\mathrm{loc}}^1(\Omega)$, so this is not a Hilbert space; on the other hand the $H^1(D)$ norms are seminorms on $H_{\mathrm{loc}}^1(\Omega)$. Similarly, $u \in \boxed{H_{\mathrm{loc}}^1(\Omega; \Delta)}$ if the restriction of u to any bounded open subset D of Ω belongs to $H^1(D; \Delta)$.

The elements of $H^1(\Omega)$ are in general not continuous, so their point evaluation is not well-defined. However we will see that their values on the boundary of Ω, or any other Lipschitz curve, are well-defined.

Exercise 3.3: (Circular wave orthogonality). For $\Omega = B_R$ a disc centred at the origin, show that the smooth Fourier–Bessel functions $J_\ell(kr)e^{i\ell\theta}$, $\ell \in \mathbb{Z}$, are orthogonal both in $L^2(B_R)$ and in $H^1(B_R)$.

It is also possible to show that they constitute a basis for the Helmholtz solution space $\{u \in H^1(B_R) : \Delta u + k^2 u = 0\}$.

Remark 3.4: (Wavenumber-weighted H^1 norms). The two terms in the definition of the $H^1(\Omega)$ norm and inner product are not dimensionally homogeneous, because ∇u has the dimension of u divided by a length (if $\mathbf{x}$ is a point in physical space). So, when dealing with Helmholtz problems, we often weigh the norm with the wavenumber $k > 0$ either as $\|v\|^2_{H^1_k(\Omega)} = |v|^2_{H^1(\Omega)} + k^2 \|v\|^2_{L^2(\Omega)}$, or $\|v\|^2_{H^1_k(\Omega)} = k^{-2} |v|^2_{H^1(\Omega)} + \|v\|^2_{L^2(\Omega)}$. The latter choice is convenient because for a plane wave v, and for many other Helmholtz solutions, $\|v\|_{H^1_k(\Omega)}$ and $\|v\|_{L^2(\Omega)}$ (and similar higher-order norms) scale in the same way with respect to k.

3.3 Spaces on boundaries

3.3.1 The circle

We will need spaces of functions defined on boundary of Lipschitz sets with regularity weaker than H^1 and stronger than L^2. How to define functions with "half derivative"?

Let $\mathbb{S}^1 := \{\mathbf{x} \in \mathbb{R}^2 : \|\mathbf{x}\| = 1\}$ be the unit circle. For a function v defined on $\mathbb{S}^1$ we write $v(\theta)$, with $\theta \in [0, 2\pi]$, for its value in polar coordinates. We say that $v \in L^2(\mathbb{S}^1)$ if $\|v\|^2_{L^2(\mathbb{S}^1)} := \int_0^{2\pi} |v|^2 \, d\theta < \infty$ and $v \in H^1(\mathbb{S}^1)$ if $\|v\|^2_{H^1(\mathbb{S}^1)} := \int_0^{2\pi} (|v|^2 + |v'|^2) \, d\theta < \infty$, where v' is the derivative in the angular coordinate.

The expansion of v in circular harmonics is $v(\theta) = \sum_{\ell \in \mathbb{Z}} \hat{v}_\ell e^{i\ell\theta}$ for a sequence of coefficients $\hat{v}_\ell \in \mathbb{C}$, which can be computed as $\hat{v}_\ell = \frac{1}{2\pi} \int_0^{2\pi} v(\theta) e^{-i\ell\theta} \, d\theta$. We can compute the $L^2(\mathbb{S}^1)$ scalar product and the $L^2(\mathbb{S}^1)/H^1(\mathbb{S}^1)$ norms using this expansion, exploiting the orthogonality $\int_0^{2\pi} e^{i\ell\theta} e^{-i\ell'\theta} \, d\theta = 2\pi\delta_{\ell,\ell'}$ and the derivation formula $\frac{\partial}{\partial\theta} e^{i\ell\theta} = i\ell e^{i\ell\theta}$:

$$(v, w)_{L^2(\mathbb{S}^1)} = \int_0^{2\pi} v(\theta)\overline{w(\theta)} \, d\theta = \int_0^{2\pi} \sum_{\ell \in \mathbb{Z}} \hat{v}_\ell e^{i\ell\theta} \sum_{\ell' \in \mathbb{Z}} \overline{\hat{w}_{\ell'} e^{i\ell'\theta}} \, d\theta = 2\pi \sum_{\ell \in \mathbb{Z}} \hat{v}_\ell \overline{\hat{w}_\ell}, \tag{27}$$

$$\|v\|^2_{L^2(\mathbb{S}^1)} = \int_0^{2\pi} |v|^2 \, d\theta = 2\pi \sum_{\ell \in \mathbb{Z}} |\hat{v}_\ell|^2, \qquad \|v\|^2_{H^1(\mathbb{S}^1)} = \int_0^{2\pi} (|v|^2 + |v'|^2) \, d\theta = 2\pi \sum_{\ell \in \mathbb{Z}} |\hat{v}_\ell|^2 (1 + \ell^2).$$

(Write down the intermediate computations.) Thus, a function defined on the circle is in $L^2(\mathbb{S}^1)$ if the sequence of its Fourier coefficients is an element of the sequence space $l^2(\mathbb{Z}) = \{(a_\ell), \ell \in \mathbb{Z}, \|(a_\ell)\|^2_{l^2} := \sum_{\ell \in \mathbb{Z}} |a_\ell|^2 < \infty\}$, and in $H^1(\mathbb{S}^1)$ if its Fourier coefficients weighted with $(1 + \ell^2)^{1/2}$ are in $l^2(\mathbb{Z})$. This means that the Fourier coefficients of functions in $H^1(\mathbb{S}^1)$ must decay faster for $\ell \to \infty$ (faster than $|\ell|^{-3/2}$) than those of the general function of $L^2(\mathbb{S}^1)$ (for which a decay slightly faster than $|\ell|^{-1/2}$ is enough).

This suggests a way to define Sobolev spaces with other regularities:

$$\boxed{\|v\|^2_{H^s(\mathbb{S}^1)} := 2\pi \sum_{\ell \in \mathbb{Z}} |\hat{v}_\ell|^2 (1 + \ell^2)^s,} \qquad \boxed{H^s(\mathbb{S}^1)} := \left\{ v(\theta) = \sum_{\ell \in \mathbb{Z}} \hat{v}_\ell e^{i\ell\theta} : \|v\|_{H^s(\mathbb{S}^1)} < \infty \right\} \quad \forall s \in \mathbb{R}. \tag{28}$$

For $s = 0$ and $s = 1$ we recover $H^0(\mathbb{S}^1) = L^2(\mathbb{S}^1)$ and $H^1(\mathbb{S}^1)$ as defined above. High-order Fourier coefficients correspond to rapidly oscillating components: imposing that they decay faster in ℓ is the same as imposing some regularity on v. So the higher s the smoother are the elements of $H^s(\mathbb{S}^1)$: for any real $s_- < s_+$, $H^{s_+}(\mathbb{S}^1) \subset H^{s_-}(\mathbb{S}^1)$ and $\|v\|_{H^{s_-}(\mathbb{S}^1)} \le \|v\|_{H^{s_+}(\mathbb{S}^1)}$. If $s > 1/2$, the elements of $H^s(\mathbb{S}^1)$ are continuous functions, if $s \ge 0$ they are $L^2(\mathbb{S}^1)$ classes of equivalence, for $s < 0$ they can only be understood as distributions.

Exercise 3.5: (Dense embeddings). Show that for all $s_- < s_+$ the space $H^{s_+}(\mathbb{S}^1)$ is a *dense* subspace of $H^{s_-}(\mathbb{S}^1)$. This means that for all $v \in H^{s_-}(\mathbb{S}^1)$ and $\epsilon > 0$ there is $w \in H^{s_+}(\mathbb{S}^1)$ with $\|v - w\|_{H^{s_-}(\mathbb{S}^1)} \le \epsilon$. Show also that $H^{s_+}(\mathbb{S}^1) \ne H^{s_-}(\mathbb{S}^1)$.

Hint: look for a common subspace of all $H^s(\mathbb{S}^1)$ that is dense in each of them.

Exercise 3.6: (Special elements of $H^s(\mathbb{S}^1)$).

- Compute the Fourier series of $\chi(\theta) = \begin{cases} 1 & 0 < \theta < \pi, \\ 0 & \pi < \theta < 2\pi. \end{cases}$ Show that $\chi \in H^s(\mathbb{S}^1)$ if and only if $s < \frac{1}{2}$.

- Can you find a $v \in H^{\frac{1}{2}}(\mathbb{S}^1) \setminus C^0(\mathbb{S}^1)$?

- Show that a delta function $\delta_{\theta_\star}$, $\theta_\star \in [0, 2\pi]$, belongs to $H^s(\mathbb{S}^1)$ if and only if $s < -\frac{1}{2}$.

Exercise 3.7: (Random Sobolev functions on boundaries). We want to visualise how the decay of the Fourier coefficients $\hat{v}_\ell$ affects the regularity of $v(\theta) = \sum_{\ell \in \mathbb{Z}} \hat{v}_\ell e^{i\ell\theta}$. To this purpose, generate and plot a function v on $\mathbb{S}^1$ with random Fourier coefficients that decay in such a way that $v \in H^{s-\epsilon}(\mathbb{S}^1) \setminus H^s(\mathbb{S}^1)$. Of course you need to truncate the series after a finite number of terms. Observe the behaviour of v for different values of s.

3.3.2   GENERAL BOUNDARIES

Given a Lipschitz bounded domain Ω, if there is a bi-Lipschitz map $\Phi : \overline{B_1} = \{|\mathbf{x}| \leq 1\} \to \overline{\Omega}$ that maps $\mathbb{S}^1$ in $\partial\Omega$, we can define the space $\boxed{H^s(\partial\Omega)}$ as the space of functions v defined on $\partial\Omega$ whose pullback $v^*(\mathbf{x}) = v(\Phi(\mathbf{x}))$ is an element of $H^s(\mathbb{S}^1)$. For $-1 \leq s \leq 1$ this gives a well-defined space $H^s(\partial\Omega)$ independently of the choice of Φ. Different maps Φ give equivalent norms. The space $H^1(\partial\Omega)$ is precisely the space of $L^2(\partial\Omega)$ functions whose tangential first derivative $\nabla_T v$ is in $L^2(\partial\Omega)$; moreover $v \mapsto (\int_{\partial\Omega}(|v|^2 + |\nabla_T v|^2)\, \mathrm{d}s)^{1/2}$ is an equivalent norm on $H^1(\partial\Omega)$.

If we do not have such a map Φ, $H^s(\partial\Omega)$ (for $-1 \leq s \leq 1$) can be defined in a slightly more complicated way, using the cover of $\partial\Omega$ from the definition of a Lipschitz set and a so-called "partition of unity", see [McLean00, pp. 98–99].

Several other definitions of the spaces $H^s(\partial\Omega)$ exist and can be found in the literature. The norms obtained with different definitions are equivalent (for $-1 \leq s \leq 1$) but not necessarily equal.

In most of these notes we will use $H^s(\partial\Omega)$ only for $s = \pm 1/2$: $H^{\frac{1}{2}}(\partial\Omega) \subset L^2(\partial\Omega) \subset H^{-\frac{1}{2}}(\partial\Omega)$.

3.3.3   DUALITY PRODUCT

An important property of these spaces is that $H^{-s}(\partial\Omega)$ can be identified to the anti-dual space of $H^s(\partial\Omega)$, i.e. the space of anti-linear continuous functionals on $H^s(\partial\Omega)$. Let us look at what this means in the case of $\mathbb{S}^1$. If $v, w \in L^2(\mathbb{S}^1)$, we have seen in (27) that we can write their scalar product as the scalar product of the Fourier coefficients in the sequence space $l^2(\mathbb{Z})$ (times 2π). We want to use the same $l^2(\mathbb{Z})$ product of Fourier coefficients also when either v or w is not in $L^2(\mathbb{S}^1)$. The Fourier coefficients of this function decay slowly, thus for the series in (27) to be finite we need the other function (w or v) to have fast-converging Fourier coefficients, i.e. to be smoother. We define the **duality product**

$$\langle v, w \rangle_{\mathbb{S}^1} = \left\langle \sum_{\ell \in \mathbb{Z}} \hat{v}_\ell e^{i\ell\theta}, \sum_{\ell \in \mathbb{Z}} \hat{w}_\ell e^{i\ell\theta} \right\rangle_{\mathbb{S}^1} := 2\pi \sum_{\ell \in \mathbb{Z}} \hat{v}_\ell \overline{\hat{w}_\ell}$$

whenever the sum is bounded. If $v \in H^s(\mathbb{S}^1)$ and $w \in H^{-s}(\mathbb{S}^1)$ for some $s \in \mathbb{R}$ then this series is bounded: by the Cauchy–Schwarz inequality in $l^2(\mathbb{Z})$,

$$|\langle v, w \rangle_{\mathbb{S}^1}| \leq 2\pi \sum_{\ell \in \mathbb{Z}} (1 + \ell^2)^{s/2} |\hat{v}_\ell| (1 + \ell^2)^{-s/2} |\hat{w}_\ell| \leq \|v\|_{H^s(\mathbb{S}^1)} \|w\|_{H^{-s}(\mathbb{S}^1)}.$$

Moreover, if $v, w \in L^2(\mathbb{S}^1)$, then the duality product coincides with the L^2 inner product: $\langle v, w \rangle_{\mathbb{S}^1} = \int_{\mathbb{S}^1} v(\theta)\overline{w}(\theta)\, \mathrm{d}\theta$.

Similarly, it is possible to define a duality product $\langle \cdot, \cdot \rangle_{\partial\Omega}$ on $\partial\Omega$, i.e. a sesquilinear form acting on Sobolev functions defined on $\partial\Omega$ such that

$$|\langle v, w \rangle_{\partial\Omega}| \leq C \|v\|_{H^{\frac{1}{2}}(\partial\Omega)} \|w\|_{H^{-\frac{1}{2}}(\partial\Omega)} \qquad \forall v \in H^{\frac{1}{2}}(\partial\Omega),\ w \in H^{-\frac{1}{2}}(\partial\Omega),\ \text{and}$$

$$\langle v, w \rangle_{\partial\Omega} = \int_{\partial\Omega} v\overline{w}\, \mathrm{d}s, \qquad \text{if } w \in L^2(\partial\Omega).$$

Because of this, we sometimes abuse the notation and write the duality product simply as $\int_{\partial\Omega} v\overline{w}\, \mathrm{d}s$, even when one of the two distributions is not in L^2 and the product is not strictly speaking an integral. We write $\langle v, w \rangle_{\partial\Omega}$ also when $v \in H^{-\frac{1}{2}}(\partial\Omega)$ and $w \in H^{\frac{1}{2}}(\partial\Omega)$. To be more clear we might write $\langle v, w \rangle_{H^{\frac{1}{2}}(\partial\Omega) \times H^{-\frac{1}{2}}(\partial\Omega)}$ and $\langle v, w \rangle_{H^{-\frac{1}{2}}(\partial\Omega) \times H^{\frac{1}{2}}(\partial\Omega)}$, depending on the regularity of the arguments.

Exercise 3.8: (Dual norms). Let the domain Ω admit a bi-Lipschitz map $\Phi : \overline{B_1} \to \overline{\Omega}$ as above. For each v, w defined on $\partial\Omega$ let v^*, w^* be their pullbacks on $\mathbb{S}^1$ and define $\|v\|_{H^s(\Gamma)} := \|v^*\|_{H^s(\mathbb{S}^1)}$ and $\langle v, w\rangle_\Gamma := \langle v^*, w^*\rangle_{\mathbb{S}^1}$.

Show that $\|v\|_{H^s(\Gamma)} = \sup_{0 \neq w \in H^{-s}(\Gamma)} \frac{|\langle v, w\rangle_\Gamma|}{\|w\|_{H^{-s}(\Gamma)}}$.

Hint: show it first for $\Gamma = \mathbb{S}^1$.

Remark 3.9: (Integrals and restrictions of $H^{-\frac{1}{2}}$ distributions). For any element $v \in H^{-s}(\mathbb{S}^1)$, $s > 0$, even if $v \notin L^1(\mathbb{S}^1)$, we can compute its "integral" as a duality product $\int_{\mathbb{S}^1} v \, ds = \langle v, 1\rangle_{\mathbb{S}^1}$, because the constant function $1 \in C^\infty(\mathbb{S}^1) \subset H^s(\mathbb{S}^1)$.

On the other hand, Exercise 3.6 shows that (non-constant) piecewise-constants do not belong to $H^{\frac{1}{2}}(\partial\Omega)$. This is equivalent to say that we cannot test $v \in H^{-\frac{1}{2}}(\mathbb{S}^1)$ against the characteristic function of a an arc subset of $\mathbb{S}^1$, so we cannot compute the integral of arbitrary $v \in H^{-\frac{1}{2}}(\mathbb{S}^1)$ over subsets. I.e. $\int_{\mathbb{S}^1} v \, ds$ makes sense, while $\int_{\mathbb{S}^1 \cap \{x_2 > 0\}} v \, ds$ might be not well-defined. Restricting an element of $H^s(\mathbb{S}^1)$ to an arc and extending back to zero is guaranteed to give an element of $H^s(\mathbb{S}^1)$ only if $|s| < \frac{1}{2}$. The same hold for general shapes.[13]

3.3.4 TRACE OPERATORS

These spaces are closely related to **trace operators**. Given a smooth function $v \in C^1(\overline{\Omega})$, we define its **Dirichlet and Neumann traces**, respectively, as

$$\boxed{\gamma v := v|_{\partial\Omega}, \qquad \partial_\mathbf{n} v := \mathbf{n} \cdot \gamma(\nabla v)}$$

where $\mathbf{n}$ is the outward-pointing unit normal vector field on $\partial\Omega$ (which is defined almost everywhere if the domain is Lipschitz, by Rademacher theorem). Can we define these traces for more general functions, such as elements of Sobolev spaces?

Theorem 3.10: (Trace theorem). The Dirichlet trace γ can be extended to a surjective continuous operator mapping $\gamma : H^1(\Omega) \to H^{\frac{1}{2}}(\partial\Omega)$. The kernel of γ is $H_0^1(\Omega)$.

The Neumann trace $\partial_\mathbf{n}$ can be extended to a surjective continuous operator $\partial_\mathbf{n} : H^1(\Omega; \Delta) \to H^{-\frac{1}{2}}(\partial\Omega)$.

This theorem says that the spaces $H^{\frac{1}{2}}(\partial\Omega)$ and $H^{-\frac{1}{2}}(\partial\Omega)$ are precisely the spaces of the Dirichlet and the Neumann traces of $H^1(\Omega)$ and $H^1(\Omega; \Delta)$ functions, respectively. See [McLean00, Thm. 3.37, 3.40(ii)] (for the Dirichlet trace, using $k = 1$ in the book's notation) and [Spence14, p. 6] for more details.[14]

The trace operators are local, i.e. γv and $\partial_\mathbf{n} v$ depend only on the value of v in an arbitrary small neighbourhood of $\partial\Omega$. Thus, if Ω is unbounded (but $\partial\Omega$ is still bounded), in the trace theorem we can substitute $H^1(\Omega)$ and $H^1(\Omega; \Delta)$ with $H^1_{\mathrm{loc}}(\Omega)$ and $H^1_{\mathrm{loc}}(\Omega; \Delta)$, respectively.

Exercise 3.11: (Equivalent norms on boundaries). Prove that the following are equivalent norms on $H^{\pm\frac{1}{2}}(\partial\Omega)$:

$$\|u\|_{H^{\frac{1}{2}}_\#(\partial\Omega)} := \inf\{\|U\|_{H^1(\Omega)} : \gamma U = u\}, \qquad \|u\|_{H^{-\frac{1}{2}}_\#(\partial\Omega)} := \inf\{\|U\|_{H^1(\Omega;\Delta)} : \partial_\mathbf{n} U = u\}.$$

Hint: use that all continuous linear surjective operators between Hilbert spaces admit continuous right inverses [SBH19, Lemma 4.1].

Remark 3.12: (Sobolev spaces on $\mathbb{R}^n$). We defined Sobolev spaces with non-integer exponents s on the unit circle $\mathbb{S}^1$, however they can be defined on $\mathbb{R}^n$ and all its open subsets. We sketch a brief description of these spaces, but we point out that we will not use them in the rest of this course (apart from a brief mention in §6.3.4).

To define $H^s(\mathbb{R}^n)$, since $\mathbb{R}^n$ is unbounded, instead of Fourier series one has to use the Fourier transform, i.e. switch from a discrete ($\ell \in \mathbb{Z}$) to a continuous ($\boldsymbol{\xi} \in \mathbb{R}^n$) spectral parameter. The Fourier transform of $u \in L^1(\mathbb{R}^n)$ is $\widehat{u}(\boldsymbol{\xi}) := (2\pi)^{-n/2} \int_{\mathbb{R}^n} u(\mathbf{x}) e^{-i\boldsymbol{\xi}\cdot\mathbf{x}} \, d\mathbf{x} \in L^\infty(\mathbb{R}^n)$. For a tempered distribution $u \in \mathcal{S}^*(\mathbb{R}^n)$, its Fourier transform $\widehat{u} \in \mathcal{S}^*(\mathbb{R}^n)$ is defined by its action on Schwartz functions $\varphi \in \mathcal{S}(\mathbb{R}^n)$ as $\langle \widehat{u}, \varphi\rangle := \langle u, \widehat{\varphi}\rangle_{\mathbb{R}^n}$, where $\langle \cdot, \cdot\rangle_{\mathbb{R}^n}$ is the duality product between $\mathcal{S}^*(\mathbb{R}^n)$ and $\mathcal{S}(\mathbb{R}^n)$ that extends the $L^2(\mathbb{R}^n)$ scalar product. We say that $u \in H^s(\mathbb{R}^n)$ for $s \in \mathbb{R}$ if $\widehat{u}$ is locally integrable and $\|u\|^2_{H^s(\mathbb{R}^n)} := \int_{\mathbb{R}^n} (1 + |\boldsymbol{\xi}|^2)^s |\widehat{u}(\boldsymbol{\xi})|^2 d\boldsymbol{\xi} < \infty$. The smoothness of u is measured in terms of decay or growth of $\widehat{u}$ at infinity. Plancherel theorem

---

[13]A different concrete and instructive explanation of the same facts, making use of the trace theorem below, can be found in Remark 2.5.1 of the book [Boffi, Brezzi, Fortin, Mixed Finite Element Methods and Applications, 2013].

[14]The continuity of the Neumann trace in Theorem 3.10 is a consequence of the continuity of the normal-component trace of vector fields $\mathbf{w} \mapsto \mathbf{w}|_{\partial\Omega} \cdot \mathbf{n}$, from $H(\mathrm{div}; \Omega) := \{\mathbf{w} \in L^2(\Omega)^2 : \mathrm{div}\,\mathbf{w} \in L^2(\Omega)\}$ to $H^{-\frac{1}{2}}(\partial\Omega)$, [SBH19, Thm. 6.1].

$\|u\|_{L^2(\mathbb{R}^n)} = \|\widehat{u}\|_{L^2(\mathbb{R}^n)}$ implies that $H^0(\mathbb{R}^n) = L^2(\mathbb{R}^n)$. Combined with $\widehat{\nabla u} = \mathrm{i}\boldsymbol{\xi}\widehat{u}$, for $s = 1$ we deduce that $\|u\|_{H^1(\mathbb{R}^n)}^2 = \int_{\mathbb{R}^n}(|u|^2 + |\nabla u|^2)\,\mathrm{d}\mathbf{x}$, in agreement with §3.2. Properties analogous to those seen for $H^s(\mathbb{S}^1)$ hold for these spaces, such as the duality between $H^s(\mathbb{R}^n)$ and $H^{-s}(\mathbb{R}^n)$, the dense embeddings $H^{s_+}(\mathbb{R}^n) \subset H^{s_+}(\mathbb{R}^n)$ for $s_+ > s_-$, and the equivalence between $u \in H^m(\mathbb{R}^n)$ with $m \in \mathbb{N}$ and the square-integrability of the partial derivatives of u of order up to m.

For open subsets $\Omega \subset \mathbb{R}^n$, $H^s(\Omega)$ is the space of the restrictions to Ω of elements of $H^s(\mathbb{R}^n)$, and its norm is $\|u\|_{H^s(\Omega)} := \inf\{\|U\|_{H^s(\mathbb{R}^n)} : U|_\Omega = u\}$. If Ω is Lipschitz, then one can define a norm equivalent to $\|\cdot\|_{H^s(\Omega)}$ for any $s > 0$ in terms of double singular integrals (Slobodeckij–Gagliardo norms). Note that the definition of $H^s(\Omega)$ using restrictions is meaningful for *open* subsets only: the spaces on the *boundaries* of Lipschitz sets $\Omega \subset \mathbb{R}^n$ introduced earlier in this section can be related to the spaces introduced here using charts, i.e. sufficiently smooth bijections between open sets of $\mathbb{R}^{n-1}$ and subsets of $\partial\Omega$.

A clear and rich introduction to these space is available in [McLean00, Ch. 3].

3.4 GREEN'S IDENTITIES

The divergence (or Gauss) theorem says that for any $\mathbf{F} \in C^1(\overline{\Omega})^2$ we have $\int_\Omega \mathrm{div}\,\mathbf{F}\,\mathrm{d}\mathbf{x} = \int_{\partial\Omega} \mathbf{F}\cdot\mathbf{n}\,\mathrm{d}s$, where $\mathbf{n}$ is the outward pointing unit normal vector field on $\partial\Omega$, [McLean00, Thm. 3.34]. The product rule for the divergence is $\mathrm{div}[w\mathbf{G}] = \nabla w\cdot\mathbf{G} + w\,\mathrm{div}\,\mathbf{G}$. The combination of these two ingredients gives the multidimensional integration-by-parts formula[15]:

$$\int_\Omega \nabla w\cdot\mathbf{G}\,\mathrm{d}\mathbf{x} + \int_\Omega w\,\mathrm{div}\,\mathbf{G}\,\mathrm{d}\mathbf{x} = \int_{\partial\Omega} w\mathbf{G}\cdot\mathbf{n}\,\mathrm{d}s \qquad \forall w \in C^1(\overline{\Omega}), \mathbf{G} \in C^1(\overline{\Omega})^2. \tag{29}$$

Taking $\mathbf{G}$ as a gradient, with simple manipulations we get **Green's first and second identity** for the Helmholtz equation: for $u, w \in C^2(\overline{\Omega})$, $k \in \mathbb{R}$

$$\int_\Omega (\Delta u + k^2 u)w\,\mathrm{d}\mathbf{x} = \int_{\partial\Omega} \partial_\mathbf{n} u\,\gamma w\,\mathrm{d}s + \int_\Omega (k^2 uw - \nabla u\cdot\nabla w)\,\mathrm{d}\mathbf{x}, \tag{30}$$

$$\int_\Omega \Big((\Delta u + k^2 u)w - u(\Delta w + k^2 w)\Big)\,\mathrm{d}\mathbf{x} = \int_{\partial\Omega} (\partial_\mathbf{n} u\,\gamma w - \gamma u\,\partial_\mathbf{n} w)\,\mathrm{d}s. \tag{31}$$

Exercise 3.13: (Complete proof). Write in detail the proof of (30)–(31) for $u, w \in C^2(\overline{\Omega})$.

Do these identities hold for Sobolev functions?

> **Proposition 3.14: (Green's identities in Sobolev spaces).** If Ω is a bounded Lipschitz domain, Green's first identity (30) holds for $u \in H^1(\Omega; \Delta)$ e $w \in H^1(\Omega)$. Green's second identity (31) holds for $u, v \in H^1(\Omega; \Delta)$.
> The boundary integrals must be understood as the duality products $\langle\partial_\mathbf{n} u, \gamma\overline{w}\rangle_{\partial\Omega}$ and $\langle\gamma u, \partial_\mathbf{n}\overline{w}\rangle_{\partial\Omega}$.

Green's identities are the main tools in the derivation of boundary integral equations. This is the reason why the Sobolev spaces we need are $H^1(\Omega)$, $H^1(\Omega; \Delta)$ and their trace spaces $H^{\pm\frac{1}{2}}(\partial\Omega)$. The proof of Proposition 3.14 can be found in [Spence14, Lemma 4.1–4.2].

Remark 3.15: (Glueing together H^1 functions). Let Ω_1, Ω_2 and $\Omega = \Omega_1 \cup \Sigma \cup \Omega_2$ be three Lipschitz domains, where $\Omega_1 \cap \Omega_2 = \emptyset$, $\Sigma \neq \emptyset$, and $\Sigma = (\partial\Omega_1 \cup \partial\Omega_2) \setminus \partial\Omega \subset \partial\Omega_1 \cap \partial\Omega_2$ is the Lipschitz interface separating Ω_1 and Ω_2.
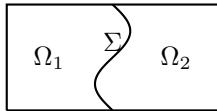
For $u_1 \in H^1(\Omega_1)$ and $u_2 \in H^1(\Omega_2)$ let $u \in L^2(\Omega)$ be such that $u|_{\Omega_j} = u_j$. Then $u \in H^1(\Omega)$ if and only if the Dirichlet traces of u_1 and u_2 restricted to Σ coincide, i.e. $(\gamma_{\Omega_1 \to \partial\Omega_1} u_1)|_\Sigma = (\gamma_{\Omega_2 \to \partial\Omega_2} u_2)|_\Sigma$.

In particular, if $u_1 \in H_0^1(\Omega_1)$, then the zero extension $u \in L^2(\Omega)$ with $u|_{\Omega_2} = 0$ belongs to $H^1(\Omega)$.

Moreover, given $u_1 \in H^1(\Omega_1; \Delta)$ and $u_2 \in H^1(\Omega_2; \Delta)$, then $u \in H^1(\Omega; \Delta)$ if both Dirichlet and Neumann traces of u_1 and u_2 coincide on Σ.

The first statement can be proved by taking the vector field $\mathbf{w} \in L^2(\Omega)^2$ such that $\mathbf{w}|_{\Omega_j} = \nabla u_j$, $j = 1, 2$, and verifying that it is the distributional gradient of u, as in Remark 3.2, by testing against any $\boldsymbol{\varphi} \in \mathcal{D}(\Omega)^2$ and integrating by parts with formula (29). The second statement is proved similarly.

---

[15]Here we do not explicitly write the trace operators because we have assumed that the functions involved are continuous up to the boundary. Identity (29) holds also for $w \in H^1(\Omega)$ and $\mathbf{G} \in H(\mathrm{div};\Omega)$ (defined in footnote 14), with the obvious traces in the boundary integral.

3.5 VARIATIONAL PROBLEMS, FREDHOLM THEORY, GÅRDING INEQUALITY

As we do for Laplace equation, we typically write Helmholtz problems in variational form. The abstract linear **variational problem** in the (complex) Hilbert space H is

$$\text{find} \quad u \in H \qquad \text{such that} \quad \mathcal{A}(u,w) = \mathcal{F}(w) \qquad \forall w \in H, \tag{32}$$

where $\mathcal{A}$ is a sesquilinear form in H and $\mathcal{F}$ is a anti-linear functional in H. We recall that an anti-linear functional satisfies $\mathcal{F}(\lambda v + \mu w) = \bar{\lambda}\mathcal{F}(v) + \bar{\mu}\mathcal{F}(w)$ for all $\lambda, \mu \in \mathbb{C}$ and $v, w \in H$. A sesquilinear form is linear in the first argument and anti-linear in the second one.

Given a variational problem such as (32), the (conforming) **Galerkin method** consists of choosing an N-dimensional subspace $V_N \subset H$ and a basis $\varphi_1, \dots, \varphi_N$, and of looking for a solution of the problem restricted to V_N:

$$\text{find} \quad u_N \in V_N \qquad \text{such that} \quad \mathcal{A}(u_N, w_N) = \mathcal{F}(w_N) \qquad \forall w_N \in V_N. \tag{33}$$

This is achieved computationally by solving the $N \times N$ linear algebraic system $\underline{\underline{\mathbf{A}}}\mathbf{U} = \mathbf{F}$ where $A_{j,m} := \mathcal{A}(\varphi_m, \varphi_j)$, $F_j := \mathcal{F}(\varphi_j)$ and $u_N = \sum_{j=1}^N U_j \varphi_j$.

Given a continuous sesquilinear form $\mathcal{A}$, we can associate a linear bounded operator $A : H \to H^*$ by $(Au)(w) = \langle Au, w \rangle_{H^* \times H} = \mathcal{A}(u,w)$ for all $u, w \in H$, where H^* is the anti-dual of H, [Spence14, Lemma 5.4]. The operator A admits a continuous inverse if and only if, for all $\mathcal{F} \in H^*$, the variational problem (32) is well-posed.

In the case of Laplace equation, the crucial result from functional analysis is **Lax–Milgram** theorem: if $\mathcal{A}$ is **continuous** ($|\mathcal{A}(u,w)| \le C_{\mathcal{A}} \|u\|_H \|w\|_H \ \forall u, w \in H$) and **coercive**[16] ($\Re\{\mathcal{A}(w,w)\} \ge \gamma_{\mathcal{A}} \|w\|_H^2 \ \forall w \in H$), and $\mathcal{F}$ is continuous ($|\mathcal{F}(w)| \le C_{\mathcal{F}} \|w\|_H \ \forall w \in H$), then the corresponding variational problem is well-posed ([Brezis11, Cor. 5.8], [McLean00, Lemma 2.32]). Moreover, several good properties of all Galerkin discretisations follow (well-posedness, stability bounds, quasi-optimality, bounds on the number of linear solver iterations, ...).

Unfortunately, for most variational formulations of the Helmholtz equation coercivity does not hold, so we cannot rely on Lax–Milgram. The branch of functional analysis that we need is called "Fredholm theory" and studies compact perturbations of operators. Good introductions to Fredholm theory are in [McLean00, Ch. 2] and [Brezis11, §6.2]. As recounted in [McLean00, Ch. 1], this theory, which nowadays is written in the abstract language of Hilbert spaces and linear operators, originated from the work[17] of Ivar Fredholm on integral equations, which in turn relies on previous works by Vito Volterra. We recall the definitions of two classes of bounded linear operators between Hilbert (or Banach) spaces; see e.g. [Sayas06, p. 21].

Definition 3.16: (Compact and Fredholm operators). A linear operator $K : H_1 \to H_2$ is **compact** if the image of a bounded sequence admits a converging subsequence ($(v_j)_{j \in \mathbb{N}} \subset H_1, \|v_j\|_H \le C \ \forall j \in \mathbb{N} \Rightarrow \exists j_m \to \infty, w \in H_2$ such that $Kv_{j_m} \to w$).
A bounded linear operator is a **Fredholm operator** if it is sum of an invertible one and a compact one (more precisely, we should say it is a Fredholm operator of index 0).

---

[18] We can think at Fredholm operators as "small" perturbations of invertible operators. The main result is the "Fredholm alternative", which, in its simplest form, reads as follows; [Brezis11, Thm. 6.6(c)], [SBH19, §8.1, 8.6].

Theorem 3.17: (Fredholm alternative). Let $T : H_1 \to H_2$ be a Fredholm operator.
T is injective if and only if it is surjective. In this case its inverse T^{-1} is bounded.

---

[16]Here terminology can be confusing. Coercivity is sometimes called "sign-definiteness", "V-ellipticity", "strong ellipticity", or "strict coercivity", see [Spence14, §5.2]; [McLean00, p. 43] says that $\mathcal{A}$ is "positive and bounded below". In some of these cases, the word "coercive" is used for sesquilinear forms satisfying a Gårding inequality, which is a weaker condition, e.g. [McLean00, eq. (2.7)]. Here we follow the convention of [Spence14] and [Brezis11, §5.3].

[17][Fredholm, *Sur une classe d'équations fonctionnelles*, 1903]

[18]Well, this is not exactly the definition you find in functional analysis textbooks. E.g. [Brezis11, p. 168] defines $T : H_1 \to H_2$ (continuous operator between Hilbert spaces, for simplicity) as "Fredholm with index Ind(T)" if $\dim(\ker T), \dim(\text{Im}\,T)^\perp < \infty$ and Ind$(T) := \dim(\ker T) - \dim(\text{Im}\,T)^\perp$. Let us check that this definition, with index 0, is equivalent to ours.

An invertible operator is Fredholm with index 0; then by [Brezis11, p. 169, $\star$1(c)] any operator in the form invertible+compact as in Definition 3.16 is Fredholm with index 0.

Conversely, assume that $T : H_1 = (\ker T \oplus (\ker T)^\perp) \to H_2 = (\text{Im}\,T \oplus (\text{Im}\,T)^\perp)$ is Fredholm with index 0. Let $\{\phi_1, \dots, \phi_n\}$ be an orthonormal basis of $\ker T$ and $\{\psi_1, \dots, \psi_n\}$ be an orthonormal basis of $(\text{Im}\,T)^\perp$ (which are both finite-dimensional and have the same dimension). Define $K : H_1 \to H_2$ as $K\phi_j = \psi_j$ and $Kv = 0 \ \forall v \in (\ker T)^\perp$; this operator has finite rank, so it is compact. Then $L = T + K$ is an invertible operator and $T = L - K$ is in the form invertible+compact, as desired.

To verify that an operator is Fredholm we will always use Definition 3.16.

This theorem has this name because it states that when we have a Fredholm operator T then only two "alternatives" are possible: either T is injective and surjective, or is neither injective nor surjective. Fredholm alternative says that if we want to prove that a Fredholm operator is invertible, then it suffices to prove its injectivity. A useful idea to keep in mind is that, under this respect, Fredholm operators behave like square matrices.[19]

How do we use Fredholm alternative? The general strategy is the following. We will show that some linear operator T mapping "problem solution" to "problem data" are Fredholm. When we can show that the homogeneous problem (with data equal to 0) only admits the trivial solution (i.e. T is injective), Fredholm alternative guarantees that *all* data admit a solution (i.e. T is surjective), which is unique by injectivity, and that the solution is controlled by the data (i.e. T^{-1} is bounded). **A linear problem whose "solution-to-data" operator is Fredholm is well-posed if the same operator is injective.**

Typically, in time-harmonic problems, sesquilinear forms are not coercive but satisfy a weaker inequality, called Gårding inequality.

Definition 3.18: (Gårding inequality). Let $H \subset V$ be two Hilbert spaces provided with the norms $\|\cdot\|_H$ and $\|\cdot\|_V$, and let the embedding $H \hookrightarrow V$ be continuous. A sesquilinear form satisfies a Gårding inequality if there exists two positive constants α and C_V such that

$$\Re\{\mathcal{A}(v,v)\} \geq \alpha \|v\|_H^2 - C_V \|v\|_V^2 \qquad \forall v \in H. \tag{34}$$

---

[20] Here we follow the notation of [Spence14, §5.3], where the letters H and V are swapped with respect to the classical choice for Hilbert triples (as in [Brezis11, p. 136] and [McLean00, p. 44]).

The main use of Gårding inequality comes from the next result, see [Spence14, Theorem 5.20].

Proposition 3.19: (Gårding $\Rightarrow$ Fredholm). Assume that H and V are as in Definition 3.18, the embedding $H \hookrightarrow V$ is compact and the continuous sesquilinear form $\mathcal{A}(\cdot,\cdot)$ satisfies the Gårding inequality (34). Then the operator $A : H \to H^*$ associated to $\mathcal{A}(\cdot,\cdot)$ is Fredholm.

Proof. Let $i : H \to V$ be the (compact) inclusion map, and $T : V \to H^*$ defined by $\langle Tv, w \rangle_{H^* \times H} = (v, iw)_V$, for $v \in V$ and $w \in H$, where $(\cdot, \cdot)_V$ is the scalar product in V. Then, by Cauchy–Schwarz in V, T is continuous: $\|Tv\|_{H^*} = \sup_{w \in H} \frac{|\langle Tv, w \rangle_{H^* \times H}|}{\|w\|_H} \leq \sup_{w \in H} \frac{\|v\|_V \|iw\|_V}{\|w\|_H} \leq \|v\|_V \|i\|_{H \to V}$. Define $B := A + C_V T \circ i : H \to H^*$, where $C_V > 0$ is the value in (34). Since $T \circ i$ is compact, in order to prove that A is Fredholm, it is enough to see that B is invertible. Then the sesquilinear form

$$\mathcal{B}(u,w) := \langle Bu, w \rangle_{H^* \times H} = \langle Au, w \rangle_{H^* \times H} + C_V \langle T \circ iu, w \rangle_{H^* \times H} = \mathcal{A}(u,w) + C_V (iu, iw)_V, \qquad u, w \in H,$$

is continuous and coercive in H, which, by Lax–Milgram, implies that B is invertible. (Actually we have proved something stronger, that A is sum of a compact operator and a *coercive* one.) $\qquad \square$

Proposition 3.19 and Theorem 3.17 imply that, in order to prove well-posedness of a variational problem (32) whose sesquilinear form $\mathcal{A}(\cdot,\cdot)$ satisfies a Gårding inequality, it suffices to study the homogeneous problem (with $\mathcal{F} = 0$):

Corollary 3.20: (Well-posedness from Gårding). Assume that:

- $H \subset V$ are Hilbert spaces and the embedding $H \hookrightarrow V$ is compact,

- the sesquilinear form $\mathcal{A}(\cdot,\cdot)$ is continuous in H and satisfies the Gårding inequality (34),

- the homogeneous variational problem, $\mathcal{A}(u_0, w) = 0$ for all $w \in H$, admits only the trivial solution $u_0 = 0$.

Then also the inhomogeneous problem (32) is well-posed, for any $\mathcal{F} \in H^*$.

To be able to exploit Corollary 3.20, we need to know when the embedding between two function spaces is compact. A classical result, called Rellich embedding theorem, says that $H^1(\Omega) \hookrightarrow L^2(\Omega)$ is

---

[19]Indeed, an invertible linear operator between finite-dimensional spaces corresponds to a square matrix. All finite-range operators are compact because all bounded sequences of $\mathbb{R}^n$ and $\mathbb{C}^n$ admit converging subsequences. Thus the operators between finite-dimensional spaces that are Fredholm are precisely those associated to square matrices. We know from linear algebra that a square matrix is injective if and only if it is surjective. This proves the Fredholm alternative in the case of operators between finite-dimensional spaces.

(In this $\mathbb{C}^n \to \mathbb{C}^n$ case, Fredholm operators are compact, but in infinite dimensions a Fredholm operator is not compact.)

[20]We could take a more general definition using the inequality $\Re\{\sigma \mathcal{A}(v,v)\} \geq \alpha \|v\|_H^2 - C_V \|v\|_V^2$ for some $0 \neq \sigma \in \mathbb{C}$ (the same σ for all v). Then all consequences of the Gårding inequality would follow precisely in the same way. However all variational problems with $\mathcal{A}(\cdot,\cdot)$ that satisfy this inequality can be reduced to equivalent problems satisfying (34) simply by multiplying the sesquilinear form and the linear functional by σ.

compact, when Ω is a bounded Lipschitz domain[21]. Similarly, one can show that $H^{s_+}(\partial\Omega) \hookrightarrow H^{s_-}(\partial\Omega)$ is compact for all $s_+ > s_-$, [Nédélec01, Theorem 2.5.7].

Exercise 3.21: (Compactness of Sobolev embeddings). Let $s_- < s_+$ be real numbers. Show the compactness of Sobolev embedding $i : H^{s_+}(\mathbb{S}^1) \to H^{s_-}(\mathbb{S}^1)$, in the simple case of the boundary of the unit circle.

The key tool to use is [Brezis11, Cor. 6.2]: given a linear operator $T : H_1 \to H_2$ and $T_j : H_1 \to H_2$ finite-rank operators (i.e. with finite-dimensional image) for $j \in \mathbb{N}$, if $\|T - T_j\|_{H_1 \to H_2} \to 0$ then T is compact.

Construct a sequence of finite-rank "truncated embedding" operators $i_L : H^{s_+}(\mathbb{S}^1) \to H^{s_-}(\mathbb{S}^1)$ for $L \in \mathbb{N}$, such that

$$\|i - i_L\|^2_{H^{s_+}(\mathbb{S}^1) \to H^{s_-}(\mathbb{S}^1)} \leq \frac{1}{(1 + L^2)^{s_+ - s_-}}.$$

Exercise 3.22: (Compact and Fredholm operators in sequence spaces). Let l^2 be the Hilbert space of squared-summable complex sequences $x = (x_j)_{j \in \mathbb{N}}$, $x_j \in \mathbb{C}$, equipped with $\|x\|^2_{l^2} = \sum_{j \in \mathbb{N}} |x_j|^2$.

- Define the right and left complex shift operators $R, L : l^2 \to l^2$ as $(Rx)_1 = 0$, $(Rx)_{j+1} = x_j$ and $(Lx)_j = x_{j+1}$ for $j \in \mathbb{N}$. Show that R and L are neither Fredholm nor compact.

  Are the composition LR and RL either Fredholm or compact? Which of L, R, LR, RL is invertible?

- Show that for any $J \in \mathbb{N}$ the truncation operator $T_J : l^2 \to l^2$ defined by $(T_Jx)_j = x_j$ if $j \leq J$ and $(T_Jx)_j = 0$ if $j > J$ is compact.

- Show that the operator $T : l^2 \to l^2$ defined by $Tx = (x_3, 0, -x_3, 2x_4, 2x_5, \ldots, (Tx)_j = 2x_j, \ldots)$ is Fredholm.

An extensive description of the relations between variational problems satisfying Lax–Milgram assumptions, Gårding inequality or the inf-sup inequality, and the consequences for the Galerkin method, can be found in [Spence14, §5.3]; see also §6.3.1 below.

---

[21]See e.g. [Brezis11, Thm. 9.16] ánd [SBH19, Prop. 7.5] for a more general version.

4 Boundary value problems for the Helmholtz equation

4.1 Plane waves reflected by a straight line

To understand what happens when a wave hits an impenetrable obstacle we start with a very simple case that can be solved analytically. Let $u^{\mathrm{Inc}}(\mathbf{x}) = \mathrm{e}^{\mathrm{i}k\mathbf{x}\cdot\mathbf{d}}$ be a plane wave with $|\mathbf{d}| = 1$, $d_1 \geq 0$ and $d_2 \leq 0$ (i.e. propagating rightward and downward in the plane, $\searrow$). This is called the "**incoming field**", or "**incident field**". Assume that we truncate the domain of propagation to the upper half plane $\Omega^+ = \{x_2 > 0\}$ and on the horizontal line $\Gamma = \{x_2 = 0\}$ we impose some boundary conditions that reflect the impinging wave. We call u^{Scat} the reflected wave, i.e. the "**scattered field**", and $u^{\mathrm{Tot}} = u^{\mathrm{Inc}} + u^{\mathrm{Scat}}$ the "**total field**". u^{Tot} is the physical field we would measure in a point of the half plane.
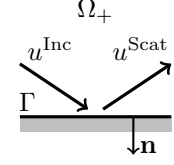
Given u^{Inc}, which is a datum, we now want to find u^{Tot} that satisfies the Helmholtz equation in the upper half plane, and satisfies some desired homogeneous boundary conditions on Γ. This is the same as saying that we want u^{Scat} that satisfies the Helmholtz equation in the same region, and satisfies boundary conditions that depend on u^{Inc} on Γ.

By the law of reflection, we expect u^{Scat} to propagate upwards and to make with the horizontal line Γ the same angle as u^{Inc}, $\nearrow$. This means that u^{Scat} is a plane wave with direction $\widetilde{\mathbf{d}} = (d_1, -d_2)$: $u^{\mathrm{Scat}}(\mathbf{x}) = \mathsf{R}\mathrm{e}^{\mathrm{i}k\widetilde{\mathbf{d}}\cdot\mathbf{x}} = \mathsf{R}\mathrm{e}^{\mathrm{i}k(x_1 d_1 - x_2 d_2)}$ for some reflection coefficient $\mathsf{R} \in \mathbb{C}$ that gives the amplitude and the phase of u^{Scat} itself. The coefficient R depends on the particular type of boundary condition chosen.

- When the line Γ is sound-soft, the Dirichlet trace of the total field u^{Tot} vanishes on Γ:

$$0 = u^{\mathrm{Tot}}(x_1, 0) = u^{\mathrm{Inc}}(x_1, 0) + u^{\mathrm{Scat}}(x_1, 0) = \mathrm{e}^{\mathrm{i}kx_1 d_1} + \mathsf{R}\mathrm{e}^{\mathrm{i}kx_1 d_1} \qquad \forall x_1 \in \mathbb{R} \qquad \Rightarrow \mathsf{R} = -1.$$

- When the line Γ is sound-hard, the Neumann trace of the total field u^{Tot}, i.e. its normal derivative, vanishes on Γ:

$$0 = \frac{\partial u^{\mathrm{Tot}}}{\partial x_2}(x_1, 0) = \frac{\partial}{\partial x_2}\Big(u^{\mathrm{Inc}}(x_1, 0) + u^{\mathrm{Scat}}(x_1, 0)\Big) = \mathrm{i}kd_2\mathrm{e}^{\mathrm{i}kx_1 d_1} - \mathsf{R}\mathrm{i}kd_2\mathrm{e}^{\mathrm{i}kx_1 d_1} \quad \forall x_1 \in \mathbb{R} \quad \Rightarrow \mathsf{R} = 1.$$

- To impose the impedance boundary condition $\frac{\partial u^{\mathrm{Tot}}}{\partial \mathbf{n}} - \mathrm{i}k\vartheta u^{\mathrm{Tot}} = 0$ with $\vartheta > 0$, we recall that $\mathbf{n}$ is the outward-pointing unit normal vector on Γ so $\mathbf{n} = (0, -1)$. In this case we have

$$0 = \frac{\partial u^{\mathrm{Tot}}}{\partial \mathbf{n}} - \mathrm{i}k\vartheta u^{\mathrm{Tot}} = -\frac{\partial u^{\mathrm{Tot}}}{\partial x_2} - \mathrm{i}k\vartheta u^{\mathrm{Tot}} = \Big(\mathrm{i}kd_2(-1 + \mathsf{R}) - \mathrm{i}k\vartheta(1 + \mathsf{R})\Big)\mathrm{e}^{\mathrm{i}kx_1 d_1}.$$

This vanishes for $d_2(-1 + \mathsf{R}) = \vartheta(1 + \mathsf{R})$, i.e. $\mathsf{R} = \frac{d_2 + \vartheta}{d_2 - \vartheta}$.

Summarising, the fields are

$$
\begin{aligned}
u^{\mathrm{Inc}}(\mathbf{x}) &= \mathrm{e}^{\mathrm{i}k(x_1 d_1 + x_2 d_2)}, \\
u^{\mathrm{Scat}}(\mathbf{x}) &= \mathsf{R}\mathrm{e}^{\mathrm{i}k(x_1 d_1 - x_2 d_2)}, \\
u^{\mathrm{Tot}}(\mathbf{x}) &= \mathrm{e}^{\mathrm{i}k(x_1 d_1 + x_2 d_2)} + \mathsf{R}\mathrm{e}^{\mathrm{i}k(x_1 d_1 - x_2 d_2)},
\end{aligned}
\qquad \text{with } \mathsf{R} =
\begin{cases}
-1 & \text{for sound-soft } \Gamma, \\
1 & \text{for sound-hard } \Gamma, \\
\frac{d_2 + \vartheta}{d_2 - \vartheta} \in (-1, 1) & \text{for impedance } \Gamma.
\end{cases}
$$

The plane waves reflected by sound-soft or sound-hard interfaces have the same amplitude of the incoming plane waves and either opposite (sound-soft) or the same (sound-hard) phase. On the other hand, since $|\mathsf{R}| < 1$, the waves reflected by an impedance line have amplitude smaller than the incoming wave: the impedance boundary absorbs some of the wave energy. The amount of wave that is reflected and the amount that is absorbed depend on the direction of the incoming wave; in particular, if $\vartheta \leq 1$ the impedance boundary does not reflect (but absorbs completely) the impinging waves propagating in direction $\mathbf{d} = (\sqrt{1 - \vartheta^2}, -\vartheta)$. An impedance boundary with $\vartheta = 1$ does not reflect the waves hitting perpendicularly. For another point of view on energy preservation and absorption by different boundary conditions, see Exercise 4.18.

For $\vartheta \to 0$ the impedance boundary condition converges to the sound-hard one, and consistently $\mathsf{R} \to 1$; for $\vartheta \to \infty$ it converges to the sound-soft boundary condition and $\mathsf{R} \to -1$.

Here we have considered a wave with infinite front hitting an infinite, perfectly flat barrier: clearly this is not a realistic problem, but it helps to get an intuition of what happens when a wave hits an impenetrable obstacle. A perturbation of Γ, such as the graph of a bounded surface, is termed **rough surface** in the scattering literature; when it is periodic in x_1 it is also called **diffraction grating**.

Remark 4.1: (On unbounded domains: PDE + BCs $\not\Rightarrow$ BVP). When we solve a well-posed boundary value problem the solution is typically determined by the PDE and by the boundary conditions. Here we have used something more. Let us look for example at the sound-soft case. Given u^{Inc}, *any* combination $u_\lambda^{\text{Scat}}(\mathbf{x}) = -\lambda e^{ik(x_1 d_1 + x_2 d_2)} - (1-\lambda)e^{ik(x_1 d_1 - x_2 d_2)}$ satisfies the Helmholtz equation and the boundary condition $u_\lambda^{\text{Scat}} = -u^{\text{Inc}}$ on Γ. We have chosen the case $\lambda = 0$ because from the law of reflection we expect the scattered field to propagate upwards. We will see that in all problems posed on unbounded domains we need to select the waves propagating in the desired direction, and that this is equivalent to imposing conditions "at infinity".

Remark 4.2: (General wave reflected by a straight line). The same reasoning made above shows that if u^{Inc} is any wave propagating downwards, then the reflected wave $u_D^{\text{Scat}}(\mathbf{x}) = -u^{\text{Inc}}(x_1, -x_2)$ propagates upwards and $u^{\text{Inc}} + u_D^{\text{Scat}}$ vanishes on Γ. So $u_D^{\text{Tot}} = u^{\text{Inc}} + u_D^{\text{Scat}}$ is the total field in the presence of a sound-soft line.

You can see the reflection of the Herglotz function $u^{\text{Inc}}(\mathbf{x}) = \int_{-\pi/3}^{-\pi/6} e^{ik(x_1 \cos\varphi + x_2 \sin\varphi)} \, \mathrm{d}\varphi$ by a sound-soft horizontal line in Figure 9 and in the animation on the course webpage[9].

Similarly, $u_N^{\text{Scat}}(\mathbf{x}) = u^{\text{Inc}}(x_1, -x_2)$ propagates upwards and $\frac{\partial}{\partial \mathbf{n}}(u^{\text{Inc}} + u_N^{\text{Scat}})$ vanishes on Γ, so $u_N^{\text{Tot}} = u^{\text{Inc}} + u_N^{\text{Scat}}$ is the reflection of any downward u^{Inc} by a sound-hard line.

For an impedance line Γ, the argument is slightly more complicated: since the reflection coefficient R depends on the direction of the incoming wave, to compute u^{Scat} we need to be able to decompose u^{Tot} in plane waves with different directions and reflect each one of them with its own coefficient. This is possible if u^{Inc} is a Herglotz function with kernel supported in the lower half of the unit circle ($g(\varphi) = 0$ for $0 < \varphi < \pi$).

Figure 9: Reflection of the Herglotz function with kernel $g(\varphi) = \chi_{(-\frac{\pi}{3}, -\frac{\pi}{6})}(\varphi)$ by the sound-soft line $\{x_2 = 0\}$. See Remark 4.2.
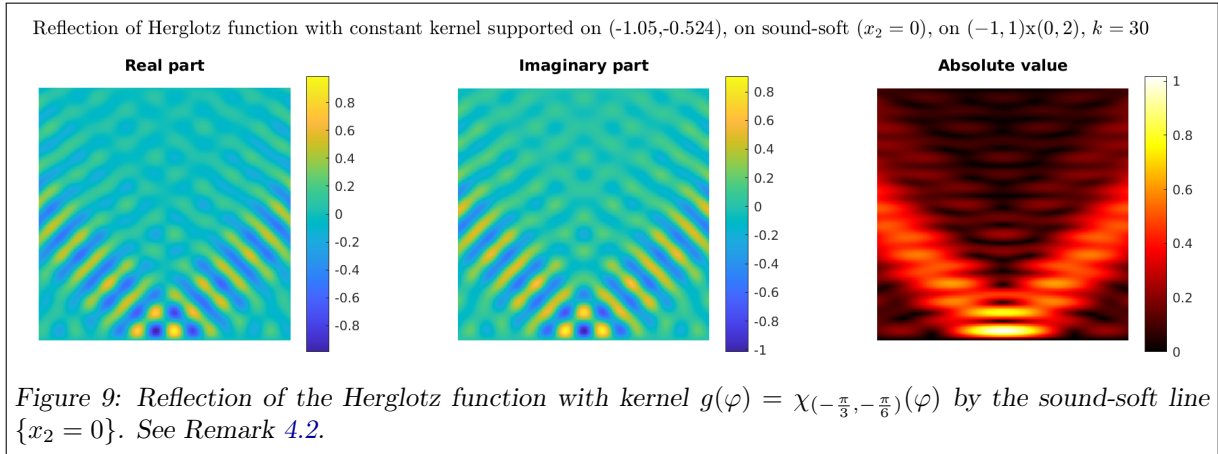
Exercise 4.3: (Neumann reflection of Herglotz function). Plot the total field when the incoming field is the same Herglotz function as in Figure 9 and in Remark 4.2, but the horizontal line Γ acts as a Neumann boundary. Start from the Matlab file provided.

Repeat the same for an impedance boundary.

Exercise 4.4: (Neumann traces on sound-soft boundaries and vice versa). For the problem of a plane wave u^{Inc} impinging on $\Gamma = \{x_2 = 0\}$ as described above, show that, $\forall x \in \mathbb{R}$,

- if Γ is a sound-soft boundary then $\partial_{\mathbf{n}} u^{\text{Scat}}(x, 0) = \partial_{\mathbf{n}} u^{\text{Inc}}(x, 0)$ and $\partial_{\mathbf{n}} u^{\text{Tot}}(x, 0) = 2\partial_{\mathbf{n}} u^{\text{Inc}}(x, 0)$;

- if Γ is a sound-hard boundary then $u^{\text{Scat}}(x, 0) = u^{\text{Inc}}(x, 0)$ and $u^{\text{Tot}}(x, 0) = 2u^{\text{Inc}}(x, 0)$;

- if Γ is an impedance boundary then $(\partial_{\mathbf{n}} - ik\widetilde{\vartheta})u^{\text{Scat}} = (\partial_{\mathbf{n}} - ik\widetilde{\vartheta})u^{\text{Inc}}$ for $\widetilde{\vartheta} = \frac{(d_2)^2}{\vartheta}$.

These formulas motivate the "physical optics approximation" for high-frequency scattering by convex obstacles, see Remark 5.36.

Exercise 4.5: (Reflection of vector plane waves). Consider a vector plane wave $\mathbf{A}e^{ik\mathbf{d}\cdot\mathbf{x}}$ that is solution of Maxwell's equations (14) as in Exercise 2.3. Compute the plane wave reflected by the horizontal plane $\{\mathbf{x} \in \mathbb{R}^3 : x_3 = 0\}$ equipped with PEC boundary conditions $\mathbf{E} \times \mathbf{n} = \mathbf{0}$. Recall that the amplitude of the reflected wave must be orthogonal to its propagation direction.

The reflection of elastic waves is more complicated: an impinging pressure (or shear) wave generates a reflected waves that is sum of a pressure and a shear wave. This phenomenon is called "mode conversion" and is due to the boundary conditions, which involve all three Cartesian components of the fields; see [BK00, pp. 140–143].

4.2   Helmholtz boundary value problems in bounded domains

Let $\Omega \subset \mathbb{R}^2$ be a bounded, open, Lipschitz set. The Dirichlet BVP for the Helmholtz equation is: given a source term f defined in Ω and a boundary datum g_{D} defined on $\partial\Omega$ find u on Ω such that

$$\Delta u + k^2 u = -f \quad \text{in } \Omega, \qquad \gamma u = g_{\mathrm{D}} \quad \text{on } \partial\Omega. \tag{35}$$

We know that the Dirichlet problem for the Poisson equation (problem (35) with $k = 0$) is well-posed when the data f, g_{D} are sufficiently smooth. Despite the Helmholtz equation looks like an innocuous low-order perturbation of the Laplace equation, well-posedness of the Helmholtz Dirichlet problem is not guaranteed.

We start from a simple example. Let Ω be the rectangle $(0, L_1) \times (0, L_2)$. Then for all $j_1, j_2 \in \mathbb{N}$ the field $u_{j_1,j_2}(\mathbf{x}) = \sin(\frac{j_1\pi}{L_1} x_1) \sin(\frac{j_2\pi}{L_2} x_2)$ vanishes on $\partial\Omega$ and is solution of $\Delta u + k_{j_1,j_2}^2 u = 0$ with $k_{j_1,j_2}^2 = \frac{j_1^2\pi^2}{L_1^2} + \frac{j_2^2\pi^2}{L_2^2}$. So there are infinitely many values of k such that the homogeneous ($f = 0$ and $g_{\mathrm{D}} = 0$) Helmholtz Dirichlet BVP admits non-trivial solutions. It follows that for these values of k the problem (35) is not well-posed: if there is a solution then it cannot be unique.

Solutions of the homogeneous Helmholtz Dirichlet problem are called **Dirichlet eigenfunctions** of the Laplacian with **eigenvalue** $\Lambda = k^2$, as they satisfy the eigenproblem $-\Delta u = \Lambda u$, $\gamma u = 0$. The corresponding value of k is a **resonant wavenumber**, and $\omega = kc$ is a **resonant frequency**.

As a second example, if $\Omega = B_R$ is the disc of radius R, then the circular waves $J_\ell(kr)\mathrm{e}^{\pm\mathrm{i}\ell\theta}$ are Dirichlet eigenfunctions for $\Lambda = k^2$ and k such that kR is a zero of the ℓth Bessel function J_ℓ (recall the plots in the left panel of Figure 5 and the top panel of Figure 6: each J_ℓ has infinitely many zeros).

In other domains we find the same situation as in the two examples described, even if we cannot compute eigenvalues and eigenfunctions explicitly; see [SBH19, §9] for the spectral theory of elliptic operators.

4.2.1   Variational formulations of interior BVPs, well-posedness, eigenvalues

To understand the problem in more general bounded Lipschitz domains, we study the problem from a variational point of view. From Green's first identity (30), the variational problem for the Helmholtz Dirichlet BVP (35) with homogeneous boundary conditions $g_{\mathrm{D}} = 0$ is

$$\text{find } u \in H_0^1(\Omega) \text{ such that } \quad \mathcal{A}(u, w) := \int_\Omega (\nabla u \cdot \nabla\overline{w} - k^2 u\overline{w})\, \mathrm{d}\mathbf{x} = \int_\Omega f\overline{w}\, \mathrm{d}\mathbf{x} =: \mathcal{F}(w) \quad \forall w \in H_0^1(\Omega). \tag{36}$$

The sesquilinear form $\mathcal{A}(\cdot, \cdot)$ and the linear functional $\mathcal{F}(\cdot)$ are continuous in $H_0^1(\Omega)$. On the other hand, $\mathcal{A}(\cdot, \cdot)$ is not coercive (for k sufficiently large), as the two terms ($\nabla u \nabla\overline{w}$ and $-k^2 u\overline{w}$) have opposite signs, see Exercise 4.8 or [Spence14, Lemma 6.2]. However, it satisfies a Gårding inequality (34) with $\alpha = 1$ and $C_V = k^2 + 1$:

$$\Re\{\mathcal{A}(w, w)\} = \mathcal{A}(w, w) = \|w\|_{H^1(\Omega)}^2 - (k^2 + 1) \|w\|_{L^2(\Omega)}^2 \qquad \forall w \in H^1(\Omega).$$

Proposition 3.19, together with the compactness of $H_0^1(\Omega)$ in $L^2(\Omega)$, gives that the operator $A : H_0^1(\Omega) \to (H_0^1(\Omega))^*$, $\boxed{A : u \mapsto f, \text{ is Fredholm}}$.[22] Corollary 3.20 of Fredholm alternative then implies that, given Ω and k, only two situations can happen:

- If Ω and k are such that the homogeneous ($f = 0$) problem (36) admits only the trivial solution $u = 0$, then also problem (36) with any $f \in L^2(\Omega)$ (or more generally $\mathcal{F} \in (H_0^1(\Omega))^*$) admits a unique solution.

- On the other hand, if there is a $u \neq 0$ such that $\mathcal{A}(u, w) = 0$ $\forall w \in H_0^1(\Omega)$, then the problem (36) is not well-posed for *any* f. It might have no solutions for some f, and many solutions for some other f.

---

[22]If A is Fredholm, what are the invertible and the compact operators that sum to $A : H_0^1(\Omega) \to (H_0^1(\Omega))^*$?

We can split the sesquilinear form as $\mathcal{A}(u, w) = \mathcal{A}_0(u, w) + \mathcal{K}(u, w)$ with $\mathcal{A}_0(u, w) := \int_\Omega \nabla u \cdot \nabla\overline{w}\, \mathrm{d}\mathbf{x}$ and $\mathcal{K}(u, w) := (-k^2) \int_\Omega u\overline{w}\, \mathrm{d}\mathbf{x}$. Then $\mathcal{A}_0(\cdot, \cdot)$ is the sesquilinear form associated to the (well-posed) Laplace–Dirichlet BVP in $H_0^1(\Omega)$, so it is continuous and coercive (by Poincaré inequality), thus the operator A_0 associated, i.e. $\langle A_0 u, w\rangle_{(H_0^1(\Omega))^* \times H_0^1(\Omega)} = \mathcal{A}_0(u, w)$, is invertible. This operator is simply the Laplacian $A_0 = -\Delta : H_0^1(\Omega) \to (H_0^1(\Omega))^*$. The operator $K : H_0^1(\Omega) \to (H_0^1(\Omega))^*$ associated to the second sesquilinear form, i.e. $\langle Ku, w\rangle_{(H_0^1(\Omega))^* \times H_0^1(\Omega)} = \mathcal{K}(u, w)$, is $-k^2$ times the embedding of $H_0^1(\Omega)$ in $(H_0^1(\Omega))^*$, which is a compact operator (the dual is a space larger than $L^2(\Omega)$).

The trick, hidden in Proposition 3.19, to decompose the Helmholtz "solution-to-data" operator A is to write the analogous operator for the Laplace equation (A_0, invertible) and to verify that the remainder ($K = A - A_0$) is compact as it comes from the lower-order term in the PDE. We will use again the "Helmholtz = Laplace + compact low-order perturbation" trick.

We have proved part of the following proposition. To prove the remaining part (the existence, discreteness and divergence at infinity of the eigenvalues), one needs the spectral theory of self-adjoint compact operators, see e.g. [McLean00, Ch. 2] or [Brezis11, §6]. To treat inhomogeneous Dirichlet boundary conditions $g_D \neq 0$, one uses a "lifting", i.e. a $u_D \in H^1(\Omega)$ such that $\gamma u_D = g_D$ (which exists because of the surjectivity of the trace operator), and then solves for $u_0 = u - u_D \in H_0^1(\Omega)$.

Proposition 4.6: (Well-posedness of the Helmholtz–Dirichlet BVP). For a Lipschitz bounded domain Ω, there exist a sequence of positive numbers $k_1 < k_2 < \ldots$, with $k_j \to \infty$, such that:

- If $k = k_j$ for some j, then the Dirichlet problem (35) is not well-posed.
  In particular, the homogeneous case with $f = 0$ and $g_D = 0$ admits non-trivial solutions.

- If $0 < k \neq k_j$ for all j, then the Dirichlet problem (35) is well-posed in $H^1(\Omega)$ for all $f \in L^2(\Omega)$ and $g_D \in H^{\frac{1}{2}}(\partial\Omega)$.

The smallest of the values k_j equals the inverse of the Poincaré constant of Ω: the smallest value C_P such that $\|u\|_{L^2(\Omega)} \leq C_P \|\nabla u\|_{L^2(\Omega)}$ for all $u \in H_0^1(\Omega)$ is $C_P = 1/k_1$ (this is an easy consequence of the existence of an orthogonal basis of $H_0^1(\Omega)$ made of eigenfunctions).

Exercise 4.7: (Helmholtz–Neumann BVP).

- What are the eigenvalues and the eigenfunctions for the Laplacian with Neumann boundary conditions $\partial_n u = 0$ on the rectangle and on the disc?

- Show that the positive Neumann eigenvalues for a rectangle coincide with the Dirichlet eigenvalues but the eigenfunctions differ. (On the contrary, using subtle properties of the Bessel functions it is possible to see that there are no Neumann eigenvalues of the disc that are also Dirichlet eigenvalues.)

- Write the variational formulation of the Helmholtz–Neumann BVP with inhomogeneous conditions $\partial_n u = g_N \in H^{-\frac{1}{2}}(\partial\Omega)$: the sesquilinear form coincides with that in (36) but the linear functional and the function space differ.

- What are the eigenvalues and the eigenfunctions for the Laplacian on the rectangle when Dirichlet conditions are imposed on some of the sides and Neumann conditions on the others?

A result analogue to Proposition 4.6 holds for the Neumann BVP. The main differences are that the first eigenvalue is $k_1 = 0$ (with multiplicity equal to the number of connected components of Ω), the function space is $H^1(\Omega)$, and the datum regularity is $H^{-\frac{1}{2}}(\partial\Omega)$. Similar considerations hold also for problems with mixed boundary conditions, i.e. with Dirichlet conditions on part of $\partial\Omega$ and Neumann on the remaining part.

Exercise 4.8: (No coercivity for $k > k_1$).
Let u_1, u_2 be Dirichlet eigenfunctions in Ω, associated to different eigenvalues k_1^2 and k_2^2 and normalised as $\|u_1\|_{L^2(\Omega)} = \|u_2\|_{L^2(\Omega)} = 1$. Let $k_1 < k < k_2$, and define $w = u_1 \pm \sqrt{\frac{k^2 - k_1^2}{k_2^2 - k^2}}\, u_2$. Show that $\mathcal{A}(w, w) = 0$.

Deduce that $\mathcal{A}(\cdot, \cdot)$ is not coercive for all k^2 larger than the first Dirichlet eigenvalue.

Hint: recall (or prove) that eigenfunctions associated to different eigenvalues are orthogonal both in $L^2(\Omega)$ and in $H^1(\Omega)$ norms.

Exercise 4.9: (Domain scaling and eigenvalues).
Let Ω be a bounded domain, $\rho > 0$ a constant factor, and $\widehat{\Omega} = \rho\Omega = \{\hat{\mathbf{x}} = \rho\mathbf{x} : \mathbf{x} \in \Omega\}$ be a dilation of Ω. Let Λ be a Dirichlet (or Neumann) eigenvalue of Ω. Show that $\widehat{\Lambda} = \Lambda/\rho$ is a Dirichlet (Neumann, respectively) eigenvalue of $\widehat{\Omega}$.

Deduce that any given $\Lambda > 0$ is Dirichlet eigenvalue of the discs B_ρ only for countably many radii ρ. Given $R > 0$, show that $\Lambda > 0$ is Dirichlet eigenvalue of the discs B_ρ contained in B_R only for a finite number (possibly zero) of radii ρ. Circles with radius ρ can be replaced by the images of diameter ρ of a given domain under similarities (e.g. all squares, or all equilateral triangles,...).

Exercise 4.9 allows to prove the following useful lemma. We will see a different proof as a consequence of Theorem 5.15.

Lemma 4.10: (Helmholtz solutions with both zero traces are zero). Let u be a solution of the homogeneous Helmholtz equation $\Delta u + k^2 u = 0$ in a bounded Lipschitz domain Ω. If both traces on $\partial\Omega$ of u vanish, i.e. $\gamma u = \partial_n u = 0$, then $u = 0$ in Ω.

Proof. By contradiction, assume $u \neq 0$. Let $R > 0$ be such that $\overline{\Omega} \subset B_R$, the disc of radius R. By Remark 3.15, the zero-extension $\widetilde{u} \in L^2(B_R)$, defined as $\widetilde{u}|_\Omega = u$ and $\widetilde{u}|_{B_R \setminus \overline{\Omega}} = 0$, belongs to $H^1(B_R; \Delta)$.

So $\Delta \widetilde{u} \in L^2(B_R)$ and $\Delta \widetilde{u} + k^2 \widetilde{u} = 0$ in the whole of B_R. Since the trace of $\widetilde{u}$ on ∂B_R is 0, $\widetilde{u}$ is a Dirichlet eigenfunction of B_R and k^2 is a Dirichlet eigenvalue. The radius R is arbitrary: k^2 is a Dirichlet eigenvalue for all discs $B_{R'}$ with any $R' > R$. This is in contradiction with Exercise 4.9; the contradiction is resolved only if $\widetilde{u} = 0$, so also $u = 0$. $\qquad\square$

Lemma 4.10 means that a given function u cannot be simultaneously Dirichlet and Neumann eigenfunction of the Laplacian in Ω.

Exercise 4.11: (Absorption gives well-posedness.). Show that the Dirichlet and the Neumann problems

$$\Delta u + k^2 u = -f \quad \text{in } \Omega, \qquad \gamma u = 0 \quad \text{on } \partial\Omega, \quad \text{or}$$
$$\Delta u + k^2 u = -f \quad \text{in } \Omega, \qquad \partial_{\mathbf{n}} u = g_{\mathrm{N}} \quad \text{on } \partial\Omega,$$

are well-posed if $\Im k > 0$, $f \in L^2(\Omega)$ and $g_{\mathrm{N}} \in H^{-\frac{1}{2}}(\partial\Omega)$.

Hint: First write the two BVPs as variational problems $\mathcal{A}(u,w) = \mathcal{F}(w)$ in $H^1_0(\Omega)$ and $H^1(\Omega)$, respectively. Then use Lax–Milgram theorem. To prove the coercivity $|\mathcal{A}(w,w)| \geq c \|w\|^2_{H^1(\Omega)}$ of the sesquilinear form obtained, first control the L^2 norm of u, then the H^1 seminorm by using the triangle inequality.

Deduce a bound on $\|u\|_{H^1(\Omega)}$. The bounding constant C will blow up for $\Im k \searrow 0$.

If instead of sound-soft and sound-hard conditions we have impedance ones we obtain a different result. Consider the **impedance BVP**:

$$\Delta u + k^2 u = -f \quad \text{in } \Omega, \qquad \partial_{\mathbf{n}} u - \mathrm{i}k\vartheta\, \gamma u = g_I \quad \text{on } \partial\Omega, \tag{37}$$

for $\vartheta > 0$, $f \in L^2(\Omega)$, $g_I \in H^{-\frac{1}{2}}(\partial\Omega)$. Its variational form is: find $u \in H^1(\Omega)$ such that

$$\mathcal{A}_I(u,w) := \int_\Omega (\nabla u \cdot \nabla \overline{w} - k^2 u \overline{w})\, \mathrm{d}\mathbf{x} - \mathrm{i}k\vartheta \int_{\partial\Omega} \gamma u\, \gamma\overline{w}\, \mathrm{d}s = \int_\Omega f\overline{w}\, \mathrm{d}\mathbf{x} + \int_{\partial\Omega} g_I\, \gamma\overline{w}\, \mathrm{d}s =: \mathcal{F}_I(w) \quad \forall w \in H^1(\Omega). \tag{38}$$

As before, the sesquilinear form is continuous, coercive only for small k, and satisfies a Gårding inequality since $\Re\{\mathcal{A}_I(w,w)\} = \mathcal{A}(w,w)$. So, by Corollary 3.20, to check the well-posedness we only have to look at the homogeneous problem. If u_0 satisfies (38) with $\mathcal{F}_I = 0$ (i.e. $f = 0$ and $g_I = 0$), taking the imaginary part of $\mathcal{A}_I(u_0, u_0) = 0$, we see that $\gamma u_0 = 0$ on $\partial\Omega$, and from the boundary condition that also $\partial_{\mathbf{n}} u_0 = 0$ on $\partial\Omega$. Then, since $\Delta u_0 + k^2 u_0 = 0$, Lemma 4.10 implies that $u_0 = 0$.

Proposition 4.12: (Well-posedness of interior impedance BVP). The impedance BVP (37) (equivalently, (38)) is well-posed for all $k > 0$.

A slightly different proof can be found in [SBH19, §8.8]; see also [CGLS12, Thm. 2.3].

The Fredholm alternative implies that the solution of the impedance BVP (37) exists and is unique, and also that its $H^1(\Omega_-)$ norm is controlled by the norm of the data (f and g_I). However, the bounding constant is not explicit as in the situations where we can use Lax–Milgram theorem.

Differently from the Dirichlet and the Neumann BVP form $\mathcal{A}(\cdot, \cdot)$, the impedance BVP sesquilinear form $\mathcal{A}_I(\cdot, \cdot)$ is not self-adjoint. This is consistent with the fact that Dirichlet and Neumann eigenvalues are real, while the impedance BVP has no real eigenvalues.

4.2.2 Remarks on eigenvalues, eigenfunctions and interior BVPs

So far we studied the well-posedness of interior Helmholtz BVPs and the presence of eigenvalues. In the following remarks and exercises we observe some properties of eigenfunctions and BVPs. Recall that we have already seen in Remark 1.22 how Dirichlet and Neumann eigenfunctions correspond to TM and TE modes propagating in a waveguide.

Remark 4.13: (What kind of waves are the eigenfunctions?). We have observed in §4.1 that Dirichlet and Neumann boundary conditions reflect waves without losing energy. Roughly speaking, we can interpret Dirichlet and Neumann eigenfunctions as waves that bounce around in Ω forever, without any damping. At the right wavenumber the interference of the wave with itself is constructive (after a full round of bounces the wave has precisely the same phase it started with), so, in a sense, it can exist without a source; see Exercises 4.14–4.15. For example, if Ω is a disc, one can imagine a wave propagating along a regular polygon inscribed in Ω, reflected by $\partial\Omega$ at every corner of the polygon. These are called **creeping waves**, as they "crawl" around $\partial\Omega$ and are small in the centre of Ω, or **whispering gallery modes** (from some circular buildings where a whisper can be heard in any place close to the wall but not in the centre); see Figure 10.

On the other hand, impedance boundary conditions and complex wavenumbers entail some energy absorption (see Exercise 4.18): in this case the waves cannot propagate forever and there are no eigenfunctions for any $k > 0$.

For high frequencies $k \nearrow \infty$ Helmholtz solutions resemble more and more trajectories of particles, or billiard balls on a table, or light rays if the particles are photons. The study of the relationships between the dynamics of "billiard trajectories" and the properties of PDEs with a vanishingly small parameter ($h = k^{-1}$ in $h^2 \Delta u + u = 0$) is the topic of "semiclassical analysis" (the name comes from the analogy with the relation *particles : waves = classical physics : quantum physics*).

Unit disc eigenfunction, $k = 13.3543$: $u(x) = J_9(kr)e^{i9t}$

Figure 10: The Dirichlet eigenfunction $J_9(kr)\mathrm{e}^{\mathrm{i}9\theta}$ with $k = 13.3543$ on the unit disc. This is a typical "creeping wave" or "whispering gallery mode", as it is concentrated along the boundary of the domain.
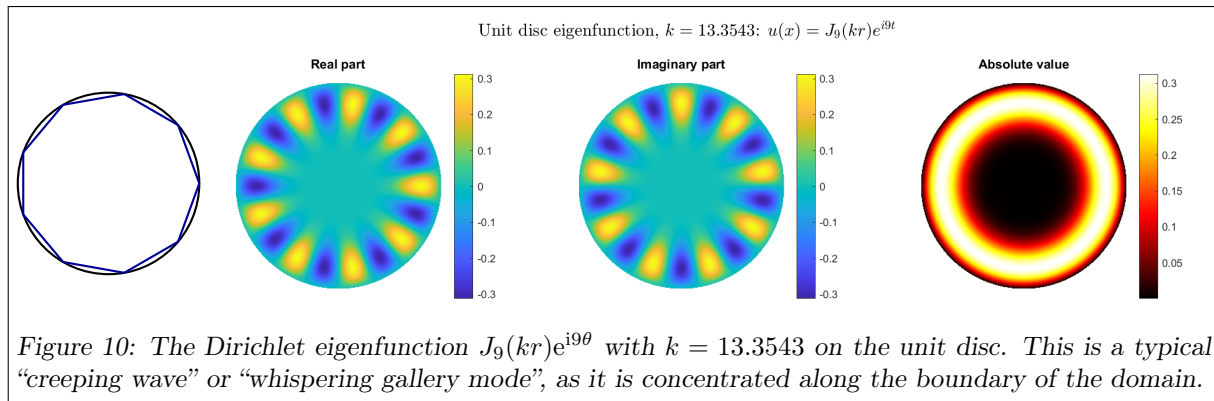
Exercise 4.14: (Billiards and eigenfunctions). Show that for all pairs $j_1, j_2 \in \mathbb{N}$ there is a closed "billiard trajectory" in the unit square $\Omega = (0,1)^2$ whose length is an integer multiple of the wavelength $\lambda_{j_1,j_2} = \frac{2\pi}{k_{j_1,j_2}} = \frac{2}{\sqrt{j_1^2 + j_2^2}}$ of the Dirichlet eigenfunction with indices j_1, j_2.

A "billiard trajectory" is the trajectory of a particle leaving from a point in Ω, moving in a straight line, that is reflected when it hits $\partial\Omega$ with the equal-angle law, and that never hits the corners of Ω. It is closed if it is a loop, i.e. the particle repeats it infinitely many time.
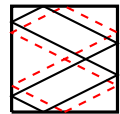
Exercise 4.15: (Plane waves and eigenfunctions of the square).
Fix $j_1, j_2 \in \mathbb{N}$ and define the plane wave $u_{\searrow}(\mathbf{x}) = \mathrm{e}^{\mathrm{i}\pi(j_1 x_1 - j_2 x_2)}$. Write the wave $u_{\nearrow}$ defined as the sound-soft reflection of $u_{\searrow}$ on the line $\{x_2 = 0\}$, using the rules learned in §4.1. Extend these rules to write the wave $u_{\nwarrow}$ defined as the reflection of $u_{\nearrow}$ on the line $\{x_1 = 1\}$, and $u_{\swarrow}$ as the reflection of $u_{\nwarrow}$ on the line $\{x_2 = 1\}$. Show that the reflection of $u_{\swarrow}$ on the line $\{x_1 = 0\}$ is $u_{\searrow}$.
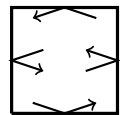
We have found a wave that after four sound-soft reflections on the lines corresponding to the sides of the square $(0,1)^2$ is identical to itself.

Show that $u_{\searrow} + u_{\nearrow} + u_{\nwarrow} + u_{\swarrow}$ is (a multiple of) one of the eigenfunctions of $(0,1)^2$ described at the beginning of this section.

Exercise 4.16: (Resonances are denser at higher frequencies). For any domain Ω, the resonant wavenumbers become denser and denser when their value increase.

Compute numerically and plot all resonant wavenumbers k_j of the unit disc, namely the zeros of all smooth Bessel functions J_ℓ, smaller than a given $k_{\max}$.

Which of them correspond to eigenvalues with multiplicity 1 and which to multiplicity 2? Is there any eigenvalue with multiplicity larger than 2?

Plot the "counting function" $N(k) := \#\{$resonant wavenumbers k_j of $B_1, k_j \leq k\}$, where the resonances are counted with their multiplicity.

A famous result called "Weyl law" states that, for any Lipschitz bounded $\Omega \subset \mathbb{R}^2$ with Lebesgue measure $|\Omega|$, the number of Dirichlet eigenvalues (counted with multiplicity) smaller than a given Λ is approximately $\frac{|\Omega|}{4\pi}\Lambda$. Then the counting function is $N(k) \approx \frac{|\Omega|}{4\pi}k^2$. In particular, the number of resonant wavenumbers in the interval $(k, k+\delta]$ for a fix $\delta > 0$ is $N(k+\delta) - N(k) \approx \frac{|\Omega|}{4\pi}(2k\delta + \delta^2)$, which grows linearly in k.

Do the same for the unit square $(0,1)^2$ (or any rectangle): in this case you can compute analytically all resonant wavenumbers.

A comparison of $N(k)$ and Weyl law for the unit disc and square in the range $k \in (0, 100)$ is plotted in Figure 11. See also [Runborg12, Rem. 2].
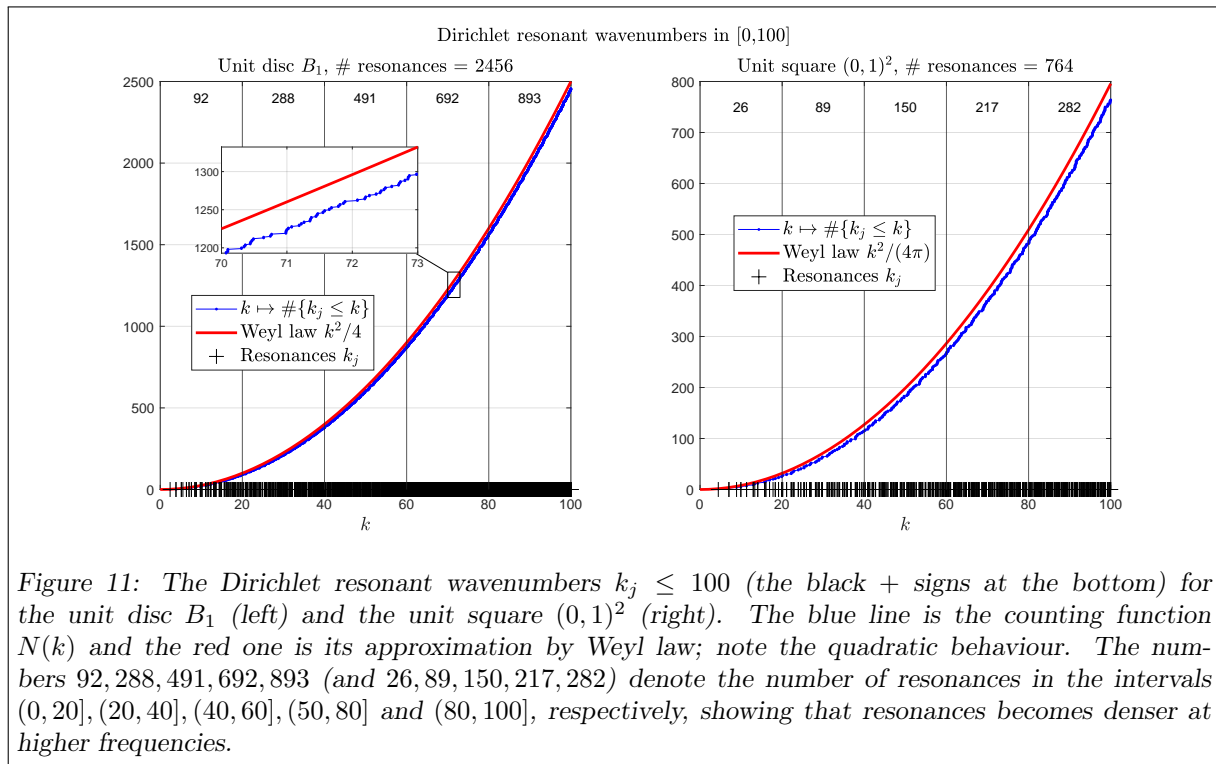
Figure 11: The Dirichlet resonant wavenumbers $k_j \leq 100$ (the black + signs at the bottom) for the unit disc B_1 (left) and the unit square $(0,1)^2$ (right). The blue line is the counting function $N(k)$ and the red one is its approximation by Weyl law; note the quadratic behaviour. The numbers $92, 288, 491, 692, 893$ (and $26, 89, 150, 217, 282$) denote the number of resonances in the intervals $(0, 20], (20, 40], (40, 60], (50, 80]$ and $(80, 100]$, respectively, showing that resonances becomes denser at higher frequencies.

Remark 4.17: (Resonances in different dimensions and musical instruments). In one dimension, the Laplacian is simply the second derivative and its eigenvalue are easy to compute. E.g. on the interval $\Omega = (0, L)$, the Dirichlet resonant wavenumbers are $k_j = \frac{j\pi}{L}$ for $j \in \mathbb{N}$ and the corresponding eigenfunctions are $u_j(x) = \sin(k_j x)$. These frequencies k_j are equally spaced, while the resonant wavenumbers of a two-dimensional domain are distributed more irregularly (see e.g. Figure 11). This has important consequences in music.

Musical instruments produce different notes by exciting resonances. Most instruments rely on the vibrations of a one-dimensional part: air columns in wind instruments and strings in guitars, pianos, and violins (then other parts, such as the soundboard, amplify and modify the sound produced by the strings). The different frequencies excited when plucking a string or blowing a flute are related to one another as the resonant wavenumbers of a one-dimensional interval, so they can produce harmonious sounds. On the other hand, the sound of a drum depends on the disordered resonances of a two-dimensional object, its membrane, leading to a "less musical" sound. The book [Heller13] describes in detail how different musical instruments produce sound.

Exercise 4.18: (Energy conservation and dissipation in time domain). Let $\Omega \subset \mathbb{R}^n$ be a bounded Lipschitz domain with outward-pointing unit normal $\mathbf{n}$, $T > 0$, and let U be a sufficiently smooth real-valued function defined on $\overline{\Omega} \times [0, T]$. Define the "acoustic energy" of U at time $t \in [0, T]$ as the sum of a potential and a kinetic term:

$$\mathcal{E}(U; t) := \frac{1}{2} \int_\Omega \left(|\nabla U(\mathbf{x}, t)|^2 + \frac{1}{c^2} \left(\frac{\partial U}{\partial t}(\mathbf{x}, t) \right)^2 \right) \mathrm{d}\mathbf{x}.$$

- Show that

$$\frac{\partial \mathcal{E}(U; t)}{\partial t} = \int_\Omega \left(\frac{1}{c^2} \frac{\partial^2 U}{\partial t^2} - \Delta U \right) \frac{\partial U}{\partial t} \, \mathrm{d}\mathbf{x} + \int_{\partial \Omega} \partial_\mathbf{n} U \, \frac{\partial U}{\partial t} \, \mathrm{d}s.$$

- Assume that U is solution of the homogeneous wave equation (6), and either U satisfies homogeneous Dirichlet ($\gamma U = 0$ on $\partial \Omega \times [0, T]$) or Neumann ($\partial_\mathbf{n} U = 0$ on $\partial \Omega \times [0, T]$) conditions.

  Deduce that its energy remains constant in time: $\mathcal{E}(U; t) = \mathcal{E}(U; 0)$ for all t.

- Deduce that if the wave solution U satisfies the homogeneous impedance boundary condition $\partial_\mathbf{n} U + \frac{\theta}{c} \frac{\partial U}{\partial t} = 0$ with $\theta > 0$ (recall §1.1.1), then the energy decreases in time: $\mathcal{E}(U; t_2) \leq \mathcal{E}(U; t_1)$ for all $0 \leq t_1 < t_2 \leq T$.

  This is the case of "passive" boundary surfaces; "active" surfaces have $\theta < 0$ and produce energy.

Remark 4.19: (Limiting amplitude principle). We know from §1.2 that a solution $u(\mathbf{x})$ of a Helmholtz BVP corresponds to a time-harmonic $U(\mathbf{x}, t)$ that solves the wave equation. Can we compute or approximate u by solving an initial–boundary value problem (IBVP) for the wave equation?

For instance, if u solves the Dirichlet BVP (35), then $U(\mathbf{x},t) = \Re\{u(\mathbf{x})\mathrm{e}^{-\mathrm{i}\omega t}\}$ solves the Dirichlet IBVP

$$
\begin{aligned}
\frac{1}{c^2}\frac{\partial^2 U}{\partial t^2}(\mathbf{x},t) - \Delta U(\mathbf{x},t) &= \Re\{f(\mathbf{x})\mathrm{e}^{-\mathrm{i}\omega t}\} && \text{in } \Omega \times (0,T), \\
U(\mathbf{x},0) &= u_0(\mathbf{x}) && \text{in } \Omega, \\
\frac{\partial U}{\partial t}(\mathbf{x},0) &= u_1(\mathbf{x}) && \text{in } \Omega, \\
U(\mathbf{x},t) &= \Re\{g_{\mathrm{D}}(\mathbf{x})\mathrm{e}^{-\mathrm{i}\omega t}\} && \text{on } \partial\Omega \times (0,T).
\end{aligned}
\tag{39}
$$

with $u_0 = \Re u$ and $u_1 = \omega\Im u$ and any choice of $T > 0$. This is a well-posed problem, but we cannot use it to find u because the initial conditions u_0, u_1 require to know u itself.

On the other hand, we can easily check that the solution U of any IBVP in the form (39) can be decomposed as $U = \Re\{u_\star(\mathbf{x})\mathrm{e}^{-\mathrm{i}\omega t}\} + \widetilde{U}$, where the two terms solve

$$
\begin{cases}
-\Delta u_\star - k^2 u_\star = f & \text{in } \Omega, \\
u_\star = g_{\mathrm{D}} & \text{on } \partial\Omega,
\end{cases}
\qquad
\begin{cases}
\dfrac{1}{c^2}\dfrac{\partial^2 \widetilde{U}}{\partial t^2}(\mathbf{x},t) - \Delta\widetilde{U}(\mathbf{x},t) = 0 & \text{in } \Omega \times (0,T), \\[2mm]
\widetilde{U}(\mathbf{x},0) = u_0(\mathbf{x}) - \Re u_\star(\mathbf{x}) & \text{in } \Omega, \\[2mm]
\dfrac{\partial\widetilde{U}}{\partial t}(\mathbf{x},0) = u_1(\mathbf{x}) - \omega\Im u_\star(\mathbf{x}) & \text{in } \Omega, \\[2mm]
\widetilde{U}(\mathbf{x},t) = 0 & \text{on } \partial\Omega \times (0,T).
\end{cases}
$$

This means that any wave IBVP solution with time-harmonic data is sum of a time-harmonic term ($u_\star$) and a "transient" wave solution ($\widetilde{U}$) generated only by the initial conditions (i.e. with zero source and boundary conditions). The same argument holds for Neumann or impedance boundary conditions.

Assume that, for some class of initial data, after some time $T^\dagger$ the term $\widetilde{U}$ "dies out", i.e. $\widetilde{U}(\mathbf{x},t) \approx 0$ for $t \geq T^\dagger$. This means that, after a possibly large time, the value of U depends only on the source and the boundary data, while the initial data have been "forgotten". Then, $U(\mathbf{x},t) \approx \Re\{u_\star(\mathbf{x})\mathrm{e}^{-\mathrm{i}\omega t}\}$ for $t \geq T^\dagger$ and $u_\star(\mathbf{x}) \approx U(\mathbf{x},\frac{2\pi j}{\omega}) + \mathrm{i}U(\mathbf{x},\frac{2\pi j + \pi/2}{\omega})$ for some $j \in \mathbb{N}$ with $\frac{2\pi j}{\omega} \geq T^\dagger$. So we can compute the Helmholtz solution $u_\star$ by solving the IBVP (39) with some choice of u_0, u_1 (e.g. $u_0 = u_1 = 0$), instead of solving the Helmholtz BVP (35). This is analogous to the convergence in time of solutions of parabolic PDEs with time-independent sources to solutions of elliptic PDEs (e.g., if $-\frac{\partial V}{\partial t} + \Delta V = f$, $\gamma V = g$, then $\lim_{t\to\infty} V = v$ with $-\Delta v = f$, $\gamma v = g$). The fact that wave solutions with time-harmonic sources converge to Helmholtz solutions for large times is called "**limiting amplitude principle**" and is a classical topic in mathematical physics[23].

Is this assumption true? For Dirichlet and Neumann problems in bounded domains: no, it is false because energy is preserved for all times and transient solutions $\widetilde{U}$ never decay, as proved in Exercise 4.18. On the other hand, for problems posed in unbounded domains, such as those that we will consider from §4.3, if the geometry is "non-trapping", i.e. no wave can be trapped but they all dissipate towards infinity, then the limiting amplitude principle holds. The presence of damping, either in the volume as in Exercises 1.5 and 1.14 or in impedance boundary conditions, is another way to ensure the decay to zero of the transient solution $\widetilde{U}$ and thus the validity of the limiting amplitude principle.

Some numerical methods for approximating Helmholtz BVPs by solving wave IBVPs have been developed, exploiting efficient time-stepping schemes and enforcing convergence to time-periodic solutions. Two examples are the "WaveHoltz method"[24] and the "controllability method"[25].

4.3 EXTERIOR BOUNDARY VALUE PROBLEMS

A typical problem in computational wave propagation is that of **scattering**. In a scattering problem we want to compute how a given incoming wave is perturbed by the interaction with an obstacle. Here we consider only bounded, sound-soft obstacles.

Different physical phenomena intervene in the interaction between a wave and an obstacle: reflection, diffraction and refraction. When the obstacle is perfectly flat and impenetrable, as in §4.1, the wave is simply reflected. When the obstacle is not flat but curved or has corners, the wave is also diffracted: this will be our main concern. When the obstacle is penetrable, the wave is also refracted (recall Remark 1.15).

We fix some notation. Let $\boxed{\Omega_-} \subset \mathbb{R}^2$ be a bounded Lipschitz domain, denote $\boxed{\Omega_+} := \mathbb{R}^2 \setminus \overline{\Omega_-}$ and $\boxed{\Gamma} = \partial\Omega_-$. We will always assume that Ω_+ is connected, i.e. Ω_- has no holes. We choose the unit normal

[23][Morawetz, The limiting amplitude principle, CPAM 1962]
[24][Appelö, Garcia, Runborg, WaveHoltz: Iterative solution of the Helmholtz equation via the wave equation, SISC 2020]
[25][Grote, Tang, On controllability methods for the Helmholtz equation, JCAM 2019]

vector field $\boxed{\mathbf{n}}$ on Γ that points out of Ω_- and into Ω_+. We need to take traces of fields defined in Ω_- and in Ω_+: for clarity we write $\boxed{\gamma^\pm}$ and $\boxed{\partial_{\mathbf{n}}^\pm}$ for the traces taken from Ω_+ and Ω_-. If $u \in H^1_{\mathrm{loc}}(\mathbb{R}^2)$ then $\gamma^+ u = \gamma^- u$ by Remark 3.15 (and we may write γu); if instead $u \in H^1_{\mathrm{loc}}(\Omega_- \cup \Omega_+)$ then $\gamma^+ u$ and $\gamma^- u$ might differ. The same holds for the Neumann traces $\partial_{\mathbf{n}}^\pm$ and the $H^1(\cdot; \Delta)$ spaces.

Let $\boxed{u^{\mathrm{Inc}}}$ be the incoming wave, or incident wave, a given Helmholtz solution which will be the datum of our scattering problem. We want to find the field $\boxed{u^{\mathrm{Scat}}}$ scattered by Ω_-, that is a Helmholtz solution in the exterior domain Ω_+ and such that $\gamma(u^{\mathrm{Tot}}) = 0$ on Γ, where $\boxed{u^{\mathrm{Tot}}} = u^{\mathrm{Inc}} + u^{\mathrm{Scat}}$. We see in the next section that these two conditions are not enough to determine u^{Scat}.

4.3.1 EXAMPLE: SCATTERING BY A DISC

Let us consider a simple example using separation of variables. Assume that (i) $\Omega_- = B_R$ is the disc of radius $R > 0$ centred at the origin, and (ii) the trace of u^{Inc} on Γ is a circular harmonic, in polar coordinates $(\gamma^+ u^{\mathrm{Inc}})(R, \theta) = \mathrm{e}^{\mathrm{i}\ell\theta}$ for some $\ell \in \mathbb{Z}$. From §2.3, we know that all fields in the form[26]

$$u^{\mathrm{Scat}}_\lambda(r, \theta) = -\lambda \frac{H^{(1)}_\ell(kr)}{H^{(1)}_\ell(kR)} \mathrm{e}^{\mathrm{i}\ell\theta} - (1 - \lambda) \frac{H^{(2)}_\ell(kr)}{H^{(2)}_\ell(kR)} \mathrm{e}^{\mathrm{i}\ell\theta}, \qquad \lambda \in \mathbb{C}, \tag{40}$$

are Helmholtz solutions in Ω_+ and satisfy $\gamma^+(u^{\mathrm{Inc}} + u^{\mathrm{Scat}}_\lambda) = 0$ on the circle Γ. Which value of λ should we choose?

The scattered field is produced by the interaction of the obstacle Ω_- and the incoming field u^{Inc}. So it should look like a wave propagating away from Ω_- towards infinity.

First of all, we would like $|u(\mathbf{x})|$ to decrease to zero for $r \to \infty$ (the further we are from a sound source, the weaker the sound we hear). In particular if $|u(\mathbf{x})|^2 \sim r^{-1}$ for $r \to \infty$, then the "energy" $\int_{\{|\mathbf{x}|=R\}} |u|^2 \, \mathrm{d}s$ is bounded for $R \to \infty$. All Fourier–Bessel and Fourier–Hankel functions decay as $\sqrt{2/(\pi kr)}$ for $r \to \infty$, so this does not help choosing λ. All fields $u^{\mathrm{Scat}}_\lambda$ in (40) belong to $L^2_{\mathrm{loc}}(\Omega_+)$ and $H^1_{\mathrm{loc}}(\Omega_+)$, but none of them belongs to $L^2(\Omega_+)$: function spaces do not select the desired λ.

If we plot u^{Scat} in a position $\mathbf{x}$ very far from Ω_-, we expect it to point away from Ω_-, i.e. radially towards infinity. We would like u^{Scat} close to $\mathbf{x}$ to look like a plane wave pointing away from Ω_-, i.e. in the direction $\mathbf{d} = \frac{\mathbf{x}}{r}$:
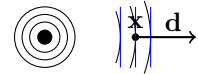
$$u^{\mathrm{Scat}}(\mathbf{x}) \approx A\mathrm{e}^{\mathrm{i}k\mathbf{x}\cdot\frac{\mathbf{x}}{r}} = A\mathrm{e}^{\mathrm{i}kr} \qquad \mathbf{x} = (r\cos\theta, r\sin\theta).$$

Here $A \in \mathbb{C}$ includes the amplitude, proportional to $\frac{1}{\sqrt{r}}$, and the phase of the wave.

We recall that Bessel functions with large arguments can be approximated by the following formulas, [CK2, (3.105)]:

$$J_\ell(z) = \sqrt{\frac{2}{\pi z}} \cos\left(z - \frac{\ell\pi}{2} - \frac{\pi}{4}\right)\left(1 + \mathcal{O}\left(\frac{1}{z}\right)\right), \quad Y_\ell(z) = \sqrt{\frac{2}{\pi z}} \sin\left(z - \frac{\ell\pi}{2} - \frac{\pi}{4}\right)\left(1 + \mathcal{O}\left(\frac{1}{z}\right)\right), \quad z \to \infty.$$

Recalling the relations (23) between Bessel and Hankel functions, we can write the scattered field as

$$u^{\mathrm{Scat}}_\lambda(\mathbf{x}) \approx -\sqrt{\frac{2}{\pi kr}}\left(\lambda \frac{\mathrm{e}^{\mathrm{i}(kr - \frac{\ell\pi}{2} - \frac{\pi}{4} + \ell\theta)}}{H^{(1)}_\ell(kR)} + (1 - \lambda)\frac{\mathrm{e}^{\mathrm{i}(-kr + \frac{\ell\pi}{2} + \frac{\pi}{4} + \ell\theta)}}{H^{(2)}_\ell(kR)}\right)\left(1 + \mathcal{O}\left(\frac{1}{kr}\right)\right). \tag{41}$$

We see that the $H^{(1)}_\ell$ term gives a factor $\mathrm{e}^{\mathrm{i}kr}$, while $H^{(2)}_\ell$ term gives a factor $\mathrm{e}^{-\mathrm{i}kr}$. This means that only the first component is propagating outward, while the second one is directed towards the origin. So we want to keep the first term only and choose $\lambda = 1$.

Another way to see that the $\mathrm{e}^{\mathrm{i}kr}$ terms are outgoing is to recall the meaning of time-harmonic waves, as described in §1.2. For $u(\mathbf{x}) = r^{-1/2}\mathrm{e}^{\mathrm{i}kr}$, the time-dependent field (10) is $U(\mathbf{x}, t) = r^{-1/2}\cos(kr - \omega t) = r^{-1/2}\cos(k(r - ct))$ which spreads (in time) radially from the origin. Conversely, $\tilde{u}(\mathbf{x}) = r^{-1/2}\mathrm{e}^{-\mathrm{i}kr} = \overline{u}(\mathbf{x})$ gives $\tilde{U}(\mathbf{x}, t) = r^{-1/2}\cos(kr + \omega t) = U(\mathbf{x}, -t)$ which moves towards the origin. See also Figure 13 for another way of reading the direction of propagation of a Fourier–Hankel function.

Exercise 4.20: (Circular wave motion). Using the Matlab code provided, make time-harmonic animations of different combinations of Fourier–Bessel and Fourier–Hankel functions and observe in which direction they propagate.

---

[26]Here we have chosen the Hankel functions, as opposed to J_ℓ and Y_ℓ, because they are different from 0 for all values of kR, so we can normalise as written.

Figure 12: (Ex. *4.21.*) *Scattering of a plane wave with direction* $\mathbf{d} = (\frac{\sqrt{3}}{2}, \frac{1}{2})$ *by a a sound-soft disc with radius 0.25 at $k = 30$. Top: scattered field; bottom: total field. We can observe that the u^{Scat} field is strongest in the shadow region, and has phase opposite to u^{Inc}, so that u^{Tot} is minimal there. In u^{Tot} we see the complicated pattern produced by the interference between u^{Scat} and u^{Inc}.*

For a general u^{Inc}, we can expand its trace on the circle Γ in circular harmonics as $u^{\mathrm{Inc}}(R, \theta) = \sum_{\ell \in \mathbb{Z}} a_\ell \mathrm{e}^{\mathrm{i}\ell\theta}$. The scattered field and the total field are then

$$u^{\mathrm{Scat}}(r, \theta) = -\sum_{\ell \in \mathbb{Z}} a_\ell \frac{H_\ell^{(1)}(kr)}{H_\ell^{(1)}(kR)} \mathrm{e}^{\mathrm{i}\ell\theta}, \qquad u^{\mathrm{Tot}}(\mathbf{x}) = u^{\mathrm{Inc}}(\mathbf{x}) + u^{\mathrm{Scat}}(\mathbf{x}).$$

This choice ensures that (i) u^{Scat} is Helmholtz solution in Ω_+, (ii) $\gamma^+ u^{\mathrm{Tot}} = 0$ on Γ, and (iii) u^{Scat} is made of outgoing waves only. This expression of the scattered field as combination of Fourier–Hankel functions is called **multipole expansion**. In electromagnetics similar expansions are also called "Mie series".

You can see an example of scattered field computed with this formula in Figure 12 and on the webpage[9].

Exercise 4.21: (Scattering of a plane wave by a disc). Let u^{Inc} be a plane wave with direction $\mathbf{d}$.
Compute the field scattered by a disc of radius R using Jacobi–Anger formula (25).
Reproduce the plots in Figure 12.
The sum over $\ell \in \mathbb{Z}$ has to be truncated at $|\ell| \leq \ell_{\max}$, with $\ell_{\max}$ (slightly) larger than kR. Plot the magnitude of the coefficients $\hat{u}_\ell$ in $u^{\mathrm{Scat}}(\mathbf{x}) = \sum_{\ell \in \mathbb{Z}} \hat{u}_\ell H_\ell^{(1)}(kr) \mathrm{e}^{\mathrm{i}\ell\theta}$ to justify this choice.

Exercise 4.22: (Scattering of a circular wave by a disc).

1. Using the "Graf's addition theorem" in [DLMF, eq. 10.23.7], derive the formula

$$H_0^{(1)}(k|\mathbf{x} - \mathbf{y}|) = \sum_{\ell \in \mathbb{Z}} H_\ell^{(1)}(k|\mathbf{y}|) \mathrm{e}^{-\mathrm{i}\ell\theta_{\mathbf{y}}} J_\ell(k|\mathbf{x}|) \mathrm{e}^{\mathrm{i}\ell\theta_{\mathbf{x}}} \qquad \forall \mathbf{x}, \mathbf{y} \in \mathbb{R}^2, \quad |\mathbf{x}| < |\mathbf{y}|. \tag{42}$$

Here $\theta_{\mathbf{x}}$ and $\theta_{\mathbf{y}}$ are the angular coordinates of $\mathbf{x}$ and $\mathbf{y}$.

2. Let $u^{\mathrm{Inc}}(\mathbf{x}) = H_0^{(1)}(k|\mathbf{x} - \mathbf{y}|)$ be a 0-order Fourier–Hankel function centred at $\mathbf{y} \in \mathbb{R}^2 \setminus \overline{B_R}$, $R > 0$. Show that, for this incoming field, the field scattered by the disc B_R, is

$$u^{\mathrm{Scat}}(r, \theta) = \sum_{\ell \in \mathbb{Z}} \frac{J_\ell(kR) H_\ell^{(1)}(k|\mathbf{y}|) \mathrm{e}^{-\mathrm{i}\ell\theta_{\mathbf{y}}}}{H_\ell^{(1)}(kR)} H_\ell^{(1)}(kr) \mathrm{e}^{\mathrm{i}\ell\theta} \qquad r > R.$$

3. Plot the scattered and the total fields.
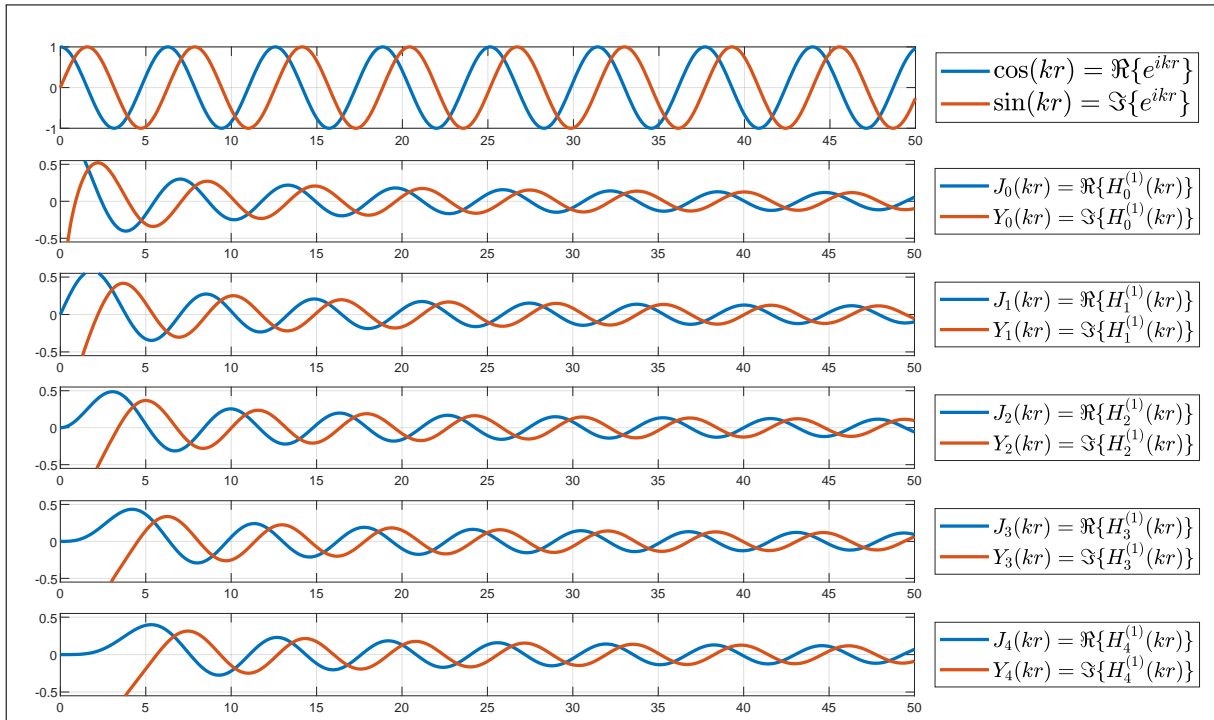
Figure 13: *How can we see that $u(\mathbf{x}) = H_\ell^{(1)}(kr)e^{i\ell\theta}$ moves outwards from its definition? In this figure we compare the real part (blue continuous lines) and the imaginary part (red dashed line) of these circular waves for $\ell = 1, 2, 3, 4$ and $k = 1$ along a ray from the origin $(0,0)$ (left) to the point $(50,0)$ (right). We see that the imaginary part is always slightly "ahead" of the real part. Recall Exercise 1.13: the time-dependent wave $U(\mathbf{x}, t)$, after taking value $\Re u(x)$ will take value $\Im u(x)$. From the figures we see that this means that u is moving from left to right, i.e. from the origin towards infinity.*
For comparison, in the first row we see the real and the imaginary parts of a plane wave propagating to the right.

4.3.2 SOUND-SOFT SCATTERING PROBLEMS

We have seen how to select "outgoing" waves using the expansion in polar coordinates. How to do the same when this expansion is not available, namely when Ω_- is not a circle?

The radial dependence of all the outgoing terms in the circular wave approximation (41) is $\frac{1}{\sqrt{r}}e^{ikr}$ (ignoring high-order terms). Deriving with respect to the radial direction r we have $\partial_r(\frac{1}{\sqrt{r}}e^{ikr}) = ik\frac{1}{\sqrt{r}}e^{ikr} - \frac{1}{2}r^{-3/2}e^{ikr}$. So, if u^{Scat} is a linear combination of $H_\ell^{(1)}(kr)e^{i\ell\theta}$ for different ℓs, then it satisfies $\partial_r u^{\mathrm{Scat}} - iku^{\mathrm{Scat}} = \mathcal{O}(r^{-3/2})$. On the other hand, the bad terms $H_\ell^{(2)}(kr)e^{i\ell\theta}$ satisfy only the condition with the opposite sign $\partial_r u + iku = \mathcal{O}(r^{-3/2})$ (recall that $H_\ell^{(2)} = \overline{H_\ell^{(1)}}$). This suggests the following classical definition[27].

> **Definition 4.23: (Radiating/outgoing solution).** Let u be an $H_{\mathrm{loc}}^1(\mathbb{R}^2 \setminus \overline{B_R})$ solution of the Helmholtz equation in the complement of a ball. We say that u is **radiating**, or **outgoing**, if it satisfies the **Sommerfeld radiation condition**:
> $$|\partial_r u - iku| = o(r^{-1/2}) \qquad r \to \infty. \tag{43}$$

Sommerfeld condition is meant to hold uniformly in all directions, namely

$$\lim_{r \to \infty} \sup_{\theta \in [0, 2\pi]} \sqrt{r}|\partial_r u(r, \theta) - iku(r, \theta)| = 0.$$

Since radiating solutions can be expanded in series of Fourier–Hankel functions, Sommerfeld condition (43) is equivalent (for Helmholtz solutions only) to the apparently stronger condition

$$\exists C, R > 0 \quad \text{such that} \quad |\partial_r u(r, \theta) - iku(r, \theta)| \leq Cr^{-3/2} \qquad \forall r > R, \quad \theta \in [0, 2\pi].$$

---

[27]For the history of the Sommerfeld radiation condition see [Schot, Eighty years of Sommerfeld's radiation condition, 1992].

Sommerfeld condition also implies that $\lim_{R\to\infty}\int_{\partial B_R}|\partial_r u - \mathrm{i}ku|^2\,\mathrm{d}s = 0$, $\partial B_R = \{\mathbf{x}:|\mathbf{x}|=R\}$. The approximation (41) implies that all linear combinations of $H_\ell^{(1)}(kr)\mathrm{e}^{\mathrm{i}\ell\theta}$ that converge outside of some ball are radiating. On the the other hand, no $H_\ell^{(2)}(kr)\mathrm{e}^{\mathrm{i}\ell\theta}$ term is allowed in radiating functions. The complex-conjugate of a radiating function is not radiating.

A more rigorous derivation of the Sommerfeld radiation condition can be done using the "limiting absorption principle": first consider the problem with absorption, i.e. $\Im k > 0$, where the $\mathrm{e}^{\mathrm{i}kr}$ behaviour corresponds to solutions decaying towards infinity, then study the limit for $\Im k \searrow 0$.

We can now define the class of exterior boundary value problems that we will consider in the following.

Definition 4.24: (Exterior Dirichlet problem—EDP). Let Ω_- be a bounded Lipschitz domain, $k > 0$ and $g_\mathrm{D} \in H^{\frac{1}{2}}(\Gamma)$. We say that $u \in H^1_\mathrm{loc}(\Omega_+)$ satisfies the exterior Helmholtz Dirichlet problem if

$$
\begin{aligned}
\Delta u + k^2 u &= 0 && \text{in } \Omega_+, \\
\gamma^+ u &= g_\mathrm{D} && \text{on } \Gamma, \\
u \text{ is radiating.} &&&
\end{aligned}
\tag{44}
$$

In the language of scattering theory:

Definition 4.25: (Sound-soft scattering problem—SSSP). Let Ω_- a bounded Lipschitz domain, $k > 0$ and u^Inc is a Helmholtz solution in a neighbourhood of Γ. We say that $u^\mathrm{Scat} \in H^1_\mathrm{loc}(\Omega_+)$ satisfies the sound-soft scattering problem if

$$
\begin{aligned}
\Delta u^\mathrm{Scat} + k^2 u^\mathrm{Scat} &= 0 && \text{in } \Omega_+, \\
\gamma^+(u^\mathrm{Scat} + u^\mathrm{Inc}) &= 0 && \text{on } \Gamma, \\
u^\mathrm{Scat} \text{ is radiating.} &&&
\end{aligned}
\tag{45}
$$

The sound-soft scattering problem is an exterior Dirichlet problem with $u = u^\mathrm{Scat}$ and $g_\mathrm{D} = -\gamma^+ u^\mathrm{Inc}$. We will see in §4.4 that problems (44) and (45) are well-posed.

Figure 14: Diagram of the sound-soft scattering problem (45).
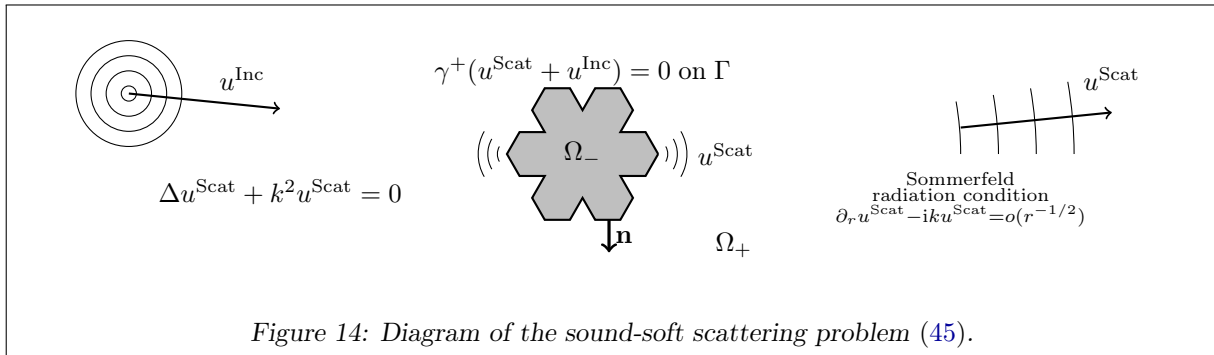
In Definition 4.25 we have assumed that u^Inc is defined only in a neighbourhood of the scatterer's boundary. If the incoming wave is a plane wave, then of course it is defined in the whole of $\mathbb{R}^2$, but this definition allows to include more realistic incoming waves such as "point sources", i.e. Fourier–Hankel functions centred at some point of Ω_+.

The EDP and the SSSP are defined and analysed in details in, e.g., [CK2, §3.2]. However, [CK2] focuses on the 3D case (so the powers of r in the Sommerfeld condition are different) and C^m spaces rather than Sobolev spaces; the 2D case is described more briefly in [CK2, §3.5].

Besides the EDP (44), one can define exterior Neumann and impedance BVPs, by simply replacing the boundary condition on Γ. The Sommerfeld radiation condition, being related to the field behaviour far from the scatterer, is unaffected.
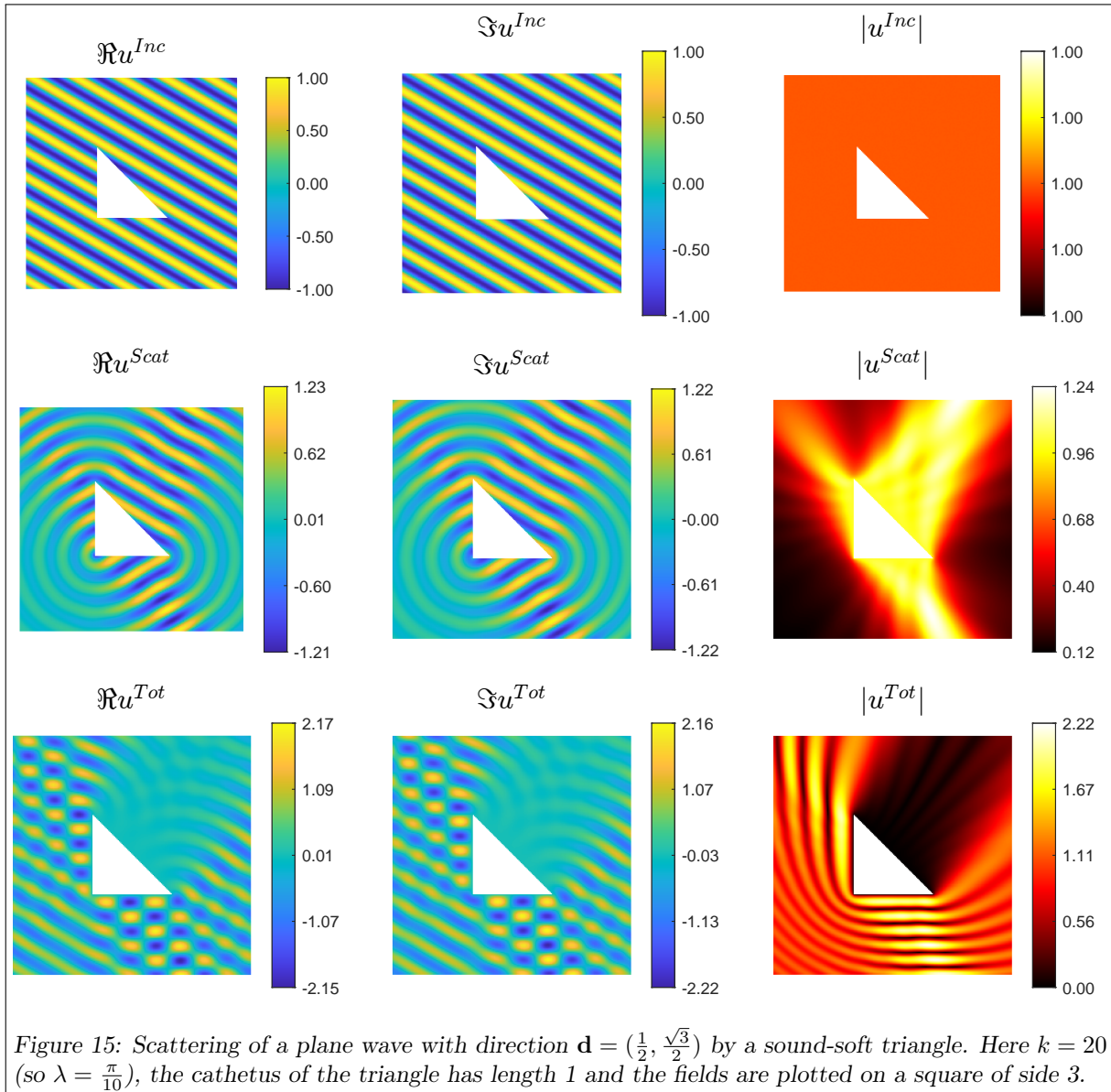
Figure 15: Scattering of a plane wave with direction $\mathbf{d} = (\frac{1}{2}, \frac{\sqrt{3}}{2})$ by a sound-soft triangle. Here $k = 20$ (so $\lambda = \frac{\pi}{10}$), the cathetus of the triangle has length 1 and the fields are plotted on a square of side 3.

4.3.3 Remarks and exercises on scattering problems

Remark 4.26: (Truncated problems). Often one does not want to deal with BVPs posed on unbounded domains such as in Definition 4.25, for example because one wants to approximate the solution with a finite element method. A possibility to reduce this problem to one posed on a bounded domain is to choose a large ball B_R (or a different shape) with $\Omega_- \subset B_R$ and solve a Helmholtz BVP on the truncated domain $B_R \cap \Omega_+$. On Γ we impose the Dirichlet condition as above. On the artificial boundary $\Gamma_R = \partial B_R$ one has to impose some artificial boundary condition that mimics the Sommerfeld radiation condition. The simplest choice is to choose impedance conditions $\partial_r u^{\text{Scat}} - iku^{\text{Scat}} = 0$ (compare with (43)). Many more efficient and more complicated boundary conditions exist. They are called absorbing, non-reflecting, radiation, generalised-impedance boundary conditions (ABC, NRBC, GIBC...); a related concept is that of perfectly matched layer (PML). The quality of an artificial boundary condition depends on the ability to absorb the waves coming from the domain and to not reflect them back. See some examples in [Ihlenburg98, Ch. 3].

Remark 4.27: (Far-field pattern). It is possible to prove (e.g. [CK2, eq. (3.109)]) that if u is a radiating Helmholtz solution, then it satisfies

$$u(\mathbf{x}) = \frac{e^{ikr}}{\sqrt{r}} \Big(u_\infty(\theta) + \mathcal{O}(r^{-1}) \Big) \qquad \text{for } r = |\mathbf{x}| \to \infty, \tag{46}$$

for a function $u_\infty \in C^\infty(\mathbb{S}^1)$ (recall that $\mathbb{S}^1$ is the unit circle, and that θ denotes the angular polar coordinate of $\mathbf{x}$). This means that, up to factoring out the phase factor e^{ikr} and the decay factor $\frac{1}{\sqrt{r}}$, when we move

Figure 16: *The Poynting vectors* $\mathbf{S}(u^{\mathrm{Scat}})$ *for the scattering problems in Figures 12 and 15. See Exercise 2.15.*
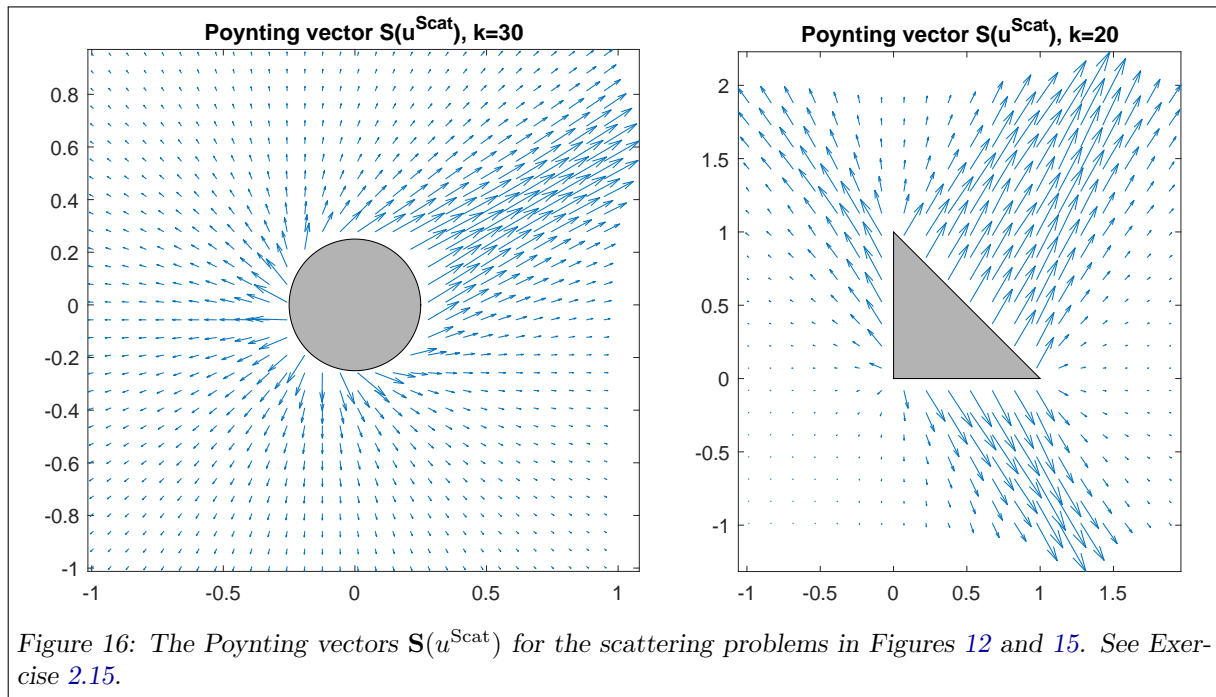
towards infinity along a straight line in the direction θ, a radiating field converges to a given value $u_\infty(\theta)$. The function u_∞ is called **far-field pattern**. If u is defined in Ω_+ and admits Dirichlet and Neumann traces on Γ, the far-field pattern can be computed using the formula

$$u_\infty(\theta) = \frac{\mathrm{e}^{\mathrm{i}\frac{\pi}{4}}}{\sqrt{8\pi k}} \int_\Gamma \left(\gamma^+ u(\mathbf{y}) \partial_{\mathbf{n}}^+ \mathrm{e}^{-\mathrm{i}k\mathbf{y}\cdot\mathbf{d}} - \partial_{\mathbf{n}}^+ u(\mathbf{y}) \mathrm{e}^{-\mathrm{i}k\mathbf{y}\cdot\mathbf{d}} \right) \mathrm{d}s(\mathbf{y}) \qquad \mathbf{d} = (\cos\theta, \sin\theta). \qquad (47)$$

The far-field pattern is one of the main quantities of interest in remote-sensing applications, for example to quantify the amount of radiation "backscattered" by an obstacle when it is hit by a wave. In electromagnetics, the "radar cross section" (RCS), which measures e.g. how stealth is an aircraft, is proportional to the logarithm of the magnitude of the far-field of the scattered electric field. You can see the far-field pattern of the wave scattered by a triangle in Figure 17.

Figure 17: *Some polar logarithmic plots (Matlab's* `polarplot` *command) of the magnitudes of far-field patterns* $\log_{10}|u_\infty|$. *In this scattering problem, a plane wave with direction* $\frac{\pi}{3}$ *hits a sound-soft triangular scatterer* ◣ *with vertices* $(0,0)$, $(1,0)$ *and* $(0,1)$, *as in Figure 15. Each plot corresponds to a different wavenumber* ($k = 5, 10, 20, 40$): *for increasing frequencies the far field becomes more complex and focused in few directions. The far-field pattern has maximal intensity in the direction* $\frac{\pi}{3}$ *of the incoming wave (up right), where the triangle projects its shadow. Two other peaks are in directions* $-\frac{\pi}{3}$ *and* $\frac{2\pi}{3}$, *corresponding to the wave reflected by the two illuminated sides. The field in all other directions is due to the diffraction by the corners. The far-field patterns were computed numerically with the BEM described in §5.2. The values* $-\min_{0\le\theta<2\pi}\log_{10}|u_\infty(\theta)|$ *(i.e. the values* $0.641, \ldots, 1.13$ *in the figure titles) have been added to* $\log_{10}|u_\infty(\theta)|$ *to ensure that the curves are positive.*

Exercise 4.28: (Far-field pattern of a plane wave scattered by a disc). Compute (as a circular harmonic expansion) and plot with Matlab the far-field pattern of the field scattered by a disc hit by a plane wave. Use the Fourier expansion computed in Exercise 4.21. Study how the far-field pattern vary with k, R and the propagation direction of u^{Inc}. Denote $u_\infty(\theta, \xi)$ the far-field for $u^{\mathrm{Inc}}(\mathbf{x}) = \mathrm{e}^{\mathrm{i}k(x_1 \cos \xi + x_2 \sin \xi)}$: can you find any symmetry between the two angles? See [CK2, Thm. 3.23].

Exercise 4.29: (Phased array). The far-field pattern u_∞ can be computed for any radiating Helmholtz solution u, non only for solutions of an EDP. Formula (47) can be applied taking as Γ any boundary such that u is a radiating Helmholtz solution in the region exterior to it. For instance, Γ can be taken as a circle ∂B_R with sufficiently large radius.

Compute and plot the far-field pattern generated by the **phased array** $u(\mathbf{x}) = \sum_{j=1}^J \mathrm{e}^{\mathrm{i}\beta j} H_0^{(1)}(k|\mathbf{x} - \mathbf{x}_j|)$, for a phase shift β and a set of aligned sources (e.g. $\mathbf{x}_j = (-\frac{1}{2} + \frac{j}{J}, 0)$ on the segment $[(-\frac{1}{2}, 0), (\frac{1}{2}, 0)]$). Plot also the near field $u(\mathbf{x})$ (see also the course page[9]). Observe how the phase shift β steers the direction of the emitted wave. What is the effect of the source spacing $|\mathbf{x}_{j+1} - \mathbf{x}_j|/\lambda$?

Phased arrays are used for **beam forming**: to emit strong (electromagnetic, usually) waves in any desired direction without moving the antenna. This is routinely used in wi-fi routers, 5G antennas, radar, sonar, and ultrasound imaging.
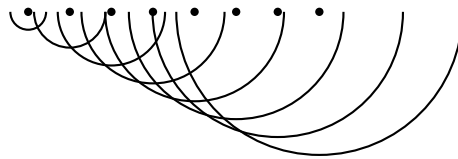
Exercise 4.30: (Poynting vector of radiating solutions). Show that the radial component of the Poynting vector $\mathbf{S}(u)$ in (26) of a non-zero radiating Helmholtz solution satisfies $(\mathbf{S}(u))(\mathbf{x}) \cdot \frac{\mathbf{x}}{r} = |u(\mathbf{x})|^2 + \frac{1}{k}\Im\{\overline{u}(\mathbf{x})\mathcal{O}(r^{-3/2})\}$ for $r = |\mathbf{x}| \to \infty$.

Remark 4.27 shows that $|u(\mathbf{x})| \sim r^{-1/2}$ for $r \to \infty$, as we could expect from the large-argument asymptotics (24) of Bessel and Hankel functions.

Deduce that, for large arguments, the Poynting vector (and so the energy flow of radiating solutions) points "outwards" towards infinity. See the examples in Figure 16.

Remark 4.31: (Direct and inverse scattering). The SSSP is a *direct* scattering problem: we know the incoming wave, we know the obstacle, we want to compute the scattered field. In applications (such as medical imaging, oil retrieval, seismic and atmospheric remote sensing, fault detection in materials, radar and sonar...) it is very important to consider also *inverse* scattering problem: given the scattered field or the far-field (typically from measurements), one wants to compute the obstacle and/or the incoming wave. Inverse problems are ill-posed and much harder than direct ones, both theoretically and computationally. Most numerical methods for the approximation of inverse problems require the numerical solution of many direct problems: this is one of the main motivations for the study of efficient methods to simulate direct scattering problems. Most of the book [CK2] is devoted to inverse scattering problems.

Remark 4.32: (Radiation conditions in 3D, electromagnetism and elasticity). In three space dimensions, the Sommerfeld condition requires a slightly faster decay of u: $|\partial_r u - \mathrm{i}ku| = o(r^{-1})$, $r \to \infty$, [CK2, Def. 2.4]. The limit $\lim_{R\to\infty} \int_{\{|\mathbf{x}|=R\}} |\partial_r u - \mathrm{i}ku|^2 \, \mathrm{d}S = 0$ is equivalent to the Sommerfeld condition both in 2D and in 3D, [CK2, p. 23].

A pair $(\mathbf{E}, \mathbf{H})$ that solves the time-harmonic Maxwell's equations (13) (with $\sigma = 0$) in the complement of a bounded domain of $\mathbb{R}^3$ is outgoing if it satisfies one of the **Silver–Müller** radiation conditions [CK2, Def. 6.6]:

$$\lim_{r\to\infty} |\mathbf{H} \times \mathbf{x} - r\mathbf{E}| = 0 \qquad \text{or} \qquad \lim_{r\to\infty} |\mathbf{E} \times \mathbf{x} + r\mathbf{H}| = 0.$$

This is equivalent to assuming that all the Cartesian components (which are Helmholtz solutions) of the fields $\mathbf{E}, \mathbf{H}$ satisfy the Sommerfeld condition, [CK2, Thm. 6.8].

A displacement field $\mathbf{u}$ that solves Navier's equations (18) in the complement of a bounded domain is outgoing if it satisfies the **Kupradze** condition: the scalar and vector potentials χ and ψ of (19) satisfy the Sommerfeld condition with wavenumber k_P and k_S, respectively, [Martin06, §1.5.1]. So all Cartesian components of radiating pressure and shear waves are radiating Helmholtz solutions.

Given a bounded Lipschitz domain in $\mathbb{R}^3$, one can define exterior boundary value problems for acoustic, electromagnetic, and elastic waves, by imposing the corresponding PDE, a suitable boundary condition (one of those seen in §1), and the appropriate radiation condition.

Remark 4.33: (TE and TM modes in electromagnetic scattering). We have see in Remark 1.22 and Exercise 1.23 that, in the presence of translational symmetry, the 3D Maxwell equations reduce to the 2D Helmholtz equation. Here we describe a similar situation, but considering scattering as opposed to propagation along a waveguide.

Given $\Omega_-, \Omega_+, \Gamma, \mathbf{n}$ as above, let $\widetilde{\Omega_-} := \Omega_- \times \mathbb{R}$, $\widetilde{\Omega_+} := \Omega_+ \times \mathbb{R}$, $\widetilde{\Gamma} := \Gamma \times \mathbb{R}$ be subsets of $\mathbb{R}^3$, and $\widetilde{\mathbf{n}} := (n_1, n_2, 0)$. Assume that $\widetilde{\Omega_-}$ is a perfect electric conductor (imagine a straight metal cable or structure with constant section) hit by a time-harmonic electromagnetic wave $(\mathbf{E}^{\mathrm{Inc}}, \mathbf{H}^{\mathrm{Inc}})$ propagating the in the homogeneous medium $\widetilde{\Omega_+}$, and assume that this is non-conductive, i.e. $\sigma = 0$. This generates a scattered field $(\mathbf{E}^{\mathrm{Scat}}, \mathbf{H}^{\mathrm{Scat}})$ in $\widetilde{\Omega_+}$. The PEC condition is $(\mathbf{E}^{\mathrm{Inc}} + \mathbf{E}^{\mathrm{Scat}}) \times \widetilde{\mathbf{n}} = \mathbf{0}$ on $\widetilde{\Gamma}$. If the incoming field propagates in the (x_1, x_2)-plane, meaning that it is independent of x_3, by translation symmetry the same is true for the scattered field. We consider two cases, see Figure 18.
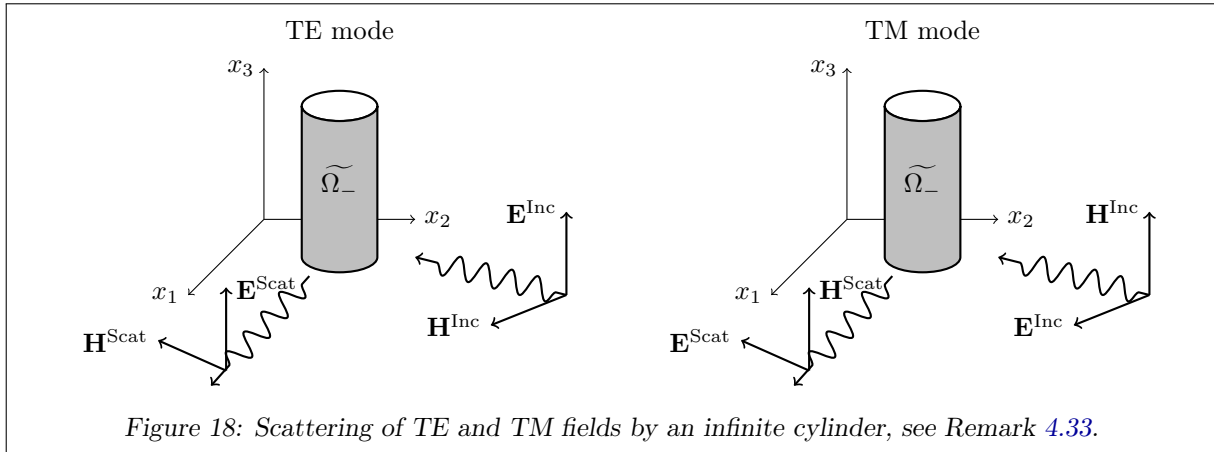
Figure 18: *Scattering of TE and TM fields by an infinite cylinder, see Remark 4.33.*

If the electric field is parallel to the x_3 axis, i.e. $\mathbf{E}^{\mathrm{Inc}}(\mathbf{x}) = (0, 0, u^{\mathrm{Inc}}(x_1, x_2))$, let u^{Scat} be the solution of the SSSP (45) for the 2D Helmholtz equation. Then $\mathbf{E}^{\mathrm{Scat}}(\mathbf{x}) = (0, 0, u^{\mathrm{Scat}}(x_1, x_2))$ and $\mathbf{H}^{\mathrm{Scat}}(\mathbf{x}) = \frac{1}{\mathrm{i}\omega\mu} \operatorname{curl} \mathbf{E}^{\mathrm{Scat}}(\mathbf{x}) = \frac{1}{\mathrm{i}\omega\mu}\left(\frac{\partial u^{\mathrm{Scat}}}{\partial x_2}, -\frac{\partial u^{\mathrm{Scat}}}{\partial x_1}, 0\right)$ solve the Maxwell equations (13) in $\widetilde{\Omega_+}$, and satisfy the PEC condition on $\widetilde{\Gamma}$. This is called a TE (transverse electric) mode because the electric field is perpendicular to the (x_1, x_2)-plane.

Instead, if the magnetic field is parallel to the x_3 axis, i.e. $\mathbf{H}^{\mathrm{Inc}}(\mathbf{x}) = (0, 0, u^{\mathrm{Inc}}(x_1, x_2))$, we compute from Maxwell equations (13) and the definitions of the curl and the vector product

$$\mathbf{E}^{\mathrm{Inc}} \times \widetilde{\mathbf{n}} = -\frac{1}{\mathrm{i}\omega\epsilon} \operatorname{curl} \mathbf{H}^{\mathrm{Inc}} \times \widetilde{\mathbf{n}} = -\frac{1}{\mathrm{i}\omega\epsilon}\left(\frac{\partial u^{\mathrm{Inc}}}{\partial x_2}, -\frac{\partial u^{\mathrm{Inc}}}{\partial x_1}, 0\right) \times (n_1, n_2, 0)$$

$$= -\frac{1}{\mathrm{i}\omega\epsilon}\left(0, 0, \frac{\partial u^{\mathrm{Inc}}}{\partial x_2}n_2 + \frac{\partial u^{\mathrm{Inc}}}{\partial x_1}n_1\right) = -\frac{1}{\mathrm{i}\omega\epsilon}(0, 0, \partial_{\mathbf{n}} u^{\mathrm{Inc}}).$$

So letting u^{Scat} be the solution of the 2D Helmholtz exterior Neumann problem in Ω_+ with datum $-\partial_{\mathbf{n}} u^{\mathrm{Inc}}$ on Γ, the fields $\mathbf{E}^{\mathrm{Scat}} = -\frac{1}{\mathrm{i}\omega\epsilon}\left(\frac{\partial u^{\mathrm{Inc}}}{\partial x_2}, -\frac{\partial u^{\mathrm{Inc}}}{\partial x_1}, 0\right)$, $\mathbf{H}^{\mathrm{Scat}} = (0, 0, u^{\mathrm{Scat}})$ solve the Maxwell equations in $\widetilde{\Omega_+}$ with PEC conditions on $\widetilde{\Gamma}$. This is a TM (transverse magnetic) mode.

Note that the TE/TM naming is apparently reversed from the waveguide case in Remark 1.22. There TE and TM modes were computed by solving Helmholtz BVPs with Neumann and Dirichlet boundary conditions, respectively, while here the boundary conditions are swapped. This is because of the different meaning given to the word "transverse". In the waveguide case (16), we call "transverse" the field that is perpendicular to the waveguide itself (so in the plane where we solve the Helmholtz equation). In the present scattering case, the transverse field is perpendicular to the plane where we solve the Helmholtz equation.

Remark 4.34: (The multipole method: scattering by several discs). In general, we cannot compute analytically the solution of a scattering problem, so we resort to numerical methods: this is what we do in §5.2. Thanks to separation of variables in polar coordinates, a simple exception is the case when the scatterer is a disc, as we have seen in §4.3.1. A more complicated case that allows separation of variables is when the scatterer is an ellipse [Martin06, §2.9]. Here we study the intermediate case of the union of a finite number of disjoint discs, for which we can compute the solution "semi-analytically": truncating an exact expansion, solving a linear system, but without discretisations.

Define $J \in \mathbb{N}$ discs $B_j := B_{R_j}(\mathbf{O}_j)$, $j = 1, \ldots, J$, with radii $R_j > 0$ and centres $\mathbf{O}_j \in \mathbb{R}^2$. Denote $D_{j,j'} := |\mathbf{O}_{j'} - \mathbf{O}_j|$ the mutual distances between the centres, and assume that the disc closures are disjoint, namely $D_{j,j'} > R_j + R_{j'}$.

Let the scatterer be $\Omega_- := \bigcup_{j=1,\ldots,J} B_j$.

We use a system of polar coordinates (r_j, θ_j) associated to each disc: for any point $\mathbf{x} \in \mathbb{R}^2$ we have $\mathbf{x} = \mathbf{O}_j + (r_j \cos \theta_j, r_j \sin \theta_j)$.

We also denote by $\theta_{j,j'}$ the angular polar coordinate of $\mathbf{O}_{j'}$ with respect to $\mathbf{O}_j$: $\mathbf{O}_{j'} - \mathbf{O}_j = (D_{j,j'} \cos \theta_{j,j'}, D_{j,j'} \sin \theta_{j,j'})$.
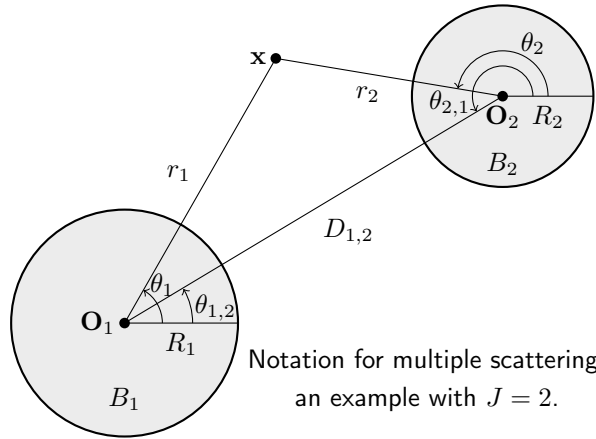
Notation for multiple scattering: an example with $J = 2$.

Assuming for simplicity that the incoming field is a plane wave, we expand it in the local polar coordinate systems using the Jacobi–Anger formula (25):

$$u^{\mathrm{Inc}}(\mathbf{x}) = \mathrm{e}^{\mathrm{i}k\mathbf{d}\cdot\mathbf{x}} = \mathrm{e}^{\mathrm{i}k(\cos\varphi, \sin\varphi)\cdot\mathbf{x}} = \mathrm{e}^{\mathrm{i}k\mathbf{d}\cdot\mathbf{O}_j} \sum_{\ell \in \mathbb{Z}} \mathrm{i}^\ell J_\ell(kr_j) \mathrm{e}^{\mathrm{i}\ell(\theta_j - \varphi)}, \qquad j = 1, \ldots, N.$$

It can be proved that the scattered field is a sum of multipole expansions, one for each disc:

there exist $c_{j,\ell} \in \mathbb{C}$ such that $\qquad u^{\mathrm{Scat}}(\mathbf{x}) = \sum_{j=1}^{J} \sum_{\ell \in \mathbb{Z}} c_{j,\ell} \dfrac{H_\ell^{(1)}(kr_j) \mathrm{e}^{\mathrm{i}\ell\theta_j}}{H_\ell^{(1)}(kR_j)} \qquad \forall \mathbf{x} \in \Omega_+.$ (48)

Provided the series converges appropriately, a function in this form is a radiating Helmholtz solution in Ω_+. We have normalised the expansions dividing by $H_\ell^{(1)}(kR_j)$ in such a way that the term multiplied to each $c_{j,\ell}$ has absolute value equal to 1 on ∂B_j.

The fundamental result relating multipole expansions with different centres is **Graf's addition theorem** [Martin06, Thm. 2.12, eq. (2.25)], [DLMF, eq. 10.23.7] (more general than (42)), which, in our notation, is:

$$H_\ell^{(1)}(kr_j) \mathrm{e}^{\mathrm{i}\ell\theta_j} = \sum_{\ell' \in \mathbb{Z}} H_{\ell-\ell'}^{(1)}(kD_{j,j'}) \mathrm{e}^{\mathrm{i}(\ell-\ell')\theta_{j,j'}} J_{\ell'}(kr_{j'}) \mathrm{e}^{\mathrm{i}\ell'\theta_{j'}} \qquad \begin{matrix} j \neq j' \in \{1, \ldots, J\}, \ \ell \in \mathbb{Z}, \\ \mathbf{x} \in \mathbb{R}^2 \text{ such that } r_{j'} < D_{j,j'}. \end{matrix}$$

This formula can be thought as the expansion of (a Fourier component of) the field outgoing from the disc B_j, "seen from" the disc $B_{j'}$, i.e. in terms of circular waves $J_{\ell'}(kr_{j'}) \mathrm{e}^{\mathrm{i}\ell'\theta_{j'}}$ centred at $\mathbf{O}_j$. Thanks to the disjointness $\overline{B_j} \cap \overline{B_{j'}} = \emptyset$, the condition $r_{j'} < D_{j,j'}$ is satisfied for $\mathbf{x} \in \partial B_{j'}$, in which case $r_{j'} = R_{j'}$.

Imposing the Dirichlet condition $u^{\mathrm{Scat}} = -u^{\mathrm{Inc}}$ on each circle ∂B_{j^*}, expanding $u^{\mathrm{Scat}} = -u^{\mathrm{Inc}}$ in sum of Fourier modes $\mathrm{e}^{\mathrm{i}\ell^*\theta_{j^*}}$ on ∂B_{j^*}, and setting the ℓ^*-th Fourier coefficient to zero, one obtains the relations:

$$c_{j^*,\ell^*} + \sum_{j \neq j^*} \sum_{\ell \in \mathbb{Z}} c_{j,\ell} \frac{H_{\ell-\ell^*}^{(1)}(kD_{j,j^*}) \mathrm{e}^{\mathrm{i}(\ell-\ell^*)\theta_{j,j^*}} J_{\ell^*}(kR_{j^*})}{H_\ell^{(1)}(kR_j)} = -\mathrm{i}^{\ell^*} \mathrm{e}^{\mathrm{i}k\mathbf{d}\cdot\mathbf{O}_j} J_{\ell^*}(kR_{j^*}) \mathrm{e}^{-\mathrm{i}\ell^*\varphi} \qquad \begin{matrix} \forall j^* = 1, \ldots, J, \\ \ell^* \in \mathbb{Z}. \end{matrix}$$
(49)

This is an infinite linear system of equations in the unknowns $(c_{j,\ell})_{j=1,\ldots,J; \ell \in \mathbb{Z}}$. Its infinite matrix can be partitioned in $J \times J$ infinite blocks, and each diagonal block (representing the self-interaction of a single disc) is the infinite identity matrix.

Truncating the infinite sums in the expansion (48), the system (49) becomes a finite linear system, whose solution is a finite coefficient vector $\mathbf{c} = (c_{j,\ell})_{j=1,\ldots,J; |\ell| \leq L_j} \in \mathbb{C}^{\sum_{j=1}^J (2L_j+1)}$. In Figure 19 we see an example of an SSSP solved in this way.

Graf's addition theorem can be extended to three dimensions, electromagnetic and elastic waves, [Martin06, Ch. 2–3]. The technique presented in this remark is an example of the **multipole method**, which is the subject of [Martin06, Ch. 4], where sound-hard problems in 2 and 3 dimensions, electromagnetic and elastic waves are considered. The first instance of this method, for transmission problems, is due to Záviška[28].

Problems involving several well-separated non-circular scatterers can profit from this technique: one can approximate the scattering solution operator for each scatterer with a numerical method, and combine them in a global system using the addition theorem. This is the basic idea of the T-matrix method [Martin06, Ch. 7].

Several videos of scientific talks given in Cambridge in 2023 on the broad topic of multiple scattering can be found at https://www.newton.ac.uk/event/mws/

---

[28][Záviška, Über die Beugung elektromagnetischer Wellen an parallelen, unendlich langen Kreiszylindern, 1913]

Figure 19: *The scattering of a plane wave with direction* $\mathbf{d} = (1,1)/\sqrt{2}$ *and wavenumber* $k = 10$ *by 12 discs of radius* $R = 0.15$, *with centres equispaced on the unit circle. The scattered field has been computed by solving a truncation (at* $|\ell| \leq 32$*) of the infinite linear system* (49)*; see also Exercise 4.35. The upper right plot shows the magnitude* $|c_{j,\ell}|$ *of the Fourier coefficients in the multipole expansion* (48)*; note the exponential decay for large* $|\ell|$ *in the semilog scale.*
The lower right plot shows the trace of $\Re\{u^{\mathrm{Scat}}\}$ *on the boundary of each circle; due to symmetry only 6 curves are visible.*
This example models a Faraday cage: disjoint sound-soft obstacles (equipotential perfect electric conductor cylinders in the TE-mode interpretation of the SSSP as in Remark 4.33) shield an incoming electromagnetic wave.

Exercise 4.35: (Implementation of multiple scattering by discs). Implement numerically the procedure described in Remark 4.34.

- Derive the infinite system of equations (49).

- Write this system in block form.

- Implement a truncation of the system (49) and solve it. Then use the coefficients $c_{j,\ell}$ to compute and plot u^{Scat} and u^{Tot} in a portion of Ω_+, using the truncated (48).

  A cautious way to truncate the expansion is to keep the terms with $|\ell| \leq \lceil kR_j \rceil + 30$ for each B_j. In the example of Figure 19, with this rule all truncated coefficients have magnitude below machine precision. With the normalisation used in (48), it is enough to look at the computed coefficients (as in the upper right plot of Figure 19) to understand if the truncation error committed is acceptable.

- To test the correctness of your implementation, compute the trace of u^{Scat} on Γ and compare it with the plane wave $-u^{\mathrm{Inc}}$.

  In the example in the figure, the ratio $\|u^{\mathrm{Tot}}\|_{L^2(\Gamma)}/\|u^{\mathrm{Inc}}\|_{L^2(\Gamma)}$ for the numerical result is of the order 10^{-15}.

  Careful: for a given disc B_j, $u^{\mathrm{Scat}}|_{\partial B_j}$ does not depend on the $c_{j,\ell}$ only, but also on the other $c_{j',\ell}$.

- Replicate the Faraday-cage example in Figure 19.

- Replicate a setting such as that in https://people.maths.ox.ac.uk/trefethen/10helmholtz.pdf

  Here a plane wave hits two circular arrays of small discs: one of them shields the field, the other generates a quasi-resonance and amplifies the field in its interior. The two circles differ only in their radius. To obtain the quasi-resonance you have to tune carefully the radius of the circle (or the wavenumber); a simple numerical optimisation can help.

4.4 Well-posedness of the exterior Dirichlet problem (EDP)

The most common proof that the EDP (44) is well-posed relies on properties of BIOs and BIEs, e.g. [CK1, Thm. 3.21] and [CK2, Thm. 3.11]. Here instead we prove the well-posedness using a variational formulation on a truncated domain and the "DtN map". However, both proofs rely on the same main tools: Fredholm theory and a "Rellich lemma", which ensures uniqueness.

4.4.1 DtN map

Let $R > 0$ be the radius of an open ball B_R centred at the origin such that $\Gamma \subset B_R$. We define the operator DtN, which acts on functions defined on ∂B_R by multiplying each terms in their Fourier expansion by the ratio of the radial derivative of the corresponding Fourier–Hankel function and the value of the Fourier–Hankel function itself:

$$\mathsf{DtN}(v) = \mathsf{DtN}\Big(\sum_{\ell \in \mathbb{Z}} \hat{v}_\ell \mathrm{e}^{\mathrm{i}\ell\theta} \Big) = \sum_{\ell \in \mathbb{Z}} T_\ell \hat{v}_\ell \mathrm{e}^{\mathrm{i}\ell\theta}, \qquad \text{for } T_\ell := \frac{k H_\ell^{(1)'}(kR)}{H_\ell^{(1)}(kR)}. \tag{50}$$

This operator is called **Dirichlet-to-Neumann (DtN) map** or **capacity operator** (see [Nédélec01, (2.6.92)] for the 3D version).

If u is a radiating solution in Ω_+, then in $\mathbb{R}^2 \setminus B_R$ it can[29] be expanded as $u(\mathbf{x}) = \sum_{\ell \in \mathbb{Z}} a_\ell H_\ell^{(1)}(kr) \mathrm{e}^{\mathrm{i}\ell\theta}$. Then its traces on ∂B_R are

$$\gamma_{\partial B_R}^+ u = \sum_{\ell \in \mathbb{Z}} a_\ell H_\ell^{(1)}(kR) \mathrm{e}^{\mathrm{i}\ell\theta} \quad \text{and} \ \ \partial_{\mathbf{n}_{B_R}}^+(u) = \sum_{\ell \in \mathbb{Z}} a_\ell k H_\ell^{(1)'}(kR) \mathrm{e}^{\mathrm{i}\ell\theta} \quad \text{thus} \ \boxed{\mathsf{DtN}(\gamma_{\partial B_R}^+ u) = \partial_{\mathbf{n}_{B_R}}^+(u).}$$

In words: **the DtN operator maps the Dirichlet trace** (on ∂B_R) **of a radiating solution to its Neumann trace** (on ∂B_R).

From the formulas ([DLMF, §10.6(i) and eq. 10.19.2]) for the derivative and the large-index asymptotics of the Hankel functions

$$H_\ell^{(1)'}(z) = \frac{H_{\ell-1}^{(1)}(z) - H_{\ell+1}^{(1)}(z)}{2}, \qquad H_\ell^{(1)}(z) \sim -\mathrm{i}\sqrt{\frac{2}{\pi}} \Big(\frac{2}{\mathrm{e}z}\Big)^\ell \ell^{\ell-\frac{1}{2}} \quad \text{for } \ell \to \infty$$

we have

$$T_\ell = k \frac{H_{\ell-1}^{(1)}(kR) - H_{\ell+1}^{(1)}(kR)}{H_\ell^{(1)}(kR)} \sim k \Big(\frac{\mathrm{e}kR}{2\ell} - \frac{2\ell}{\mathrm{e}kR}\Big) = \mathcal{O}(\ell) \qquad \ell \to \infty.$$

From the definition of the fractional norms (28) on the circle we have that DtN is continuous as an operator $\mathsf{DtN} : H^s(\partial B_R) \to H^{s-1}(\partial B_R)$ for any $s \in \mathbb{R}$: for some $C > 0$,

$$\|\mathsf{DtN}v\|_{H^{s-1}(\partial B_R)}^2 = 2\pi \sum_{\ell \in \mathbb{Z}} |\hat{v}_\ell|^2 \underbrace{|T_\ell|^2}_{\sim \ell^2}(1+\ell^2)^{s-1} \leq C \sum_{\ell \in \mathbb{Z}} |\hat{v}_\ell|^2 (1+\ell^2)^s \leq C \|v\|_{H^s(\partial B_R)}^2.$$

4.4.2 Truncated problem

The EDP (44) is equivalent to the following problem on the truncated domain $\Omega_R := B_R \cap \Omega_+$:

$$\begin{aligned}
\Delta u + k^2 u &= 0 && \text{in } \Omega_R, \\
\gamma u &= g_\mathrm{D} && \text{on } \Gamma, \\
\mathsf{DtN}(\gamma u) - \partial_\mathbf{n} u &= 0 && \text{on } \partial B_R.
\end{aligned} \tag{51}$$
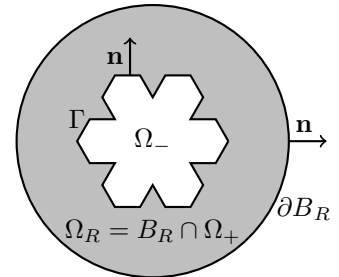
The last condition on the exterior boundary ∂B_R is equivalent to the Sommerfeld radiation condition. To write this BVP as a variational problem we define the space $H_{0,R}^1(\Omega_R) := \{u \in H^1(\Omega_R) : \gamma u = 0 \text{ on } \Gamma\}$ (the H^1 functions whose trace vanishes on the interior boundary Γ but not necessarily on ∂B_R).

---

[29]We haven't proved that *all* radiating solutions can be expanded in Fourier–Hankel series; see [CK1, Thm. 3.6] for a proof (in the 3D case) which relies on Green's representation (which we will see later). This is called Atkinson–Wilcox expansion.

From the surjectivity of the trace operator (Theorem 3.10) there exists a lifting $u_D \in H^1(\Omega_R)$ such that $\gamma^+ u_D = g_D$; it is possible to choose $u_D \in H^1(\Omega_R; \Delta)$ (e.g. by solving an auxiliary Laplace BVP). If we can solve the problem

$$
\begin{aligned}
\Delta u_0 + k^2 u_0 &= -f && \text{in } \Omega_R, \\
\gamma u_0 &= 0 && \text{on } \Gamma, && f := -\Delta u_D - k^2 u_D, \quad g_R := -\mathsf{DtN}(\gamma u_D) + \partial_{\mathbf{n}} u_D, \\
\mathsf{DtN}(\gamma u_0) - \partial_{\mathbf{n}} u_0 &= g_R && \text{on } \partial B_R,
\end{aligned}
$$

then $u = u_D + u_0$ would solve (51). (We could also choose u_D such that $g_R = 0$.) Using Green's first identity it is easy to deduce a variational problem for u_0:

$$
\text{find} \quad u_0 \in H^1_{0,R}(\Omega_R) \quad \text{such that} \quad \mathcal{A}_R(u_0, w) = \mathcal{F}_R(w) \quad \forall w \in H^1_{0,R}(\Omega_R) \quad \text{where} \tag{52}
$$

$$
\mathcal{A}_R(u_0, w) := \int_{\Omega_R} (\nabla u_0 \nabla \overline{w} - k^2 u_0 \overline{w}) \, \mathrm{d}\mathbf{x} - \int_{\partial B_R} (\mathsf{DtN}\gamma u_0)(\gamma \overline{w}) \, \mathrm{d}s,
$$

$$
\mathcal{F}_R(w) := \int_{\Omega} f \overline{w} \, \mathrm{d}\mathbf{x} - \int_{\partial B_R} g_R \gamma \overline{w} \, \mathrm{d}s.
$$

Using the continuity of the trace operator ($\gamma : H^1_{0,R}(\Omega_R) \to H^{\frac{1}{2}}(\partial B_R)$) and the DtN map ($\mathsf{DtN} : H^{\frac{1}{2}}(\partial B_R) \to H^{-\frac{1}{2}}(\partial B_R)$) we deduce the continuity of $\mathcal{A}_R$ and $\mathcal{F}_R$ in $H^1_{0,R}(\Omega_R)$. [30]

4.4.3 GÅRDING INEQUALITY

We first look at the real part of the boundary sesquilinear form associated to DtN: for all $v(\mathbf{x}) = \sum_{\ell \in \mathbb{Z}} \hat{v}_\ell \mathrm{e}^{\mathrm{i}\ell\theta} \in H^{\frac{1}{2}}(\partial B_R)$ we have

$$
\Re \int_{\partial B_R} (\mathsf{DtN}v)\overline{v} \, \mathrm{d}s(\mathbf{x}) = R \, \Re \int_0^{2\pi} \left(\sum_{\ell \in \mathbb{Z}} T_\ell \hat{v}_\ell \mathrm{e}^{\mathrm{i}\ell\theta} \right) \left(\sum_{\ell \in \mathbb{Z}} \overline{\hat{v}_\ell} \mathrm{e}^{-\mathrm{i}\ell\theta} \right) \mathrm{d}\theta = 2\pi R \sum_{\ell \in \mathbb{Z}} |\hat{v}_\ell|^2 \Re\{T_\ell\}.
$$

For any complex-valued differentiable function f of a real variable we have

$$
\Re\left\{ \frac{f'(t)}{f(t)} \right\} = \Re\left\{ \frac{f'(t)\overline{f}(t)}{|f(t)|^2} \right\} = \frac{f'(t)\overline{f}(t) + \overline{f'}(t)f(t)}{2|f(t)|^2} = \frac{1}{2|f(t)|^2} \frac{\partial(f(t)\overline{f}(t))}{\partial t} = \frac{1}{2|f(t)|^2} \frac{\partial(|f(t)|^2)}{\partial t}.
$$

Choosing $f(r) = H_\ell^{(1)}(kr)$ we have

$$
\Re\{T_\ell\} = \Re\left\{ \frac{f'(R)}{f(R)} \right\} = \frac{1}{2|H_\ell^{(1)}(kR)|^2} \frac{\partial(|H_\ell^{(1)}(kr)|^2)}{\partial r} \bigg|_{r=R} < 0
$$

since the absolute value of the Hankel function is monotonically decreasing. Combining all these ingredients we see that the sesquilinear form satisfies a Gårding inequality:

$$
\begin{aligned}
\Re\{\mathcal{A}_R(w, w)\} &= \int_{\Omega_R} (|\nabla w|^2 - k^2 |w|^2) \, \mathrm{d}\mathbf{x} - \Re \int_{\partial B_R} (\mathsf{DtN}\gamma w)\gamma \overline{w} \, \mathrm{d}s \\
&= \|\nabla w\|^2_{L^2(\Omega_R)^2} - k^2 \|w\|^2_{L^2(\Omega_R)} - 2\pi R \sum_{\ell \in \mathbb{Z}} |\hat{w}_\ell|^2 \underbrace{\Re\{T_\ell\}}_{\leq 0} \\
&\geq \|\nabla w\|^2_{L^2(\Omega_R)^2} - k^2 \|w\|^2_{L^2(\Omega_R)} = \|w\|^2_{H^1(\Omega_R)} - (k^2 + 1) \|w\|^2_{L^2(\Omega_R)},
\end{aligned}
$$

where we have expanded $(\gamma w)(\theta) = \sum_{\ell \in \mathbb{Z}} \hat{w}_\ell \mathrm{e}^{\mathrm{i}\ell\theta}$ on ∂B_R. Moreover, $H^1_{0,R}(\Omega_R)$ is compactly embedded in $L^2(\Omega_R)$. From Corollary 3.20 we have that if the homogeneous version of the variational problem (52) (find $u_0 \in H^1_{0,R}(\Omega_R)$ such that $\mathcal{A}_R(u_0, w) = 0$ for all $w \in H^1_{0,R}(\Omega_R)$) admits only the trivial solution $u_0 = 0$, then (52) is well-posed for any right-hand side.

---

[30] For a detailed analysis of the truncated problem (52), and in particular its stability and the dependence on the wavenumber, see [Chandler–Wilde, Monk, Wave-number-explicit bounds in time-harmonic scattering, SIMA 2008].

4.4.4 UNIQUENESS

We first prove the following important result, [CK1, Thm. 3.12].

Theorem 4.36: (Rellich's lemma). Let u be a radiating Helmholtz solution in Ω_+.

$$\text{If} \qquad \Im \int_{\partial B_R} \partial_{\mathbf{n}} u \, \gamma \overline{u} \, \mathrm{d}s \leq 0, \qquad \text{then} \qquad u = 0 \quad \text{in } \Omega_+.$$

Proof. As before, we assume that u admits a Fourier–Hankel expansion $u = \sum_{\ell \in \mathbb{Z}} \hat{u}_\ell \mathrm{e}^{\mathrm{i}\ell\theta} H_\ell^{(1)}(kr)$, [CK1, Thm. 3.6]. With this normalisation, on ∂B_R we have

$$\Im \int_{\partial B_R} \partial_{\mathbf{n}} u \, \gamma \overline{u} \, \mathrm{d}s = R \, \Im \int_0^{2\pi} \Big(\sum_{\ell \in \mathbb{Z}} \hat{u}_\ell \mathrm{e}^{\mathrm{i}\ell\theta} k H_\ell^{(1)'}(kr) \Big) \Big(\sum_{\ell \in \mathbb{Z}} \overline{\hat{u}_\ell} \mathrm{e}^{-\mathrm{i}\ell\theta} \overline{H_\ell^{(1)}(kr)} \Big) \, \mathrm{d}\theta$$

$$= 2\pi R \sum_{\ell \in \mathbb{Z}} |\hat{u}_\ell|^2 \Im\{ k H_\ell^{(1)'}(kR) \overline{H_\ell^{(1)}}(kR) \}$$

$$= 2\pi R \sum_{\ell \in \mathbb{Z}} |\hat{u}_\ell|^2 k \Big(Y'(kR) J(kR) - Y(kR) J'(kR) \Big) = 2\pi R \sum_{\ell \in \mathbb{Z}} |\hat{u}_\ell|^2 \frac{2}{\pi R} = 4 \sum_{\ell \in \mathbb{Z}} |\hat{u}_\ell|^2 \geq 0,$$

from the Wronskian identity [DLMF, eq. 10.5.2]. Since all terms in the series are positive, if the series is ≤ 0 then it is 0 and $\hat{u}_\ell = 0$ for all $\ell \in \mathbb{Z}$, so $u = 0$. $\qquad\square$

If we choose u_0 to be the solution of the homogeneous variational problem (52) with $\mathcal{F}_R = 0$, then

$$0 = \Im\{\mathcal{F}_R(u_0)\} = \Im\{\mathcal{A}_R(u_0, u_0)\} = -\Im \int_{\partial B_R} (\mathsf{DtN}\gamma u_0) \gamma \overline{u}_0 \, \mathrm{d}s = -\Im \int_{\partial B_R} \partial_{\mathbf{n}} u_0 \, \gamma \overline{u}_0 \, \mathrm{d}s$$

and $u_0 = 0$ by Rellich's lemma 4.36.

We can now complete the proof of the well-posedness. The homogeneous variational problem ((52) with $\mathcal{F}_R = 0$) admits only the trivial solution $u_0 = 0$ (§4.4.4) and its sesquilinear form satisfies a Gårding inequality (§4.4.3). By Corollary 3.20 the problem (52) is well-posed for all f and g_R. Thanks to the equivalence with (51), also the EDP (44) and the special case of the SSSP (45) are well-posed.

5 Boundary integral equations and the boundary element method

5.1 Single-layer potential, operator and the first BIE

We define the 2D Helmholtz **fundamental solution**:

$$\Phi_k(\mathbf{x}, \mathbf{y}) := \frac{\mathrm{i}}{4} H_0^{(1)}(k|\mathbf{x} - \mathbf{y}|), \qquad \mathbf{x} \neq \mathbf{y} \in \mathbb{R}^2. \tag{53}$$

As a function of $\mathbf{x}$, this is a radiating Fourier–Hankel function of order 0 centred at $\mathbf{y}$. It is a smooth Helmholtz solution in $\mathbb{R}^2 \setminus \{\mathbf{y}\}$ and has a singularity at $\mathbf{y}$. The roles of $\mathbf{x}$ and $\mathbf{y}$ are symmetric. It represents the field produced by a point source located in $\mathbf{y}$. The value of $\Phi_k(\mathbf{x}, \mathbf{y})$ only depends on the distance $|\mathbf{x} - \mathbf{y}|$ between the arguments (more precisely: it depends on the number of wavelengths contained in that distance: $\frac{|\mathbf{x}-\mathbf{y}|}{\lambda} = \frac{k|\mathbf{x}-\mathbf{y}|}{2\pi}$). When the arguments $\mathbf{x}, \mathbf{y}$ approach one another, the fundamental solution blows up logarithmically; more precisely, from the small-argument asymptotics of the Hankel function [DLMF, eq. 10.8.2] and the smoothness of J_0 (equivalently, [CK2, eq. (3.107)]), one can show that

$$\Phi_k(\mathbf{x}, \mathbf{y}) = -\frac{1}{2\pi} \log(k|\mathbf{x} - \mathbf{y}|) + \mathcal{R}(|\mathbf{x} - \mathbf{y}|) \qquad \text{for a function} \quad \mathcal{R} \in C^1(\mathbb{R}). \tag{54}$$

We will see in Exercise 5.24 that the normalisation factor $\frac{\mathrm{i}}{4}$ in (53) gives that, for all $\mathbf{y} \in \mathbb{R}^2$, $\Delta\Phi_k(\cdot, \mathbf{y}) + k^2\Phi_k(\cdot, \mathbf{y}) = \delta_{\mathbf{y}}$, in the sense of distributions, where $\delta_{\mathbf{y}}$ is the Dirac delta centred at $\mathbf{y}$. Moreover this coefficient will allow to write a simple Green's integral representation in §5.3.

Any linear combination $\sum_j \psi_j \Phi_k(\cdot, \mathbf{y}_j)$ of fundamental solutions centred at points $\mathbf{y} \in \overline{\Omega_-}$ satisfies the Helmholtz equation in Ω_+ and is radiating.[31] We can also take a continuous linear combination of fundamental solutions, which we write as

$$(\mathcal{S}\psi)(\mathbf{x}) := \int_\Gamma \Phi_k(\mathbf{x}, \mathbf{y})\psi(\mathbf{y}) \, \mathrm{d}s(\mathbf{y}) \qquad \mathbf{x} \in \Omega_+, \tag{55}$$

where ψ is a function on Γ. We can think at ψ as the density of acoustic sources[32] generating the field $\mathcal{S}\psi$. The function $\mathbf{x} \mapsto \Phi_k(\mathbf{x}, \mathbf{y})\psi(\mathbf{y})$ belongs to $C^\infty(\Omega_+)$ for any given $\mathbf{y} \in \Gamma$. Thus, by the differentiation under integral sign theorem, the function $\mathcal{S}\psi$ belongs to $C^\infty(\Omega_+)$, is radiating and is a solution of the Helmholtz equation, [CGLS12, Thm. 2.14]. The operator $\mathcal{S}$ is called (acoustic) **single-layer potential** or, sometimes, **simple-layer potential**. It is possible to prove that the single-layer potential is continuous as a mapping $\mathcal{S} : H^{-\frac{1}{2}}(\Gamma) \to H^1_{\mathrm{loc}}(\Omega_+)$, [CGLS12, Thm. 2.15].

This suggests to look for a solution of the EDP (44) in the form $u(\mathbf{x}) = (\mathcal{S}\psi)(\mathbf{x})$ for some "density" ψ. But, how can we find ψ? We need to relate $\mathcal{S}\psi$ to the boundary condition.

We first introduce the **single-layer operator** S:

$$(S\psi)(\mathbf{x}) := \int_\Gamma \Phi_k(\mathbf{x}, \mathbf{y})\psi(\mathbf{y}) \, \mathrm{d}s(\mathbf{y}) \qquad \mathbf{x} \in \Gamma. \tag{56}$$

The only difference between the single-layer potential $\mathcal{S}$ and operator S is that the former is evaluated in points *off* the boundary, and the latter *on* the boundary Γ. When $\psi \in C^0(\Gamma)$, then the evaluation of $(\mathcal{S}\psi)(\mathbf{x})$ is the integral of a continuous function. On the other hand, no matter the regularity of ψ, the evaluation of $(S\psi)(\mathbf{x})$ is a singular integral, because of the singularity of $\Phi_k(\mathbf{x}, \mathbf{y})$ at $\mathbf{x} = \mathbf{y}$. The single-layer operator is a first example of **boundary integral operator (BIO)**, in particular it is a **weakly singular integral operator**, as the singularity of Φ_k is logarithmic.

---

[31] This suggests a numerical method consisting in choosing N points $\mathbf{y}_1, \ldots, \mathbf{y}_N \in \Omega_-$ and in searching the coefficients $\psi_1, \ldots, \psi_N$ that minimise $\left\| \sum_{j=1}^N \psi_j \Phi_k(\cdot, \mathbf{y}_j) - g_D(\cdot) \right\|_{L^2(\Gamma)}$ (or some other norm on Γ). This is a well-known scheme called the **method of fundamental solutions** (**MFS**), see e.g. [Barnett, Betcke, Stability and convergence of the method of fundamental solutions for Helmholtz problems on analytic domains, JCP 2008]. It is simple to code and can give extremely good accuracy but has some drawbacks: it is very sensitive with respect to the location of the poles $\mathbf{y}_j$, the minimisation generally leads to ill-conditioned linear systems, it struggles to approximate solutions for scatterers with corners, it is not easily extended to 3D and does not have a complete stability and convergence theory. The **lightning method** is a modern variant of the MFS, extremely effective at approximating the solution singularities at the scatterer corners, see [Ginn, Trefethen, Lightning Helmholtz solver, arXiv:2310.01665, 2023].

[32] The terminology ("potential", "layer", "density", . . .) comes from electrostatics, i.e. the Laplace equation case $k = 0$. In this case ψ represents the surface density of electric charges generating, by Coulomb's law, the electrostatic potential $\mathcal{S}\psi$. For a simple and very brief summary see `https://cims.nyu.edu/~oneil/courses/sp19-math2840/electrostatics.pdf`

The next proposition shows that the Dirichlet trace operator relates $\mathcal{S}$ and S. This fact seems obvious from the definitions (55)–(56) of single-layer potential and operator, but its justification requires some care because of the singularity of the fundamental solution Φ_k, which appears in the definition of $\mathcal{S}$ and S. We will see in §5.4 (equation (76)) another boundary integral potential/operator pair defined by similar formulas, where the operator is not the trace of the potential.

Proposition 5.1: $\big(S = \gamma^+ \mathcal{S}\big)$. The Dirichlet trace of the single-layer potential is the single layer operator:

$$S\psi = \gamma^+(\mathcal{S}\psi) \qquad \text{for } \psi \in H^{-\frac{1}{2}}(\Gamma). \tag{57}$$

Proof. We show this (intuitively very plausible) fact when $\psi \in C^0(\Gamma)$ and Γ is a polygon.

We recall that $\mathcal{R}$ is the C^1 function introduced in (54) and we denote by $L_{\mathcal{R}} := \sup_{t \in [0, \text{diam } \Gamma]} |\mathcal{R}'(t)|$ its Lipschitz constant. We fix a point $\mathbf{x} \in \Gamma$ and a sequence $(\mathbf{x}_j)_{j \in \mathbb{N}} \subset \Omega_+ \cap B_{1/4}(\mathbf{x})$ with $\mathbf{x}_j \xrightarrow{j \to \infty} \mathbf{x}$. We denote $\epsilon_j := 2|\mathbf{x} - \mathbf{x}_j|^{1/2}$. Then

$$\begin{aligned}
|S\psi(\mathbf{x}) - \mathcal{S}\psi(\mathbf{x}_j)| &= \left| \int_\Gamma [\Phi_k(\mathbf{x}, \mathbf{y}) - \Phi_k(\mathbf{x}_j, \mathbf{y})] \psi(\mathbf{y}) \, \mathrm{d}s(\mathbf{y}) \right| \\
&\leq \|\psi\|_{L^\infty(\Gamma)} \left(\int_\Gamma |\mathcal{R}(|\mathbf{x} - \mathbf{y}|) - \mathcal{R}(|\mathbf{x}_j - \mathbf{y}|)| \, \mathrm{d}s(\mathbf{y}) + \frac{1}{2\pi} \int_\Gamma |\log(k|\mathbf{x} - \mathbf{y}|) - \log(k|\mathbf{x}_j - \mathbf{y}|)| \, \mathrm{d}s(\mathbf{y}) \right) \\
&\leq \|\psi\|_{L^\infty(\Gamma)} \left(|\Gamma| L_{\mathcal{R}} |\mathbf{x} - \mathbf{x}_j| + \int_{\Gamma \setminus B_{\epsilon_j}(\mathbf{x})} |\log|\mathbf{x} - \mathbf{y}| - \log|\mathbf{x}_j - \mathbf{y}|| \, \mathrm{d}s(\mathbf{y}) \right. \\
&\qquad\qquad \left. + \int_{\Gamma \cap B_{\epsilon_j}(\mathbf{x})} |\log|\mathbf{x} - \mathbf{y}| - \log|\mathbf{x}_j - \mathbf{y}|| \, \mathrm{d}s(\mathbf{y}) \right).
\end{aligned}$$

The first term clearly vanishes in the limit $\mathbf{x}_j \to \mathbf{x}$. Using that $|\log t - \log s| \leq \frac{|t-s|}{\min\{t,s\}}$ for all $t, s > 0$, also the second term vanishes in the same limit:

$$\begin{aligned}
\int_{\Gamma \setminus B_{\epsilon_j}(\mathbf{x})} |\log|\mathbf{x} - \mathbf{y}| - \log|\mathbf{x}_j - \mathbf{y}|| \, \mathrm{d}s(\mathbf{y}) &\leq \int_{\Gamma \setminus B_{\epsilon_j}(\mathbf{x})} \frac{||\mathbf{x} - \mathbf{y}| - |\mathbf{x}_j - \mathbf{y}||}{\min\{|\mathbf{x} - \mathbf{y}|, |\mathbf{x}_j - \mathbf{y}|\}} \, \mathrm{d}s(\mathbf{y}) \\
&\leq \frac{2|\Gamma|}{\epsilon_j} |\mathbf{x} - \mathbf{x}_j| = |\Gamma| |\mathbf{x} - \mathbf{x}_j|^{1/2}.
\end{aligned}$$

Here we used that for $\mathbf{y} \notin B_{\epsilon_j}(\mathbf{x})$ we have $|\mathbf{x} - \mathbf{y}| \geq \epsilon_j$ and $|\mathbf{x}_j - \mathbf{y}| \geq |\mathbf{x} - \mathbf{y}| - |\mathbf{x}_j - \mathbf{x}| \geq \epsilon_j - \frac{\epsilon_j^2}{4} \geq \frac{\epsilon_j}{2}$.

Now assume that $\mathbf{x}$ belongs to a side of Γ (which was assumed to be a polygon) and that ϵ_j is smaller than the distance between $\mathbf{x}$ and the closest vertex of Γ (which is true for sufficiently large j). Let $t_j \in [0, \frac{\epsilon_j}{2})$ be the distance between $\mathbf{x}$ and the point of Γ closest to $\mathbf{x}_j$. Then, recalling that $\log t = (t \log t - t)'$, the last integral term can be bounded as

$$\begin{aligned}
\int_{\Gamma \cap B_{\epsilon_j}(\mathbf{x})} &|\log|\mathbf{x} - \mathbf{y}| - \log|\mathbf{x}_j - \mathbf{y}|| \, \mathrm{d}s(\mathbf{y}) \\
&\leq \int_{-\epsilon_j}^{\epsilon_j} |\log|t|| + |\log|t - t_j|| \, \mathrm{d}t \\
&= 2\epsilon_j |\log \epsilon_j - 1| + (\epsilon_j + t_j)|\log(\epsilon_j + t_j) - 1| + (\epsilon_j - t_j)|\log(\epsilon_j - t_j) - 1| \\
&\leq C \epsilon_j |\log \epsilon_j|.
\end{aligned}$$
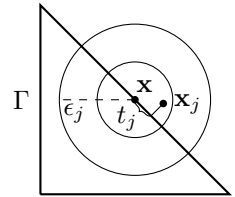
If $\mathbf{x}$ is instead a vertex of Γ, one can proceed in a similar way by treating separately the two segments of $\Gamma \cap B_{\epsilon_j}(\mathbf{x})$. From the definition of ϵ_j, all three terms in the bound on $|\mathcal{S}\psi(\mathbf{x}_j) - S\psi(\mathbf{x})|$ converge to 0 for $j \to \infty$, so $\lim_{j \to \infty} \mathcal{S}\psi(\mathbf{x}_j) = S\psi(\mathbf{x})$. We have also shown that $\mathbf{x} \mapsto \int_\Gamma \Phi_k(\mathbf{x}, \mathbf{y}) \psi(\mathbf{y}) \, \mathrm{d}s(\mathbf{y})$ is a continuous function on $\Omega_+ \cup \Gamma$ (actually it is continuous on $\mathbb{R}^2$). See [SS11, Thm. 3.3.5] for a more general proof. $\square$

If we are able to find ψ on Γ such that

$$\boxed{S\psi = g_{\mathrm{D}} \quad \text{on } \Gamma,} \tag{58}$$

where g_{D} is the Dirichlet datum of the EDP (44) (recall that $g_{\mathrm{D}} = -\gamma^+ u^{\mathrm{Inc}}$ for the SSSP (45)), then

$$\boxed{u = \mathcal{S}\psi \quad \text{in } \Omega_+} \tag{59}$$

is a radiating Helmholtz solution in Ω_+ with $\gamma^+ u = \gamma^+ \mathcal{S}\psi = S\psi = g_{\mathrm{D}}$ by (57), thus u itself is a **solution of the EDP** (44).

Equation (58) is the first example of **boundary integral equation** (BIE) and (59) is the corresponding **representation formula**. The unknown of the BIE is ψ, which is a distribution supported on Γ and does not need to have a physical meaning: for this reason this is called **indirect method**. If we could solve the BIE and compute ψ, then the solution u of the EDP could be obtained from the representation formula, which amounts to the computation of an integral on Γ for each point $\mathbf{x} \in \Omega_+$ where we want to evaluate u.

We will see in §6.1 that the BIE (58) is well-posed under some conditions on Γ and k. Moreover, in §6.3.4 (in particular (112)) we will study the regularity of the solution ψ for a polygonal scatterer, showing that $\psi \in L^2(\Gamma)$.

From the continuity of the single-layer potential $\mathcal{S} : H^{-\frac{1}{2}}(\Gamma) \to H^1_{\mathrm{loc}}(\Omega_+)$, the trace formula (57) and the trace theorem 3.10, it follows that the single-layer operator is continuous as a mapping $S : H^{-\frac{1}{2}}(\Gamma) \to H^{\frac{1}{2}}(\Gamma)$. We demonstrate this continuity in the case of the disc in Remark 5.2.

This continuity property allows us write a variational form of the BIE (58). Recall from §3.3.3 that the range $H^{\frac{1}{2}}(\Gamma)$ of S is the anti-dual of its domain $H^{-\frac{1}{2}}(\Gamma)$. So we can write the variational problem:

$$
\begin{aligned}
&\text{seek } \psi \in H^{-\frac{1}{2}}(\Gamma) \text{ such that} \\
&\mathcal{A}(\psi, \xi) := \langle S\psi, \xi \rangle_{H^{\frac{1}{2}}(\Gamma) \times H^{-\frac{1}{2}}(\Gamma)} = \langle g_{\mathrm{D}}, \xi \rangle_{H^{\frac{1}{2}}(\Gamma) \times H^{-\frac{1}{2}}(\Gamma)} =: \mathcal{F}(\xi) \qquad \forall \xi \in H^{-\frac{1}{2}}(\Gamma).
\end{aligned}
\tag{60}
$$

$\mathcal{A}(\cdot, \cdot)$ and $\mathcal{F}(\cdot)$ are the sesquilinear and the antilinear form of the variational problem. When $\xi \in L^2(\Gamma)$ the duality products $\langle \cdot, \cdot \rangle_\Gamma$ in (60) can be written as integrals over Γ. Recall that when we deal with BVPs for PDEs we obtain sesquilinear forms from integration by parts; with BIEs we simply multiply the equation by a test function and integrate (using the duality product) over Γ.
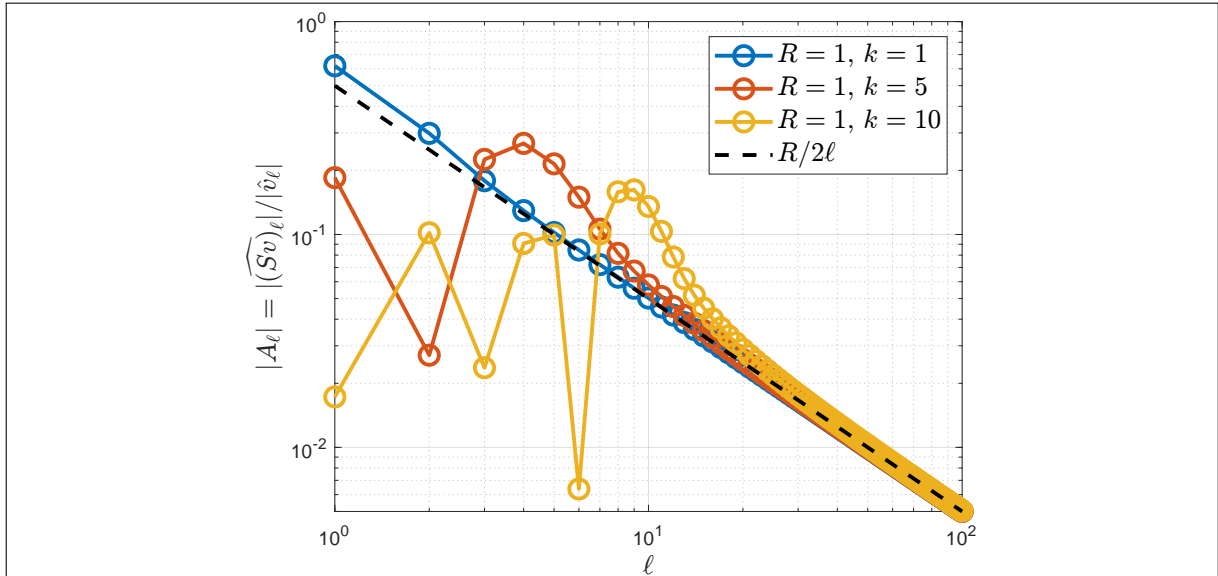
Figure 20: A log–log plot of the absolute values of the multipliers $A_\ell = \frac{\widehat{(Sv)}_\ell}{\hat{v}_\ell}$ in the circular-harmonic expansion of the single-layer operator S on the boundary of a circle. They decay proportionally to $\frac{1}{\ell}$, demonstrating the continuity of $S : H^s(\Gamma) \to H^{s+1}(\Gamma)$. Each colour correspond to a wavenumber k. See Remark 5.2.

Remark 5.2: (Continuity of the single-layer operator on the circle). We can verify the continuity $S : H^{-\frac{1}{2}}(\Gamma) \to H^{\frac{1}{2}}(\Gamma)$ for a circular boundary $\Gamma = \partial B_R = \{\mathbf{x} : |\mathbf{x}| = R\}$ for $R > 0$, where these norms can be computed from Fourier coefficients. Let $v(\theta) = \sum_{\ell \in \mathbb{Z}} \hat{v}_\ell e^{i\ell\theta}$ be a function (or distribution) defined on Γ and $\mathbf{x} = (R\cos\theta_{\mathbf{x}}, R\sin\theta_{\mathbf{x}}) \in \partial B_R$. By Graf's addition formula (42), the orthogonality of the circular harmonics, the large-index asymptotics [DLMF, eq. 10.19.1–10.19.2] for Bessel and Hankel functions

$$
(Sv)(\mathbf{x}) = \int_{\partial B_R} \Phi_k(\mathbf{x}, \mathbf{y}) v(\mathbf{y}) \, ds(\mathbf{y}) = R \int_0^{2\pi} \left(\sum_{\ell \in \mathbb{Z}} \frac{i}{4} H_\ell^{(1)}(kR) J_\ell(kR) e^{i\ell\theta_{\mathbf{x}}} e^{-i\ell\theta_{\mathbf{y}}} \right) \left(\sum_{\ell \in \mathbb{Z}} \hat{v}_\ell e^{i\ell\theta_{\mathbf{y}}} \right) d\theta_{\mathbf{y}}
$$

$$= 2\pi R \frac{\mathrm{i}}{4} \sum_{\ell \in \mathbb{Z}} H_\ell^{(1)}(kR) J_\ell(kR) \, \hat{v}_\ell \, \mathrm{e}^{\mathrm{i}\ell\theta_{\mathbf{x}}}$$

$$\Rightarrow \qquad \widehat{(Sv)}_\ell = A_\ell \hat{v}_\ell, \qquad A_\ell := \frac{\pi R \mathrm{i}}{2} H_\ell^{(1)}(kR) J_\ell(kR) \sim \frac{R}{2\ell} \qquad \ell \to \infty.$$

We say that S "diagonalises" in the Fourier basis: expanding the argument v in the $\mathrm{e}^{\mathrm{i}\ell\theta}$ basis, the action of S corresponds to a multiplication of each coefficient $\hat{v}_\ell$ by a factor A_ℓ (exactly as when we multiply a diagonal matrix and a vector). In Figure 20 we show the log–log plot of the factors $|A_\ell|$ for $0 \le \ell \le 100$, $R = 1$ and different values of k. The important observation is that the coefficients decay as $|A_\ell| \sim \ell^{-1}$.

Recalling the definition of the fractional Sobolev norms (28) on the circle, this gives that $\|Sv\|_{H^{s+1}(\partial B_R)} \le C \|v\|_{H^s(\partial B_R)}$ for all $s \in \mathbb{R}$ and all $v \in H^s(\Gamma)$, or equivalently $S : H^s(\partial B_R) \to H^{s+1}(\partial B_R)$. This bound can be proved rigorously for all boundaries Γ and for a range of s that depends on the boundary regularity.

Exercise 5.3: (Quasi-self-adjointness of S). Formula (54) implies that there is a constant $C > 0$ such that $\sup_{\mathbf{x},\mathbf{y} \in \Gamma} |\Phi_k(\mathbf{x},\mathbf{y}) + \frac{1}{2\pi} \log \frac{1}{|\mathbf{x}-\mathbf{y}|}| \le C$.

- (Difficult!) Deduce that the function $\Gamma \to \mathbb{R}$, $\mathbf{x} \mapsto \|\Phi_k(\mathbf{x},\cdot)\|_{L^2(\Gamma)}$ is bounded.

  Use the definition of Lipschitz domain.

- (Easier.) Show that the single-layer operator S is "quasi-self-adjoint" [CGLS12, p. 120], i.e. for $\psi, \phi \in L^2(\Gamma)$ it holds

$$\int_\Gamma (S\psi)\overline{\phi} \, \mathrm{d}s(\mathbf{y}) = \int_\Gamma \psi(\overline{S\phi}) \, \mathrm{d}s(\mathbf{y}).$$

  Careful: to use Fubini theorem you need to verify that the integrand is integrable (L^1) on a suitable Cartesian product set.

- Show that S is not self-adjoint, i.e., in general, $\int_\Gamma (S\psi) \, \overline{\phi} \, \mathrm{d}s(\mathbf{y}) \ne \int_\Gamma \psi \, \overline{(S\phi)} \, \mathrm{d}s(\mathbf{y})$.

5.2 Piecewise-constant BEM for the single-layer BIE

We have seen that if we were able to find a solution ψ to the BIE (58) then we would have a solution $u = \mathcal{S}\psi$ of the EDP. In general we cannot solve the BIE analytically, thus we resort to a numerical method.

The **boundary element method** (BEM) consists of choosing an N-dimensional space $V_N \subset H^{-\frac{1}{2}}(\Gamma)$ and looking for a $\psi_N \in V_N$ that approximately solves the BIE (58). There are two ways of imposing the BIE.

- **Collocation-BEM.** We choose N points $\mathbf{x}_1, \ldots, \mathbf{x}_N$ on Γ and look for

$$\psi_N \in V_N \text{ such that } (S\psi_N)(\mathbf{x}_j) = g_{\mathrm{D}}(\mathbf{x}_j), \quad j = 1, \ldots, N.$$

- **Galerkin-BEM.** We restrict the variational form (60) to the finite-dimensional space V_N, as in (33). In practice, all discrete functions we may want to consider belong to $L^2(\Gamma)$, so we can write the Galerkin-BEM as: find $\psi_N \in V_N$ such that

$$\mathcal{A}(\psi_N, \xi_N) = \int_\Gamma (S\psi_N)\overline{\xi_N} \, \mathrm{d}s = \int_\Gamma g_{\mathrm{D}}\overline{\xi_N} \, \mathrm{d}s = \mathcal{F}(\xi_N) \qquad \forall \xi_N \in V_N.$$

We recall that $H^{-\frac{1}{2}}(\Gamma)$ is a space larger than $L^2(\Gamma)$, so it accommodates discontinuous functions. This makes the construction of the discrete space V_N simpler. The simplest choice of V_N is the following: we partition the curve Γ in a mesh $\mathcal{T}_N(\Gamma)$ of N (possibly curvilinear) segments $K_1, \ldots, K_N \subset \Gamma$ (with $\bigcup_{j=1}^N \overline{K_j} = \Gamma$ and $K_j \cap K_{j'} = \emptyset$ for $j \ne j'$) and choose V_N to be the space of **piecewise constant** functions on $\mathcal{T}_N(\Gamma)$.
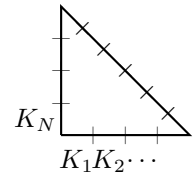
The obvious **basis** $\{\varphi_j\}_{j=1}^N$ of V_N is defined by $\varphi_j(\mathbf{x}) = 1$ if $\mathbf{x} \in K_j$ and $\varphi_j(\mathbf{x}) = 0$ if $\mathbf{x} \in \Gamma \setminus K_j$.

We expand the BEM solution in coordinates as $\boxed{\psi_N = \sum_{j=1}^N \Psi_j \varphi_j}$, where $\Psi_j = (\boldsymbol{\Psi})_j$ is the jth element of the vector $\boldsymbol{\Psi} \in \mathbb{C}^N$. So $\psi_N(\mathbf{x}) = \Psi_j$ if $\mathbf{x} \in K_j$.

With this discrete space and basis, in the collocation-BEM we choose the **collocation nodes** $\mathbf{x}_j$ such that $\mathbf{x}_j \in K_j$ for all $j = 1, \ldots, N$ and obtain the linear system $\boxed{\underline{\underline{\mathbf{A}}}^{\mathrm{Col}} \boldsymbol{\Psi} = \mathbf{F}^{\mathrm{Col}}}$, where

$$\boxed{A_{j,m}^{\mathrm{Col}} := (S\varphi_m)(\mathbf{x}_j) = \int_\Gamma \Phi_k(\mathbf{x}_j, \mathbf{y})\varphi_m(\mathbf{y}) \, \mathrm{d}s(\mathbf{y}) = \int_{K_m} \Phi_k(\mathbf{x}_j, \mathbf{y}) \, \mathrm{d}s(\mathbf{y}), \qquad F_j^{\mathrm{Col}} := g_{\mathrm{D}}(\mathbf{x}_j).} \tag{61}$$

Indeed, by the linearity of S, if ψ_N is the collocation-BEM solution then its coefficient vector $\boldsymbol{\Psi}$ solves $\underline{\underline{\mathbf{A}}}^{\mathrm{Col}}\boldsymbol{\Psi} = \mathbf{F}^{\mathrm{Col}}$:

$$F_j^{\mathrm{Col}} = g_{\mathrm{D}}(\mathbf{x}_j) = (S\psi_N)(\mathbf{x}_j) = \Big(S\sum_{m=1}^{N}\Psi_m\varphi_m\Big)(\mathbf{x}_j) = \sum_{m=1}^{N}\Psi_m(S\varphi_m)(\mathbf{x}_j) = (\underline{\underline{\mathbf{A}}}^{\mathrm{Col}}\boldsymbol{\Psi})_j.$$

To be able to evaluate the collocation-BEM right-hand side vector $\mathbf{F}^{\mathrm{Col}}$ we need $g_{\mathrm{D}} \in C^0(\Gamma)$, which is typically satisfied if the EDP comes from a scattering problem such as (45) and $g_{\mathrm{D}} = -\gamma^+ u^{\mathrm{Inc}}$.

Similarly, if ψ_N is the Galerkin-BEM solution, its coefficient vector $\boldsymbol{\Psi}$ solves $\boxed{\underline{\underline{\mathbf{A}}}^{\mathrm{Gal}}\boldsymbol{\Psi} = \mathbf{F}^{\mathrm{Gal}}}$ with

$$
\begin{aligned}
A_{j,m}^{\mathrm{Gal}} &:= \mathcal{A}(\varphi_m, \varphi_j) = \langle S\varphi_m, \varphi_j\rangle_\Gamma = \int_\Gamma (S\varphi_m)(\mathbf{x})\overline{\varphi_j}(\mathbf{x})\,\mathrm{d}s(\mathbf{x}) = \int_\Gamma\int_\Gamma \Phi_k(\mathbf{x},\mathbf{y})\varphi_m(\mathbf{y})\overline{\varphi_j}(\mathbf{x})\,\mathrm{d}s(\mathbf{y})\,\mathrm{d}s(\mathbf{x})\\
F_j^{\mathrm{Gal}} &:= \mathcal{F}(\varphi_j) = \langle g_{\mathrm{D}}, \varphi_j\rangle_\Gamma = \int_\Gamma g_{\mathrm{D}}(\mathbf{x})\overline{\varphi_j}(\mathbf{x})\,\mathrm{d}s(\mathbf{x}).
\end{aligned}
\tag{62}
$$

Choosing piecewise-constant basis functions on the elements K_j, these expressions simplify to

$$\boxed{A_{j,m}^{\mathrm{Gal}} = \int_{K_j}\int_{K_m} \Phi_k(\mathbf{x},\mathbf{y})\,\mathrm{d}s(\mathbf{y})\,\mathrm{d}s(\mathbf{x}), \qquad F_j^{\mathrm{Gal}} = \int_{K_j} g_{\mathrm{D}}(\mathbf{x})\,\mathrm{d}s(\mathbf{x}).}$$

Multiplying each row of $\underline{\underline{\mathbf{A}}}^{\mathrm{Col}}$ and $\mathbf{F}^{\mathrm{Col}}$ by the length of the corresponding element, we see that the collocation-BEM is a Galerkin-BEM with a simple 1-point quadrature. Formally, one can also think at the collocation method as a Petrov–Galerkin method with delta functions as test functions, but this is not mathematically correct in the $H^{\pm\frac{1}{2}}(\Gamma)$ framework because delta functions do not belong to $H^{-\frac{1}{2}}(\Gamma)$.

Exercise 5.4: (Testing against constants is taking means). Show that the Galerkin-BEM with piecewise-constant functions is equivalent to impose that the *integral averages* of $S\psi_N$ and g_{D} coincide on each element.

Both matrices $\underline{\underline{\mathbf{A}}}^{\mathrm{Col}}$ and $\underline{\underline{\mathbf{A}}}^{\mathrm{Gal}}$ are **dense**: this is a major difference between the BEM and the finite element method (FEM). The Galerkin matrix is also complex-symmetric, but not Hermitian.

This shortcoming of the BEM with respect to the FEM is compensated by a **dimensional reduction**: to solve a 2D problem we only need to mesh a 1D object, the boundary Γ. Thus typically BEM requires much fewer degrees of freedom (DOFs) than FEM for comparable problems and accuracies.

Another advantage of BEM is that it deals with a BVP posed on the unbounded domain Ω_+ by discretising only a bounded object, Γ. To treat the EDP with FEM one has to truncate Ω_+ as in Remark 4.26, introducing additional errors, [Ihlenburg98, §3].

The collocation-BEM is simpler to implement than the Galerkin-BEM. However, in many situations the choice of the collocation nodes adversely affects the performance of the method. To improve the numerical stability of the collocation method, often one chooses M collocation nodes with $M > N$ (oversampling) and solves an overdetermined rectangular linear system in the least-squares sense. If the datum g_{D} is discontinuous (which is possible since $H^{\frac{1}{2}}(\Gamma) \not\subset C^0(\Gamma)$), then the computation of $\mathbf{F}^{\mathrm{Col}}$ is not well-defined; on the other hand, for typical scattering problems g_{D} is continuous and piecewise smooth. Moreover, the stability and convergence theory for the Galerkin-BEM is much more complete.

A simple Galerkin-BEM simulation of the scattering of a plane wave by a polygon is shown in Figure 15. Figure 21 shows an example of a 3D collocation-BEM computation for the acoustic scattering by a jet fighter, taken from a recent paper[33].

According to [Martin06, §5.9.1], the first article proposing a BEM for the Helmholtz equation (a collocation-BEM for an exterior Neumann problem in three dimensions) was published in 1963[34].

Exercise 5.5: (Least-squares BEM). A third version of the BEM, after collocation and Galerkin, is a least-squares formulation. In this case, one looks for $\psi_N \in V_N$ such that $\int_\Gamma (S\psi_N)\overline{(S\xi_N)}\,\mathrm{d}s = \int_\Gamma g_{\mathrm{D}}\overline{(S\xi_N)}\,\mathrm{d}s$ for all $\xi_N \in V_N$. Compute the entries of the matrix $\underline{\underline{\mathbf{A}}}^{\mathrm{LS}}$ and the right-hand side $\mathbf{F}^{\mathrm{LS}}$ of the corresponding linear system. How many integrations are needed for each of them? Show that $\underline{\underline{\mathbf{A}}}^{\mathrm{LS}}$ is Hermitian and, if (58) is uniquely solvable, positive definite.

---

[33][Chaillat, Groth, Loseille, Metric-based anisotropic mesh adaptation for 3D acoustic boundary element methods, 2018]
[34][Chen, Schweikert, Sound radiation from an arbitrary body, JASA 1963]
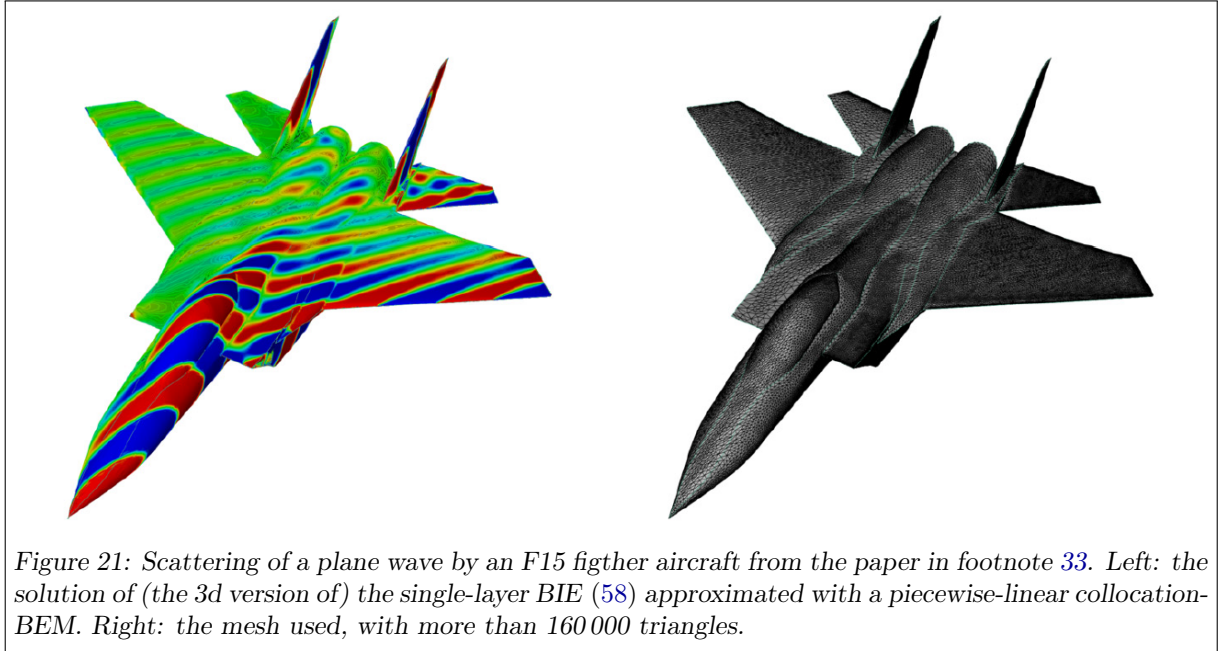
Figure 21: Scattering of a plane wave by an F15 fighter aircraft from the paper in footnote [33]. Left: the solution of (the 3d version of) the single-layer BIE (58) approximated with a piecewise-linear collocation-BEM. Right: the mesh used, with more than 160 000 triangles.

5.2.1 BEM AND QUADRATURE

From (61) and (62) we see that to compute each entry of the system matrix we need to compute an **integral of the fundamental solution**: it is a single integral on a mesh element for the collocation-BEM and a double integral on the Cartesian product of two elements for the Galerkin-BEM. To compute each entry of the right-hand side vectors, in the collocation-BEM we only need to evaluate the boundary datum g_{D} while for the Galerkin-BEM we need an integral over an element.

All these integrals require accurate **quadrature** formulas: these are among the main difficulties in a BEM implementation. In particular, for both matrices, the **diagonal entries require the approximation of singular integrals**, because of the (logarithmic) singularity of $\Phi_k(\mathbf{x}, \mathbf{y})$ at $\mathbf{x} = \mathbf{y}$.

Let us assume that Ω_- is a connected **polygon** and each mesh element is a **straight segment**. For $j = 1, \ldots, N$, the element K_j has endpoints $\mathbf{p}_j$ and $\mathbf{p}_{j+1}$ and length $h_j := |\mathbf{p}_{j+1} - \mathbf{p}_j|$ (of course $\mathbf{p}_{N+1} = \mathbf{p}_1$). The element is parametrised by $\mathbf{X}_j : (0, h_j) \to K_j$, $\mathbf{X}_j(s) := \mathbf{p}_j + s\boldsymbol{\tau}_j$, where $\boldsymbol{\tau}_j := \frac{\mathbf{p}_{j+1} - \mathbf{p}_j}{|\mathbf{p}_{j+1} - \mathbf{p}_j|}$ is the unit tangent vector to K_j.

Recalling the definition of the fundamental solution (53), the entries of the BEM matrices and vectors are then computed as integrals over intervals and rectangles:
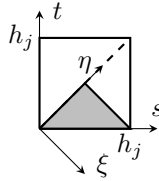
$$A_{j,m}^{\mathrm{Col}} = \frac{\mathrm{i}}{4} \int_0^{h_m} H_0^{(1)}(k|\mathbf{p}_m + s\boldsymbol{\tau}_m - \mathbf{x}_j|) \,\mathrm{d}s, \qquad F_j^{\mathrm{Col}} = g_{\mathrm{D}}(\mathbf{x}_j), \qquad F_j^{\mathrm{Gal}} = \int_0^{h_j} g_{\mathrm{D}}(\mathbf{p}_j + s\boldsymbol{\tau}_j) \,\mathrm{d}s,$$

$$A_{j,m}^{\mathrm{Gal}} = \int_0^{h_j} \left(\int_0^{h_m} \Phi_k(\mathbf{p}_j + t\boldsymbol{\tau}_j, \mathbf{p}_m + s\boldsymbol{\tau}_m) \,\mathrm{d}s \right) \mathrm{d}t = \frac{\mathrm{i}}{4} \int_0^{h_j} \left(\int_0^{h_m} H_0^{(1)}\big(k|\mathbf{p}_j - \mathbf{p}_m + t\boldsymbol{\tau}_j - s\boldsymbol{\tau}_m|\big) \,\mathrm{d}s \right) \mathrm{d}t.$$

Each diagonal entry of the collocation-BEM matrix is a singular integral, as $\mathbf{x}_j \in K_j$ for all j. A simple recipe to compute $A_{j,j}^{\mathrm{Col}}$ is to split the element in the two components of $K_j \setminus \{\mathbf{x}_j\}$ and apply Gauss quadrature on each side. To this purpose a Gauss–Legendre quadrature is a good choice, while Gauss–Lobatto rules cannot be used as they involve the value of the integrand at the endpoints, where the singularity is located. The obvious choice for the collocation nodes is to take the element midpoints: $\mathbf{x}_j = \frac{1}{2}(\mathbf{p}_j + \mathbf{p}_{j+1})$.

The jth diagonal entry of the Galerkin-BEM matrix is a double integral on the square $(0, h_j)^2 = \{0 < s, t < h_j\}$, whose integrand has a singularity along the diagonal $s = t$. One can use a quadrature formula for triangles (e.g. based on Duffy transform) on each half of the square. Alternatively, splitting the square in four triangle, exploiting the symmetries, and using the isometric change of variables $\xi = \frac{s-t}{\sqrt{2}}$, $\eta = \frac{s+t}{\sqrt{2}}$
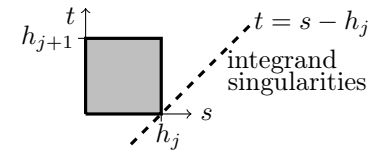
$(s = \frac{\xi+\eta}{\sqrt{2}}, t = \frac{\eta-\xi}{\sqrt{2}})$, we obtain

$$A_{j,j}^{\text{Gal}} = \int_0^{h_j} \int_0^{h_j} \frac{\mathrm{i}}{4} H_0^{(1)}(k|s-t|) \,\mathrm{d}s\,\mathrm{d}t = 4\int_0^{\frac{h_j}{\sqrt{2}}} \left(\int_\xi^{\frac{h_j}{\sqrt{2}}} \frac{\mathrm{i}}{4} H_0^{(1)}(\sqrt{2}k\xi)\,\mathrm{d}\eta \right) \mathrm{d}\xi$$
$$= \int_0^{\frac{h_j}{\sqrt{2}}} \mathrm{i}\left(\frac{h_j}{\sqrt{2}} - \xi \right) H_0^{(1)}(\sqrt{2}k\xi)\,\mathrm{d}\xi \overset{(h_j\zeta = \sqrt{2}\xi)}{=} \frac{\mathrm{i}h_j^2}{2} \int_0^1 (1-\zeta)H_0^{(1)}(kh_j\zeta)\,\mathrm{d}\zeta. \tag{63}$$

This is a one-dimensional integral with a weak singularity at the endpoint $\zeta = 0$. Its approximation with a Gauss–Legendre quadrature rule gives acceptable results.

If all elements are identical, e.g. straight segments of the same length, then also the diagonal terms are identical and they need to be computed only once: $h_j = h_{j'} \Rightarrow A_{j,j} = A_{j',j'}$.

In the Galerkin-BEM, also when two element share an endpoint we have a singularity. For example, if the segments K_j and K_{j+1} are aligned ($\boldsymbol{\tau}_j = \boldsymbol{\tau}_{j+1}$), we have

$$A_{j,j+1}^{\text{Gal}} = \int_0^{h_j} \left(\int_0^{h_{j+1}} \frac{\mathrm{i}}{4} H_0^{(1)}(k|h_j - s + t|)\,\mathrm{d}t \right) \mathrm{d}s.$$

This is a double integral on the rectangle $\{0 < s < h_j, 0 < t < h_{j+1}\}$ with a logarithmic singularity at the vertex $s = h_j$, $t = 0$. Again, since the since the weak singularity is at the boundary of the domain of integration, Gauss rules can be used.

Exercise 5.6: (BEM on non-polygonal Γ). Write the entries of the collocation- and Galerkin-BEM when Ω_- is not a polygon but a general Lipschitz domain and its boundary is defined by a parametrisation $\mathbf{X} : [0, L] \to \Gamma$.

Remark 5.7: (Gauss–Legendre quadrature). The following code computes the Gauss–Legendre nodes and weights for the interval $(0, 1)$ with the Golub–Welsch algorithm (1969). The output x, w are two length-q column vectors containing the quadrature nodes and weights, respectively. The quadrature $\sum_{j=1}^q w_j f(x_j)$ converges (for $q \to \infty$) to $\int_0^1 f(x)\,\mathrm{d}x$ for all continuous f, and it integrates exactly polynomials of degree up to $2q - 1$.

```
function [x,w] = gaussquad( q )
b     = ( 1:(q-1) ) ./ sqrt( 4*( 1:(q-1) ).^2 - 1 );
[V,D] = eig( diag(b,-1) + diag(b,1) );
x     = ( diag(D)+1 )/2;
w     = ( V(1,:).*V(1,:) )';
```

To use this quadrature on the general interval (a, b), do not forget to scale nodes and weights by the factor $b-a$: $\int_a^b f(x)\,\mathrm{d}x \approx \sum_{j=1}^q (b-a)w_j f(a + (b-a)x_j)$.

Exercise 5.8: (Singularity extraction quadrature). A typical technique to compute the singular integrals needed for the BEM is the "singularity extraction". Inserting the small-argument asymptotics (54) for the fundamental solution in the expression of $A_{j,j}^{\text{Col/Gal}}$, one can compute analytically the terms coming from the logarithm and use a standard quadrature for the remainder $\mathcal{R}$.

One of the several possible ways to implement this idea is the following. Show that, for $h > 0$,

$$\int_0^h \log\left|s - \frac{h}{2}\right| \,\mathrm{d}s = h\left(\log\frac{h}{2} - 1 \right),$$
$$\int_0^h \int_0^h \log|s-t|\,\mathrm{d}s\,\mathrm{d}t = h^2\left(\log h - \frac{3}{2} \right).$$

Use $[x(\log x - 1)]' = \log x$ and $[\frac{1}{2}x^2 \log x - \frac{1}{4}x^2]' = x\log x$, and the change of variables in (63).

Use these formulas together with (54) to approximate the BEM matrix diagonal entries $A_{j,j}^{\text{Col}}$ and $A_{j,j}^{\text{Gal}}$.

Once we have assembled and solved the BEM linear system, we have an approximation $\psi_N \in V_N$ of the solution $\psi \in H^{-\frac{1}{2}}(\Gamma)$ of the BIE (58). However to approximate the solution of the EDP (44)/SSSP (45),

we need to approximate u in the unbounded domain Ω_+. Recalling the representation formula $u = \mathcal{S}\psi$ (59), the BEM approximation of u is

$$u_N(\mathbf{x}) := (\mathcal{S}\psi_N)(\mathbf{x}) = \int_\Gamma \Phi_k(\mathbf{x}, \mathbf{y})\psi_N(\mathbf{y})\, ds(\mathbf{y}) = \sum_{j=1}^N \Psi_j \int_{K_j} \Phi_k(\mathbf{x}, \mathbf{y})\, ds(\mathbf{y}) \qquad \mathbf{x} \in \Omega_+. \qquad (64)$$

Again, each term in this sum is an integral that needs to be approximated with a quadrature formula. For all $\mathbf{x} \in \Omega_+$ the integrand is C^∞. However, if $\mathbf{x}$ lies very close to Γ the accurate evaluation of $u_N(\mathbf{x})$ requires a careful use of the quadrature as the integral is near-singular.

The function u_N computed with the BEM is an exact solution of the Helmholtz equation and exactly satisfies the Sommerfeld radiation condition. It is an approximation of the solution u of the exterior Dirichlet problem (44) only because it satisfies the boundary condition on Γ approximately.

The plots in Figure 15 have been made with the quadrature described in this section. The assembly of the Galerkin-BEM matrix and the right-hand side vector, with $N = 1\,001$ degrees of freedom, 5 Gauss quadrature points for the computation of the off-diagonal terms and for $\mathbf{F}^{\mathrm{Gal}}$, and 20 Gauss points for the terms on the diagonal of $\underline{\underline{\mathbf{A}}}^{\mathrm{Gal}}$, took less than 4 seconds on an average laptop in Matlab. With the same parameters, the assembly for the collocation method takes less than a second.
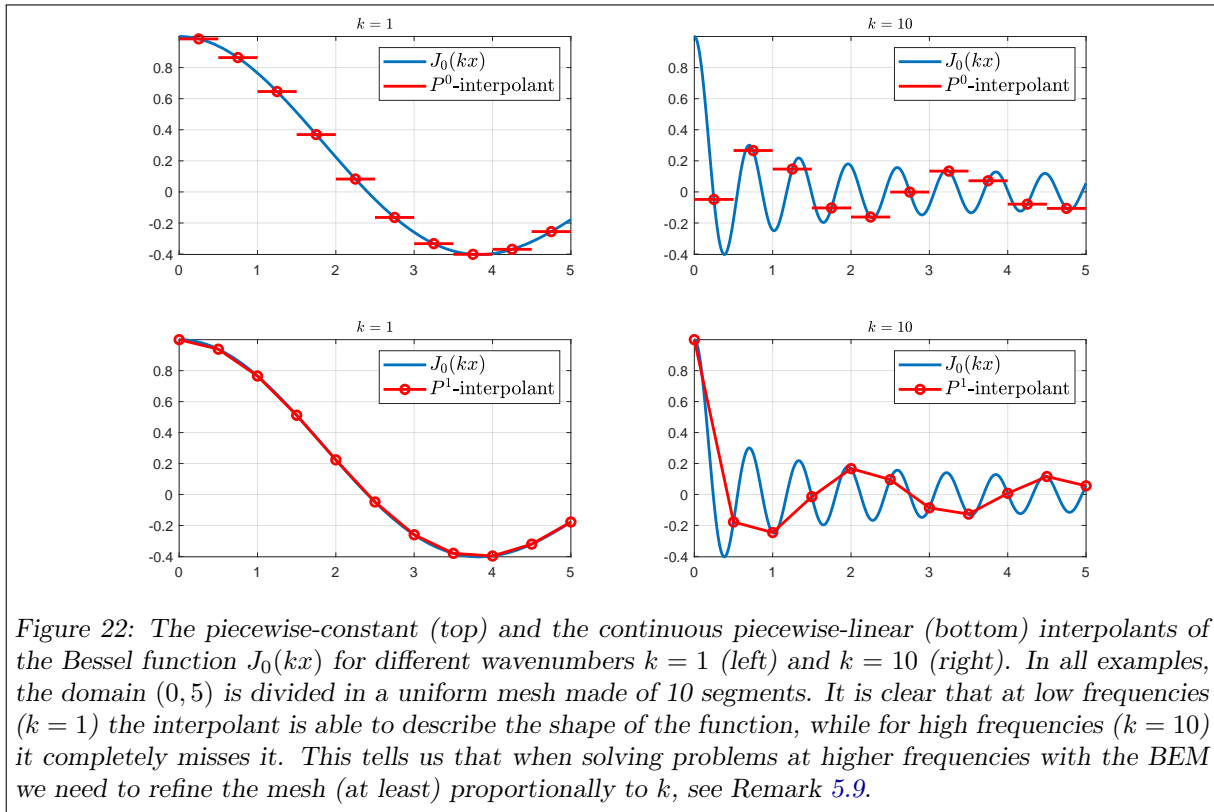
Figure 22: *The piecewise-constant (top) and the continuous piecewise-linear (bottom) interpolants of the Bessel function $J_0(kx)$ for different wavenumbers $k = 1$ (left) and $k = 10$ (right). In all examples, the domain $(0,5)$ is divided in a uniform mesh made of 10 segments. It is clear that at low frequencies $(k = 1)$ the interpolant is able to describe the shape of the function, while for high frequencies $(k = 10)$ it completely misses it. This tells us that when solving problems at higher frequencies with the BEM we need to refine the mesh (at least) proportionally to k, see Remark 5.9.*

Remark 5.9: (Resolution of oscillations). Another difficulty is due to the **oscillatory behaviour** of both Φ_k and the solution for large values of the wavenumber k.

A first issue is that to approximate the solution one needs to use more DOFs for larger values of k. See Figure 22 for a simple visual justification of this statement. A typical recipe for "engineering accuracy" (a few percent relative errors) is to use at least 10 DOFs per wavelength λ. This means that the length of each element should not exceed $\frac{\lambda}{10} = \frac{\pi}{5k}$. (Sometimes the rule of thumb is to use 6 DOFs per wavelength, corresponding roughly to $kh_j \leq 1$, for $10\%/15\%$ error.) This implies that the number of DOFs must grow like $N = \mathcal{O}(k)$ for increasing k: high-frequency problem are computationally very expensive. On the other hand, a 2D FEM needs at least $\mathcal{O}(k^2)$ DOFs as the wavelength has to be resolved in two dimensions, which is a much stronger requirement; the difficulties encountered by FEM in solving high-frequency problems are described e.g. in [Ihlenburg98] (see also §6.3.2 below).

The fundamental solution oscillates with wavelength close to $\lambda = \frac{2\pi}{k}$. Thus, even for elements K_j, K_m far from each other, in the assembly of the matrices $\underline{\underline{\mathbf{A}}}^{\mathrm{Col/Gal}}$ one has to use a sufficiently accurate quadrature formula to take into account the oscillations.

Exercise 5.10: (Gauss quadrature and oscillating functions). The q-point Gauss–Legendre quadrature corresponds to the integration of a degree-$(2q-1)$ polynomial interpolating f in q points. To integrate more oscillatory solutions, we need higher-degree polynomial interpolants, so higher-order Gauss quadratures.

Using the code in Remark 5.7, plot the Gauss–Legendre quadrature error for the approximation of $\int_0^1 f(x)\,dx$ with $f(x) = \cos(kx)e^{\sin(kx)}$, in dependence of the number of quadrature nodes and of $k > 0$. Study how the number of quadrature nodes have to be increased in dependence of k to maintain the error below a given threshold. See an example in Figure 23.
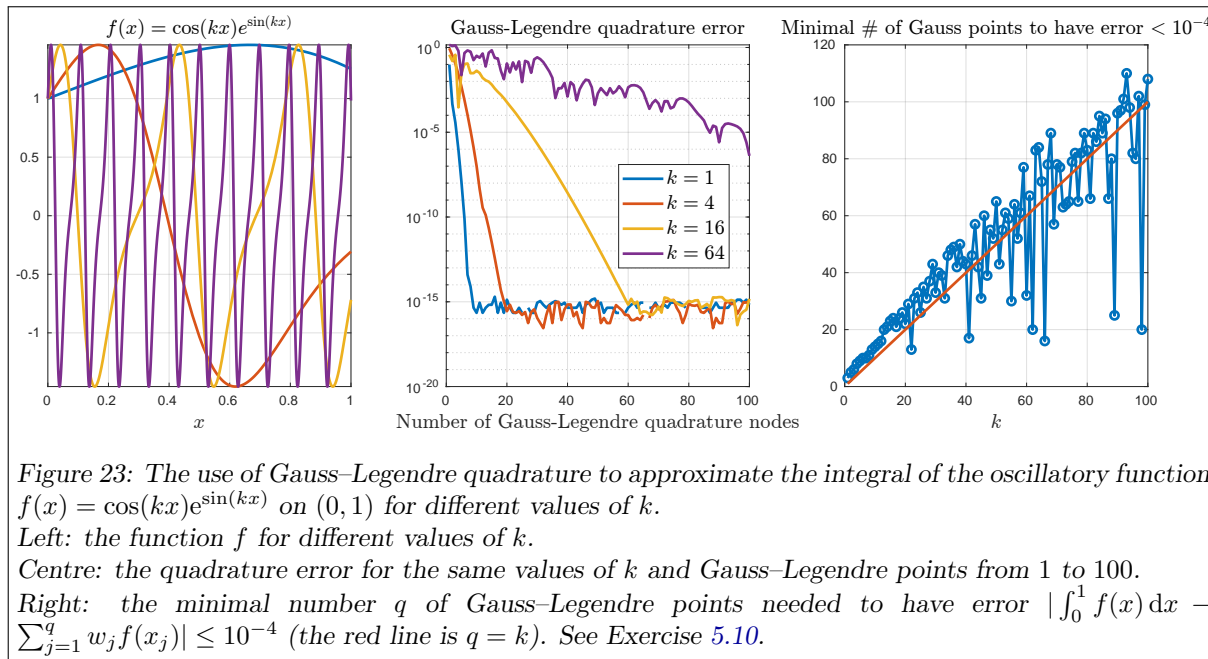
Figure 23: The use of Gauss–Legendre quadrature to approximate the integral of the oscillatory function $f(x) = \cos(kx)e^{\sin(kx)}$ on $(0,1)$ for different values of k.
Left: the function f for different values of k.
Centre: the quadrature error for the same values of k and Gauss–Legendre points from 1 to 100.
Right: the minimal number q of Gauss–Legendre points needed to have error $|\int_0^1 f(x)\,dx - \sum_{j=1}^q w_j f(x_j)| \le 10^{-4}$ (the red line is $q = k$). See Exercise 5.10.

An obvious improvement of the piecewise-constant BEM is the use of piecewise-polynomial discrete spaces of higher order. These can be discontinuous, or $C^0(\Gamma)$ or of higher continuity (at least away from corners of Γ) such as splines. The choice of basis functions, collocation points and quadrature rules is in general non-trivial. When Γ is smooth one can use also global functions such as mapped trigonometric functions, in the spirit of spectral methods. If Γ is a polygon (possibly with curvilinear sides), the BIE solution is usually singular close to its corners: to approximate it efficiently one can use a graded mesh, i.e. a mesh whose elements are smaller the closer they are to a corner.

5.2.2   BEM coding project

Implement the collocation-BEM method for the scattering of a plane wave by a polygon Ω_-.
Use a discrete space V_N of piecewise-constant functions. Choose a mesh such that the elements on a given side of Γ have equal length. Plot the scattered field u_N and the total field on a portion of Ω_+. You can use the quadrature routine provided.

A possible suggestion for the main steps in the code:

1. **Initialise** the geometric data structure. Given the vertices of the polygon, decide the number of elements on each side, and generate (for each element K_j) the endpoint $\mathbf{p}_j$, the length h_j, the tangent vector $\boldsymbol{\tau}_j$, and the collocation point $\mathbf{x}_j$, chosen as the element midpoint. Choose elements with roughly the same size.

   (In Matlab it might be convenient to treat points and vectors in the plane as complex numbers with the usual identification $\mathbb{C} \sim \mathbb{R}^2$; then the `abs` function allows for immediate computation of distances.)

2. **Assemble** the matrix $\underline{\underline{\mathbf{A}}}^{\text{Col}}$ (being careful with the quadrature) and the right-hand side $\mathbf{F}^{\text{Col}}$.

   You can use the Gauss–Legendre quadrature routine `gaussquad` provided.

3. **Solve** the linear system.

4. **Evaluate** the near-field u_N on a grid of points in 2D using the representation formula and plot it.

To generate the grid of points for the plot use `meshgrid`. To plot the field you can use one of the Matlab commands `pcolor` (used for Figure 15), `surf`, `mesh` or `contour`. To hide the grid points that lie inside Ω_- you can locate them with `inpolygon` and set them to 0 or `NaN` (or use `patch`).

Plot the total field $u_N^{\mathrm{Tot}} = u_N + u^{\mathrm{Inc}}$: if it does not vanish approaching Γ then the code is not correct.

Plenty of interesting extensions are possible:

- Choose as incident wave u^{Inc} a **fundamental solution** centred in some $\mathbf{x}_0 \in \Omega_+$. (The total field cannot be plotted close to $\mathbf{x}_0$.) You can also try more exotic incident waves, such as Herglotz functions.

- Implement the problem of the scattering by **multiple polygons**, i.e. with Ω_- made of several components. Here Matlab's "cell arrays" are useful to store vectors with different lengths in a single variable, e.g., the coordinates of the vertices of polygons with different numbers of sides.

- Implement the **Galerkin-BEM** for the same problem, on the same mesh. The only difference is in the assembly of the matrix and the right-hand side. Compare the solutions obtained with the two versions of the scheme.

- Generate a time-harmonic **animation** of the scattered and total fields.

  You can generate a .gif file using the script provided or export a video in various formats such as .avi.

- Implement the **singularity-extraction** quadrature of Exercise 5.8.

- Use meshes that are **locally refined** towards the corners of Γ to better approximate the solution singularities.

- Compute and plot the Helmholtz **Poynting vector** $\mathbf{S}(u^{\mathrm{Scat}})$ defined in Exercise 2.15 (see Figure 16).

  The Matlab command `quiver` helps. You can approximate the gradient ∇u^{Scat} with finite differences.

- Approximate the **error** committed by the scheme e.g. as $\|\psi_N - \psi_{\mathrm{ref}}\|_{L^2(\Gamma)}$ or $\|u_N - u_{\mathrm{ref}}\|_{L^2(\Omega_*)}$ where Ω_* is (a subset of) the portion of Ω_+ where you plot the near-field and $\psi_{\mathrm{ref}}/u_{\mathrm{ref}}$ are the reference solutions obtained with a very fine mesh. Plot the convergence of the error against N or h.

  Another way to estimate the accuracy of the numerical solution is provided by Remark 5.35.

- **Test** the code by solving the EDP (44) with a radiating Fourier–Hankel function centred inside Ω_- (or a linear combination of such functions) as solution u. This is not an SSSP (45) but allows to compute the near-field error $u_N - u$. In this case the solution is smooth also close to the corners of Ω_-.

- Study the dependence of the results on the **parameters**. You can see how the plots and the norms of the solution and the error vary when you change the number N of DOFs, the wavenumber k, the product kh, the quality of the quadrature, the shape of Ω_-...

  For instance: for increasing k, if the mesh is refined keeping kh constant, how does the error behave?

  How does the condition number depend on h?

  Do convergence rates differ for the scattering of a plane wave or for a prescribed Fourier–Hankel u?

- Test the code (for a square scatterer) by computing the near-field error against the **reference solution** provided.[35] This was computed with MPSpack (https://github.com/ahbarnett/mpspack). Compare your result against Figure 32.

- Implement the collocation-BEM with **oversampling**, i.e. with M collocation points, N degrees of freedom, and $M > N$. For instance take $M = cN$ for some fixed $c > 1$. Solve the rectangular linear system in the least-square sense (with the backslash command). Does the accuracy of the method improve? How does the cost increase? How does the position (equispaced, random,...) of the collocation points impact the results?

- Solve the BEM linear system using an appropriate **iterative method**, e.g. GMRES (`gmres` in Matlab). Study its performance (number of iterations to reach a given accuracy, computing time...) in dependence of the problem parameters (N, k, the shape of Ω_-,...).

---

[35]Load the .mat file provided. The vectors `gx`, `gy` contain the coordinates of the nodes of a Cartesian grid in the square $(-1.5, 1.5)^2$. The matrix `ui` contains the values of an incoming plane wave with direction $\mathbf{d} = \frac{1}{\sqrt{2}}(1, -1)$ and wavenumber $k = 20$, in the the grid points exterior to the unit circle, and 0 otherwise. The entries of the matrix `u` are: the values of the scattered field $u = u^{\mathrm{Scat}}$ in the grid points exterior to the unit circle, the values of the total field u^{Tot} in the points interior to the unit circle but exterior to the scatterer $(-0.5, 0.5)^2$, and not-a-number `nan` values inside the scatterer. You can plot the total field with the commands

```
load MPSpackBenchmarkSquareScatt.mat; pcolor(gx,gy,real(ui+u)); shading flat; axis square;
```

It is also easy to generate other benchmark solutions with MPSpack, which is a package running in Matlab.

- Extend the code to **curvilinear** polygons and/or smooth scatterers.

  The use of the arclength parametrisation of the boundary makes the implementation simpler. Make sure that the quadrature points lie on the curve Γ.

  You can test your code for a circular obstacle against the analytic solution obtained in Exercise 4.21.

- Implement a **higher-order** version of the BEM with (either $C^0(\Gamma)$ or discontinuous) piecewise-polynomial basis functions of degree $p > 0$.

- Extend the code to discrete spaces made of continuous **splines** of maximal regularity, i.e. piecewise-polynomials of degree p with continuity $C^{p-1}(\Gamma)$. In the collocation version of the scheme, for even p choose the collocation nodes as the element mid-points (as we have done for $p = 0$), for odd p choose them as the element endpoints. With this choice, the collocation-BEM is well-posed and quasi-optimal[36] for sufficiently small h.

- Implement a **spectral BEM** on a smooth curvilinear scatterer.

  Choose a smooth scatterer defined by a parametrisation $\mathbf{X} : [0, 2\pi] \to \Gamma$. E.g. a shape often used as example for scattering problems is the kite $\mathbf{X}(t) = (\cos t + 0.65(\cos 2t - 1), \ 1.5 \sin t)$, [CK2, Fig. 3.1]. For $L \in \mathbb{N}$ and $N = 2L + 1$, choose as basis functions the mapped complex exponentials $\varphi_\ell(\mathbf{x}) = \mathrm{e}^{\mathrm{i}\ell \mathbf{X}^{-1}(\mathbf{x})}$, $-L \leq \ell \leq L$, or the corresponding trigonometric functions $\sin(\ell \mathbf{X}^{-1}(\mathbf{x})), \cos(\ell \mathbf{X}^{-1}(\mathbf{x}))$.

- Apply the **uncertainty quantification** (UQ) techniques to scattering problems approximated with the BEM. For instance, how do random perturbations of the position of the vertices of a triangular scatterer affect the far-field u_∞? How does its variance depend on the wavenumber?

- . . .

The next sections provide several suggestions for further extensions of your code; see in particular the exercises.

Exercise 5.11: (Proximity resonance). Choose $u^{\mathrm{Inc}}(\mathbf{x}) = \Phi_k(\mathbf{x}, \mathbf{y})$ for a fixed source point $\mathbf{y}$ at a small distance from a straight side of a sound-soft obstacle. Compare the total field u^{Tot} when the distance between $\mathbf{y}$ and the obstacle is $\frac{\lambda}{2}$ and $\frac{\lambda}{4}$, λ being the problem wavelength. What do you observe? Can you explain it? Compare with [Heller13, p. 193], where sound-hard obstacles are considered.

Exercise 5.12: (Build your own quasi-resonance). When a plane wave impinges on a scatterer Ω_- with a simple shape, for example convex or star-shaped[37], it is possible to prove that some norm of the scattered field is stable (does not grow) for $k \to \infty$. On the contrary, if Ω_- has a cavity (part of Ω_+, which is connected) that can "trap" a wave, the scattered field in the cavity can be extremely large.

   Using your BEM code, try to find a polygonal scatterer that traps an incoming plane wave. Recall the discussion of Dirichlet eigenfunctions (which exist only for bounded regions) in §4.2. With a simple polygon with 12 sides it is not difficult to obtain a scattered field with magnitude $|u^{\mathrm{Scat}}| > 30$ in some region (with $\|u^{\mathrm{Inc}}\|_{L^\infty(\mathbb{R}^2)} = 1$).

   Careful: for a given domain only some wavenumbers will do. The computations in §4.2 might help you choosing the right k for your trapping domain.

Exercise 5.13: (BEM vs FEM). Recall the approximation of the SSSP/EDP described in Remark 4.26 and Exercise 5.17: Ω_+ is truncated to $\Omega_R = B_R \setminus \overline{\Omega_-}$ and the homogeneous impedance boundary condition $\partial_{\mathbf{n}} u^{\mathrm{Scat}} - \mathrm{i}k u^{\mathrm{Scat}} = 0$ is imposed on ∂B_R.

   Use the 2D FEM code you have implemented in the finite element course to discretise this BVP. Careful: FEM basis functions (e.g. tent functions) are real, but the right-hand side vector and the coefficients of the discrete solution are complex. Compare the results against those obtained with BEM.

   Extra: Instead of the impedance condition, impose the DtN map (50) using circular harmonics. This is harder and involves the assembly of a dense block in the matrix.

Remark 5.14: (Fast Matlab code). Often, most of the computational time in a simple BEM code is spent evaluating the fundamental solution for the assembly of $\underline{\underline{\mathbf{A}}}^{\mathrm{Col/Gal}}$ and the evaluation of u_N. You can check how much time is spent on each part of your Matlab code using the `profile` command, for instance

```
1  profile on;      MyFunctionDoingWhatever;    profile viewer
```

---

[36][Arnold, Wendland, *The convergence of spline collocation for strongly elliptic equations on curves*, Numer.Math. 1985]
[37]A domain $D \subset \mathbb{R}^n$ is called **star-shaped** with respect to a point $\mathbf{x}_0$ if, for all $\mathbf{x} \in D$, the segment with endpoints $\mathbf{x}_0$ and $\mathbf{x}$ is contained in D. It is star-shaped with respect to a subset D' if it is star-shaped with respect to all points in D'.

A simple implementation of the piecewise-constant collocation-BEM assembles the matrix $\underline{\underline{\mathbf{A}}}^{\mathrm{Col}}$ using a triple loop: over rows, columns and quadrature points. This requires $N^2 q$ calls to the function `besselh`, where q is the number of quadrature nodes per element (ignoring the different treatment needed for the diagonal terms). The evaluation of the near-field u_N on a $M \times M$ grid, for plots such as Figure 15, using a q-point quadrature approximation of (64), requires $M^2 N q$ evaluations of Φ_k, and can be easily coded with a quadruple loop and $M^2 N q$ calls to `besselh`. However, we know that Matlab is most efficient if we reduce as much as possible the use of nested loops and apply functions such as `besselh` to few vectors or matrices (as opposed to many scalars). You can observe this running

```
n = 5000; A=rand(n);
B=ones(n)*1i; C=ones(n)*1i;      % Initialise complex matrices
tic; B=besselh(0,1,A); toc
tic; for j=1:n; for jj=1:n; C(j,jj)=besselh(0,1,A(j,jj)); end; end; toc
```

Keep this in mind to write a fast Matlab code: avoid loops, vectorise operations, and reduce the number of calls to the fundamental solution.

On the other hand, the evaluation of `besselh` on so many inputs simultaneously might require too much memory (e.g. to store $N^2 q$ complex numbers instead of N^2 for the matrix assembly, $M^2 N q$ instead of M^2 for u_N) and prevents computation with large values of N, q, M. Thus, also excessive vectorisation can hinder the BEM code. To obtain an efficient code, you have to find a balance between the reduction of function calls and the memory constraints (also, do not forget to delete large temporary variables, such as the stiffness matrix, after they have been used).

5.3 GREEN'S INTEGRAL REPRESENTATION

The Green's integral representation, or Green's third identity, is an important tool to derive new BIEs and BEMs, and to understand the properties of the corresponding BVPs. It extends Green's second identity (31). We write it and prove it for bounded and unbounded Lipschitz domains.

We keep using the notation introduced in §4.3. In particular, we recall that the unit normal $\mathbf{n}$ on the boundary of the bounded domain Ω_- is defined to point outwards, into the complement Ω_+; this enters the definition of the Neumann trace $\partial_{\mathbf{n}}$. Since the fundamental solution Φ_k depends on two variables, we write $\frac{\partial \Phi_k(\mathbf{x},\mathbf{y})}{\partial n(\mathbf{x})}$ and $\frac{\partial \Phi_k(\mathbf{x},\mathbf{y})}{\partial n(\mathbf{y})}$ to make clear which is the variable with respect to which we derive and take the trace. We recall that when we write $\int_\Gamma \varphi \overline{\psi} \, \mathrm{d}s$ for $\varphi \in H^{-\frac{1}{2}}(\Gamma)$ and $\psi \in H^{\frac{1}{2}}(\Gamma)$ (or vice versa) we mean the duality product $\langle \varphi, \psi \rangle_\Gamma$.

Theorem 5.15: (Green's representation in Ω_-). Let Ω_- be a bounded Lipschitz domain and $u \in H^1(\Omega_-; \Delta) \cap C^2(\Omega_-)$ be a Helmholtz solution in Ω_-. Then:

$$\int_\Gamma \left(\partial_{\mathbf{n}}^- u(\mathbf{y}) \Phi_k(\mathbf{x},\mathbf{y}) - \gamma^- u(\mathbf{y}) \frac{\partial \Phi_k(\mathbf{x},\mathbf{y})}{\partial n(\mathbf{y})} \right) \mathrm{d}s(\mathbf{y}) = \begin{cases} u(\mathbf{x}) & \text{if } \mathbf{x} \in \Omega_-, \\ 0 & \text{if } \mathbf{x} \in \Omega_+. \end{cases} \tag{65}$$

Proof. If $\mathbf{x} \in \Omega_+$, then both u and Φ_k are Helmholtz solution in Ω_- thus the volume integral in Green's second identity (31) vanishes and what is left is (65).

If $\mathbf{x} \in \Omega_-$ we take $\epsilon > 0$ such that the ball $B_\epsilon(\mathbf{x}) := \{\mathbf{z} \in \mathbb{R}^2 : |\mathbf{z} - \mathbf{x}| < \epsilon\} \subset \Omega_-$. Applying again Green's second identity in $\Omega_- \setminus \overline{B_\epsilon(\mathbf{x})}$ we have

$$\int_\Gamma \left(\partial_{\mathbf{n}}^- u(\mathbf{y}) \Phi_k(\mathbf{x},\mathbf{y}) - \gamma^- u(\mathbf{y}) \frac{\partial \Phi_k(\mathbf{x},\mathbf{y})}{\partial n(\mathbf{y})} \right) \mathrm{d}s(\mathbf{y}) = - \int_{\partial B_\epsilon(\mathbf{x})} \left(\partial_{\mathbf{n}} u(\mathbf{y}) \Phi_k(\mathbf{x},\mathbf{y}) - \gamma u(\mathbf{y}) \frac{\partial \Phi_k(\mathbf{x},\mathbf{y})}{\partial n(\mathbf{y})} \right) \mathrm{d}s(\mathbf{y}),$$

where $\mathbf{n}$ points into the ball (this is why we have a minus sign in front of $\int_{\partial B_\epsilon(\mathbf{x})}$). We now want to take the limit for $\epsilon \searrow 0$ of the right-hand side, and see that the first term vanish, while the second converges to $u(\mathbf{x})$. The advantage of using a ball centred at $\mathbf{x}$, is that on its boundary the value of $\Phi_k(\mathbf{x}, \cdot)$ and its normal derivative are constant.
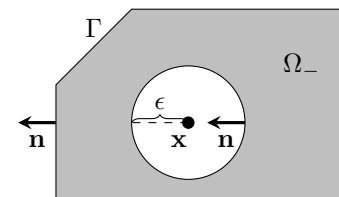
To this purpose, we need some properties of Hankel functions: the formula for the first derivative of $H_0^{(1)}$ and the asymptotics for small arguments (from [DLMF, §10.7], recall also (54)):

$$\frac{\partial}{\partial z} H_0^{(1)}(z) = -H_1^{(1)}(z), \qquad H_0^{(1)}(z) \sim \frac{2\mathrm{i}}{\pi} \log z, \qquad H_\ell^{(1)}(z) \sim -\frac{\mathrm{i}}{\pi}(\ell-1)! \frac{2^\ell}{z^\ell}, \qquad \ell \in \mathbb{N}, \qquad z \to 0. \tag{66}$$

(Here $a(z) \sim b(z)$ for $z \to 0$ means that $\lim_{z \searrow 0} \frac{a(z)}{b(z)} = 1$.)

We take the limit $\lim_{\epsilon \to 0}$ of the first term using the expression of the fundamental solution, the divergence theorem, $\operatorname{div} \nabla = \Delta$, $\Delta u = -k^2 u$, the asymptotics (66), the mean value theorem (in the form $\lim_{\epsilon \to 0} \frac{1}{\pi \epsilon^2} \int_{B_\epsilon(\mathbf{x})} f(\mathbf{y}) \, d\mathbf{y} = f(\mathbf{x})$), the boundedness of u in $\mathbf{x}$:

$$
\begin{aligned}
-\int_{\partial B_\epsilon(\mathbf{x})} \partial_{\mathbf{n}} u(\mathbf{y}) \Phi_k(\mathbf{x}, \mathbf{y}) \, ds(\mathbf{y}) &= -\frac{i}{4} H_0^{(1)}(k\epsilon) \int_{\partial B_\epsilon(\mathbf{x})} \partial_{\mathbf{n}} u(\mathbf{y}) \, ds(\mathbf{y}) \\
&= \frac{i}{4} H_0^{(1)}(k\epsilon) \int_{B_\epsilon(\mathbf{x})} \Delta u(\mathbf{y}) \, d\mathbf{y} \\
&= -\frac{i}{4} H_0^{(1)}(k\epsilon) k^2 \int_{B_\epsilon(\mathbf{x})} u(\mathbf{y}) \, d\mathbf{y} \sim -\frac{i}{4} \left(\frac{2i}{\pi} \log k\epsilon \right) k^2 \pi \epsilon^2 u(\mathbf{x}) \xrightarrow{\epsilon \searrow 0} 0.
\end{aligned}
$$

Using the expression of the radial derivative of Φ_k, the asymptotics (66), the mean value theorem $\left(\lim_{\epsilon \to 0} \frac{1}{2\pi\epsilon} \int_{\partial B_\epsilon(\mathbf{x})} f(\mathbf{y}) \, ds(\mathbf{y}) = f(\mathbf{x}) \right)$ we get

$$
\begin{aligned}
\int_{\partial B_\epsilon(\mathbf{x})} u(\mathbf{y}) \frac{\partial \Phi_k(\mathbf{x}, \mathbf{y})}{\partial n(\mathbf{y})} \, ds(\mathbf{y}) &= k \frac{i}{4} H_1^{(1)}(k\epsilon) \int_{\partial B_\epsilon(\mathbf{x})} u(\mathbf{y}) \, ds(\mathbf{y}) \\
&\sim k \frac{i}{4} \left(\frac{-2i}{\pi k \epsilon} \right) \int_{\partial B_\epsilon(\mathbf{x})} u(\mathbf{y}) \, ds(\mathbf{y}) \sim \left(\frac{1}{2\pi\epsilon} \right) 2\pi\epsilon u(\mathbf{x}) = u(\mathbf{x}).
\end{aligned}
$$

(The first of the two limits $\lim_{\epsilon \to 0} \int_{\partial B_\epsilon(\mathbf{x})} \ldots$ vanishes, while the second one is non-zero: this is because the singularity of the first derivative of the fundamental solution Φ_k is stronger than that of Φ_k itself, so it compensates the infinitesimal length of the circle on which it is integrated.) $\qquad\square$

Green's representation formula allows to compute any Helmholtz solution from its two traces.

Representation (65) also explains why we chose the coefficient $\frac{i}{4}$ in the definition (53) of Φ_k: it allows to write a simple Green's representation.

Green's representation is sometimes called "Kirchhoff–Helmholtz integral".

Remark 5.16: (Green representation and impedance BVP). From Green's representation (65), it follows immediately that if u is a Helmholtz solution in Ω_- and $\gamma^- u = \partial_{\mathbf{n}}^- u = 0$ then $u = 0$. We have already proved the same fact by other means (extending u by zero and using the discreteness of Laplace–Dirichlet eigenvalues) in Lemma 4.10. This was a key step to prove the well-posedness of the impedance interior problem (37) in Proposition 4.12.

Exercise 5.17: (Truncated BVP). Let $\Omega_R = B_R \setminus \overline{\Omega_-}$, where B_R is an open ball containing $\overline{\Omega_-}$. Write a truncation of the EDP (44) to Ω_R, as described in Remark 4.26 imposing impedance boundary conditions on ∂B_R and sound-soft conditions on Γ. Show that the BVP obtained is well-posed.

Remark 5.18: (Green's representation with volume term). If u in (65) were not Helmholtz solution we would need to add to the left-hand side of Green's representation the volume integral term $-\int_{\Omega_-} \left(\Delta u(\mathbf{y}) + k^2 u(\mathbf{y}) \right) \Phi_k(\mathbf{x}, \mathbf{y}) \, d\mathbf{y}$. When $\mathbf{x} \in \Omega_-$ the integrand is weakly singular, see (66), and the integral is well-defined.

Remark 5.19: (Green's representation in 3D). In the 3-dimensional case all the arguments are similar. The fundamental solution has the simpler expression $\Phi_k(\mathbf{x}, \mathbf{y}) = \frac{e^{ik|\mathbf{x}-\mathbf{y}|}}{4\pi|\mathbf{x}-\mathbf{y}|}$, which does not involve Bessel and Hankel function, so checking the limits for $\epsilon \searrow 0$ is simpler.

The integral over $\partial B_\epsilon(\mathbf{x})$ in the proof of Theorem 5.15 gives the same value for any path in Ω_- with winding number 1 around $\mathbf{x}$. This reminds of complex analysis, but the key ingredient here is just integration by parts. Indeed the same argument works in 3D.

To write a Green's representation formula for unbounded domains, we denote by B_R the ball of radius $R > 0$ centred at $\mathbf{0}$ and fix $\mathbf{n} = \frac{\mathbf{x}}{r}$ on ∂B_R. We work in the bounded region $B_R \cap \Omega_+$, for sufficiently large R and use Sommerfeld condition to take the limit $R \to \infty$. The unit normal $\mathbf{n}$ points into $B_R \cap \Omega_+$ on the inner boundary Γ and out of $B_R \cap \Omega_+$ on the outer boundary ∂B_R.
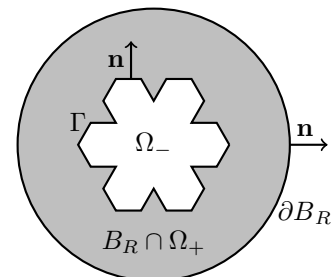
Lemma 5.20: (Properties of radiating solutions). Let Ω_- be a bounded Lipschitz domain, $\Gamma = \partial\Omega_-$, $\Omega_+ = \mathbb{R}^2 \setminus \overline{\Omega_-}$, and $u, w \in H^1_{\text{loc}}(\Omega_+; \Delta) \cap C^2(\Omega_+)$ be two *radiating* Helmholtz solutions in Ω_+. Then:

$$\lim_{R \to \infty} \int_{\partial B_R} |u|^2 \, \mathrm{d}s < \infty, \qquad \Im \int_\Gamma \partial_{\mathbf{n}} u \, \gamma \overline{u} \, \mathrm{d}s \geq 0 \qquad \lim_{R \to \infty} \int_{\partial B_R} (\partial_{\mathbf{n}} u \, w - u \partial_{\mathbf{n}} w) \, \mathrm{d}s = 0. \quad (67)$$

Proof. We first prove the boundedness of the limit of $\|u\|_{L^2(\partial B_R)}$. The imaginary part of Green's first identity (30) with $w = \overline{u}$ in $B_R \cap \Omega_+$ gives

$$\Im \int_\Gamma \partial_{\mathbf{n}} u \, \gamma \overline{u} \, \mathrm{d}s = \Im \int_{\partial B_R} \partial_{\mathbf{n}} u \, \gamma \overline{u} \, \mathrm{d}s + \underbrace{\Im \int_{B_R \cap \Omega_+} (k^2 |u|^2 - |\nabla u|^2) \, \mathrm{d}\mathbf{x}}_{=0, \text{ imaginary part of real value}}$$

$$= \frac{1}{2k} \int_{\partial B_R} \left(k^2 |u|^2 + |\partial_{\mathbf{n}} u|^2 - |\partial_{\mathbf{n}} u - iku|^2 \right) \, \mathrm{d}s,$$

where we have used the identity $|a - ib|^2 = |a|^2 + |b|^2 - 2\Re\{a\,\overline{ib}\} = |a|^2 + |b|^2 - 2\Im\{a\overline{b}\}$, which holds for all $a, b \in \mathbb{C}$, applied to $a = \partial_{\mathbf{n}} u$, $b = ku$. Taking the limit for $R \to \infty$, the term $\int_{\partial B_R} |\partial_{\mathbf{n}} u - iku|^2 \, \mathrm{d}s \to 0$, by the Sommerfeld condition (43). The left-hand side is independent of R, thus

$$\lim_{R \to \infty} \frac{1}{2k} \left(k^2 \|u\|^2_{L^2(\partial B_R)} + \|\partial_{\mathbf{n}} u\|^2_{L^2(\partial B_R)} \right) = \Im \int_\Gamma \partial_{\mathbf{n}} u \, \gamma \overline{u} \, \mathrm{d}s < \infty.$$

Since the norms are non-negative and the limit is finite, each of them is bounded, which is the desired inequality. In particular $u = \mathcal{O}(r^{-1/2})$ for $r \to \infty$. Moreover the left-hand side is non-negative, so also the second inequality is proved.

The Sommerfeld condition, together with $u, w = \mathcal{O}(r^{-1/2})$, gives the identity involving w:

$$\int_{\partial B_R} (\partial_{\mathbf{n}} u \, w - w \partial_{\mathbf{n}} u) \, \mathrm{d}s = \int_{\partial B_R} \left(\left(iku + o(R^{-1/2}) \right) w - u \left(ikw + o(R^{-1/2}) \right) \right) \, \mathrm{d}s$$

$$= \int_{\partial B_R} \left(o(R^{-1/2})\mathcal{O}(R^{-1/2}) - \mathcal{O}(R^{-1/2})o(R^{-1/2}) \right) \, \mathrm{d}s = \int_{\partial B_R} o(R^{-1}) \, \mathrm{d}s \xrightarrow{R \to \infty} 0.$$

$\square$

Recall that we have already seen in Theorem 4.36 (Rellich's lemma) a stronger version of the second inequality in (67): if this integral is 0 then $u = 0$ (see the first formula in the proof to relate the integrals on Γ and on ∂B_R).

The Sommerfeld radiation condition can be extended to problems with complex wavenumbers with $\Im k \geq 0$, Lemma 5.20 holds also in this case, see [CK1, Thm. 3.3].

Theorem 5.21: (Green's representation in Ω_+). Let Ω_- be a bounded Lipschitz domain, $\Gamma = \partial\Omega_-$, $\Omega_+ = \mathbb{R}^2 \setminus \overline{\Omega_-}$, and $u \in H^1_{\text{loc}}(\Omega_+; \Delta) \cap C^2(\Omega_+)$ be a *radiating* Helmholtz solution in Ω_+. Then:

$$-\int_\Gamma \left(\partial_{\mathbf{n}}^+ u(\mathbf{y}) \Phi_k(\mathbf{x}, \mathbf{y}) - \gamma^+ u(\mathbf{y}) \frac{\partial \Phi_k(\mathbf{x}, \mathbf{y})}{\partial n(\mathbf{y})} \right) \mathrm{d}s(\mathbf{y}) = \begin{cases} 0 & \text{if } \mathbf{x} \in \Omega_-, \\ u(\mathbf{x}) & \text{if } \mathbf{x} \in \Omega_+. \end{cases} \quad (68)$$

Proof. Let $R > 0$ be the radius of a ball such that $\Gamma \subset B_R$ and, if $\mathbf{x} \in \Omega_+$ also $\mathbf{x} \in B_R$. Then Green's representation (65) applied in $\Omega_+ \cap B_R$ gives

$$\left(\int_{\partial B_R} - \int_\Gamma \right) \left(\partial_{\mathbf{n}}^+ u(\mathbf{y}) \Phi_k(\mathbf{x}, \mathbf{y}) - \gamma^+ u(\mathbf{y}) \frac{\partial \Phi_k(\mathbf{x}, \mathbf{y})}{\partial n(\mathbf{y})} \right) \mathrm{d}s(\mathbf{y}) = \begin{cases} 0 & \text{if } \mathbf{x} \in \Omega_-, \\ u(\mathbf{x}) & \text{if } \mathbf{x} \in \Omega_+. \end{cases}$$

Taking the limit for $R \to \infty$, the integral over ∂B_R vanishes by the identity in (67) and we conclude. $\square$

Corollary 5.22: (There are no entire radiating solutions). Let $u_+ \in H^1_{\text{loc}}(\Omega_+; \Delta)$ be a radiating Helmholtz solution and $u_- \in H^1(\Omega_-; \Delta)$ a Helmholtz solution. If they have the same traces on Γ, i.e. $\gamma^+ u_+ = \gamma^- u_-$ and $\partial_{\mathbf{n}}^+ u_+ = \partial_{\mathbf{n}}^- u_-$, then $u_+ = 0$ and $u_- = 0$.
In particular, the only radiating Helmholtz solution in the whole of $\mathbb{R}^2$ is $u = 0$.

In this corollary, the assumption that the solution is radiating is necessary: plane waves and smooth Fourier–Bessel functions are Helmholtz solutions in $\mathbb{R}^2$, but not radiating. The radiating Fourier–Hankel functions are not defined in the whole of $\mathbb{R}^2$ as they are singular at the origin. Intuitively, the corollary says that all radiating solutions "go towards infinity" and they need to have a source somewhere; on the other hand, plane waves are not radiating and have "a source at infinity".

We have evaluated the integral in Green's representation in $\mathbf{x} \in \Omega_- \cup \Omega_+ = \mathbb{R}^2 \setminus \Gamma$. What about $\mathbf{x} \in \Gamma$? We extend Green's representation (65)/(68) to this case.

For $\mathbf{x} \in \Gamma$ define

$$\sigma(\mathbf{x}) := \lim_{\epsilon \to 0} \frac{1}{2\pi\epsilon} \int_{\mathbf{y} \in \Omega_-, |\mathbf{y} - \mathbf{x}| = \epsilon} \mathrm{d}s.$$

If Γ is C^1 in $\mathbf{x}$ then $\sigma(\mathbf{x}) = \frac{1}{2}$; if Γ forms an angle with opening α at $\mathbf{x}$ then $\sigma(\mathbf{x}) = \frac{\alpha}{2\pi}$. By Rademacher theorem (Lipschitz functions are differentiable a.e.), for a Lipschitz Γ, $\sigma = \frac{1}{2}$ almost everywhere on Γ.

Lemma 5.23: (Green's representation on Γ). Let $u \in H^1(\Omega_-; \Delta) \cap C^0(\overline{\Omega_-})$ be a Helmholtz solution. Then

$$\int_{\Gamma} \left(\partial_{\mathbf{n}}^- u(\mathbf{y}) \Phi_k(\mathbf{x}, \mathbf{y}) - \gamma^- u(\mathbf{y}) \frac{\partial \Phi_k(\mathbf{x}, \mathbf{y})}{\partial n(\mathbf{y})} \right) \mathrm{d}s(\mathbf{y}) = \sigma(\mathbf{x}) u(\mathbf{x}) \qquad \mathbf{x} \in \Gamma. \tag{69}$$

If $u \in H^1_{\mathrm{loc}}(\Omega_+; \Delta) \cap C^0(\overline{\Omega_+})$ is a radiating Helmholtz solution then

$$-\int_{\Gamma} \left(\partial_{\mathbf{n}}^+ u(\mathbf{y}) \Phi_k(\mathbf{x}, \mathbf{y}) - \gamma^+ u(\mathbf{y}) \frac{\partial \Phi_k(\mathbf{x}, \mathbf{y})}{\partial n(\mathbf{y})} \right) \mathrm{d}s(\mathbf{y}) = \big(1 - \sigma(\mathbf{x})\big) u(\mathbf{x}) \qquad \mathbf{x} \in \Gamma. \tag{70}$$

Proof. We prove the first identity, the second one is analogous.

For simplicity we denote the integrand with the shorthand

$$\bigstar := \partial_{\mathbf{n}}^- u(\mathbf{y}) \Phi_k(\mathbf{x}, \mathbf{y}) - \gamma^- u(\mathbf{y}) \frac{\partial \Phi_k(\mathbf{x}, \mathbf{y})}{\partial n(\mathbf{y})}.$$

For $\mathbf{x} \in \Gamma$, we apply Green's second identity on $\Omega_- \setminus \overline{B_\epsilon(\mathbf{x})}$ (see figure). Its boundary is decomposed in $\Gamma \setminus B_\epsilon(\mathbf{x})$ and $\partial B_\epsilon(\mathbf{x}) \cap \Omega_-$; on both parts we choose $\mathbf{n}$ pointing outwards:

$$0 = \int_{\partial(\Omega_- \setminus \overline{B_\epsilon(\mathbf{x})})} \bigstar \, \mathrm{d}s(\mathbf{y}) = \int_{\Gamma \setminus B_\epsilon(\mathbf{x})} \bigstar \, \mathrm{d}s(\mathbf{y}) + \int_{\partial B_\epsilon(\mathbf{x}) \cap \Omega_-} \bigstar \, \mathrm{d}s(\mathbf{y}).$$
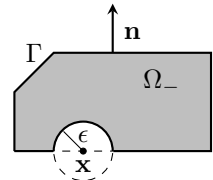
The limit for $\epsilon \to 0$ of the integral over $\Gamma \setminus B_\epsilon(\mathbf{x})$ is exactly the integral of the same integrand over the whole Γ, the left-hand side of the assertion (understood as a Cauchy principal value):

$$\int_{\Gamma} \bigstar \, \mathrm{d}s(\mathbf{y}) = \lim_{\epsilon \to 0} \int_{\Gamma \setminus B_\epsilon(\mathbf{x})} \bigstar \, \mathrm{d}s(\mathbf{y}) = -\lim_{\epsilon \to 0} \int_{\partial B_\epsilon(\mathbf{x}) \cap \Omega_-} \bigstar \, \mathrm{d}s(\mathbf{y}).$$

Proceeding as in the proof of Theorem 5.15 we see that $\lim_{\epsilon \to 0} \int_{\partial B_\epsilon(\mathbf{x}) \cap \Omega_-} \partial_{\mathbf{n}}^- u(\mathbf{y}) \Phi_k(\mathbf{x}, \mathbf{y}) \, \mathrm{d}s(\mathbf{y}) = 0$, while the last term gives:

$$\int_{\partial B_\epsilon(\mathbf{x}) \cap \Omega_-} \gamma^- u(\mathbf{y}) \frac{\partial \Phi_k(\mathbf{x}, \mathbf{y})}{\partial n(\mathbf{y})} \, \mathrm{d}s(\mathbf{y}) = k \frac{\mathrm{i}}{4} H_1^{(1)}(k\epsilon) \int_{\partial B_\epsilon(\mathbf{x}) \cap \Omega_-} u(\mathbf{y}) \, \mathrm{d}s(\mathbf{y})$$

$$\sim k \frac{\mathrm{i}}{4} \left(\frac{-2\mathrm{i}}{\pi k\epsilon} \right) \int_{\partial B_\epsilon(\mathbf{x}) \cap \Omega_-} u(\mathbf{y}) \, \mathrm{d}s(\mathbf{y}) \sim \left(\frac{1}{2\pi\epsilon} \right) 2\pi \sigma(\mathbf{x}) \epsilon u(\mathbf{x}) = \sigma(\mathbf{x}) u(\mathbf{x}).$$

$\square$

We summarise Green's representations (65), (68), (69) and (70) as follows. With u as in Lemma 5.23:

$\Delta u + k^2 u = 0$ in Ω_- :

$$\int_{\Gamma} \left(\partial_{\mathbf{n}}^- u(\mathbf{y}) \Phi_k(\mathbf{x}, \mathbf{y}) - \gamma^- u(\mathbf{y}) \frac{\partial \Phi_k(\mathbf{x}, \mathbf{y})}{\partial n(\mathbf{y})} \right) \mathrm{d}s(\mathbf{y}) = \begin{cases} u(\mathbf{x}) & \text{if } \mathbf{x} \in \Omega_-, \\ \sigma(\mathbf{x}) u(\mathbf{x}) & \text{if } \mathbf{x} \in \Gamma, \\ 0 & \text{if } \mathbf{x} \in \Omega_+, \end{cases}$$

$\Delta u + k^2 u = 0$ in Ω_+, radiating:

$$-\int_\Gamma \left(\partial_{\mathbf{n}}^+ u(\mathbf{y})\Phi_k(\mathbf{x},\mathbf{y}) - \gamma^+ u(\mathbf{y})\frac{\partial\Phi_k(\mathbf{x},\mathbf{y})}{\partial n(\mathbf{y})} \right) \mathrm{d}s(\mathbf{y}) = \begin{cases} 0 & \text{if } \mathbf{x}\in\Omega_-, \\ (1-\sigma(\mathbf{x}))u(\mathbf{x}) & \text{if } \mathbf{x}\in\Gamma, \\ u(\mathbf{x}) & \text{if } \mathbf{x}\in\Omega_+. \end{cases}$$

Exercise 5.24: (Fundamental solution and delta function). Show that the fundamental solution deserves its name: for any fixed $\mathbf{y}\in\mathbb{R}^2$, it satisfies $-\Delta\Phi_k(\cdot,\mathbf{y}) - k^2\Phi_k(\cdot,\mathbf{y}) = \delta_{\mathbf{y}}$ in distributional sense, where $\delta_{\mathbf{y}}$ is the Dirac delta at $\mathbf{y}$.

This means that $\int_{\mathbb{R}^2}\Phi_k(\mathbf{x},\mathbf{y})\big(\Delta\rho(\mathbf{x}) + k^2\rho(\mathbf{x})\big)\,\mathrm{d}\mathbf{x} = -\rho(\mathbf{y})$ for all $\rho\in\mathscr{D}(\mathbb{R}^2)$ and $\mathbf{y}\in\mathbb{R}^2$.

Hint: integrate by parts in $\mathbb{R}^2\setminus B_\epsilon(\mathbf{y})$ and take the limit for $\epsilon\to 0$ using the technique of the proof of Theorem 5.15.

Show that for $f\in\mathcal{D}(\mathbb{R}^2)$, $u(\mathbf{y}) := \int_{\mathbb{R}^2}\Phi_k(\mathbf{x},\mathbf{y})f(\mathbf{x})\,\mathrm{d}\mathbf{x}$ is solution of the inhomogeneous Helmholtz equation $-\Delta u - k^2 u = f$ and is radiating.

The operator

$$\mathcal{V}: \{f\in L^2(\mathbb{R}^2): \operatorname{supp} f \text{ is compact}\} \to H^2_{\mathrm{loc}}(\mathbb{R}^2), \qquad (\mathcal{V}f)(\mathbf{y}) := \int_{\mathbb{R}^2}\Phi_k(\mathbf{x},\mathbf{y})f(\mathbf{x})\,\mathrm{d}\mathbf{x} \qquad (71)$$

is called "volume potential" or "Newton potential" (since in the Laplace case $k=0$, with $f\ge 0$, it represent the gravitational potential generated by a mass distribution f) and is used to construct the "volume integral equations"; see [CK2, Ch. 8] and [SS11, §3.1.1].

Remark 5.25: (Distributions of charges on Ω_- or on Γ). In §5.1 we decided to try to represent a radiating solution u in Ω_+ as a single-layer potential, i.e. as a continuous linear combination of "acoustic charges" distributed on Γ. (In §5.4 and §6.2.1 we will see that we could proceed similarly representing u as a combination of "acoustic dipoles" on Γ.) Is this representation sufficiently rich or are we loosing some generality? Can we represent some more radiating fields if we distribute the charges in the whole scatterer $\overline{\Omega_-}$?

To answer these questions, let $u(\mathbf{x}) = \int_{\Omega_-}\Phi(\mathbf{x},\mathbf{y})f(\mathbf{y})\mathrm{d}\mathbf{y}$ for some density f supported on Ω_- (or $u = \mathcal{V}f$ in the notation of (71)). By Exercise 5.24, u is well defined on $\mathbb{R}^2$, is radiating, and $\Delta u + k^2 u = -f$ in $\mathbb{R}^2$. Can we write $u = \mathcal{S}\psi$ for some surface charge density ψ on Γ?

Assume that k^2 is not a Dirichlet eigenvalue of Ω_-. Let $w\in H^1(\Omega_-;\Delta)$ be the solution of $\Delta w + k^2 w = 0$ in Ω_- with boundary condition $\gamma^- w = \gamma^\pm u$. Set $\psi := \partial_{\mathbf{n}}^-(w - u) \in H^{-\frac{1}{2}}(\Gamma)$. Then, using Green's second identity (31), for $\mathbf{x}\in\Omega_+$,

$$\begin{aligned}
\mathcal{S}\psi(\mathbf{x}) &= \int_\Gamma \Phi(\mathbf{x},\mathbf{y})\partial_{\mathbf{n}}^-\big(w(\mathbf{y})-u(\mathbf{y})\big)\mathrm{d}s(\mathbf{y}) \\
&= \int_\Gamma \left(\Phi(\mathbf{x},\mathbf{y})\partial_{\mathbf{n}}^-\big(w(\mathbf{y})-u(\mathbf{y})\big) - \partial_{\mathbf{n}}^-\Phi(\mathbf{x},\mathbf{y})\underbrace{\gamma^-\big(w(\mathbf{y})-u(\mathbf{y})\big)}_{=0 \text{ by def. of } w} \right)\mathrm{d}s(\mathbf{y}) \\
&= \int_{\Omega_-} \left(\Phi(\mathbf{x},\mathbf{y})\underbrace{(\Delta+k^2)w(\mathbf{y})}_{=0} - \Phi(\mathbf{x},\mathbf{y})\underbrace{(\Delta+k^2)u(\mathbf{y})}_{=-f} - \underbrace{(\Delta+k^2)\Phi(\mathbf{x},\mathbf{y})}_{=0,\text{ as } \mathbf{x}\in\Omega_+, \mathbf{y}\in\Omega_-}\big(w(\mathbf{y})-u(\mathbf{y})\big) \right)\mathrm{d}\mathbf{y} \\
&= \mathcal{V}f(\mathbf{x}) = u(\mathbf{x}).
\end{aligned}$$

This means that, away from eigenvalues, any radiating solution written as superposition of charges in Ω_- (with density f) can also be written as superposition of charges on Γ (with density ψ), i.e. as a single-layer potential. (This is easier to imagine in the Laplace case, thinking at distributions of electric charge or mass, and Coulomb or gravitational potentials.)

What if k^2 is a Dirichlet eigenvalue of Ω_-? We will see in §6.1.1 that in this case the single-layer BIE (58) is not even well-posed. To represent *all* radiating solution in Ω_+, for *all* $k > 0$, we need to use Green's representation (68) instead of the single-layer one (59); we will do this in §6.2.

Exercise 5.26: (Huygens' principle). Consider the SSSP (45) with incoming field u^{Inc} that is Helmholtz solution in a neighbourhood of $\overline{\Omega_-}$. Using Green's representation formulas, show that $u^{\mathrm{Scat}} = -\mathcal{S}\partial_{\mathbf{n}}^+ u^{\mathrm{Tot}}$ and $u^{\mathrm{Tot}} = u^{\mathrm{Inc}} - \mathcal{S}\partial_{\mathbf{n}}^+ u^{\mathrm{Tot}}$ in Ω_+. In [CK2, p. 64], this formula is called Huygens' principle.

Exercise 5.27: (Discrete-valued field). Find a field $u\in C^\infty(\mathbb{R}^2)$ and a bounded, Lipschitz, connected domain Ω_- such that the function $Z: \mathbf{x}\mapsto \left|\int_\Gamma\big(\partial_{\mathbf{n}}^- u(\mathbf{y})\Phi_k(\mathbf{x},\mathbf{y}) - \gamma^- u(\mathbf{y})\frac{\partial\Phi_k(\mathbf{x},\mathbf{y})}{\partial n(\mathbf{y})}\big)\,\mathrm{d}s(\mathbf{y})\right|$ takes exactly the values $0,1,2,4$ for $\mathbf{x}\in\mathbb{R}^2$.

Despite the function Z is defined by the same formula for all $\mathbf{x}\in\mathbb{R}^2$, it takes exactly 4 different values.

5.4 Double-layer potential and operator

Green's representation formulas (65) and (68) mean that all Helmholtz solutions in Ω_- and all radiating Helmholtz solutions in Ω_+ can be written as boundary integrals over Γ. The integral of $\partial_{\mathbf{n}} u\, \Phi_k$ is the single-layer potential $\mathcal{S}\psi$ for $\psi = \partial_{\mathbf{n}}^\pm u$ we already know from (55). Now we are evaluating $(\mathcal{S}\psi)(\mathbf{x})$ for both $\mathbf{x} \in \Omega_+$ and $\mathbf{x} \in \Omega_-$, so we are extending the definition of the single-layer potential (55) to all points in the complement of Γ:

$$(\mathcal{S}\psi)(\mathbf{x}) := \int_\Gamma \Phi_k(\mathbf{x}, \mathbf{y}) \psi(\mathbf{y})\, \mathrm{d}s(\mathbf{y}) \qquad \mathbf{x} \in \Omega_+ \cup \Omega_-.$$

In particular, for any $\psi \in H^{-\frac{1}{2}}(\Gamma)$, $\mathcal{S}\psi$ is a Helmholtz solution both in Ω_- and Ω_+ and is radiating. With the same reasoning as in Proposition 5.1, the Dirichlet traces from both sides of Γ coincide:

$$\gamma^+(\mathcal{S}\psi) = \gamma^-(\mathcal{S}\psi) = S\psi.$$

In particular, if $\psi \in C^0(\Gamma)$, then $\mathcal{S}\psi \in C^\infty(\mathbb{R}^2 \setminus \Gamma)$ admits an extension in $C^0(\mathbb{R}^2)$ but not in $C^1(\mathbb{R}^2)$ because, as we will see, the normal derivative of $\mathcal{S}\psi$ is discontinuous across Γ.

The second term in (65) and (68) is a new potential:

$$(\mathcal{D}\psi)(\mathbf{x}) := \int_\Gamma \frac{\partial \Phi_k(\mathbf{x}, \mathbf{y})}{\partial n(\mathbf{y})} \psi(\mathbf{y})\, \mathrm{d}s(\mathbf{y}) \qquad \mathbf{x} \in \Omega_- \cup \Omega_+. \tag{72}$$

This is called acoustic **double-layer potential**.[38] For a function ψ on Γ, sufficiently smooth, $\mathcal{S}\psi$ is a smooth Helmholtz solution in both Ω_- and Ω_+, and satisfies the radiation condition. It can be proved that it is continuous as mapping $\mathcal{D} : H^{\frac{1}{2}}(\Gamma) \to H^1_{\mathrm{loc}}(\Omega_- \cup \Omega_+)$, [CGLS12, Thm. 2.15] (here we need the density to be in $H^{\frac{1}{2}}(\Gamma)$, while for the single-layer potential $H^{-\frac{1}{2}}(\Gamma)$ was enough, this is because the singularity of $\nabla\Phi_k$ is stronger than that of Φ_k).

Then Green's representation can be written as:

$$\begin{array}{ll} \text{if } u \text{ is Helmholtz solution in } \Omega_- : & u = \mathcal{S}\partial_{\mathbf{n}}^- u - \mathcal{D}\gamma^- u \quad \text{in } \Omega_-, \\ \text{if } u \text{ is radiating Helmholtz solution in } \Omega_+ : & u = -\mathcal{S}\partial_{\mathbf{n}}^+ u + \mathcal{D}\gamma^+ u \quad \text{in } \Omega_+. \end{array} \tag{73}$$

This means that any radiating Helmholtz solution is known once we know the "Cauchy data" γu and $\partial_{\mathbf{n}} u$, i.e. its Dirichlet and Neumann traces.

As we did for the single-layer, we can define the **double-layer operator**:

$$(D\psi)(\mathbf{x}) := \int_\Gamma \frac{\partial \Phi_k(\mathbf{x}, \mathbf{y})}{\partial n(\mathbf{y})} \psi(\mathbf{y})\, \mathrm{d}s(\mathbf{y}) \qquad \mathbf{x} \in \Gamma. \tag{74}$$

If Γ is of class C^2 and $\psi \in C^0(\Gamma)$, then $D\psi$ is well-defined as a standard (weakly singular) integral and $S\psi \in C^0(\Gamma)$. On the other hand, if Γ is only Lipschitz and $\psi \in L^2(\Gamma)$, then $D\psi$ must be understood as Cauchy principal value:

$$(D\psi)(\mathbf{x}) = \lim_{\epsilon \to 0} \int_{\Gamma \cap \{\mathbf{y} : |\mathbf{y} - \mathbf{x}| > \epsilon\}} \frac{\partial \Phi_k(\mathbf{x}, \mathbf{y})}{\partial n(\mathbf{y})} \psi(\mathbf{y})\, \mathrm{d}s(\mathbf{y}) \qquad \text{a.e. } \mathbf{x} \in \Gamma.$$

Then $D\psi \in L^2(\Gamma)$.

Exercise 5.28: (Double-layer operator on straight segments). Assume that $\Gamma_* \subset \Gamma$ is a straight segment and that $\psi \in C^0(\Gamma)$ is supported in Γ_*. Show that $(D\psi)(\mathbf{x}) = 0$ for all for all $\mathbf{x} \in \Gamma_*$.

Hint: you do not need the precise value of Φ_k but only that it depends only on $|\mathbf{x} - \mathbf{y}|$.

We have seen in (57) that $S = \gamma\mathcal{S}$. One might expect that $D = \gamma\mathcal{D}$, but this is not the case.

The assertions of Lemma 5.23, Green's representation on the boundary, can be written in terms of layer operators as (compare against (73))

$$S\partial_{\mathbf{n}}^- u - D\gamma^- u = \sigma\gamma^- u, \qquad D\gamma^+ u - S\partial_{\mathbf{n}}^+ u = (1-\sigma)\gamma^+ u. \tag{75}$$

---

[38]The double-layer potential has this name because it can be thought as the acoustic potential generated by two "sheets" of charges with opposite signs, parallel to Γ, in the limit when the distance between the sheets decreases to 0 (from $\frac{\partial \Phi_k(\mathbf{x}, \mathbf{y})}{\partial n(\mathbf{y})} = \lim_{\delta \to 0} \frac{1}{2\delta}(\Phi_k(\mathbf{x}, \mathbf{y} + \delta\mathbf{n}) - \Phi_k(\mathbf{x}, \mathbf{y} - \delta\mathbf{n}))$. In electrostatics (Laplace equation) this would be a layer of dipoles.

Now let u be a Helmholtz solution in Ω_- and denote $\psi := \gamma^- u \in H^{\frac{1}{2}}(\Gamma)$. We have

$$\psi = \gamma^- u \overset{\overset{\text{Green repr.}}{(65)}}{=} \gamma^- \mathcal{S} \partial_{\mathbf{n}}^- u - \gamma^- \mathcal{D} \psi \overset{\overset{\text{single-layer}}{\text{trace }(57)}}{=} S \partial_{\mathbf{n}}^- u - \gamma^- \mathcal{D} \psi \qquad \text{and} \qquad \sigma \psi \overset{(75)}{=} S \partial_{\mathbf{n}}^- u - D \psi$$

Taking the difference between these two equations we have the Dirichlet **trace formula for the double-layer potential**:

$$\boxed{\gamma^- \mathcal{D} \psi = D \psi - (1 - \sigma)\psi, \qquad \gamma^+ \mathcal{D} \psi = D \psi + \sigma \psi.} \tag{76}$$

The second of these equations is obtained similarly using (68) in place of (65) and (70) in place of (69). Recall that $\sigma = \frac{1}{2}$ in all smooth points, so (76) reads almost everywhere as

$$\gamma^\pm \mathcal{D} \psi = D \psi \pm \frac{1}{2} \psi, \quad \text{or, in operator form,} \quad \gamma^\pm \mathcal{D} = D \pm \frac{1}{2} I,$$

where I is the identity operator. All these formulas tell us that the Dirichlet trace of $\mathcal{D}$ is not simply D but a correction term is needed, due to the singular behaviour of $\frac{\partial \Phi_k}{\partial n}$. Taking the difference between the two equations in (76), the correction terms $\pm \frac{1}{2} \psi$ give the **jump relation**:

$$[\![\gamma \mathcal{D} \psi]\!] := \gamma^+ \mathcal{D} \psi - \gamma^- \mathcal{D} \psi = \psi.$$

Given a ψ on the boundary Γ, the double-layer potential $\mathcal{D} \psi$ is a radiating Helmholtz solution in the complement of Γ, whose jump on Γ is ψ itself.

For simplicity, in the following we write $\frac{1}{2}$ instead of σ and $1 - \sigma$, with the implicit convention that equalities on Γ hold almost everywhere (everywhere except at corners).

5.5 NEUMANN TRACES OF THE POTENTIALS: TWO MORE BIOs AND JUMP RELATIONS

In the previous section we have learned how to construct fields in $\Omega_- \cup \Omega_+$ from distributions defined on Γ:

$$\forall \psi \in H^{-\frac{1}{2}}(\Gamma), \quad \forall \varphi \in H^{\frac{1}{2}}(\Gamma), \qquad \mathcal{S} \psi, \, \mathcal{D} \varphi \in H^1(\Omega_-; \Delta) \times H_{\mathrm{loc}}^1(\Omega_+; \Delta) \tag{77}$$

are radiating Helmholtz solution in the complement of the boundary Γ. Moreover, the Dirichlet traces of $\mathcal{S} \psi$ coincide: $\gamma^+ \mathcal{S} \psi = \gamma^- \mathcal{S} \psi$, so $\mathcal{S} \psi \in H_{\mathrm{loc}}^1(\mathbb{R}^2; \Delta)$, while $\mathcal{D} \varphi$ is discontinuous on Γ, (76).

We now want to look at the Neumann traces of $\mathcal{S} \psi$, $\mathcal{D} \varphi$. To this purpose, we need to introduce two more BIOs (the last ones!): the **adjoint double-layer operator** D' and the **hypersingular operator** H:

$$\boxed{(D' \varphi)(\mathbf{x}) := \int_\Gamma \frac{\partial \Phi_k(\mathbf{x}, \mathbf{y})}{\partial n(\mathbf{x})} \varphi(\mathbf{y}) \, ds(\mathbf{y}), \qquad (H \varphi)(\mathbf{x}) := \frac{\partial}{\partial n(\mathbf{x})} \int_\Gamma \frac{\partial \Phi_k(\mathbf{x}, \mathbf{y})}{\partial n(\mathbf{y})} \varphi(\mathbf{y}) \, ds(\mathbf{y}), \quad \mathbf{x} \in \Gamma.} \tag{78}$$

Note that D' differs from D only in that the normal derivation is taken with respect to a different variable of Φ_k. If Γ is not C^2 or $\varphi \notin C^0(\Gamma)$, the adjoint double-layer operator has to be understood as a principal value integral, in the same way as D. Its name and notation are due to the identity $\int_\Gamma (D\varphi)\psi \, ds = \int_\Gamma \varphi(D'\psi) \, ds$, valid for all $\varphi, \psi \in L^2(\Gamma)$, which can be proved using Fubini theorem and with some complications due to the singularity of the integrand, [CGLS12, eq. (2.37)].

The hypersingular operator is more complicated: it has to be understood as a limit $(H\varphi)(\mathbf{x}) = \lim_{\mathbf{z} \to \mathbf{x}} \mathbf{n}(\mathbf{x}) \cdot \nabla(\mathcal{D}\varphi)(\mathbf{z})$, for a suitable choice of the points $\mathbf{z}$, [CGLS12, eq. (2.36)]. In its definition we are not allowed to move $\frac{\partial}{\partial n(\mathbf{x})}$ inside the integral because the second derivatives of Φ_k are not integrable.

The main properties of the BIOs are their relations with the traces of the two layer potentials:

$$\boxed{\begin{aligned} \gamma^\pm \mathcal{S} &= S, & \gamma^\pm \mathcal{D} &= D \pm \frac{1}{2} I, \\ \partial_{\mathbf{n}}^\pm \mathcal{S} &= D' \mp \frac{1}{2} I, & \partial_{\mathbf{n}}^\pm \mathcal{D} &= H. \end{aligned}} \tag{79}$$

Here I is the identity operator. We have already derived the formulas of the Dirichlet traces, those for the Neumann ones are proved in a similar way, [CK1, §2.4–2.5]. Taking the difference between outer and inner traces we find the **jump relations** (we have already encountered those for the Dirichlet traces)

$$\boxed{\begin{aligned} [\![\gamma \mathcal{S} \psi]\!] &= \gamma^+ \mathcal{S} \psi - \gamma^- \mathcal{S} \psi = 0, & [\![\gamma \mathcal{D} \psi]\!] &= \gamma^+ \mathcal{D} \psi - \gamma^- \mathcal{D} \psi = \psi, \\ [\![\partial_{\mathbf{n}} \mathcal{S} \psi]\!] &= \partial_{\mathbf{n}}^+ \mathcal{S} \psi - \partial_{\mathbf{n}}^- \mathcal{S} \psi = -\psi, & [\![\partial_{\mathbf{n}} \mathcal{D} \psi]\!] &= \partial_{\mathbf{n}}^+ \mathcal{D} \psi - \partial_{\mathbf{n}}^- \mathcal{D} \psi = 0. \end{aligned}} \tag{80}$$

From (79), using (77) and the trace theorem 3.10, the mapping (continuity) properties of the BIOs follow:

$$S : H^{-\frac{1}{2}}(\Gamma) \to H^{\frac{1}{2}}(\Gamma),$$
$$D : H^{\frac{1}{2}}(\Gamma) \to H^{\frac{1}{2}}(\Gamma),$$
$$D' : H^{-\frac{1}{2}}(\Gamma) \to H^{-\frac{1}{2}}(\Gamma),$$
$$H : H^{\frac{1}{2}}(\Gamma) \to H^{-\frac{1}{2}}(\Gamma).$$
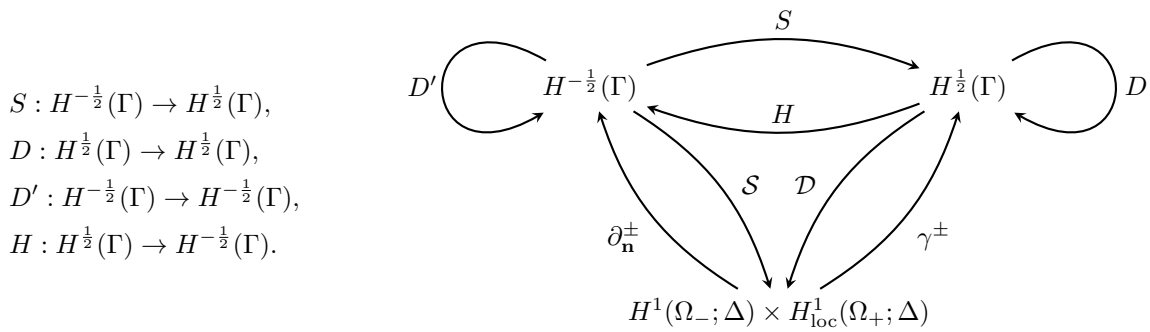
From (79) we also see that all four operators are averages of traces of the potentials:

$$S = \{\!\{\gamma \mathcal{S}\}\!\} = \frac{\gamma^+ \mathcal{S} + \gamma^- \mathcal{S}}{2}, \qquad D = \{\!\{\gamma \mathcal{D}\}\!\} = \frac{\gamma^+ \mathcal{D} + \gamma^- \mathcal{D}}{2},$$
$$D' = \{\!\{\partial_\mathbf{n} \mathcal{S}\}\!\} = \frac{\partial_\mathbf{n}^+ \mathcal{S} + \partial_\mathbf{n}^- \mathcal{S}}{2}, \qquad H = \{\!\{\partial_\mathbf{n} \mathcal{D}\}\!\} = \frac{\partial_\mathbf{n}^+ \mathcal{D} + \partial_\mathbf{n}^- \mathcal{D}}{2}.$$

These formulas can be taken as alternative rigorous definitions of the four BIOs, given those of the two layer potentials (see e.g. [SBH19, §14.2] for a PDE different from Helmholtz).

Remark 5.29: (BIOs notation). There is no universal notation for boundary integral operators and sometimes the same symbol is used by different authors to mean different BIOs: comparing references can be a nightmare. To help navigating the literature, we list here the notation used in several references[39] on BIEs for Helmholtz (some of these only consider the 3D case).

	Φ_k (53)	$\mathcal{S}$ (55)	$\mathcal{D}$ (72)	S (56)	D (74)	D' (78)	H (78)
[Spence14, p. 36], [CGLS12, pp. 108–113]	Φ_k	$\mathcal{S}_k$	$\mathcal{D}_k$	S_k	D_k	D'_k	H_k
[Sayas06, §3,§11.1]	ϕ	$\mathcal{S}_\Gamma$	$\mathcal{D}_\Gamma$	V_Γ	K_Γ	K_Γ^t	W_Γ
[CK1, §2.7], [CK2, (3.8–11)]	Φ			S	K	K'	T
[Nédélec01, p. 116]	E			S	D	D^*	N
[SS11, §3.9]	G_k	S_k	D_k	V_k	K_k	K'_k	W_k
[McLean00, pp. 217–218]	G	SL	DL	S	T	$\widetilde{T}$	R
[Martin06, §5.1–5.3]	G	S	D	S	K	$\overline{K}^*$	N
[Hsiao and Wendland 2008, §2.1]	E_k	V_k	W_k	V_k	K_k	K'_k	D_k
[Antoine 2012, §3.3]	G	L	S	$\mathcal{L}$	$\mathcal{N}$	$\mathcal{D}$	$\mathcal{S}$
[Steinbach 2008, §6.9] (W used for Laplace d.l.p.)	U_k^*	$\widetilde{V}_k$		V_k	K_k	K'_k	D_k

Moreover, in some cases the hypersingular operator H is defined with the opposite sign, e.g. [Sayas06, §11.1] and [McLean00, eq. (7.3)]. In other cases all four BIOs include a factor 2 [CK2, eq. (3.8–11)] (to avoid the factor $\frac{1}{2}$ in the trace relations). [Martin06, eq. (5.1)] defines the fundamental solution as (-2) times our (standard) definition.

Exercise 5.30: (Double-layers operators on the disc). Let $\Omega_- = B_R$ be a disc of radius $R > 0$.
   Show that $(\mathbf{x} - \mathbf{y}) \cdot \mathbf{n}(\mathbf{x}) = (\mathbf{x} - \mathbf{y}) \cdot \mathbf{n}(\mathbf{y})$ for all $\mathbf{x}, \mathbf{y} \in \Gamma$.
   Deduce that, for the disc, double-layer and adjoint double-layer operators coincide: $D = D'$.

Remark 5.31: (Explicit double-layer formulas). Using $\frac{\partial}{\partial z} H_0^{(1)}(z) = -H_1^{(1)}(z)$, we can write more explicit formulas for the double-layer and the adjoint double-layer operators:

$$(D\psi)(\mathbf{x}) = \frac{\mathrm{i}k}{4} \int_\Gamma H_1^{(1)}(k|\mathbf{x} - \mathbf{y}|) \frac{(\mathbf{x} - \mathbf{y}) \cdot \mathbf{n}(\mathbf{y})}{|\mathbf{x} - \mathbf{y}|} \psi(\mathbf{y}) \, \mathrm{d}s(\mathbf{y}),$$
$$(D'\psi)(\mathbf{x}) = \frac{\mathrm{i}k}{4} \int_\Gamma H_1^{(1)}(k|\mathbf{x} - \mathbf{y}|) \frac{(\mathbf{y} - \mathbf{x}) \cdot \mathbf{n}(\mathbf{x})}{|\mathbf{x} - \mathbf{y}|} \psi(\mathbf{y}) \, \mathrm{d}s(\mathbf{y}).$$

---

[39]The last three in the table are: [Hsiao, Wendland, Boundary integral equations, Springer 2008]
[Antoine, Introduction to integral equations for time harmonic acoustic scattering problems, notes 2012]
[Steinbach, Numerical approximation methods for elliptic boundary value problems, Springer 2008]

From this formulas, we see that if Γ is a polygon and E is one of its edges, the points $\mathbf{y} \in E$ do not contribute to the computation of $(D\psi)(\mathbf{x})$ for $\mathbf{x} \in E$, because $(\mathbf{x} - \mathbf{y}) \cdot \mathbf{n}(\mathbf{y}) = 0$. So $H_1^{(1)}$ is evaluated only for $|\mathbf{x} - \mathbf{y}| > \operatorname{dist}(\mathbf{x}, \partial E)$, i.e. away from the singularity. The singularity in the integrand has to be treated carefully when $\mathbf{x}$ is very close to a corner, while it is harmless otherwise. If Γ is smooth then $\frac{(\mathbf{x}-\mathbf{y}) \cdot \mathbf{n}(\mathbf{y})}{|\mathbf{x}-\mathbf{y}|} \to 0$ for $\mathbf{y} \to \mathbf{x}$, partially compensating the strong singularity of $H_1^{(1)}$.

Remark 5.32: (Regularisation of the hypersingular operator). On sufficiently smooth domains, the hypersingular operator H can be computed with a "regularisation" technique. This circumvents the strong singularity in the kernel with two applications of the single-layer operator S:

$$(H\psi)(\mathbf{x}) = \partial_\tau \int_\Gamma \Phi_k(\mathbf{x}, \mathbf{y}) \partial_\tau \psi(\mathbf{y}) \, \mathrm{d}s(\mathbf{y}) + k^2 \int_\Gamma \Phi_k(\mathbf{x}, \mathbf{y}) \mathbf{n}(\mathbf{x}) \cdot \mathbf{n}(\mathbf{y}) \psi(\mathbf{y}) \, \mathrm{d}s(\mathbf{y}),$$

$$\langle H\psi, \varphi \rangle_\Gamma = -\langle S\partial_\tau \psi, \partial_\tau \varphi \rangle_\Gamma + k^2 \langle S(\psi \mathbf{n}), \varphi \mathbf{n} \rangle_\Gamma$$

$$= \int_\Gamma \int_\Gamma \Phi_k(\mathbf{x}, \mathbf{y}) \left(-\partial_\tau \psi(\mathbf{x}) \overline{\partial_\tau \varphi}(\mathbf{y}) + k^2 \mathbf{n}(\mathbf{x}) \cdot \mathbf{n}(\mathbf{y}) \psi(\mathbf{x}) \overline{\varphi}(\mathbf{y}) \right) \mathrm{d}s(\mathbf{y}) \, \mathrm{d}s(\mathbf{x}).$$

Here $\partial_\tau = (-n_2, n_1) \cdot \nabla$ denotes the tangential derivative along Γ. Note the presence of the scalar product $\mathbf{n}(\mathbf{x}) \cdot \mathbf{n}(\mathbf{y})$ between the unit normals. This formula can be found in [McLean00, Ex. 9.6][40]. The 3D version of this formula is in [McLean00, Thm. 9.15] (for the Helmholtz equation) and [SS11, Thm. 3.3.22] (for more general PDEs).

Exercise 5.33: (Calderón calculus). Given a bounded Lipschitz scatterer Ω_-, we can collect the Dirichlet and the Neumann traces (either from Ω_- or Ω_+) in a vector-valued **Cauchy trace**:

$$\boldsymbol{\gamma}_C^\pm := (\gamma^\pm, \partial_\mathbf{n}^\pm) \ : \ H_{\mathrm{loc}}^1(\Omega_\pm; \Delta) \to \mathcal{H}, \qquad \text{where } \mathcal{H} := H^{\frac{1}{2}}(\Gamma) \times H^{-\frac{1}{2}}(\Gamma).$$

For $k > 0$, we define the **Calderón projectors** $P^\pm$ as the operator matrices

$$P^\pm : \mathcal{H} \to \mathcal{H}, \qquad P^\pm := \pm \begin{pmatrix} \gamma^\pm \mathcal{D} & -\gamma^\pm \mathcal{S} \\ \partial_\mathbf{n}^\pm \mathcal{D} & -\partial_\mathbf{n}^\pm \mathcal{S} \end{pmatrix} = \frac{1}{2} I \pm \begin{pmatrix} D & -S \\ H & -D' \end{pmatrix} = \begin{pmatrix} \frac{1}{2} \pm D & \mp S \\ \pm H & \frac{1}{2} \mp D' \end{pmatrix}.$$

(When we say "Helmholtz solution" it is understood that the wavenumber is k.)

- Check the equality between the expressions of $P^\pm$ using the trace formulas (79).
- Let u^+ be a radiating Helmholtz solution in Ω_+ and u^- a Helmholtz solution in Ω_-.
  Use the Green representations (73), $u^\pm = \pm(\mathcal{D}\gamma^\pm u^\pm - \mathcal{S}\partial_\mathbf{n}^\pm u^\pm)$, to show that

$$P^\pm \boldsymbol{\gamma}^\pm u^\pm = \boldsymbol{\gamma}^\pm u^\pm.$$

- Let $\boldsymbol{\phi} = (\phi_1, \phi_2) \in \mathcal{H}$. Define $u = \mathcal{D}\phi_1 - \mathcal{S}\phi_2 \in H_{\mathrm{loc}}^1(\Omega_+ \cup \Omega_-; \Delta)$. Show that $\boldsymbol{\gamma}_C^\pm u = \pm P^\pm \boldsymbol{\phi}$.
- Deduce that the Calderón operators are indeed projectors, i.e. $(P^\pm)^2 = P^\pm$ in $\mathcal{H}$.
- Deduce the operator identities

$$D^2 - SH = (D')^2 - HS = \frac{1}{4} I, \qquad DS = SD', \qquad HD = D'H. \tag{81}$$

- Since the projectors satisfy $P^+ + P^- = I$, they project on complementary subspaces of $\mathcal{H}$:

$$\forall \boldsymbol{\phi} \in \mathcal{H}, \quad \boldsymbol{\phi} = P^- \boldsymbol{\phi}^- + P^+ \boldsymbol{\phi}^+ \quad \text{where } \boldsymbol{\phi}^\pm = P^\pm \boldsymbol{\phi}.$$

- Let $\boldsymbol{\phi} \in \mathcal{H}$ be such that $P^\pm \boldsymbol{\phi} = \boldsymbol{\phi}$. Deduce that $\boldsymbol{\phi} = \boldsymbol{\gamma}_C^\pm u^\pm$, where $u^\pm \in H_{\mathrm{loc}}^1(\Omega_\pm; \Delta)$ is a (radiating, if the sign is $+$) Helmholtz solution.
  Hint: define $u^\pm = \pm(\mathcal{D}\phi_1 - \mathcal{S}\phi_2)|_{\Omega_\pm}$.
- The Calderón projectors allow to identify the Cauchy traces of Helmholtz solutions in the two domains $\Omega_\pm$. The space $\mathcal{H}$ is direct sum of $\ker P^+$ and $\ker P^-$. For all $\boldsymbol{\phi} \in \mathcal{H}$,

$$P^+ \boldsymbol{\phi} = \mathbf{0} \quad \Longleftrightarrow \quad P^- \boldsymbol{\phi} = \boldsymbol{\phi} \quad \Longleftrightarrow \quad \boldsymbol{\phi} = \boldsymbol{\gamma}_C^- u^-$$
$$\text{where } u^- \text{ is a Helmholtz solution in } \Omega_-,$$
$$P^- \boldsymbol{\phi} = \mathbf{0} \quad \Longleftrightarrow \quad P^+ \boldsymbol{\phi} = \boldsymbol{\phi} \quad \Longleftrightarrow \quad \boldsymbol{\phi} = \boldsymbol{\gamma}_C^+ u^+$$
$$\text{where } u^+ \text{ is a radiating Helmholtz solution in } \Omega_+. \tag{82}$$

---

[40] Also, eq. (4) in [Domínguez, Lu, Sayas, A Nyström method for the 2-dimensional Helmholtz hypersingular equation, 2014]

Calderón projectors are described in [CGLS12, pp. 117–118] (for the Helmholtz equation) and [SBH19, §14.4] (for the reaction–diffusion equation). They are often used to design new BIEs and preconditioners for the BEM, exploiting formulas (81). For instance, if one wants to solve a BIE for the operator S, as we have been doing in this section, pre-multiplying left- and right-hand sides of the BIE by the hypersingular operator $-4H$ gives a BIE for the operator $I - 4(D')^2$, which is a compact perturbation of the identity when the domain is smooth, [SS11, §3.9.3]. An accurate discretisation of this BIE gives a well-conditioned matrix whose eigenvalues cluster at 1, so its solution with an iterative solver might require very few iterations. However, the assembly of the system may require the construction of compatible "dual meshes" and be extremely complicated. This "Calderón operator preconditioning" is particularly relevant and well-studied in computational electromagnetism.

5.6 Single-layer potential in Ω_-, value of ψ and far-field pattern

Consider the SSSP (45) and the corresponding single-layer BIE $S\psi = g_D$ (58). The representation formula $u^{\mathrm{Scat}} = (\mathcal{S}\psi)|_{\Omega_+}$ (59) gives the value of the scattered field in Ω_+ as a single-layer potential. Denote by u^- the same potential evaluated inside the scatterer Ω_-, i.e. $u^- = (\mathcal{S}\psi)|_{\Omega_-}$. Then u^- is a Helmholtz solution in Ω_- with trace $\gamma^- u^- = \gamma^- \mathcal{S}\psi = S\psi = g_D = -\gamma u^{\mathrm{Inc}}$. We now assume that: (i) k^2 is not a Dirichlet eigenvalue and (ii) u^{Inc} is an incoming wave that is Helmholtz solution also in Ω_-, e.g. a plane wave. Then, by the uniqueness of the solution of the interior Helmholtz Dirichlet problem (Proposition 4.6),

$$(\mathcal{S}\psi)|_{\Omega_-} = u^- = -u^{\mathrm{Inc}}|_{\Omega_-}. \tag{83}$$

This equality has a few useful consequences.

From one of the jump relations (80) we can relate the BIE density ψ to a "physical" quantity, the Neumann trace of the total field:

$$\psi = -[\![\partial_{\mathbf{n}}\mathcal{S}\psi]\!] = \partial_{\mathbf{n}}^- \mathcal{S}\psi - \partial_{\mathbf{n}}^+ \mathcal{S}\psi = \partial_{\mathbf{n}}(-u^{\mathrm{Inc}}) - \partial_{\mathbf{n}}^+ u^{\mathrm{Scat}} = -\partial_{\mathbf{n}}^+ u^{\mathrm{Tot}}. \tag{84}$$

This allows to compute the Neumann trace of the scattered field from the data and the BIE solution as

$$\partial_{\mathbf{n}}^+ u^{\mathrm{Scat}} = -\psi - \partial_{\mathbf{n}} u^{\mathrm{Inc}}.$$
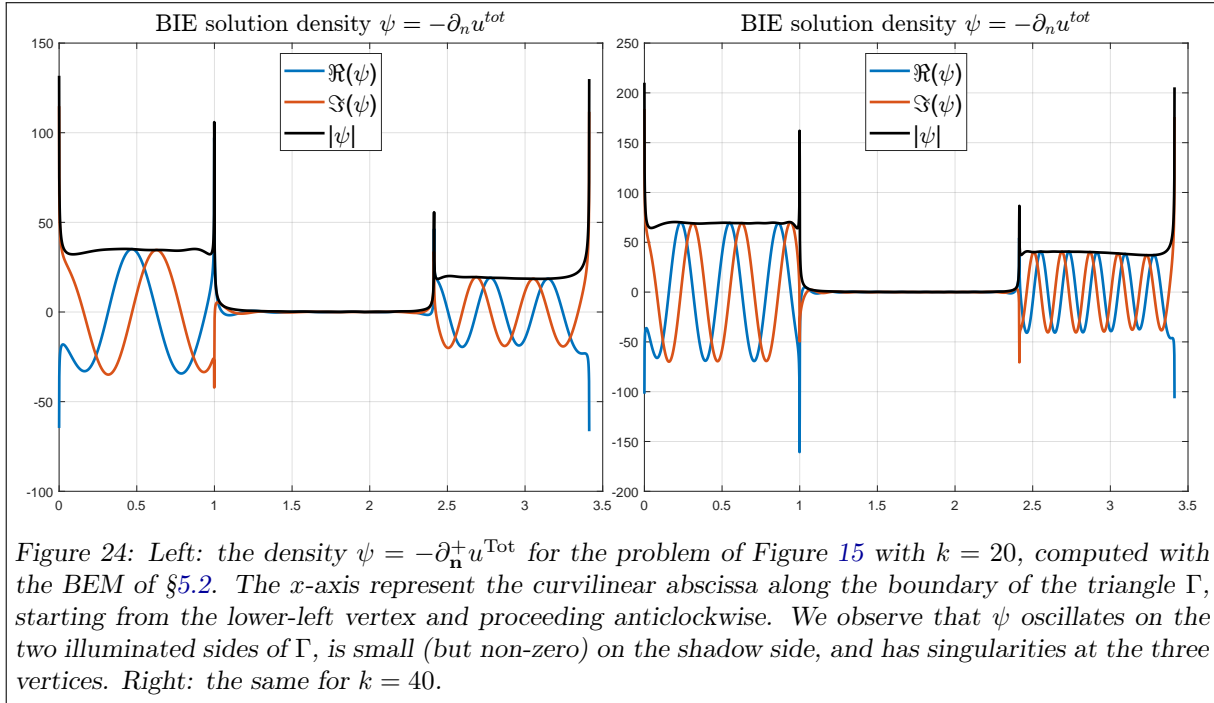
Figure 24: *Left: the density $\psi = -\partial_{\mathbf{n}}^+ u^{\mathrm{Tot}}$ for the problem of Figure 15 with $k = 20$, computed with the BEM of §5.2. The x-axis represent the curvilinear abscissa along the boundary of the triangle Γ, starting from the lower-left vertex and proceeding anticlockwise. We observe that ψ oscillates on the two illuminated sides of Γ, is small (but non-zero) on the shadow side, and has singularities at the three vertices. Right: the same for $k = 40$.*

We recall from Remark 4.27 that the far-field pattern of the scattered field is the function $u_\infty \in C^\infty(\mathbb{S}^1)$ such that $u^{\mathrm{Scat}}(\mathbf{x}) = \frac{\mathrm{e}^{\mathrm{i}kr}}{\sqrt{r}}(u_\infty(\theta) + \mathcal{O}(r^{-1}))$. Its explicit formula (47) requires the value of $\partial_{\mathbf{n}}^+ u^{\mathrm{Scat}}$ on Γ. We can use the formula that we have just obtained to compute the far-field pattern of the scattered field (solution of the SSSP (45)) from the BIE (58) solution ψ:

$$u_\infty(\theta) = \frac{\mathrm{e}^{\mathrm{i}\frac{\pi}{4}}}{\sqrt{8\pi k}} \int_\Gamma \left(\gamma^+ u^{\mathrm{Scat}}(\mathbf{y})\partial_{\mathbf{n}}\mathrm{e}^{-\mathrm{i}k\mathbf{y}\cdot\mathbf{d}} - \partial_{\mathbf{n}}^+ u^{\mathrm{Scat}}(\mathbf{y})\mathrm{e}^{-\mathrm{i}k\mathbf{y}\cdot\mathbf{d}} \right) \mathrm{d}s(\mathbf{y})$$

$$= \frac{e^{i\frac{\pi}{4}}}{\sqrt{8\pi k}} \int_\Gamma \Big(-\gamma u^{\mathrm{Inc}}(\mathbf{y}) \partial_\mathbf{n} e^{-ik\mathbf{y}\cdot\mathbf{d}} + \big(\psi(\mathbf{y}) + \partial_\mathbf{n} u^{\mathrm{Inc}}(\mathbf{y})\big) e^{-ik\mathbf{y}\cdot\mathbf{d}} \Big) \,\mathrm{d}s(\mathbf{y}) \tag{85}$$

$$= \frac{e^{i\frac{\pi}{4}}}{\sqrt{8\pi k}} \int_\Gamma \psi(\mathbf{y}) e^{-ik\mathbf{y}\cdot\mathbf{d}} \,\mathrm{d}s(\mathbf{y}) \qquad\qquad \mathbf{d} = (\cos\theta, \sin\theta).$$

The last equality comes from Green's second identity (31) in Ω_-, applied to u^{Inc} and the plane wave $\mathbf{y} \mapsto e^{-ik\mathbf{y}\cdot\mathbf{d}}$ (recall that here we have assumed that the datum u^{Inc} is a Helmholtz solution in Ω_-).

Exercise 5.34: (Far-field pattern with BEM). Use your BEM code to approximate the far-field pattern of the field scattered by a polygon; see an example in Figure 17.

Remark 5.35: (Checking BEM accuracy). The formula $(\mathcal{S}\psi + u^{\mathrm{Inc}})|_{\Omega_-} = 0$ is useful to check the correctness of a BEM implementation of the BIE (58). The routine used to evaluate the numerical near-field $u_N = \mathcal{S}\psi_N$ in a portion of Ω_+ can be used to approximate $\mathcal{S}\psi$ in Ω_-. The value $|\mathcal{S}\psi_N + u^{\mathrm{Inc}}|$ in Ω_- must be small for an accurate BEM implementation and must decrease to 0 when the BEM mesh is refined.

Choose a simple domain Υ compactly contained in Ω_- and test your BEM code by computing the value $\big\|\mathcal{S}\psi_N + u^{\mathrm{Inc}}\big\|_{L^2(\Upsilon)} / \big\|u^{\mathrm{Inc}}\big\|_{L^2(\Upsilon)}$ and see how this ratio depends on the problem parameters and on the numerical ones (k, Ω_-, N, quadrature,...). (The reason for taking Υ instead of Ω_- is that the convergence to zero of $(\mathcal{S}\psi_N + u^{\mathrm{Inc}})(\mathbf{x})$ for $N \to \infty$ is slow for $\mathbf{x} \in \Omega_-$ close to Γ.)

Remark 5.36: (Kirchhoff/physical optics approximation). We know from the analysis in §4.1 that, when a plane wave $u^{\mathrm{Inc}}(\mathbf{x}) = e^{ik\mathbf{x}\cdot\mathbf{d}}$ is reflected by an infinite flat Dirichlet obstacle, then the corresponding total field satisfies $\partial_\mathbf{n} u^{\mathrm{Tot}} = 2\partial_\mathbf{n} u^{\mathrm{Inc}}$, where $\mathbf{n}$ is the unit normal to the obstacle. We can imagine that when the same wave hits a flat part of a "very large", convex, bounded, obstacle Ω_- then, at least locally, it behaves as if the obstacle was infinite. For a time-harmonic wave, "very large" means much larger than the problem wavelength $\lambda = \frac{2\pi}{k}$. This suggests to approximate the BIE solution $\psi = -\partial_\mathbf{n}^+ u^{\mathrm{Tot}}$ with

$$\psi^{\mathrm{PO}} := \begin{cases} -2\partial_\mathbf{n} u^{\mathrm{Inc}} = -2ik\mathbf{d}\cdot\mathbf{n}\, u^{\mathrm{Inc}} & \text{on the part of } \Gamma \text{ where } \mathbf{d}\cdot\mathbf{n} \le 0 \text{ i.e., in the part illuminated by } u^{\mathrm{Inc}}, \\ 0 & \text{on the part of } \Gamma \text{ where } \mathbf{d}\cdot\mathbf{n} > 0 \text{ i.e., in the shadow part of } \Gamma. \end{cases}$$

(Recall Exercise 4.4.) This is equivalent to approximating $\partial_\mathbf{n}^+ u^{\mathrm{Scat}}$ with $\partial_\mathbf{n}^+ u^{\mathrm{Inc}}$ on the illuminated part and with $-\partial_\mathbf{n}^+ u^{\mathrm{Inc}}$ on the shadow part. Then one can compute $u^{\mathrm{PO}} = \mathcal{S}(\psi^{\mathrm{PO}})$ as an approximation of u^{Scat}. Numerically, this only requires approximating the representation formula, with no need to solve linear systems or to approximate BIEs. This is called **Kirchhoff** or **physical optics** approximation (sometimes **geometrical optics** approximation), see [CK2, pp. 64] and [CGLS12, §3]. Physically, it corresponds to taking into account only the reflection of the incoming wave disregarding more subtle phenomena such as diffraction by the corners and/or the curved parts of Γ. This can be accurate only for large values of k. See Figure 25 for an example.
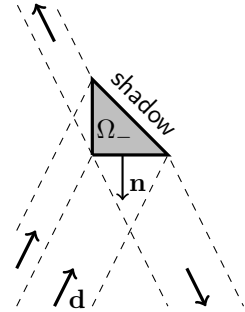
Figure 24 suggests that indeed, for the example with triangular Ω_- of Figure 15, ψ is close to 0 on the hypotenuse (in the shadow) and close to $-2\partial_\mathbf{n} e^{ik\mathbf{x}\cdot\mathbf{d}}$ on the other sides. The physical optics approximation completely misses the singularities of ψ at the corners of the polygon.

Exercise 5.37: (Physical optics approximation vs BEM). Compute the physical optics approximation ψ^{PO} and u^{PO} and plot them against ψ_N and u_N for a given u^{Inc} and a convex polygon, or for a disc (as in Figure 25). Plot some norm of their difference as function of the wavenumber.

Remark 5.38: (Geometrical theory of diffraction). The Kirchhoff approximation described in Remark 5.36 does not include diffraction phenomena, e.g. it incorrectly predicts $\partial_\mathbf{n} u^{\mathrm{Tot}} = 0$ in the shadow region $\{\mathbf{x} \in \Gamma : \mathbf{d}\cdot\mathbf{n}(\mathbf{x}) > 0\}$ of the boundary. An improvement is the **geometrical theory of diffraction** (GTD) developed by J.B. Keller. Assume that Ω_- is a convex polygon and that the incoming field is a plane wave. Let $\mathbf{x} : [0, L_j] \to \Gamma_j$ be the arclength parametrisation of the side Γ_j of Ω_-. The GTD predicts that

$$\psi\big(\mathbf{x}(s)\big) = -\partial_\mathbf{n} u^{\mathrm{Tot}}\big(\mathbf{x}(s)\big) = \psi^{\mathrm{PO}}\big(\mathbf{x}(s)\big) + v_j^+(s) e^{iks} + v_j^-(L_j - s) e^{-iks},$$

where $v_j^\pm$ are non-oscillatory functions that are singular at $s = 0$ and smooth for $s > 0$. This means that $\psi|_{\Gamma_j}$ is sum of the physical-optics approximation and of two waves creeping along Γ in opposite directions and that singularities may appear only at corners. This is consistent with what we see in Figure 24 and is the starting point for the construction of the very efficient **hybrid numerical-asymptotic** (HNA) BEM schemes, see [CGLS12, §3].

Remark 5.39: (Scattering by screens). A sound-soft obstacle does not need to have a positive volume to scatter acoustic waves. Imagine a plane wave propagating in direction $\mathbf{d} = (0, -1)$ hitting the sound-soft rectangle $\Omega_- = (0, 1) \times (0, \delta)$ for small δ. The region immediately underneath the obstacle lies in the "shadow" of Ω_- and the total field will be small, whatever the value of the rectangle thickness $\delta > 0$. In the limit $\delta \searrow 0$, the scatterer volume vanishes, but the scattered field does not. Indeed, we can consider compact scatterers $\Gamma \subset \mathbb{R}^2$ with empty interior that are segments or Lipschitz curves. These scatterers are usually called **screens** or **cracks**. See a simple example in Figure 26.
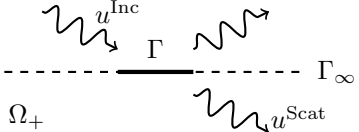
   The corresponding SSSP is identical to (45) where $\Omega_+ = \mathbb{R}^2 \setminus \Gamma$. We can define the single-layer operator and potential on Γ as in §5.1, consider the BIE $S\psi = g_{\mathrm{D}}$, and the scattered field is $u^{\mathrm{Scat}} = \mathcal{S}\psi$. The Dirichlet traces of u^{Scat} on both sides of Γ are equal to the trace of $-u^{\mathrm{Inc}}$, while the Neumann traces of u^{Scat} from the two sides differ. The BIE solution ψ turns out to be the difference (the jump) between the two Neumann traces of u^{Scat} on the two sides of Γ.

   An important difference from problem (45) with a Lipschitz Ω_-, is that when Γ is a screen then the unbounded propagation domain Ω_+ is not a Lipschitz domain, and both u^{Scat} and u^{Tot} have a strong singularity at the endpoints of Γ. In particular, $\psi \notin L^2(\Gamma)$ (compare with (112)). The function spaces needed to appropriately formulate BVPs and BIEs on screens are slightly more complicated than $H^{\pm \frac{1}{2}}(\Gamma)$, to account for the singular behaviour at the endpoints.

   A special property of flat screens, i.e. screens contained in a straight line (or a plane in 3D) is that the sesquilinear forms associated to the Helmholtz single-layer and the hypersingular operators are coercive.[41]

   Exercise 5.40 studies another special feature of the scattering by flat screens.

Exercise 5.40: (Babinet principle). Let $\Gamma_\infty = \{(x_1, 0), x_1 \in \mathbb{R}\} \subset \mathbb{R}^2$ be a horizontal line in the plane. Let $u^{\mathrm{Inc}}(\mathbf{x}) = \mathrm{e}^{\mathrm{i}k(x_1 d_1 + x_2 d_2)}$ be a downward-pointing plane wave, with $d_2 < 0$. Let $\Gamma \subset \Gamma_\infty$ be a flat screen, i.e. a bounded union of disjoint closed segments, and $\Omega_+ = \mathbb{R}^2 \setminus \Gamma$. Let u^{Scat} be the solution of the problem described in Remark 5.39: a radiating Helmholtz solution in Ω_+ with trace $g_{\mathrm{D}} = -u^{\mathrm{Inc}}$ on Γ. From Remark 5.39, $u^{\mathrm{Scat}}(\mathbf{x}) = \mathcal{S}\psi(\mathbf{x}) = \int_\Gamma \Phi_k(\mathbf{x}, \mathbf{y}) \psi(\mathbf{y}) \, \mathrm{d}s(\mathbf{y})$, for ψ supported on Γ. Define

$$w(\mathbf{x}) = \begin{cases} u^{\mathrm{Inc}}(\mathbf{x}) + \mathrm{e}^{\mathrm{i}k(x_1 d_1 - x_2 d_2)} + u^{\mathrm{Scat}}(\mathbf{x}) & x_2 > 0, \\ -u^{\mathrm{Scat}}(\mathbf{x}) & x_2 < 0. \end{cases}$$

Recall from §4.1 that $\mathrm{e}^{\mathrm{i}k(x_1 d_1 - x_2 d_2)}$ is the reflection of u^{Inc} by the infinite line Γ_∞ equipped with sound-hard boundary conditions.

- Show that u^{Scat} is even-symmetric with respect to Γ_∞: $u^{\mathrm{Scat}}(x_1, -x_2) = u^{\mathrm{Scat}}(x_1, x_2)$, and $\frac{\partial u^{\mathrm{Scat}}}{\partial x_2}(x_1, 0) = 0$ for $(x_1, 0) \in \Gamma_\infty \setminus \Gamma$.

- Show that w is a Helmholtz solution in $\mathbb{R}^2 \setminus (\Gamma_\infty \setminus \Gamma) = \Omega_+ \cup \Gamma$. In particular, it is smooth across Γ.

- Show that $\frac{\partial w}{\partial x_2}(x_1, 0) = 0$ on $\Gamma_\infty \setminus \Gamma$.

This means that w is the total field obtained when u^{Inc} hits the unbounded screen $\Gamma_\infty \setminus \Gamma$ equipped with sound-hard boundary conditions.

   This is **Babinet's principle**: the scattering by a Dirichlet screen Γ is the "complementary" of the scattering by the Neumann screen Γ_∞ with aperture Γ. Here "complementary" means that the scattered fields for the two problems in the lower half plane are opposite to one another.[42] See Figure 27 for an example.

   When electromagnetic waves are involved, Babinet's principle states that the electric field scattered by a perfectly conducting (PEC) screen Γ corresponds to the magnetic field diffracted and transmitted by the complementary aperture $\Gamma_\infty \setminus \Gamma$, and vice versa (so one swaps electric↔magnetic fields, instead of Dirichlet↔Neumann boundary conditions). The field scattered by a flat screen, approximated for instance with the BEM, can be used to compute the classical aperture "diffraction patterns".

---

[41][Chandler-Wilde, Hewett, Wavenumber-explicit continuity and coercivity estimates in acoustic scattering by planar screens, IEOT 2015]

[42]See [Bouwkamp, Diffraction theory, 1954], in particular pp. 38–39 and pp. 45–46 for acoustic and electromagnetic waves.

Scattering by unit disc: comparison with Kirchhoff approximation. $\Re\{u^{Scat}\}$, $k = 10$, 200 Gauss points, relative L^2 error $= 0.20675$

Exact solution   **Kirchhoff physical optics approximation**   **Difference**

Scattering by unit disc: comparison with Kirchhoff approximation. $\Re\{u^{Scat}\}$, $k = 30$, 200 Gauss points, relative L^2 error $= 0.14645$

Exact solution   **Kirchhoff physical optics approximation**   **Difference**

Scattering by unit disc: comparison with Kirchhoff approximation. $\Re\{u^{Scat}\}$, $k = 100$, 200 Gauss points, relative L^2 error $= 0.10051$

Exact solution   **Kirchhoff physical optics approximation**   **Difference**

Figure 25: The Kirchhoff (physical optics) approximation of the scattering by a sound-soft disc.
Left: the field $\Re\{u^{\mathrm{Scat}}\}$ scattered by the unit disc B_1, hit by a horizontal plane wave for different wavenumbers $k \in \{10, 30, 100\}$. This has been computed with the multipole expansion as in Figure 12.
Centre: the approximation $\Re\{u^{\mathrm{PO}}\}$ computed as the single-layer potential applied to the density ψ^{PO} defined in Remark 5.36. Numerically, u^{PO} has been computed with 200-point Gauss–Legendre quadrature on the left half of the disc boundary (recall that $\psi^{\mathrm{PO}} = 0$ in the shadow part).
Right: the error $\Re\{u - u^{\mathrm{PO}}\}$ committed by the Kirchhoff approximation. This is not a numerical error but it contains the diffracted waves that are not taken into account by this approximation. The error is higher near the "shadow boundary", i.e. the part of Γ separating the lit and the shadow parts. The $\|u^{\mathrm{Scat}} - u^{\mathrm{PO}}\|_{L^2((-2,2)^2 \setminus B_1)}/\|u^{\mathrm{Scat}}\|_{L^2((-2,2)^2 \setminus B_1)}$ relative error is reported for each example and decreases with the wavenumber.

Figure 26: The scattering of a plane wave with $k = 20$, $\mathbf{d} = (0, -1)$, impinging on the rectangle $(0,1) \times (-0.1, 0)$ (left) and on the screen $[0,1] \times \{0\}$ (right). The imaginary part of the total field is plotted on $(-1, 2) \times (-1.5, 1.5)$.
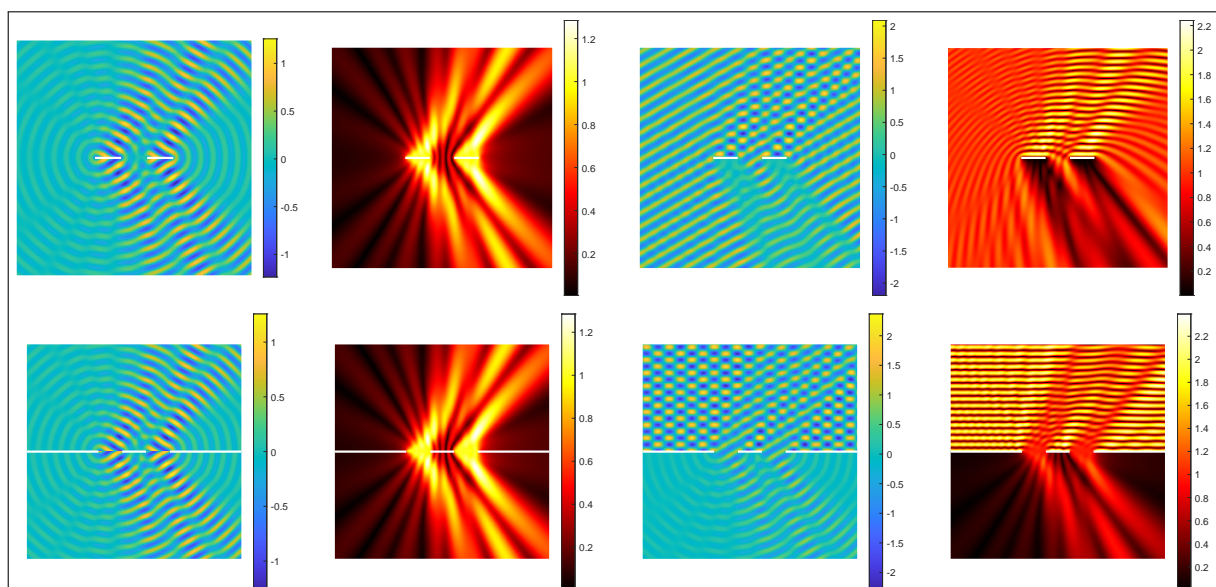
Figure 27: An illustration of Babinet's principle (Exercise 5.40). A plane wave with wavenumber $k = 40$ and direction $\mathbf{d} = (\cos\frac{\pi}{3}, -\sin\frac{\pi}{3})$ is scattered by the 2-component sound-soft screen $\Gamma = ([0, \frac{1}{3}] \cup [\frac{2}{3}, 1]) \times \{0\}$ (top row), and is transmitted by an aperture with the shape of Γ in the infinite sound-hard screen $\Gamma_\infty = \{x_2 = 0\}$ (bottom row). The real and the imaginary parts of the scattered and total fields are plotted in the square $(-1, 2) \times (-1.5, 1.5)$. The scattered field for the two problems is identical in the upper half plane and have opposite signs in the lower half plane.

6 Well-posedness, other BIEs, and error analysis

6.1 Well-posedness of the single-layer BIE

We want to study the well-posedness of the single-layer BIE $S\psi = g_{\mathrm{D}}$ (58). To this purpose, we want to verify that the single-layer operator $S : H^{-\frac{1}{2}}(\Gamma) \to H^{\frac{1}{2}}(\Gamma)$ is (i) injective and (ii) Fredholm. When both conditions are satisfied, then Fredholm alternative (Theorem 3.17) implies that S is invertible and the BIE is well-posed. However, injectivity is not always true: the EDP (44) is always well-posed (§4.4) but its BIE (58) might fail.

6.1.1 Injectivity of the single-layer operator

As in §4.2, two cases may happen:

- If $\Lambda = k^2$ is a Dirichlet eigenvalue in Ω_-, then there exists an eigenfunction $w \neq 0$ such that $\Delta w + k^2 w = 0$ and $\gamma^- w = 0$. Define $\psi = \partial_{\mathbf{n}}^- w$. By Green's representation (65), $w = \mathcal{S}\partial_{\mathbf{n}}^- w - \mathcal{D}\gamma^- w = \mathcal{S}\partial_{\mathbf{n}}^- w = \mathcal{S}\psi$. Then $\psi \neq 0$ because otherwise $w = \mathcal{S}\psi$ would be zero, and $S\psi = \gamma^- \mathcal{S}\psi = \gamma^- w = 0$. In this case the single-layer operator is not injective: $0 \neq \psi \in \ker S$. The BIE (58) is not well-posed.

- If $\Lambda = k^2$ is not a Dirichlet eigenvalue in Ω_-, then assume that $S\psi = 0$ and define $u = \mathcal{S}\psi$. We have that $u^- = u|_{\Omega_-}$ is Helmholtz solution in Ω_- and $\gamma^- u^- = \gamma^- \mathcal{S}\psi = S\psi = 0$. But the interior homogeneous Helmholtz Dirichlet BVP is well-posed by Proposition 4.6 and admits only the solution $u^- = 0$. Similarly $u^+ = u|_{\Omega_+}$ is a radiating Helmholtz solution in Ω_+ with $\gamma^+ u^+ = \gamma^+ \mathcal{S}\psi = S\psi = 0$. By the well-posedness of the EDP of §4.4 also $u^+ = 0$. The jump relation (80) gives $\psi = -[\![\partial_{\mathbf{n}}\mathcal{S}\psi]\!] = -\partial_{\mathbf{n}}^+ u^+ + \partial_{\mathbf{n}}^- u^- = 0$, so the single-layer operator is injective.

Combining with Proposition 4.6 we obtain the following fact.

Lemma 6.1: (Injectivity of S). For each bounded, Lipschitz $\Omega_- \subset \mathbb{R}^2$, there exist a sequence of positive number $k_1 < k_2 < \ldots$, $\lim_{j\to\infty} k_j = \infty$, such that S is injective if and only if $k \neq k_j$ for all $j \in \mathbb{N}$.

These values are called **spurious resonances** or **spurious frequencies**. Even if the BIE (58) is not solvable in this case, the EDP (44) is well-posed: the interior eigenvalues affect and spoil the BIE formulation of the exterior problem. This can be understood as follows: the same BIE solves both an exterior and an interior Helmholtz Dirichlet problem (with solutions $(\mathcal{S}\psi)|_{\Omega_+}$ and $(\mathcal{S}\psi)|_{\Omega_-}$), when the latter is not well-posed then the BIE cannot be well-posed either. In §6.2 we will see other (slightly more complicated) BIEs that always admit a solution.

Exercise 6.2: (Spurious frequencies and BEM). We observe how spurious resonances affect numerical computations. Plot the condition number of the BEM matrix $\underline{\underline{\mathbf{A}}}^{\mathrm{Col/Gal}}$ and the accuracy test of Remark 5.35 (e.g. $\left\|\mathcal{S}\psi_N + u^{\mathrm{Inc}}\right\|_{L^2(\Gamma)}$) for several values of k close to a resonance to see how they blow up.

Hint: choose Ω_- as a square, so that the values of k_j are easily computed by hand as in §4.2.

6.1.2 The single-layer operator is Fredholm

We now want to show that the single-layer operator $S : H^{-\frac{1}{2}}(\Gamma) \to H^{\frac{1}{2}}(\Gamma)$ is Fredholm, i.e. it is sum of an invertible and a compact operator.

We define the single-layer operator for Laplace equation $-\Delta u = 0$ as

$$(S_0\psi)(\mathbf{x}) := -\frac{1}{2\pi} \int_\Gamma \log \frac{|\mathbf{x} - \mathbf{y}|}{d} \psi(\mathbf{y})\, \mathrm{d}s(\mathbf{y}), \qquad \mathbf{x} \in \Gamma, \tag{86}$$

where d is a positive parameter[43] satisfying $d > \mathrm{diam}(\Gamma) = \sup_{\mathbf{x},\mathbf{y}\in\Gamma} |\mathbf{x} - \mathbf{y}|$.

Given a positive number c, we also define the single-layer operator for the homogeneous reaction–diffusion equation (in this setting sometimes called "Yukawa equation" [SBH19], or "modified Helmholtz equation" [Spence14]) $-\Delta u + c^2 u = 0$ as

$$(S_c\psi)(\mathbf{x}) := \frac{1}{2\pi} \int_\Gamma K_0(c|\mathbf{x} - \mathbf{y}|)\psi(\mathbf{y})\, \mathrm{d}s(\mathbf{y}), \qquad \mathbf{x} \in \Gamma, \tag{87}$$

---

[43]Different values of d give different "versions" of the single-layer. This corresponds to adding a constant to S_0; recall the following difference between Laplace and Helmholtz solutions: $\Delta u = 0 \Rightarrow \Delta(u + C) = 0$ but $(\Delta + k^2)u = 0 \Rightarrow (\Delta + k^2)(u + C) \neq 0$ for all constants $C \neq 0$. This is related to the fact that the 2D Laplace fundamental solution does not decay to 0 at infinity. We will see in Remark 6.8 that the precise value of d only matters to ensure the coercivity of S_0. This is not true in 3D, where there is no need for the parameter d.

where $K_0(t) := \frac{i\pi}{2} H_0^{(1)}(it)$ for $t \geq 0$ is the "modified Bessel function of the second kind". [44] Formally, S_c equals the single-layer operator for the Helmholtz equation with purely imaginary wavenumber (i.e. with ic in place of k).

The following two facts hold:

Lemma 6.3: (Single-layer: compactness of $S - S_c$ and coercivity of S_c). For all $c \geq 0$,

- $S - S_c : H^{-\frac{1}{2}}(\Gamma) \to H^{\frac{1}{2}}(\Gamma)$ is compact;

- $S_c : H^{-\frac{1}{2}}(\Gamma) \to H^{\frac{1}{2}}(\Gamma)$ is coercive, i.e. $\exists \alpha_c > 0$ such that $\langle S_c \psi, \psi \rangle_\Gamma \geq \alpha_c \|\psi\|^2_{H^{-\frac{1}{2}}(\Gamma)} \quad \forall \psi \in H^{-\frac{1}{2}}(\Gamma)$.

In the next pages we explain where Lemma 6.3 comes from, but we do not give a complete proof.

Note that we allow also the case $c = 0$: S_c can stand either for the Laplace or for the reaction–diffusion operator.

The second item of Lemma 6.3 and Lax–Milgram theorem imply that $S_c : H^{-\frac{1}{2}}(\Gamma) \to H^{\frac{1}{2}}(\Gamma)$ is invertible and that the corresponding BIE (for Laplace or reaction–diffusion) $S_c \psi = g$ is well-posed for all $g \in H^{\frac{1}{2}}(\Gamma)$. From Definition 3.16, $S = S_c + (S - S_c)$ is a Fredholm operator. Moreover, the sesquilinear form $\mathcal{A}(\cdot, \cdot)$ defined in (60) and used to define and implement the Galerkin-BEM method is sum of a coercive and a compact form: $\mathcal{A}(\psi, \xi) = \langle S\psi, \xi \rangle_\Gamma = \langle S_c \psi, \xi \rangle_\Gamma + \langle (S - S_c)\psi, \xi \rangle_\Gamma$.

By Fredholm alternative 3.17, S is invertible if and only if it is injective. By §6.1.1, the single-layer BIE $S\psi = g_D$ is well-posed (i.e. S is invertible) if and only if $-k^2$ is not a Dirichlet eigenvalue for Ω_-. Combining with what we already know about the eigenvalues, we obtain the following fact.

Theorem 6.4: (Single-layer BIE well-posedness). For each Ω_- there exist a sequence of positive numbers $k_1 < k_2 < \ldots$, $\lim_{j \to \infty} k_j = \infty$, such that the BIE $S\psi = g_D$ is well-posed for all $g_D \in H^{\frac{1}{2}}(\Gamma)$ if and only if $k \neq k_j$ for all $j \in \mathbb{N}$.

We repeat: Theorem 6.4 follows from Lemma 6.3, Lax–Milgram theorem, Fredholm alternative 3.17, and Lemma 6.1.

Why do we consider both the Laplace (S_0) and the reaction–diffusion (S_c) cases? To prove the Fredholm property of S any of them would be enough. On one hand, the Laplace single-layer S_0 is easier to study because it does not require special functions, while, on the other hand, the coercivity is easier to prove for S_c than for S_0 (in 2D). [45]

We study the properties of compactness and coercivity in the following, starting from the case of a circular scatterer.

Remark 6.5: (Helmholtz=Laplace+low-order, once again). This decomposition of the Helmholtz operator in a "Laplace part" and "whatever is left" should remind you the technique used in §4.2 for Helmholtz problems on bounded domains. In that case, using the Gårding inequality, we have decomposed the Helmholtz sesquilinear form (either $\mathcal{A}$ of (36) or $\mathcal{A}_I$ of (38)) in a coercive part corresponding to an elliptic equation and a compact perturbation term multiple of $k^2 \int_\Omega u \overline{u} \, d\mathbf{x}$.

Remark 6.6: (Helmholtz vs coercive cases: BIE well-posedness and Galerkin method). The coercivity of S_0 implies that the single-layer BIE for the Laplace equation $S_0 \psi = g_D$ is always well-posed. Moreover, as we are in a Lax–Milgram setting, every Galerkin-BEM discretisation of the variational problem $\langle S_0 \psi, \xi \rangle_\Gamma = \langle g_D, \xi \rangle_\Gamma$ is well-posed, quasi-optimal and gives symmetric positive-definite matrices.

This is not true in the Helmholtz case. To ensure well-posedness of the Galerkin method, some conditions on the discrete space are needed (roughly speaking, it must have sufficiently good approximation properties). Under these conditions, we have a quasi-optimality estimate as in Céa lemma. We sketch this theory in §6.3.

---

[44] This is defined from the complex-analytic extension of $H_0^{(1)}$ to complex argument, in such a way that K_0 is a real-valued, positive, monotonically decreasing function; see [DLMF, eq. 10.27.8]. It satisfies $K_0(t) \sim -\log t$ for $t \to 0$ and $K_0(t) \sim \sqrt{\pi/2t}\, e^{-t}$ for $t \to \infty$, [DLMF, eq. 10.25.3 and 10.30.3]. It is easy to see that it satisfies the "modified Bessel equation" $t^2 K_0''(t) + t K_0'(t) - t^2 K_0(t) = 0$ and from this that $-\Delta_\mathbf{x} \Phi_c(\mathbf{x}, \mathbf{y}) + c^2 \Phi_c(\mathbf{x}, \mathbf{y}) = \delta_\mathbf{y}(\mathbf{x})$ where $\Phi_c(\mathbf{x}, \mathbf{y}) := \frac{1}{2\pi} K_0(c|\mathbf{x} - \mathbf{y}|) = \frac{i}{4} H_0^{(1)}(ic|\mathbf{x} - \mathbf{y}|)$.

[45] We write also the fundamental solutions of the Helmholtz, Laplace and reaction–diffusion PDEs in $\mathbb{R}^3$:

$$\Delta u + k^2 u = 0 \to \Phi_k(\mathbf{x}, \mathbf{y}) = \frac{e^{ik|\mathbf{x}-\mathbf{y}|}}{4\pi|\mathbf{x} - \mathbf{y}|}, \quad \Delta u = 0 \to \Phi_0(\mathbf{x}, \mathbf{y}) = \frac{1}{4\pi|\mathbf{x} - \mathbf{y}|}, \quad -\Delta u + c^2 u = 0 \to \Phi_c(\mathbf{x}, \mathbf{y}) = \frac{e^{-c|\mathbf{x}-\mathbf{y}|}}{4\pi|\mathbf{x} - \mathbf{y}|}$$

([Spence14, §9.1]). Differently from the 2D case, all three fundamental solutions can be written as special instances of Φ_c with complex c (or Φ_k with complex k). In particular, in 3D the Laplace case is the limit for $k \searrow 0$ or $c \searrow 0$ of the other two.

6.1.3 CONTINUITY, COMPACTNESS AND COERCIVITY OF SINGLE-LAYER BIOS ON A CIRCLE

Let K be a BIO on the circle ∂B_R with kernel $\kappa : (0, \infty) \to \mathbb{C}$, i.e.

$$(Kv)(\mathbf{x}) = \int_{\partial B_R} \kappa(|\mathbf{x} - \mathbf{y}|) v(\mathbf{y}) \, \mathrm{d}s(\mathbf{y}), \tag{88}$$

for v defined on Γ. The distance between two points on the circle can be computed using polar coordinates:

$$|\mathbf{x} - \mathbf{y}| = |R e^{i\theta_\mathbf{x}} - R e^{i\theta_\mathbf{y}}| = R|1 - e^{i(\theta_\mathbf{x} - \theta_\mathbf{y})}| = R\sqrt{2 - 2\cos(\theta_\mathbf{x} - \theta_\mathbf{y})}.$$

The action of the operator K on a function v can be written as the multiplication of the Fourier coefficients of the argument $v(\mathbf{x}) = \sum_{\ell \in \mathbb{Z}} \hat{v}_\ell e^{i\ell\theta}$ by some coefficients K_ℓ:

$$(Kv)(\mathbf{x}) = \int_{\partial B_R} \kappa(|\mathbf{x} - \mathbf{y}|) v(\mathbf{y}) \, \mathrm{d}s(\mathbf{y}) = R \int_0^{2\pi} \kappa(R\sqrt{2 - 2\cos(\theta_\mathbf{x} - \theta)}) \sum_{\ell \in \mathbb{Z}} \hat{v}_\ell e^{i\ell\theta} \, \mathrm{d}\theta \qquad (\alpha = \theta - \theta_\mathbf{x})$$

$$= \sum_{\ell \in \mathbb{Z}} \hat{v}_\ell e^{i\ell\theta_\mathbf{x}} \underbrace{R \int_0^{2\pi} \kappa(R\sqrt{2 - 2\cos\alpha}) e^{i\ell\alpha} \, \mathrm{d}\alpha}_{=: K_\ell} = \sum_{\ell \in \mathbb{Z}} \hat{v}_\ell K_\ell \, e^{i\ell\theta_\mathbf{x}}.$$

If $K_\ell = \mathcal{O}(\ell^a)$ for some $a \in \mathbb{R}$ then, from the definition (28) of the Sobolev spaces on the circular boundary, $K : H^s(\partial B_R) \to H^{s-a}(\partial B_R)$ as a bounded operator. But, how to estimate the coefficients K_ℓ?

The values K_ℓ are the Fourier coefficients of the function $\alpha \mapsto R\kappa(R\sqrt{2 - 2\cos\alpha})$ on $(0, 2\pi)$. Parseval's theorem ($\int_0^{2\pi} |f(\theta)|^2 \, \mathrm{d}\theta = 2\pi \sum_{\ell \in \mathbb{Z}} |\hat{f}_\ell|^2$) implies that the Fourier coefficients of an $L^2(0, 2\pi)$ function decay as $o(\ell^{-1/2})$. As we have seen in §3.3 using that $(e^{i\ell\theta})' = i\ell e^{i\ell\theta}$, if $f' \in L^2(0, 2\pi)$ then $\hat{f}_\ell = o(\ell^{-3/2})$.

The function $\alpha \mapsto R\sqrt{2 - 2\cos\alpha}$ is Lipschitz (you can verify that its derivative is $\pm\sqrt{\frac{1 + \cos\alpha}{2}}$). Thus, if $\kappa \in L^2(0, 2R)$ then $K_\ell = o(\ell^{-1/2})$, if moreover $\kappa' \in L^2(0, 2R)$ then $K_\ell = o(\ell^{-3/2})$. So, useful relations between the properties of the kernel κ and the continuity of the operator K in the form (88) are

$$\kappa \in L^2(0, 2R) \implies K : H^s(\partial B_R) \to H^{s+\frac{1}{2}}(\partial B_R), \qquad \kappa \in H^1(0, 2R) \implies K : H^s(\partial B_R) \to H^{s+\frac{3}{2}}(\partial B_R).$$

(From the formulas above, the properties of $\kappa(t)$ for $t > 2R$, the diameter of the circle, are irrelevant.)

What are the kernels of the Helmholtz and Laplace single-layer operators? We have

$$K = S \qquad \implies \qquad \kappa(t) = \frac{i}{4} H_0^{(1)}(kt) \qquad\qquad \in L^2(0, 2R),$$

$$K = S_0 \qquad \implies \qquad \kappa(t) = -\frac{1}{2\pi} \log\frac{|t|}{d} \qquad\qquad \in L^2(0, 2R),$$

$$K = S - S_0 \qquad \implies \qquad \kappa(t) = \frac{i}{4} H_0^{(1)}(kt) + \frac{1}{2\pi} \log\frac{|t|}{d} \qquad \in H^1(0, 2R).$$

The first line gives $S : H^s(\partial B_R) \to H^{s+\frac{1}{2}}(\partial B_R)$. This is not new: we already mentioned that $S : H^{-\frac{1}{2}}(\Gamma) \to H^{\frac{1}{2}}(\Gamma)$ for all Lipschitz boundaries, which, for $s = -\frac{1}{2}$, is a stronger result. We have also seen from the numerical computations in Figure 20 and Remark 5.2 that $K_\ell \sim \ell^{-1}$, so we cannot expect any stronger continuity property than this.

We now look at the difference between Helmholtz and Laplace single-layer operators $S - S_0$ (on ∂B_R). From the asymptotic formula $H_0^{(1)}(z) = i\frac{2}{\pi} \log z + 1 + i\frac{2}{\pi}(\gamma - 2) + \mathcal{O}(z^2)$ by, e.g., [DLMF, eq. 10.8.2] with the Euler's constant $\gamma \approx 0.57721$ we have that κ is bounded and κ' is bounded (with a jump at 0 because of the $\sqrt{2 - 2\cos\alpha}$ term). So $S - S_0 : H^{-\frac{1}{2}}(\partial B_R) \to H^1(\partial B_R)$. (In Figure 28 we demonstrate numerically a stronger continuity property, i.e. that $S - S_0 : H^{-\frac{1}{2}}(\partial B_R) \to H^{\frac{5}{2}}(\partial B_R)$.) Since the inclusion $\iota : H^1(\partial B_R) \to H^{\frac{1}{2}}(\partial B_R)$ is compact, then **the difference between the two single-layers** $S - S_0 : H^{-\frac{1}{2}}(\partial B_R) \to H^{\frac{1}{2}}(\partial B_R)$ **is compact.**[46]

Precisely the same holds with S_c in place of S_0: this is because the corresponding kernels $\kappa(t) = -\frac{1}{2\pi} \log\frac{|t|}{d}$ and $\kappa(t) = \frac{1}{2\pi} K_0(c|t|)$ have the same behaviour at $t = 0$.

---

[46]Recall that the property of compactness of an operator depends heavily on the norms of the function spaces chosen as domain and codomain. E.g. the identity operator $I : H^1(\Omega) \to H^1(\Omega)$ is not compact for a bounded Lipschitz Ω, but when we view it as $I : H^1(\Omega) \to L^2(\Omega)$ (and we call it embedding) then it is compact (Rellich theorem). The technique used in this section is very standard: we show that an operator K maps in a space that is slightly smoother (here $H^1(\partial B_R)$) than the desired domain (here $H^{\frac{1}{2}}(\partial B_R)$), then we compose the operator with the embedding (here $\iota : H^1(\partial B_R) \to H^{\frac{1}{2}}(\partial B_R)$) and if this embedding is compact the same holds for $\iota \circ K$. Recall that the composition of a continuous operator and a compact one is compact; you can prove this from the definition.
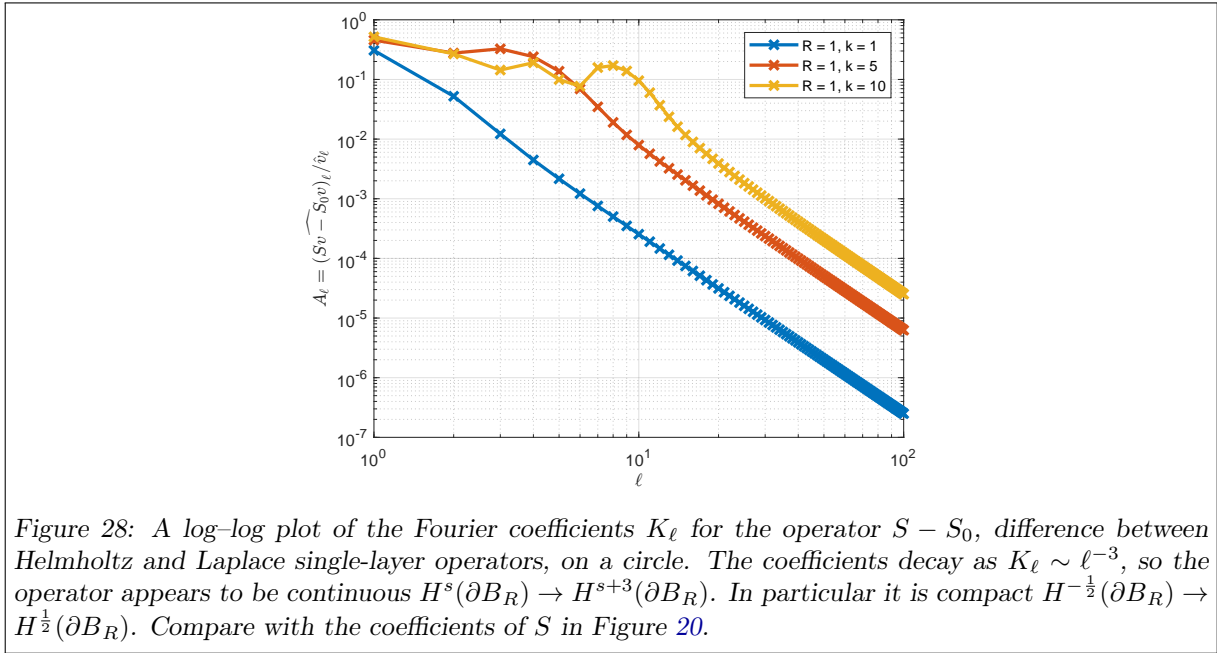
Figure 28: *A log–log plot of the Fourier coefficients K_ℓ for the operator $S - S_0$, difference between Helmholtz and Laplace single-layer operators, on a circle. The coefficients decay as $K_\ell \sim \ell^{-3}$, so the operator appears to be continuous $H^s(\partial B_R) \to H^{s+3}(\partial B_R)$. In particular it is compact $H^{-\frac{1}{2}}(\partial B_R) \to H^{\frac{1}{2}}(\partial B_R)$. Compare with the coefficients of S in Figure 20.*

We can use the expansion in circular harmonics also to check the coercivity of an integral operator. The sesquilinear form associated to K diagonalises in the Fourier basis (recall §3.3):

$$\langle Kv, w \rangle_{\partial B_R} = \left\langle \sum_{\ell \in \mathbb{Z}} \hat{v}_\ell K_\ell e^{i\ell\theta_{\mathbf{x}}}, \sum_{m \in \mathbb{Z}} \hat{w}_\ell e^{im\theta_{\mathbf{x}}} \right\rangle_{\partial B_R} = 2\pi R \sum_{\ell \in \mathbb{Z}} \hat{v}_\ell K_\ell \overline{\hat{w}_\ell}.$$

If $K_\ell \in \mathbb{R}$ and $K_\ell \geq c(1+\ell^2)^s$ for all ℓ and some $c > 0$, $s \in \mathbb{R}$ [47], then $|\langle Kv, v \rangle_{\partial B_R}| \geq 2\pi Rc \sum_{\ell \in \mathbb{Z}} |\hat{v}_\ell|^2 (1+\ell^2)^s = c \|v\|^2_{H^s(\partial B_R)}$, i.e. K is coercive in $H^s(\partial B_R)$.

Now look at the Laplace single-layer, i.e. K with $\kappa(t) = -\frac{1}{2\pi} \log \frac{|t|}{d}$. Since $\kappa(R\sqrt{2 - 2\cos(t)})$ is real and even-symmetric, its Fourier coefficients K_ℓ are real.

Exercise 6.7: (Laplace single-layer Fourier coefficients). Compute numerically the coefficients K_ℓ for the Laplace single-layer S_0 and verify that they satisfy $K_\ell(1 + \ell^2)^{\frac{1}{2}} > c$. (For $R = 1$, $c \approx \frac{1}{2}$.)

From this exercise it follows that the **Laplace single-layer operator S_0 is coercive in $H^{-\frac{1}{2}}(\partial B_R)$**. The same argument can be repeated for S_c.

We have verified, partly with numerical experiments, both items in Lemma 6.3 for the case $\Gamma = \mathbb{S}^1$.

6.1.4   COMPACTNESS OF $S - S_0$

We sketch the main ideas used to prove the compactness of $(S - S_0) : H^{-\frac{1}{2}}(\Gamma) \to H^{\frac{1}{2}}(\Gamma)$. Making them precise and rigorous is not trivial.

The key result to prove compactness of BIOs is the following: an operator $K : L^2(\Gamma) \to L^2(\Gamma)$ in the form $(Kv)(\mathbf{x}) = \int_\Gamma \kappa(|\mathbf{x} - \mathbf{y}|)v(\mathbf{y}) \, ds(\mathbf{y})$ is compact if the kernel $\kappa : [0, \text{diam}\,\Gamma] \to \mathbb{C}$ is a *bounded* function (L^∞).

From the asymptotic expansion of the Hankel function at the origin, as in §6.1.3, we see that the kernel $\kappa(t) = \frac{i}{4} H_0^{(1)}(kt) + \frac{1}{2\pi} \log \frac{t}{d}$ of $S - S_0$ is bounded (and continuous). The operator T defined by $Tv = (Sv - S_0 v)'$, where the derivative is the tangential derivative along Γ, also has a bounded (but discontinuous) kernel, for the same reason. From this it follows that $S - S_0 : L^2(\Gamma) \to H^1(\Gamma)$ is a compact operator. However we want to lower the Sobolev exponents of both spaces by $\frac{1}{2}$.

From functional analysis ([McLean00], Thm. 2.17) we know that if an operator $K : H_1 \to H_2$ is compact, then its adjoint $K^* : H_2^* \to H_1^*$ (defined by $(K^*\varphi)(\psi) = \varphi(K\psi)$ for $\varphi \in H_2^*$ and $\psi \in H_1$) is also compact.

Fubini's theorem implies that the single-layer is self-adjoint (up to conjugation) in $L^2(\Gamma)$: $\int_\Gamma (S\varphi)\psi \, ds = \int_\Gamma \varphi(S\psi) \, ds$ for all $\varphi, \psi \in L^2(\Gamma)$ (recall Exercise 5.3). The same holds for S_0. Thus the adjoint of

---

[47] More generally, if the K_ℓ are complex we can also take $\Re\{\sigma K_\ell\} > c(1+\ell^2)^s$ for some $\sigma \in \mathbb{C}$, $|\sigma| = 1$. E.g., K is coercive in $L^2(\partial B_R)$ ($s = 0$) if there exists a straight line in the complex plane $\mathbb{C}$ that separates the origin from all K_ℓ.

$S - S_0 : L^2(\Gamma) \to H^1(\Gamma)$ is the extension of $S - S_0$ itself to $(S - S_0)^* = S - S_0 : H^{-1}(\Gamma) \to L^2(\Gamma)$, where $H^{-1}(\Gamma)$ is the dual of $H^1(\Gamma)$ as in §3.3.3, and is compact.

A technique called "operator interpolation" (see, e.g., [SBH19, §9.8] or [McLean00, §B]) allows to deduce from the compactness of $S - S_0$ in $L^2(\Gamma) \to H^1(\Gamma)$ and in $H^{-1}(\Gamma) \to L^2(\Gamma)$ the boundedness and the compactness in all intermediate spaces $S - S_0 : H^{s-1}(\Gamma) \to H^s(\Gamma)$ for $0 < s < 1$, in particular the compactness of $S - S_0 : H^{-\frac{1}{2}}(\Gamma) \to H^{\frac{1}{2}}(\Gamma)$.

The same reasoning follows verbatim if we take S_c for $c > 0$ (87) in place of S_0 (86): the key point is the boundedness of the kernel of $S - S_c$ and of $v \mapsto (Sv - S_c v)'$. This follows from the fact that all kernels considered have the same singularity at 0. A different proof of the compactness of $S - S_c$ can be obtained by adapting that in [SBH19, Thm. 14.12].
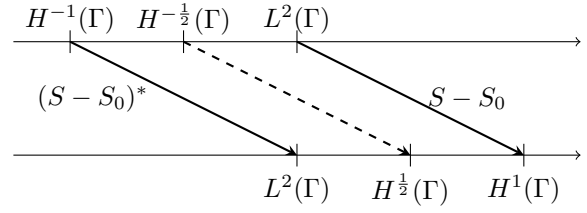
6.1.5 COERCIVITY OF S_c

We sketch the proof of the coercivity of the reaction–diffusion single-layer operator S_c. The coercivity of the Laplace single-layer operator S_0 is slightly more complicated; we discuss it in Remark 6.8.

Most of the results derived and stated in the previous sections (traces, jumps, …) for the Helmholtz equation hold also for the reaction–diffusion equation, using $\Phi_c(\mathbf{x}, \mathbf{y}) = \frac{1}{2\pi} K_0(c|\mathbf{x} - \mathbf{y}|)$ as fundamental solution.

Fix $\psi \in H^{-\frac{1}{2}}(\Gamma)$ and denote $u = \mathcal{S}_c \psi \in H^1(\Omega_-, \Delta) \times H^1_{\mathrm{loc}}(\Omega_+, \Delta)$, $\mathcal{S}_c$ being the reaction–diffusion single-layer potential. Then $-\Delta u + c^2 u = 0$ in $\Omega_- \cup \Omega_+$, $[\![\gamma u]\!] = 0$ and $[\![\partial_{\mathbf{n}} u]\!] = -\psi$, in analogy to (80). From the properties of K_0, both u and its radial derivative decay exponentially to 0 for $|\mathbf{x}| \to \infty$.

Integration by parts (Green's first identity (30) with $k = \mathrm{i}c$) on Ω_- gives the identity

$$\|\nabla u\|^2_{L^2(\Omega_-)} + c^2 \|u\|^2_{L^2(\Omega_-)} = \int_{\Omega_-} (\nabla u \cdot \nabla \overline{u} + c^2 u \overline{u})\, \mathrm{d}\mathbf{x} = \int_{\Gamma} \partial_{\mathbf{n}}^- u\, \gamma^- \overline{u}\, \mathrm{d}s.$$

Proceeding similarly to §5.3 and exploiting the decay of u and $\frac{\partial u}{\partial r}$, the same holds in Ω_+:

$$\|\nabla u\|^2_{L^2(\Omega_+)} + c^2 \|u\|^2_{L^2(\Omega_+)} = \lim_{R \to \infty} \left(\|\nabla u\|^2_{L^2(\Omega_+ \cap B_R)} + c^2 \|u\|^2_{L^2(\Omega_+ \cap B_R)} \right) \tag{89}$$

$$= \lim_{R \to \infty} \int_{\Omega_+ \cap B_R} (\nabla u \cdot \nabla \overline{u} + c^2 u \overline{u})\, \mathrm{d}\mathbf{x}$$

$$= \lim_{R \to \infty} \left(-\int_{\Gamma} \partial_{\mathbf{n}}^+ u\, \gamma^+ \overline{u}\, \mathrm{d}s + \underbrace{\int_{\partial B_R} \partial_{\mathbf{n}} u\, \overline{u}\, \mathrm{d}s}_{\xrightarrow{R \to \infty} 0} + \int_{\Omega_+ \cap B_R} \underbrace{(-\Delta u + c^2 u)}_{=0} \overline{u}\, \mathrm{d}\mathbf{x} \right) = -\int_{\Gamma} \partial_{\mathbf{n}}^+ u\, \gamma^+ \overline{u}\, \mathrm{d}s.$$

(Note that the $H^1(\Omega_+)$ norm would not be bounded if $u = \mathcal{S}\psi$, with the Helmholtz single-layer potential, because in this case u would have a slower decay at infinity.)

Taking the normal trace of vector fields, $\mathbf{v} \mapsto \mathbf{v}|_\Gamma \cdot \mathbf{n}$, is continuous as an operator from $H(\mathrm{div}; \Omega_\pm)$ to $H^{-\frac{1}{2}}(\Gamma)$ ([SBH19, Thm. 6.1], recall footnote 14):

$$\|\mathbf{v}|_\Gamma \cdot \mathbf{n}\|^2_{H^{-\frac{1}{2}}(\Gamma)} \le C_{\mathrm{tr}} \left(\|\mathbf{v}\|^2_{L^2(\Omega_\pm)^2} + \|\mathrm{div}\, \mathbf{v}\|^2_{L^2(\Omega_\pm)} \right) \tag{90}$$

$$\forall \mathbf{v} \in H(\mathrm{div}; \Omega_\pm) := \left\{ \mathbf{v} \in L^2(\Omega_\pm)^2; \mathrm{div}\, \mathbf{v} \in L^2(\Omega_\pm) \right\}.$$

Here $C_{\mathrm{tr}} > 0$ only depends on Γ. Applying this to ∇u, whose divergence is in L^2 because $\Delta u = c^2 u$, allows to control the Neumann traces with the L^2 norms of the gradient and the Laplacian of u. Combining all these results we have that, for all $\psi \in H^{-\frac{1}{2}}(\Gamma)$,

$$\|\psi\|^2_{H^{-\frac{1}{2}}(\Gamma)} = \|[\![\partial_{\mathbf{n}} u]\!]\|^2_{H^{-\frac{1}{2}}(\Gamma)} \qquad\qquad \psi = -[\![\partial_{\mathbf{n}} u]\!]$$

$$\le 2 \left(\|\partial_{\mathbf{n}}^- u\|^2_{H^{-\frac{1}{2}}(\Gamma)} + \|\partial_{\mathbf{n}}^+ u\|^2_{H^{-\frac{1}{2}}(\Gamma)} \right) \qquad\qquad \text{triangle inequality}$$

$$\le 2 C_{\mathrm{tr}} \left(\|\nabla u\|^2_{L^2(\Omega_-)^2} + \|\Delta u\|^2_{L^2(\Omega_-)} + \|\nabla u\|^2_{L^2(\Omega_+)^2} + \|\Delta u\|^2_{L^2(\Omega_+)} \right) \qquad \begin{array}{l}\text{normal trace continuity}\\ \text{in } H(\mathrm{div}; \Omega_\pm)\ (90)\end{array}$$

$$\le 2 C_{\mathrm{tr}} \max\{1, c^2\} \int_{\Omega_- \cup \Omega_+} (\nabla u \cdot \nabla \overline{u} + c^2 u \overline{u})\, \mathrm{d}\mathbf{x} \qquad\qquad \Delta u = c^2 u$$

$$= 2C_{\mathrm{tr}} \max\{1, c^2\} \int_{\Gamma} (\partial_{\mathbf{n}}^- u \gamma^- \overline{u} - \partial_{\mathbf{n}}^+ u \gamma^+ \overline{u}) \, \mathrm{d}s \qquad \text{Green's 1st identity (89)}$$

$$= 2C_{\mathrm{tr}} \max\{1, c^2\} \int_{\Gamma} -[\![\partial_{\mathbf{n}} u]\!] \gamma \overline{u} \, \mathrm{d}s \qquad \gamma^+ u = \gamma^- u$$

$$= 2C_{\mathrm{tr}} \max\{1, c^2\} \int_{\Gamma} \psi \overline{S_c \psi} \, \mathrm{d}s \qquad [\![\partial_{\mathbf{n}} u]\!] = -\psi, \quad \gamma u = \gamma S_c \psi = S_c \psi$$

$$= 2C_{\mathrm{tr}} \max\{1, c^2\} \int_{\Gamma} (S_c \psi) \overline{\psi} \, \mathrm{d}s \qquad \overline{S_c \psi} = S_c \overline{\psi}, \quad \int_{\Gamma} \psi S_c \phi \, \mathrm{d}s = \int_{\Gamma} (S_c \psi) \phi \, \mathrm{d}s.$$

This is precisely the coercivity of S_c in $H^{-\frac{1}{2}}(\Gamma)$.

Remark 6.8: (Coercivity of S_0 in 3D and 2D). The proof of the coercivity of the Laplace single-layer operator S_0 in $\mathbb{R}^3$ works exactly in the same way setting $c = 0$, noting that the algebraic decay of u for $|\mathbf{x}| \to \infty$ is enough to ensure $\nabla u \in L^2(\Omega_+)^3$ (see [SBH19, §14.6–7])

In $\mathbb{R}^2$ the proof of the coercivity of S_0 is more complicated; here we follow [Steinbach 2008, Thm. 6.22–23][48] and [McLean00, Thm. 8.12–16]. The key difference is that the relation $\|\nabla u\|_{L^2(\Omega_+)}^2 = -\int_{\Gamma} \partial_{\mathbf{n}}^+ u \, \gamma^+ \overline{u} \, \mathrm{d}s$ for $u = S_0 \psi$ only holds if ψ satisfies the 0-average condition $\langle \psi, 1 \rangle_{\Gamma} = 0$. This is due to the absence of decay to zero of the fundamental solution Φ_0 at infinity. Thus the reasoning above gives the coercivity of S_0 in $H_*^{-\frac{1}{2}}(\Gamma) := \{\psi \in H^{-\frac{1}{2}}(\Gamma) : \langle \psi, 1 \rangle_{\Gamma} = 0\}$.

To deal with the general case ($\psi \in H^{-\frac{1}{2}}(\Gamma)$ instead of $\psi \in H_*^{-\frac{1}{2}}(\Gamma)$) we have to work a bit more. Lax–Milgram and the coercivity for 0-average densities ensure that there exists a unique (non zero)

$$\beta_* \in H_*^{-\frac{1}{2}}(\Gamma) \qquad \langle S_0 \beta_*, \xi_* \rangle_{\Gamma} = \langle S_0 1, \xi_* \rangle_{\Gamma} \qquad \forall \xi_* \in H_*^{-\frac{1}{2}}(\Gamma).$$

Define $\beta_{\mathrm{eq}} := \frac{1}{|\Gamma|}(1 - \beta_*) \in H^{-\frac{1}{2}}(\Gamma)$. The two densities $\beta_*, \beta_{\mathrm{eq}}$ only depend on Γ. Then β_{eq} is real-valued, $\langle \beta_{\mathrm{eq}}, 1 \rangle_{\Gamma} = 1$, and $\langle S_0 \beta_{\mathrm{eq}}, \xi_* \rangle_{\Gamma} = 0$ for all $\xi_* \in H_*^{-\frac{1}{2}}(\Gamma)$, so $S_0 \beta_{\mathrm{eq}}$ is constant on Γ. Recalling the definition (86) of S_0,

$$(S_0 \beta_{\mathrm{eq}})(\mathbf{x}) = \frac{1}{2\pi} \int_{\Gamma} \beta_{\mathrm{eq}}(\mathbf{y}) \big(\log d - \log |\mathbf{x} - \mathbf{y}| \big) \, \mathrm{d}s(\mathbf{y})$$

$$= \frac{1}{2\pi} \log d \int_{\Gamma} \beta_{\mathrm{eq}}(\mathbf{y}) \, \mathrm{d}s(\mathbf{y}) - \frac{1}{2\pi} \int_{\Gamma} \beta_{\mathrm{eq}}(\mathbf{y}) \log |\mathbf{x} - \mathbf{y}| \, \mathrm{d}s(\mathbf{y})$$

$$= \frac{1}{2\pi} \log d - \frac{1}{2\pi} \int_{\Gamma} \beta_{\mathrm{eq}}(\mathbf{y}) \log |\mathbf{x} - \mathbf{y}| \, \mathrm{d}s(\mathbf{y}) \qquad \forall \mathbf{x} \in \Gamma.$$

This is where we need the (so far unused) parameter $d > 0$: if d is sufficiently large then $S_0 \beta_{\mathrm{eq}} > 0$. It is possible to show that $d > \mathrm{diam}\,\Gamma$ is enough to guarantee that $S_0 \beta_{\mathrm{eq}} > 0$.[49] Then also

$$\langle S_0 \beta_{\mathrm{eq}}, \beta_{\mathrm{eq}} \rangle_{\Gamma} = S_0 \beta_{\mathrm{eq}} \langle 1, \beta_{\mathrm{eq}} \rangle_{\Gamma} = S_0 \beta_{\mathrm{eq}} > 0.$$

We want to decompose a general $\psi \in H^{-\frac{1}{2}}(\Gamma)$ in a $H_*^{-\frac{1}{2}}(\Gamma)$ component and a remainder: instead of taking a constant remainder as one might expect, we take a remainder whose image under S_0 is constant, i.e. a multiple of β_{eq}. For all $\psi \in H^{-\frac{1}{2}}(\Gamma)$ define

$$\psi_* := \psi - \langle \psi, 1 \rangle_{\Gamma} \beta_{\mathrm{eq}} \quad \Rightarrow \quad \langle \psi_*, 1 \rangle_{\Gamma} = \langle \psi, 1 \rangle_{\Gamma} \Big(1 - \langle \beta_{\mathrm{eq}}, 1 \rangle_{\Gamma} \Big) = 0.$$

Now we use the decomposition $\psi = \psi_* + \langle \psi, 1 \rangle_{\Gamma} \beta_{\mathrm{eq}}$ to show the positivity of the single-layer potential:

$$\langle S_0 \psi, \psi \rangle_{\Gamma} = \langle S_0 (\psi_* + \langle \psi, 1 \rangle_{\Gamma} \beta_{\mathrm{eq}}), \psi_* + \langle \psi, 1 \rangle_{\Gamma} \beta_{\mathrm{eq}} \rangle_{\Gamma}$$

$$= \langle S_0 \psi_*, \psi_* \rangle_{\Gamma} + 2 \langle \psi, 1 \rangle_{\Gamma} \underbrace{\langle S_0 \beta_{\mathrm{eq}}, \psi_* \rangle_{\Gamma}}_{=0} + |\langle \psi, 1 \rangle_{\Gamma}|^2 \underbrace{\langle S_0 \beta_{\mathrm{eq}}, \beta_{\mathrm{eq}} \rangle_{\Gamma}}_{>0} \ge C \Big(\|\psi_*\|_{H^{-\frac{1}{2}}(\Gamma)}^2 + |\langle \psi, 1 \rangle_{\Gamma}|^2 \Big),$$

which gives coercivity when combined with the triangle inequality

$$\|\psi\|_{H^{-\frac{1}{2}}(\Gamma)} \le \|\psi_*\|_{H^{-\frac{1}{2}}(\Gamma)} + |\langle \psi, 1 \rangle_{\Gamma}| \, \|\beta_{\mathrm{eq}}\|_{H^{-\frac{1}{2}}(\Gamma)} \le C \Big(\|\psi_*\|_{H^{-\frac{1}{2}}(\Gamma)} + |\langle \psi, 1 \rangle_{\Gamma}| \Big).$$

---

[48][Steinbach, Numerical approximation methods for elliptic boundary value problems, Springer 2008]

[49]The value $e^{\int_{\Gamma} \beta_{\mathrm{eq}}(\mathbf{y}) \log |\mathbf{x} - \mathbf{y}| \, \mathrm{d}s(\mathbf{y})}$, which is independent of $\mathbf{x} \in \Gamma$, is called "logarithmic capacity of Γ", while β_{eq} is the "equilibrium density". In 2D electrostatic, the electric charge on an insulated conductor Ω_- distributes on the boundary Γ proportionally to β_{eq}, in such a way that the electrostatic potential $S_0 \beta_{\mathrm{eq}}$ is constant on Γ and takes value $\mathcal{S}_0 \beta_{\mathrm{eq}}$ in Ω_+.

Exercise 6.9: (Laplace single-layer parameter d). Using the BIO expansion in §6.1.3 show that for a circle $\Gamma = \partial B_R$, we have $\beta_* = 0$, $\beta_{eq} = \frac{1}{2\pi R}$, $S_0 \beta_{eq} = \frac{1}{2\pi R} S_0 1 = \frac{1}{2\pi} \log \frac{d}{R}$. Thus $d > R$ is enough to prove the coercivity of S_0 on $H^{-\frac{1}{2}}(\partial B_R)$.

Hint: use that $\int_0^{2\pi} \log \sqrt{2 - 2\cos\alpha}\, d\alpha = 0$ and the properties of the logarithm.

6.2 THE BIE ZOO

We have seen that the single-layer BIE fails for some values of k. We want to derive some other BIEs that allow to compute the solution of the EDP/SSSP also for these values of k. We write a total of six BIEs; their properties are summarised in Table 1.

First of all, it is instructive to recall how we found the BIE (58). We wrote the solution u of the EDP (44) as a single-layer $u = \mathcal{S}\psi$, then we took the Dirichlet trace γ^+ of this representation, and from one of the trace formulas (79) obtained the BIE $S\psi = g_{\mathrm{D}}$ (recall that we need to impose the boundary condition $\gamma^+ u = g_{\mathrm{D}}$). Also for the other BIEs the key steps are the same:

(i) choose a potential representation,

(ii) take a trace using (79).

6.2.1 INDIRECT DOUBLE-LAYER BIE

If instead of a single-layer we assume that the EDP solution is a double-layer potential

$$u = \mathcal{D}\psi, \qquad \psi \in H^{\frac{1}{2}}(\Gamma),$$

taking the Dirichlet trace γ^+ (79) we obtain

$$\boxed{\left(\frac{1}{2} + D\right)\psi = g_{\mathrm{D}}} \quad \text{in } H^{\frac{1}{2}}(\Gamma), \qquad \psi \in H^{\frac{1}{2}}(\Gamma). \tag{91}$$

This is another BIE for the same BVP. Here and in the following, $\frac{1}{2}$ stands for the identity operator multiplied by the number $\frac{1}{2}$, i.e. the equation is to be read $\frac{1}{2}\psi + D\psi = g_{\mathrm{D}}$.

According to [Martin06, §5.9.1], (91) is the first BIE studied for Helmholtz exterior Dirichlet problems by Kupradze in the 1930s.

Equation (91) can be discretised with collocation-BEM or Galerkin-BEM in the same way as §5.2. We encounter a couple of difficulties. A first difference is that the singularity of D is stronger than that of S, so the quadrature requires more care.

A second difference is that this BIE is posed in $H^{\frac{1}{2}}(\Gamma)$ instead of $H^{-\frac{1}{2}}(\Gamma)$. The functions of $H^{\frac{1}{2}}(\Gamma)$ are in general not necessarily continuous, but if they are piecewise-polynomial then they must also be continuous. This implies that the BEM discrete space V_N cannot be made of piecewise-constant functions (recall Exercise 3.6). The simplest choice is to take V_N as the space of **continuous piecewise-linear functions** on a mesh.

Is the BIE (91) well-posed? I.e. is the operator $(\frac{1}{2} + D) : H^{\frac{1}{2}}(\Gamma) \to H^{\frac{1}{2}}(\Gamma)$ invertible? As proved in [CGLS12, Thm. 2.25], this operator is Fredholm. To study the injectivity, once again we have to look at some interior problem.

Exercise 6.10: (Injectivity of $\frac{1}{2} + D$). Show the following.

- If w is a Neumann eigenfunction in Ω_- for $\Lambda = k^2$, then its trace $\psi = \gamma^- w$ satisfies $\frac{1}{2}\psi + D\psi = 0$.

  Hint: use Green's representation.

- If $\Lambda = k^2$ is not a Neumann eigenvalue in Ω_-, then $\frac{1}{2} + D$ is injective.

  Hint: take $u = \mathcal{D}\psi$ for $\psi \in \ker(\frac{1}{2} + D)$. Use the well-posedness of the EDP and both jump relations.

- Deduce that the BIE (91) is injective if and only if k^2 is not a Neumann eigenfunction.

  From this exercise it follows that the BIE (91) is well-posed except for a discrete set of frequencies.

Remark 6.11: (What is ψ?). If ψ is solution of (91), then $u^- = (\mathcal{D}\psi)|_{\Omega_-}$ is Helmholtz solution in Ω_- with Neumann trace $\partial_{\mathbf{n}}^- u^- = \partial_{\mathbf{n}}^+ u$. Differently from §5.6, this is not immediately related to the incoming field u^{Inc}. However, if k^2 is not a Neumann eigenvalue, u^- is well-defined as a solution of an interior Neumann problem. From the jump relation (80), $\psi = [\![\gamma \mathcal{D}\psi]\!] = \gamma^+ u - \gamma^- u^- = g_{\mathrm{D}} - \gamma^- u^-$. The solution of the BIE (91) is the difference between the datum g_{D} and the Dirichlet trace of the solution of an auxiliary interior Neumann problem, whose boundary datum is the Neumann trace of u itself.

6.2.2 Direct BIE

We have constructed two BIEs (58) and (91) by searching for EDP solutions in the form $u = \mathcal{S}\psi$ and $u = \mathcal{D}\psi$, respectively. Green's representation formula (73) allows to represent any radiating solution u in Ω_+ as linear combination of both potentials applied to the traces of u itself:

$$u = -\mathcal{S}\partial_{\mathbf{n}}^+ u + \mathcal{D}\gamma^+ u.$$

When u is solution of the EDP, one of the traces is given: $\gamma^+ u = g_{\mathrm{D}}$. So we can choose as unknown the other one: $\psi = \partial_{\mathbf{n}}^+ u$. How to obtain a BIE from this?

Taking the Dirichlet and the Neumann traces γ^+ and $\partial_{\mathbf{n}}^+$ of Green's representation and using the trace formulas (79), we obtain

$$\boxed{S\psi = \left(D - \frac{1}{2}\right)g_{\mathrm{D}}} \qquad \text{in } H^{\frac{1}{2}}(\Gamma), \tag{92}$$

$$\boxed{\left(\frac{1}{2} + D'\right)\psi = Hg_{\mathrm{D}}} \qquad \text{in } H^{-\frac{1}{2}}(\Gamma). \tag{93}$$

We reiterate that here the unknown stands for the Neumann datum and the underlying representation formula is that coming from Green's formula:

$$\psi = \partial_{\mathbf{n}}^+ u \quad \in H^{-\frac{1}{2}}(\Gamma), \qquad u = -\mathcal{S}\psi + \mathcal{D}g_{\mathrm{D}} \quad \text{in } \Omega_+.$$

Some terminology. BIEs such as (92)–(93) whose unknown is the missing Cauchy datum are called **direct** BIEs; BIEs such as (58) and (91) where the unknown is not directly linked to the EDP are called **indirect**. In general, a linear BIE with BIO T and data f can be written as $\alpha\psi + T\psi = f$: if $\alpha = 0$ then the BIE is called "of the first kind", if α is a non-zero coefficient then it is called "of the second kind". Thus BIEs (58) and (92) are called BIEs of the **first kind**, as the unknown ψ only appears as argument of a BIO, while (91) and (93) are called of the **second kind** as the unknown ψ also appears outside the integral operator ($\alpha = \frac{1}{2}$ in both cases).

The first-kind direct BIE (92) has at the left-hand side the same operator S as the indirect BIE (58) we know well. The right-hand side instead is slightly more complicated, as it involves the double-layer operator. So (92) is well-posed exactly when (58) is, i.e. away from Dirichlet eigenvalues. The matrix $\underline{\underline{\mathbf{A}}}^{\mathrm{Col/Gal}}$ of a BEM implementation for this formulation is identical to the matrix for the same method applied to (58). The right-hand side vector $\mathbf{F}^{\mathrm{Col/Gal}}$ is slightly more complicated to code and more expensive to compute as it requires the implementation of the double-layer operator.

The second-kind direct BIE (93) has at the left-hand side the *adjoint* of the operator present in the indirect BIE (91). Theorem 1.28 of [CK1] implies that $(\frac{1}{2} + D')$ is injective if and only if $(\frac{1}{2} + D)$ is injective (this requires the Fredholm property of the operators). So (93) is well-posed away from Neumann eigenvalues, exactly as (91). The implementation of a BEM discretisation of (93) also requires an approximation of the hypersingular operator H (78) for the right-hand side.

Finally, the evaluation of u_N in the volume through the Green's representation formula is slightly more complicated for the direct BIEs (92)–(93) than for the indirect ones ((58) and (91)), because it involves both the single- and the double-layer potential (applied to the unknown and the datum, respectively).

6.2.3 Indirect combined-field integral equation: Brakhage–Werner equation

We have seen four different BIEs for the same EDP, and none of them is invertible for *all* positive values of k, which is quite disappointing. However all is not lost: the formulations considered were deduced from some special representations of u in terms of layer potentials, we need to choose some other such representation.

We now choose, arbitrarily, to search for some u in the form

$$u = (\mathcal{D} - \mathrm{i}\eta\mathcal{S})\psi, \qquad \psi \in H^{\frac{1}{2}}(\Gamma) \tag{94}$$

where $\eta > 0$ is a parameter. Taking the Dirichlet trace, this is solution of the EDP if ψ is solution of

$$\boxed{\left(\frac{1}{2} + D - \mathrm{i}\eta S\right)\psi = g_{\mathrm{D}}} \quad \text{in } H^{\frac{1}{2}}(\Gamma). \tag{95}$$

The operator $A := (\frac{1}{2} + D - \mathrm{i}\eta S) : H^{\frac{1}{2}}(\Gamma) \to H^{\frac{1}{2}}(\Gamma)$ is Fredholm.[50] Is it injective?

Let $A\psi = 0$ for some $\psi \in H^{\frac{1}{2}}(\Gamma)$. Define u as in (94). Then $u|_{\Omega_+}$ is solution of the EDP with $g_{\mathrm{D}} = 0$, so $u = 0$ in Ω_+ and $\gamma^+ u = \partial_{\mathbf{n}}^+ u = 0$. The jump relations (80) give

$$-\gamma^- u = [\![\gamma u]\!] = [\![\gamma(\mathcal{D}\psi - \mathrm{i}\eta\mathcal{S}\psi)]\!] = [\![\gamma\mathcal{D}\psi]\!] = \psi$$
$$-\partial_{\mathbf{n}}^- u = [\![\partial_{\mathbf{n}} u]\!] = [\![\partial_{\mathbf{n}}(\mathcal{D}\psi - \mathrm{i}\eta\mathcal{S}\psi)]\!] = [\![-\mathrm{i}\eta\partial_{\mathbf{n}}\mathcal{S}\psi]\!] = \mathrm{i}\eta\psi \qquad \Rightarrow \qquad \partial_{\mathbf{n}}^- u - \mathrm{i}\eta\gamma^- u = 0.$$

So $u|_{\Omega_-}$ is solution of a homogeneous impedance BVP (37) in Ω_- with $\vartheta = \frac{\eta}{k}$. From the well-posedness of the impedance BVP (§4.2 and Proposition 4.12) $u = 0$ and from the jump relation again $\psi = -\gamma^- u = 0$. We conclude that the operator A is injective.

> The BIE (95) is well-posed for all Γ, $k > 0$, $\eta > 0$ and $g_{\mathrm{D}} \in H^{\frac{1}{2}}(\Gamma)$.

We have finally found a BIE that is invertible for all wavenumbers! The BIE (95) is often called **Brakhage–Werner equation** (even if it was introduce independently in three papers[51] by Brakhage and Werner, Leis and Panič, all in 1965).

Exercise 6.12: (Brakhage–Werner density). Let ψ be the solution of the Brakhage–Werner BIE (95) and $u = (\mathcal{D} - \mathrm{i}\eta\mathcal{S})\psi$ in $\Omega_+ \cup \Omega_-$. Use the trace formulas (79) to show that $\partial_{\mathbf{n}}^- u - \mathrm{i}\eta\gamma^- u = \partial_{\mathbf{n}}^+ u - \mathrm{i}\eta\gamma^+ u$ (careful with the signs!).

Deduce, using the jump relations, that the solution ψ of the BIE is the jump between the Dirichlet traces of the EDP solution $u|_{\Omega_+}$ and the solution $u|_{\Omega_-}$ of an impedance BVP in Ω_- with data $\partial_{\mathbf{n}}^+ u - \mathrm{i}\eta\gamma^+ u$ and impedance parameter $\vartheta = \frac{\eta}{k}$. (The relation with an impedance BVP further confirms the well-posedness of the BIE.)

6.2.4 Direct combined-field integral equation: Burton–Miller equation

Can we find a *direct* method that is well-posed for all values of k? We know that $\psi = \partial_{\mathbf{n}}^+ u$ solves both direct equations (92)–(93). We take a linear combination of the two equations:

$$\boxed{\left(\frac{1}{2} + D' - \mathrm{i}\eta S\right)\psi = \left[H - \mathrm{i}\eta\left(D - \frac{1}{2}\right)\right]g_{\mathrm{D}}} \quad \text{in } H^{-\frac{1}{2}}(\Gamma). \tag{96}$$

Again, here $\eta > 0$ is a parameter. This is called **Burton–Miller**[52] or (direct) **combined-field** integral equation (CFIE). This is a second-kind direct equation, so, as in §6.2.2, the density and the representation formula are

$$\psi = \partial_{\mathbf{n}}^+ u \quad \in H^{-\frac{1}{2}}(\Gamma) \qquad \text{and} \qquad u = -\mathcal{S}\partial_{\mathbf{n}}^+ u + \mathcal{D}\gamma^+ u = -\mathcal{S}\psi + \mathcal{D}g_{\mathrm{D}} \quad \text{in } \Omega_+.$$

The operator $A' := (\frac{1}{2} + D' - \mathrm{i}\eta S) : H^{-\frac{1}{2}}(\Gamma) \to H^{-\frac{1}{2}}(\Gamma)$ at the left-hand side differs from the operator A of the Brakhage–Werner equation only in that D is substituted by D'.

To study the injectivity of A', let $A'\psi = 0$ and $u = -\mathcal{S}\psi$. Then $\partial_{\mathbf{n}}^- u - \mathrm{i}\eta\gamma^- u = -A'\psi = 0$, so $u = 0$ in Ω_- by the well-posedness of the homogeneous interior impedance BVP. By the jump formula $\gamma^+ u = \gamma^- u$, $u|_{\Omega_+}$ is solution of the homogeneous EDP, so it also vanish, and $\psi = -[\![\partial_{\mathbf{n}}\mathcal{S}\psi]\!] = [\![u]\!] = 0$.

Similarly to the previous section, A' is also Fredholm, thus the BIE (96) is well-posed.

Under some strong regularity and convexity assumptions on the scatterer Ω_-, the operators A and A' are coercive in $L^2(\Gamma)$, [CGLS12, §5.7, Thm. 5.25]: in these cases all Galerkin-BEM discretisations of the formulations (95) and (96) are well-posed and quasi-optimal.

Remark 6.13: (Combined-field integral equation for scattering problems). Imagine that we want to solve a scattering problem (45) with an incoming wave u^{Inc} defined over a neighbourhood of $\overline{\Omega_-}$ (for example a plane wave).

---

[50]We have mentioned in §6.2.1, without proof, that $\frac{1}{2} + D$ is Fredholm. The single-layer operator is continuous as a map $S : H^{\frac{1}{2}}(\Gamma) \to H^1(\Gamma)$ ([CGLS12, Thm. 2.25], recall Remark 5.2 for the circle), thus, by composition with the embedding of Sobolev spaces, it is compact as a map $S : H^{\frac{1}{2}}(\Gamma) \to H^{\frac{1}{2}}(\Gamma)$. Finally, A is a compact perturbation of a Fredholm operator, so it is Fredholm as well.

[51][Brakhage, Werner, Über das Dirichletsche Außenraumproblem für die Helmholtzsche Schwingungsgleichung, 1965]
[Leis, Zur Dirichletschen Randwertaufgabe des Außenraumes der Schwingungsgleichung, 1965]
[Panič, On the solubility of exterior boundary-value problems for the wave equation and for a system of Maxwell eq.s, 1965]

[52][Burton, Miller, The application of integral equation methods to the numerical solution of some exterior boundary-value problems, PRSA 1971]

Green's representation (65)–(68) applied to u^{Scat} in Ω_+ and to u^{Inc} in Ω_- gives

$$\mathcal{D}\gamma^+ u^{\text{Scat}} - \mathcal{S}\partial_{\mathbf{n}}^+ u^{\text{Scat}} = u^{\text{Scat}}, \qquad \mathcal{D}\gamma^+ u^{\text{Inc}} - \mathcal{S}\partial_{\mathbf{n}}^+ u^{\text{Inc}} = \mathcal{D}\gamma^- u^{\text{Inc}} - \mathcal{S}\partial_{\mathbf{n}}^- u^{\text{Inc}} = 0 \qquad \text{in } \Omega_+.$$

Summing these two equalities and using that $\gamma^+ u^{\text{Tot}} = 0$, we have

$$\mathcal{S}(-\partial_{\mathbf{n}}^+ u^{\text{Tot}}) = \mathcal{D}\gamma^+ u^{\text{Tot}} - \mathcal{S}\partial_{\mathbf{n}}^+ u^{\text{Tot}} = u^{\text{Scat}} = u^{\text{Tot}} - u^{\text{Inc}} \qquad \text{in } \Omega_+.$$

(We already knew this from §5.6 in the case where k^2 is not a Dirichlet eigenvalue, now it is clear that this assumption is not needed.) The exterior Dirichlet and Neumann traces of this identity give

$$-S\partial_{\mathbf{n}}^+ u^{\text{Tot}} \overset{(79)}{=} \gamma^+ \mathcal{S}(-\partial_{\mathbf{n}}^+ u^{\text{Tot}}) = \gamma^+ u^{\text{Tot}} - \gamma^+ u^{\text{Inc}} \overset{(45)}{=} -\gamma^+ u^{\text{Inc}},$$

$$\left(\frac{1}{2} - D'\right)\partial_{\mathbf{n}}^+ u^{\text{Tot}} \overset{(79)}{=} \partial_{\mathbf{n}}^+ \mathcal{S}(-\partial_{\mathbf{n}}^+ u^{\text{Tot}}) = \partial_{\mathbf{n}}^+ u^{\text{Tot}} - \partial_{\mathbf{n}}^+ u^{\text{Inc}} \qquad \Rightarrow \qquad \left(\frac{1}{2} + D'\right)\partial_{\mathbf{n}}^+ u^{\text{Tot}} = \partial_{\mathbf{n}}^+ u^{\text{Inc}}.$$

As before, we linearly combine these two identities using a coupling parameter $\eta > 0$:

$$\boxed{\left(\frac{1}{2} + D' - \mathrm{i}\eta S\right)\psi = \partial_{\mathbf{n}}^+ u^{\text{Inc}} - \mathrm{i}\eta\, \gamma^+ u^{\text{Inc}}, \qquad\qquad \psi = \partial_{\mathbf{n}}^+ u^{\text{Tot}}.} \qquad (97)$$

This is a variant of the Burton–Miller formulation (96): since the integral operator to be inverted is the same (A'), the BIE is well-posed for all $k > 0$.

Equation (97) is simpler to implement than (96) because the right-hand side does not need any integral operator. On the other hand, the right-hand side involves *both traces* $\gamma^+ u^{\text{Inc}}$ and $\partial_{\mathbf{n}}^+ u^{\text{Inc}}$ of the incoming field, so this BIE cannot be used if only the Dirichlet trace $g_{\text{D}} = -\gamma^+ u^{\text{Inc}}$ is known.

Another important difference is that the unknown in (97) is $\psi = \partial_{\mathbf{n}}^+ u^{\text{Tot}}$, as opposed to $\partial_{\mathbf{n}}^+ u^{\text{Scat}}$ in (96). Thus the corresponding representation formula is simply $\boxed{u^{\text{Scat}} = -\mathcal{S}\psi}$.

For more on the BIE (97), see [CGLS12, §2.10] and the reference in footnote 30.

A modification of this BIE that is continuous and coercive in $L^2(\Gamma)$ for any bounded star-shaped Lipschitz domain has recently been discovered, see [CGLS12, §2.9].

Remark 6.14: (Choice of the parameter η). How to choose the coupling parameter $\eta > 0$ in (95) and (96)? From the expression of A and A', we can guess that η has the dimension of the inverse of a length: η multiplies the operator S which acts as the inverse of a derivation ($S : H^{-\frac{1}{2}}(\Gamma) \to H^{\frac{1}{2}}(\Gamma)$) and is added to the identity. So plausible choices are $\eta \sim k$ or $\eta \sim \frac{1}{\mathrm{diam}\,(\Gamma)}$. It turns out that $\eta = k$ is also a good choice to reduce the condition number of a BEM discretisation of either (95) or (96) for large values of k.

6.2.5 Further remarks on the BIEs and extensions

In these notes we have been focussing on exterior problems. However, BIEs can be used for BVPs posed on bounded domains such as those in §4.2; see [CGLS12, §2, e.g. table 2.1].

Remark 6.15: (Variational formulations of II kind BIEs). In the first-kind equations (58) and (92) the operator to be inverted is S, which maps $H^{-\frac{1}{2}}(\Gamma)$ (the space where we look for the unknown) to its dual $H^{\frac{1}{2}}(\Gamma)$. So testing the BIEs against elements of the same space is simple: the sesquilinear form $\mathcal{A}_S(\psi, \xi) = \langle S\psi, \xi\rangle_\Gamma$ is well-defined for $\psi, \xi \in H^{-\frac{1}{2}}(\Gamma)$ and involves the extension $\langle \cdot, \cdot\rangle_\Gamma$ of the $L^2(\Gamma)$ scalar product. This is why in the implementation of the Galerkin-BEM matrix $\underline{\underline{\mathbf{A}}}^{\text{Gal}}$ we are allowed to use integrals over Γ (recall that we chose piecewise-polynomial basis functions, which are in $L^2(\Gamma)$).

For the second-kind integral equations we have to be more careful. E.g., in (96), the operator A' maps $H^{-\frac{1}{2}}(\Gamma)$ to itself. So, we cannot write $\langle A'\psi, \xi\rangle_\Gamma$ for $\psi, \xi \in H^{-\frac{1}{2}}(\Gamma)$ because it is not defined, but should use the sesquilinear form $(A'\psi, \xi)_{H^{-\frac{1}{2}}(\Gamma)}$, where $(\cdot, \cdot)_{H^{-\frac{1}{2}}(\Gamma)}$ is the scalar product in $H^{-\frac{1}{2}}(\Gamma)$. Implementing a BEM discretisation of this variational problem is hard, as it requires to evaluate the non-local $H^{-\frac{1}{2}}(\Gamma)$ scalar product.[53]

On the other hand, if the EDP datum g_{D} is at least in $H^1(\Gamma)$, which is the case for smooth incoming waves, then the right-hand side $[H - \mathrm{i}\eta(D - \frac{1}{2})]g_{\text{D}} \in L^2(\Gamma)$ so we can use the variational formulation

$$(A'\psi, \xi)_{L^2(\Gamma)} = \int_\Gamma \left(\frac{1}{2} + D' - \mathrm{i}\eta S\right)\psi\, \overline{\xi}\, \mathrm{d}s = \int_\Gamma \left[H - \mathrm{i}\eta\left(D - \frac{1}{2}\right)\right]g_{\text{D}}\overline{\xi}\, \mathrm{d}s \qquad \forall \xi \in L^2(\Gamma),$$

---

[53]On a circular boundary $\Gamma = \mathbb{S}^1$, this would be easier as the scalar product is computed from the circular harmonics expansion: $\left(\sum_{\ell \in \mathbb{Z}} \hat{v}_\ell \mathrm{e}^{\mathrm{i}\ell\theta}, \sum_{\ell \in \mathbb{Z}} \hat{w}_\ell \mathrm{e}^{\mathrm{i}\ell\theta}\right)_{H^{-\frac{1}{2}}(\mathbb{S}^1)} = 2\pi \sum_{\ell \in \mathbb{Z}} \hat{v}_\ell \overline{\widetilde{w}_\ell}(1 + \ell^2)^{-\frac{1}{2}}$ (recall definition (28)). Still, unless the Fourier coefficients of all the functions involved are already known, this is more complicated than the simple integral appearing in the $\langle \cdot, \cdot\rangle_\Gamma$ duality.

and look for $\psi \in L^2(\Gamma)$. This is well-posed because A' is Fredholm also as a mapping $A' : L^2(\Gamma) \to L^2(\Gamma)$, [CGLS12, Thm. 2.27]. The Galerkin-BEM is then implemented with the same techniques of §5.2.

An alternative would be to use a Petrov–Galerkin approach: take test functions in a space different from the trial space. For example one can seek $\psi \in H^{-\frac{1}{2}}(\Gamma)$ such that $\langle A'\psi, \xi \rangle_\Gamma = \langle [H - i\eta(D - \frac{1}{2})]g_D, \xi \rangle_\Gamma$ for all $\xi \in H^{\frac{1}{2}}(\Gamma)$. The Galerkin-BEM discretisation of this problem can use piecewise-constant trial functions ψ_N and continuous piecewise-linear test functions ξ_N. The two discrete spaces have to be defined on different compatible "dual" meshes.

All this applies also to the second-kind direct BIE (93).

On the other hand, the indirect BIEs (91) and (95) are posed in $H^{\frac{1}{2}}(\Gamma)$, so we can use the $L^2(\Gamma)$ scalar product to write the variational form ($\int_\Gamma A\psi \, \overline{\xi} \, ds = \int_\Gamma g_D \overline{\xi} \, ds$ for all $\xi \in H^{\frac{1}{2}}(\Gamma)$ for (95)) but we need to use discrete functions that are continuous on Γ, e.g. piecewise-linear polynomials.

Remark 6.16: (Advantages of direct formulations). The BEM approximation of Burton–Miller equation (96) is slightly more complicated and expensive than Brakhage–Werner (95), as the right-hand side involves two BIOs. Similarly, the direct equations (92)&(93) require a more complicated right-hand side and representation formula than (58)&(91). What is the advantage of a direct formulation against an indirect one?

In a direct formulation, if we have some information on the properties of the EDP solution u we can include it in the design of the approximating space V_N to improve its accuracy and efficiency. For instance, in some situations, PDE theory and high-frequency asymptotics (recall the GTD mentioned in Remark 5.38) permit to estimate the location and the strength of the singularities of $\psi = \partial_\mathbf{n}^+ u^{\mathrm{Scat}}$, its oscillations, the different behaviour in the shadow and the illuminated parts of Γ; see, e.g., Figure 24[54]. This knowledge allows to construct discrete spaces V_N that ensure high accuracy with small numbers of DOFs. This is the basic idea underlying the "hybrid numerical-asymptotic" (HNA) methods that are the main concern of [CGLS12].

In an indirect method, the BIE solution ψ depends also on the trace of some interior problem (see Rem 6.11 and Ex. 6.12), so its efficient approximation would require also the knowledge of the corresponding eigenfunction, which is not directly related to the physical scattering problem and might contain expensive-to-approximate "unphysical" singularities.

Moreover, often the quantity of interest is not u^{Scat} or u^{Tot} in Ω_+, but something dependent on $\partial_\mathbf{n}^+ u^{\mathrm{Scat}}$, such as the far-field pattern u_∞ (46). This is easily and accurately computed with a direct method or with (58), but not with (91) and (95).

	BIE	representation formula	density $\psi =$	unknown ψ in	direct/ indirect	kind	fails for
(58)	$S\psi = g_D$	$u = \mathcal{S}\psi$	$-\partial_\mathbf{n}^+ u^{\mathrm{Tot}}$	$H^{-\frac{1}{2}}(\Gamma)$	indirect	I	Dir. eig.
(91)	$(\frac{1}{2} + D)\psi = g_D$	$u = \mathcal{D}\psi$	Rem.6.11	$H^{\frac{1}{2}}(\Gamma)$	indirect	II	Neum. eig.
(92)	$S\psi = (D - \frac{1}{2})g_D$	$u = \mathcal{D}g_D - \mathcal{S}\psi$	$\partial_\mathbf{n}^+ u$	$H^{-\frac{1}{2}}(\Gamma)$	direct	I	Dir. eig.
(93)	$(\frac{1}{2} + D')\psi = Hg_D$	$u = \mathcal{D}g_D - \mathcal{S}\psi$	$\partial_\mathbf{n}^+ u$	$H^{-\frac{1}{2}}(\Gamma)$	direct	II	Neum. eig.
(95)	$(\frac{1}{2} + D - i\eta S)\psi = g_D$	$u = (\mathcal{D} - i\eta\mathcal{S})\psi$	Ex. 6.12	$H^{\frac{1}{2}}(\Gamma)$	indirect	II	never!
(96)	$(\frac{1}{2} + D' - i\eta S)\psi$ $= [H - i\eta(D - \frac{1}{2})]g_D$	$u = \mathcal{D}g_D - \mathcal{S}\psi$	$\partial_\mathbf{n}^+ u$	$H^{-\frac{1}{2}}(\Gamma)$	direct	II	never!
(97)	$(\frac{1}{2} + D' - i\eta S)\psi$ $= \partial_\mathbf{n}^+ u^{\mathrm{Inc}} - i\eta\gamma^+ u^{\mathrm{Inc}}$	$u^{\mathrm{Scat}} = -\mathcal{S}\psi$	$\partial_\mathbf{n}^+ u^{\mathrm{Tot}}$	$H^{-\frac{1}{2}}(\Gamma)$	direct	II	never!

Table 1: Six (+1) BIEs for the EDP (44).
They are described in [CK1]: (58) (3.44), (91) (3.26), (92) (3.83), (93) (3.81), (95) (3.51), (96) (3.84).
The BIE (97) can be used only for the SSSP (45) as it requires both traces of u^{Inc}.

Remark 6.17: (BIO diagonalisation on the circle and BIE stability). Let $\Gamma = \mathbb{S}^1$, the unit circle. Then, all the integral operators we have encountered diagonalise in the circular harmonic basis. This means that $\mathrm{e}^{i\ell\theta}$ is eigenfunction of S, K, K' and H for all $\ell \in \mathbb{Z}$. In particular the operators take the values

$$S\mathrm{e}^{i\ell\theta} = \frac{i\pi}{2} J_\ell(k) H_\ell^{(1)}(k) \mathrm{e}^{i\ell\theta},$$

$$D\mathrm{e}^{i\ell\theta} = D'\mathrm{e}^{i\ell\theta} = \left(\frac{i\pi k}{2} J_\ell(k) H_\ell^{(1)\prime}(k) + \frac{1}{2}\right)\mathrm{e}^{i\ell\theta} = \left(\frac{i\pi k}{2} J_\ell(k)' H_\ell^{(1)}(k) - \frac{1}{2}\right)\mathrm{e}^{i\ell\theta}, \qquad \ell \in \mathbb{Z}, k > 0$$

---

[54]Figure 24 shows the density ψ for the indirect BIE (58). However we have seen in §5.6 that the solution of this BIE has the physical interpretation $\psi = -\partial_\mathbf{n}^+ u^{\mathrm{Tot}}$, while this is not true for the solutions of the other indirect BIEs (91) and (95).

$$He^{i\ell\theta} = \frac{i\pi k^2}{2} J'_\ell(k) H^{(1)}_\ell{}'(k) e^{i\ell\theta}.$$

This implies that the (spectral) Galerkin-BEM matrix with basis $\{e^{i\ell\theta}\}_{\ell=-L,\dots,L}$, for any BIE on the unit circle, gives a diagonal matrix.

This offers a very simple way to study the spurious resonances of the BIEs. We denote $\lambda_{T,\ell}$ the eigenvalue of an operator T associated to $e^{i\ell\theta}$, i.e. $Te^{i\ell\theta} = \lambda_{T,\ell}e^{i\ell\theta}$. In Figure 29 we plot the values $\|(\underline{\underline{\mathbf{A}}}^{\mathrm{Gal}})^{-1}\| = \inf_{\ell\in\{-L,\dots,L\}} |\lambda_{T,\ell}|^{-1}$ for $L = 30$ as a function of the wavenumber k. Large values of this norm signal that the linear system is close to singular, and that the corresponding BIE is not invertible for nearby values of k. We observe these instabilities near the (square roots of the) Dirichlet eigenvalues for the operator $T = S$ (corresponding to the BIEs (58) and (92)) and near the Neumann eigenvalues for the operator $T = \frac{1}{2} + D$ (corresponding to the BIEs (91) and (93), since 'taking the adjoint' does not change the operator norm). On the other hand, the operator $T = A = \frac{1}{2} + D - ikS$ of the BIEs (95) and (96) is bounded uniformly. (Here we have chosen $\eta = k$ in accordance to Remark 6.14, while choosing $\eta = \max\{k,1\}$ would stabilise the operator also for $k \to 0$, which is a Neumann eigenvalue.)
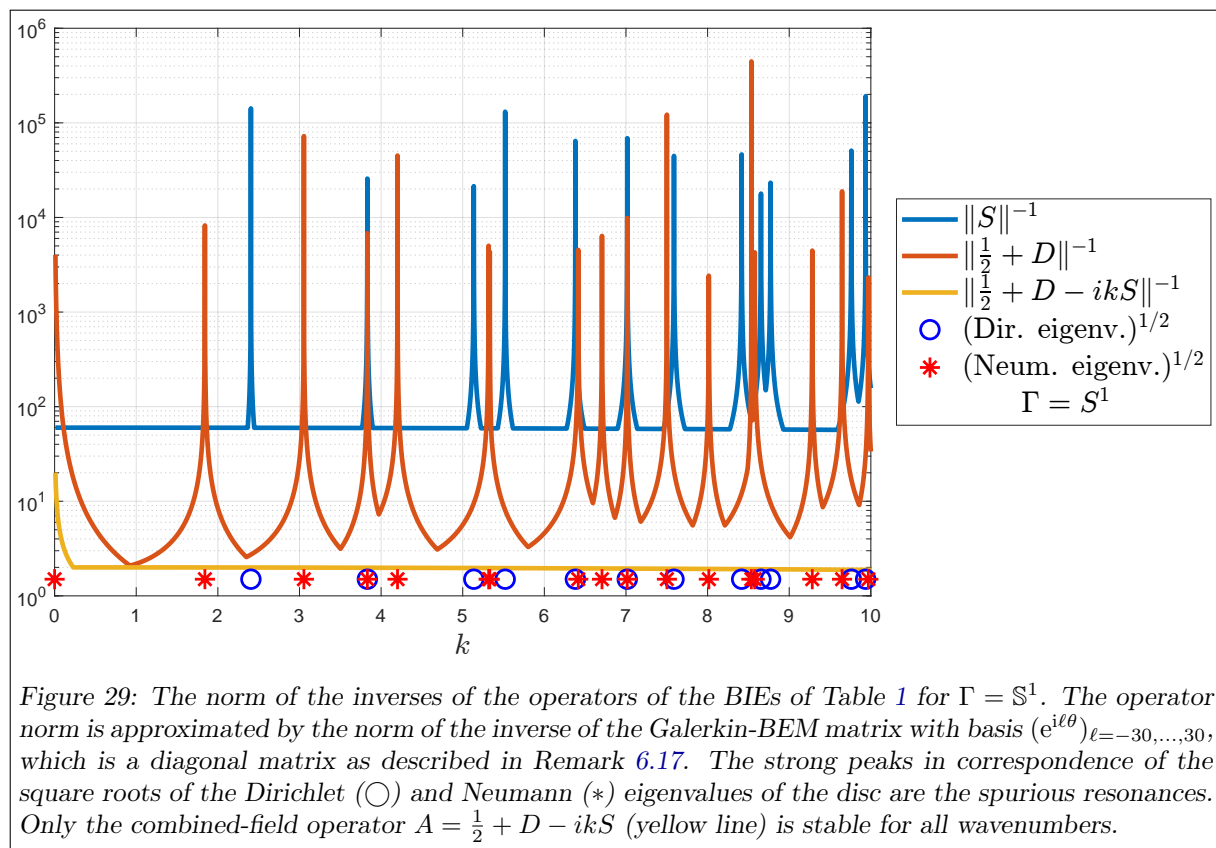
Figure 29: *The norm of the inverses of the operators of the BIEs of Table 1 for $\Gamma = \mathbb{S}^1$. The operator norm is approximated by the norm of the inverse of the Galerkin-BEM matrix with basis $(e^{i\ell\theta})_{\ell=-30,\dots,30}$, which is a diagonal matrix as described in Remark 6.17. The strong peaks in correspondence of the square roots of the Dirichlet $(\bigcirc)$ and Neumann $(*)$ eigenvalues of the disc are the spurious resonances. Only the combined-field operator $A = \frac{1}{2} + D - ikS$ (yellow line) is stable for all wavenumbers.*

Remark 6.18: (The CHIEF method). A different way to deal with spurious resonances and ensure the solvability of the BEM linear system even when k^2 is a Dirichlet eigenvalue of Ω_- is the Combined Helmholtz Integral Equation Formulation (CHIEF) proposed in 1968[55]. We know from (83) that $(S\psi)|_{\Omega_-} = -u^{\mathrm{Inc}}|_{\Omega_-}$, where ψ is the solution of the single-layer BIE (58). The CHIEF augments the BEM linear system $\underline{\underline{\mathbf{A}}}\psi = \mathbf{F}$ with a few more equations $(\mathcal{S}\psi_N)(\mathbf{z}_j) = -u^{\mathrm{Inc}}(\mathbf{z}_j)$ for some points $\mathbf{z}_j \in \Omega_-$, $j = 1,\dots,M$. This gives an overdetermined linear system that can be solved in the least-squares sense. At least some of the points $\mathbf{z}_j$ need to be away from the nodal lines of the eigenfunction corresponding to k^2, which of course is not known, so their choice is delicate (in particular for large frequencies).

Remark 6.19: (Exterior Neumann problem). So far we have only considered exterior Dirichlet problems. All techniques and results can be extended to the **exterior Neumann problem**: find $u \in H^1_{\mathrm{loc}}(\Omega_+)$ such that

$$\Delta u + k^2 u = 0 \quad \text{in } \Omega_+, \qquad \partial^+_{\mathbf{n}} u = g_{\mathrm{N}} \quad \text{on } \Gamma, \qquad u \text{ radiating}, \tag{98}$$

---

[55][Schenck, Improved integral formulation for acoustic radiation problems, JASA 1968]

where $g_{\mathrm{N}} \in H^{-\frac{1}{2}}(\Gamma)$ is a boundary datum. The corresponding **sound-hard scattering problem** is

$$\Delta u^{\mathrm{Scat}} + k^2 u^{\mathrm{Scat}} = 0 \quad \text{in } \Omega_+, \qquad \partial_{\mathbf{n}}^+(u^{\mathrm{Scat}} + u^{\mathrm{Inc}}) = 0 \quad \text{on } \Gamma, \qquad u^{\mathrm{Scat}} \text{ radiating,}$$

which is a special case of (98) for $g_{\mathrm{N}} = -\partial_{\mathbf{n}}^+ u^{\mathrm{Inc}}$. The tools needed to construct BIEs for this problem are the same already introduced: the four BIOs (S, D, D', H), the two layer potentials $(\mathcal{S}, \mathcal{D})$ and their relations. We can construct six BIEs, proceeding precisely as we have done for the Dirichlet case in the previous sections: see the summary in Table 2. Coding a BEM for the exterior Neumann problem is slightly harder than for the EDP (44) because there is no BIE involving only the single-layer operator S and many of the BIEs listed require the hypersingular operator H. See also [Sayas06, §11].

Exercise 6.20: (BIEs for the exterior Neumann problem). Derive the six BIEs in Table 2 for the exterior Neumann problem (98). Start from the representation formulas and use the trace relations (79).

[CK1] eq.#	BIE	representation formula	density $\psi =$	direct/ indirect	kind	fails for
(3.29)	$(-\frac{1}{2} + D')\psi = g_{\mathrm{N}}$	$u = \mathcal{S}\psi$		indirect	II	Dir. eig.
(3.47)	$H\psi = g_{\mathrm{N}}$	$u = \mathcal{D}\psi$	$\gamma^+ u^{\mathrm{Tot}}$	indirect	I	Neum. eig.
(3.82)	$(-\frac{1}{2} + D)\psi = Sg_{\mathrm{N}}$	$u = \mathcal{D}\psi - \mathcal{S}g_{\mathrm{N}}$	$\gamma^+ u$	direct	II	Dir. eig.
(3.85)	$H\psi = (\frac{1}{2} + D')g_{\mathrm{N}}$	$u = \mathcal{D}\psi - \mathcal{S}g_{\mathrm{N}}$	$\gamma^+ u$	direct	I	Neum. eig.
(3.53)	$(-\frac{1}{2} + D' + \mathrm{i}\eta H)\psi = g_{\mathrm{N}}$	$u = (\mathcal{S} + \mathrm{i}\eta\mathcal{D})\psi$		indirect	II	never
(3.86)	$(-\frac{1}{2} + D + \mathrm{i}\eta H)\psi$ $= (S + \mathrm{i}\eta(\frac{1}{2} + D'))g_{\mathrm{N}}$	$u = \mathcal{D}\psi - \mathcal{S}g_{\mathrm{N}}$	$\gamma^+ u$	direct	II	never

Table 2: Six BIEs for the exterior Neumann problem (98). *The first column indicates the equation number in [CK1]. Note the symmetry with the Dirichlet case in Table 1.*

Exercise 6.21: (BIO diagonalisation on the circle). (i) Read carefully Remark 6.17 and reproduce Figure 29. (ii) Repeat the same for the exterior Neumann problem described in Remark 6.19.

Exercise 6.22: (Exterior impedance problem). Consider the exterior impedance problem

$$\Delta u + k^2 u = 0 \quad \text{in } \Omega_+, \qquad \partial_{\mathbf{n}}^+ u + \mathrm{i}k\vartheta\,\gamma^+ u = g_I \quad \text{on } \Gamma, \qquad u \text{ radiating,} \qquad (99)$$

for $g_I \in H^{-\frac{1}{2}}(\Gamma)$ and $\vartheta \in L^\infty(\Gamma)$, $\operatorname{ess\,inf} \vartheta > 0$. (For the interior impedance BVP (37) on Ω_- we used the condition with opposite sign $\partial_{\mathbf{n}}^- u - \mathrm{i}k\vartheta\gamma^- u = g_I$: the two choices are consistent because $\mathbf{n}$, entering the definition of $\partial_{\mathbf{n}}^\pm$, points in Ω_+ and out of Ω_-.)

- Using Lemma 5.20, prove that (99) admits at most one solution.

- Show that $u = \mathcal{S}\psi$, for $\psi \in H^{-\frac{1}{2}}(\Gamma)$ solution of the BIE $(\frac{1}{2} - D' - \mathrm{i}k\vartheta S)\psi = -g_I$, is solution of (99). Show that the operator of this BIE is injective if and only if k^2 is not a Dirichlet eigenvalue in Ω_-.

- Show that $u = (\mathcal{S} + \mathrm{i}\eta\mathcal{D})\psi$ solves (99) if ψ is solution of the combined-field BIE

$$\left(\frac{1 + k\vartheta\eta}{2} - \mathrm{i}\vartheta k S + \eta\vartheta k D - D' - \mathrm{i}\eta H\right)\psi = -g_I.$$

Finally, show that the operator of this BIE is injective for all $k > 0$ and $\eta > 0$.

For help and more details, see [CK1, §3.7].

6.3 Error analysis of the Galerkin method applied to Gårding-type problems

6.3.1 Abstract variational framework

We recall the general variational problem (32) and its Galerkin approximation (33):

$$\text{find} \quad u \in H \qquad \text{such that} \quad \mathcal{A}(u, w) = \mathcal{F}(w) \qquad \forall w \in H, \qquad (100)$$

$$\text{find} \quad u_N \in V_N \qquad \text{such that} \quad \mathcal{A}(u_N, w_N) = \mathcal{F}(w_N) \qquad \forall w_N \in V_N, \qquad (101)$$

where H is a Hilbert space, $V_N \subset H$ is a finite-dimensional subspace, $\mathcal{A}(\cdot,\cdot)$ and $\mathcal{F}(\cdot)$ are a sesquilinear and a continuous antilinear functional on H.

If $\mathcal{A}(\cdot,\cdot)$ is continuous and coercive in H, the stability and error analysis of the Galerkin method is simple, thanks to Lax–Milgram theorem and Céa lemma. Unfortunately, the variational problems studied in this course fall outside of this framework. The key result to extend Céa lemma to problems satisfying a Gårding inequality is the following theorem. This is a modification of the classical "Aubin–Nitsche duality trick" used also in finite element analysis; in the context of Helmholtz problems it is often called "Schatz argument"[56]. Here we closely follow [Spence14, Thm. 5.21].

Theorem 6.23: (Galerkin method for Gårding inequality). Let $H \subset V$ be Hilbert spaces and the inclusion be compact. Let $\mathcal{A}(\cdot,\cdot)$ be a continuous sesquilinear form on H that satisfies the Gårding inequality (34):

$$|\mathcal{A}(v,w)| \leq C_{\mathcal{A}} \|v\|_H \|w\|_H, \qquad \Re\{\mathcal{A}(v,v)\} \geq \alpha \|v\|_H^2 - C_V \|v\|_V^2, \qquad \forall v,w \in H \qquad (\alpha, C_V, C_{\mathcal{A}} > 0).$$

Assume that the only $u_0 \in H$ such that $\mathcal{A}(u_0,v) = 0$ for all $v \in H$ is $u_0 = 0$ (so that the variational problem (100) is well-posed for any right-hand side). Let $\mathcal{F}(\cdot)$ be a continuous linear functional on H and u be the solution of the variational problem (100).
Given $f \in V$, let $z_f \in H$ be the solution of the **adjoint problem**

$$\mathcal{A}(v, z_f) = (v, f)_V \qquad \forall v \in H, \tag{102}$$

where $(\cdot,\cdot)_V$ is the scalar product in V. Let V_N be a finite-dimensional subspace of H and define

$$\eta(V_N) := \sup_{f \in V, f \neq 0} \min_{v_N \in V_N} \frac{\|z_f - v_N\|_H}{\|f\|_V}. \tag{103}$$

If $\eta(V_N)$ satisfies the **threshold condition**

$$\eta(V_N) \leq \frac{1}{C_{\mathcal{A}}} \sqrt{\frac{\alpha}{2C_V}}, \tag{104}$$

then the Galerkin method (101) is **well-posed** and its solution u_N satisfies the **quasi-optimality** bound

$$\|u - u_N\|_H \leq \frac{2C_{\mathcal{A}}}{\alpha} \min_{v_N \in V_N} \|u - v_N\|_H. \tag{105}$$

The statement of this theorem is not simple and requires some explanation. Our goal is to prove that the Galerkin method is well-posed and the quasi-optimality bound (105) holds. This ensures that the Galerkin error $\|u - u_N\|_H$ is controlled by the best-approximation error, i.e. by the best error achievable if we knew the exact solution u and we tried to approximate it with the discrete space V_N. Quasi-optimality holds for all finite-dimensional subspaces $V_N \subset H$ when we are in a Lax–Milgram setting, i.e. when $\mathcal{A}(\cdot,\cdot)$ is coercive. The bad news is that this is not true for all V_N if $\mathcal{A}(\cdot,\cdot)$ only satisfies a Gårding inequality. The good news is that well-posedness and quasi-optimality hold if V_N "has sufficiently good approximation properties". How do we measure the approximation properties of a discrete space? The "adjoint approximability parameter" $\eta(V_N)$ in (103) precisely quantifies how well V_N approximates the solution of the "adjoint problem" (102), whose datum f is an arbitrary element of the larger space V. The smaller $\eta(V_N)$, the better the approximation offered by V_N. If the "threshold condition" (104) holds, i.e. $\eta(V_N)$ is smaller than a certain quantity that depends on $\mathcal{A}(\cdot,\cdot)$, then we have what we want: the well-posedness of the Galerkin method and its quasi-optimality.[57]

In brief, Theorem 6.23 states, in a precise quantitative way, the following:

> if the discrete space is sufficiently fine, then the Galerkin method (applied to a well-posed Gårding-type problem) is well-posed and quasi-optimal.

If we have a dense sequence of discrete spaces $(V_N)_{N \in \mathbb{N}}$ (i.e. such that $\lim_{N \to \infty} \inf_{v_N \in V_N} \|v - v_N\|_H = 0$ for all $v \in H$) then the theorem states that the Galerkin method eventually converges. Typically, for

---

[56][Schatz, *An observation concerning Ritz-Galerkin methods with indefinite bilinear forms*, Math. Comput. 1974]

[57]A (surprising) theorem by Gohberg and Fel'dman (1971) states that, given a continuous linear operator $A : H \to H$, this is sum of a coercive and a compact operator if and only if the Galerkin method for $(Au, v)_H = (f, v)_H$ converges for all sequences $(H_N)_{N \in \mathbb{N}}$ of nested finite-dimensional subspaces such that $\lim_{N \to \infty} \inf_{u_N \in H_N} \|u - u_N\|_H = 0$ for all $u \in H$. In words: the Galerkin method converges for all dense subspace sequences iff the problem is a compact perturbation of a coercive problem. In this section we are studying the implication "compactly-perturbed problem⇒Galerkin convergence", the converse means that we cannot expect this to hold in a much more general setting.

constant-degree piecewise-polynomial FEM or BEM, this means that the method is guaranteed to be well-posed and quasi-optimal if the mesh employed is sufficiently fine. In the next sections we analyse a couple of examples coming from discretisations of the Helmholtz equation.

The phenomenon described by Theorem 6.23 is often observed numerically. When we approximate a Laplace-type problem with a sequence of meshes we observe a reduction of the error starting from the first mesh refinements. For a Helmholtz-type problem, mesh refinement does not give any improvement in the solution until some threshold h_0 on the mesh size h is reached; for $h < h_0$ we observe convergence of the error to zero.

Proof of Theorem 6.23. We follow [Spence14, Thm. 5.21].[58]

We first assume that the Galerkin method (101) admits a solution u_N. We recall the Galerkin orthogonality $\mathcal{A}(u - u_N, v_N) = 0$ which holds for all $v_N \in V_N$. In the following bound we use the adjoint problem (102) with source term $f = u - u_N$ and denote by $w_N \in V_N$ the element minimising the ratio in the definition (103) of the approximability parameter $\eta(V_N)$. We first control the (weaker) V norm of the Galerkin error, exploiting the adjoint problem:

$$
\begin{aligned}
\|u - u_N\|_V^2 &= \mathcal{A}(u - u_N, z_{u-u_N}) &&\text{adjoint problem (102)} \\
&= \mathcal{A}(u - u_N, z_{u-u_N} - w_N) &&\text{Galerkin orthogonality} \\
&\leq C_{\mathcal{A}} \|u - u_N\|_H \|z_{u-u_N} - w_N\|_H &&\text{continuity of } \mathcal{A}(\cdot, \cdot) \\
&\leq C_{\mathcal{A}}\eta(V_N) \|u - u_N\|_H \|u - u_N\|_V &&\text{definition of } \eta(V_N) \text{ (103)} \\
&\leq \sqrt{\frac{\alpha}{2C_V}} \|u - u_N\|_H \|u - u_N\|_V &&\text{threshold condition (104).}
\end{aligned}
$$

Then also the (stronger) H norm of the error can be controlled:

$$
\begin{aligned}
\alpha \|u - u_N\|_H^2 &\leq \Re\{\mathcal{A}(u - u_N, u - u_N)\} + C_V \|u - u_N\|_V^2 &&\text{Gårding inequality (34)} \\
&= \Re\{\mathcal{A}(u - u_N, u - v_N)\} + C_V \|u - u_N\|_V^2 &&\text{Galerkin orthogonality, } \forall v_N \in V_N \\
&\leq C_{\mathcal{A}} \|u - u_N\|_H \|u - v_N\|_H + C_V \|u - u_N\|_V^2 &&\text{continuity of } \mathcal{A}(\cdot, \cdot) \\
&\leq C_{\mathcal{A}} \|u - u_N\|_H \|u - v_N\|_H + \frac{\alpha}{2} \|u - u_N\|_H^2
\end{aligned}
$$

where in the last step we used the previous bound (after simplifying a term and squaring). Moving the last term to the left-hand side of the equation, and simplifying $\|u - u_N\|_H$, we obtain the desired quasi-optimality bound (105).

Taking $v_N = 0$ in (105) and using the triangle inequality, we have the stability estimate $\|u_N\|_H \leq (1 + \frac{2C_{\mathcal{A}}}{\alpha}) \|u\|_H$. By the injectivity assumption stipulated in the theorem, if $\mathcal{F} = 0$ then $u = 0$ and, by this stability bound, also $u_N = 0$. This means that the solution of the Galerkin method (101) is at most unique. Since the method is equivalent to a square $N \times N$ linear system, uniqueness implies well-posedness. We conclude that u_N exists, so the assumption made at the beginning of the proof is justified. □

Remark 6.24: (Galerkin method for compactly perturbed problem). A related error analysis of the Galerkin approximation of variational problems whose sesquilinear form is sum of a coercive and a compact one is presented in [SBH19, §8.9]. This theory is simpler, does not use the adjoint problem, and it is slightly more general: it does not require the Gårding inequality but only the Fredholm property. On the other hand, the threshold condition (104) and the quasi-optimality bound (105) obtained this way are not explicit.

Exercise 6.25: (Parameter tuning). Show that if we assume $\eta(V_N) \leq \frac{1}{C_{\mathcal{A}}} \sqrt{\frac{\alpha}{bC_V}}$ for some $b > 1$ instead of (104), then the quasi-optimality constant $\frac{2C_{\mathcal{A}}}{\alpha}$ in (105) can be substituted by $\frac{b}{b-1} \frac{C_{\mathcal{A}}}{\alpha}$.

This means that, with this proof, we can win at most a factor $\sqrt{2}$ in the threshold on $\eta(V_N)$ (i.e. allow a slightly coarser discrete space), paying with a poorer quasi-optimality constant. Conversely (choosing $b > 2$) one can reduce by a factor at most 2 the quasi-optimality constant, paying with a more restrictive threshold condition. In brief: in Theorem 6.23 we arbitrarily chose the factor 2 that appears in (104) and (105), but other choices do not give substantial improvements.

In the next two sections we sketch how to apply Theorem 6.23 to two exemplary problems: the FEM for the interior Helmholtz problem, and the BEM for the exterior Dirichlet problem.[59] Once we have the

---

[58]This proof should remind you the derivation of error estimates on the L^2 norm of the error of classical finite elements for elliptic problems.

[59]In the BEM case, we only consider the single-layer BIE (58), see [CGLS12, §6.1–3] for a survey of the corresponding results for the CFIE operators of §6.2.3–6.2.4. In this case the injectivity assumption is satisfied for all $k > 0$. Studying the k-dependence of $C_{\mathcal{A}}/\alpha$ and η for different geometries, meshes and polynomial degrees is an active area of research.

quasi-optimality, to obtain error bounds with convergence rates we need to know the regularity of the variational problem solution: we do this for the BEM in §6.3.4. We use several results from the theory of Sobolev spaces, PDEs, BIOs and FEMs, without justifying their use in full details.

6.3.2   FEM error analysis for interior problems

To better understand Theorem 6.23 we apply it to the simplest problem we know in this setting: the variational formulation (36) of the interior Helmholtz Dirichlet problem (35). Here $\Omega \subset \mathbb{R}^2$ is a bounded Lipschitz domain,

$$H = H_0^1(\Omega), \qquad V = L^2(\Omega), \qquad \mathcal{A}(u, w) = \int_\Omega (\nabla u \nabla \overline{w} - k^2 u \overline{w}) \, d\mathbf{x}.$$

It is convenient to use a dimensionally-homogeneous version of the $H^1(\Omega)$ norm, weighted with the wavenumber k:

$$\|v\|_{H_k^1(\Omega)}^2 := |v|_{H^1(\Omega)}^2 + k^2 \|v\|_{L^2(\Omega)}^2 .$$

With this norm, the constants in the Gårding inequality and in the continuity of $\mathcal{A}(\cdot, \cdot)$ are

$$\alpha = 1, \qquad C_V = 2k^2, \qquad C_\mathcal{A} = 1.$$

For each $f \in L^2(\Omega)$, the adjoint problem (102) consists in finding $z_f \in H_0^1(\Omega)$ such that

$$\int_\Omega (\nabla v \nabla \overline{z_f} - k^2 v \overline{z_f}) \, d\mathbf{x} = \int_\Omega v \overline{f} \, d\mathbf{x} \qquad \forall v \in H_0^1(\Omega),$$

where at the right-hand side we simply have the $V = L^2(\Omega)$ scalar product. Taking the complex conjugate, this is again (36), the variational formulation of the interior Helmholtz Dirichlet problem:

$$\Delta z_f + k^2 z_f = -f \quad \text{in } \Omega, \qquad \gamma u = 0 \quad \text{on } \partial \Omega.$$

This is because the Helmholtz Dirichlet problem is self-adjoint: it coincides with its adjoint. We assume that k^2 is not a Dirichlet eigenvalue in Ω: this corresponds to the assumption made in the theorem that the homogeneous problems admits only the trivial solution. Well-posedness comes with stability, also for the adjoint problem: $\|z_f\|_{H_k^1(\Omega)} \leq C_{\text{stab}} \|f\|_{L^2(\Omega)}$, for some $C_{\text{stab}} > 0$ depending on k and Ω but independent of f (and which may be difficult to estimate).

Since $z_f \in H_0^1(\Omega)$ and $\Delta z_f = -f - k^2 z_f \in L^2(\Omega)$, by elliptic regularity [Ihlenburg98, Prop. 2.24], if Ω is a smooth or convex domain then $z_f \in H^2(\Omega)$ and $\|z_f\|_{H^2(\Omega)} \leq C_{H^2} \|f + k^2 z_f\|_{L^2(\Omega)} \leq C_{H^2}(1 + kC_{\text{stab}}) \|f\|_{L^2(\Omega)}$ for some $C_{H^2} > 0$ depending on Ω. Assume V_N is the space of piecewise-linear finite elements on a quasi-uniform, shape-regular triangulation of Ω with mesh size h. Classical finite-element approximation estimates (Bramble–Hilbert lemma, e.g. as in [Ihlenburg98, eq. (4.1.10)]) state that $\inf_{v_N \in V_N} \|v - v_N\|_{H_k^1(\Omega)} \leq C_{BH} h \|v\|_{H^2(\Omega)}$ for all $v \in H^2(\Omega)$ and for some C_{BH} that depends on Ω, k and the "chunkiness" of the mesh elements[60]. Collecting all these bounds:

$$\inf_{v_N \in V_N} \|z_f - v_N\|_{H_k^1(\Omega)} \leq C_{BH} h \|z_f\|_{H^2(\Omega)} \leq h C_{BH} C_{H^2}(1 + kC_{\text{stab}}) \|f\|_{L^2(\Omega)} \qquad \forall f \in L^2(\Omega).$$

We have obtained a bound on the adjoint approximability parameter defined in (103):

$$\eta(V_N) \leq h C_{BH} C_{H^2}(1 + kC_{\text{stab}}).$$

Then the threshold condition (104) is satisfied if $h \leq h_\star$, where

$$h_\star := \frac{1}{C_\mathcal{A} C_{BH} C_{H^2}(1 + kC_{\text{stab}})} \sqrt{\frac{\alpha}{2C_V}} \leq \frac{1}{2k \, C_{BH} C_{H^2}(1 + kC_{\text{stab}})}. \tag{106}$$

If the finite element mesh size h is smaller than this value, then the method is well-posed and the quasi-optimality bound (105) holds:

$$\|u - u_N\|_{H_k^1(\Omega)} \leq 2 \min_{v_N \in V_N} \|u - v_N\|_{H_k^1(\Omega)} .$$

This gives a recipe to choose a suitable mesh and predict what is the computational effort required for the FEM to approximate the solution u of the Dirichlet problem (35) to a desired accuracy. The piecewise-linear FEM eventually converges in $H^1(\Omega)$ norm with the same linear convergence rate as for coercive problems, but the onset of the convergence depends on k (see Remark 6.27 and Figure 30).

---

[60]More precisely, $\inf_{v_N \in V_N} \|v - v_N\|_{H_k^1(\Omega)} \leq C'_{BH}(h + h^2 k) |v|_{H^2(\Omega)}$ for C'_{BH} independent of k.

Exercise 6.26: (Galerkin method for the impedance problem). Repeat the argument of this section for the FEM applied to the interior impedance problem (38). Which of the assumptions in Theorem 6.23 comes for free?
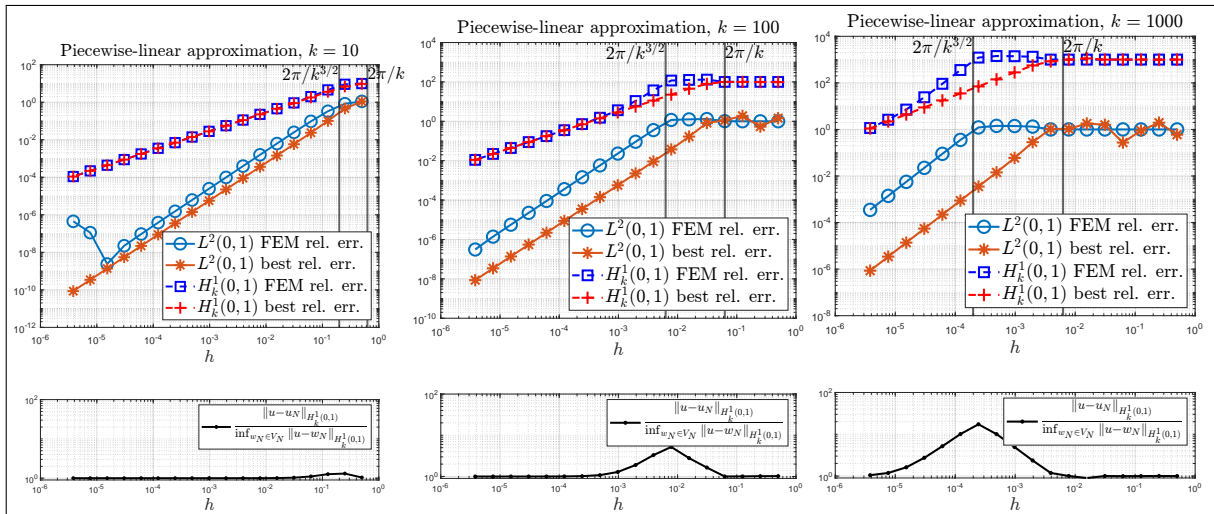
Figure 30: Error analysis of the finite element approximation of an interior impedance Helmholtz BVP. We consider the simple 1D problem $u'' + k^2 u = 0$, $u'(0) + iku(0) = 2ik$, $u'(1) - iku(1) = 0$ on the interval $\Omega = (0,1)$ for $k = 10, 100, 1000$. We approximate $u(x) = e^{ikx}$ with piecewise-linear finite elements on uniform meshes with element size h and $N = 1 + 1/h$ DOFs.

In blue we see the Galerkin relative error $\frac{\|u-u_N\|_\bullet}{\|u\|_\bullet}$ in $L^2(0,1)$ ($\bigcirc$ markers) and $H^1_k(0,1)$ ($\square$ markers) norms plotted against $h \in \{2^{-1}, 2^{-2}, \ldots, 2^{-18}\}$. We compare against the $L^2(0,1)$ ($*$ markers) and $H^1_k(0,1)$ ($+$ markers) best approximation errors (computed by the orthogonal projection with the relevant matrices). We observe three regimes:
(i) for $\frac{2\pi}{k} \lesssim h$ (right) u is not approximated at all, the wave is not resolved by the discrete space;
(ii) for $\frac{2\pi}{k^{3/2}} \lesssim h \lesssim \frac{2\pi}{k}$ (centre) the best approximation error decays with optimal order, while the Galerkin error remains roughly constant;
(iii) for $h \lesssim \frac{2\pi}{k^{3/2}}$ (left part of each plot) the Galerkin error decays with optimal rate.
The lower plots show the quasi-optimality ratio.
The presence of the regime (ii) (in which the Galerkin solution performs much worse than the best approximation) and the growth of the quasi-optimality ratio for increasing values of k are signals of the pollution effect. See Remark 6.27 and Exercise 6.28.

Remark 6.27: (k-dependence in the FEM). We observe that the mesh size threshold $h_\star$ decreases with $k \to \infty$: this means that higher frequencies require finer meshes (and larger linear systems: in 2D the number of DOFs involved in a standard FEM discretisation is proportional to h^{-2}). In Remark 5.9 we explained why $h \lesssim k^{-1}$ is needed to maintain a given level of approximation for large k. Here instead we are not looking at the approximability of the solution, but at the stability of the Galerkin scheme: the bound on $h_\star$ is needed to ensure well-posedness and quasi-optimality.

Moreover, we observe that $h_\star$ grows more than linearly in k^{-1}.[61] So, while $h = \mathcal{O}(k^{-1})$ ($N \approx k^2$ DOFs) is enough to ensure good approximation properties, we need finer meshes with $h = \mathcal{O}(k^{-a})$ ($N \approx k^{2a}$ DOFs) for some $a > 1$ to ensure stability, and thus FEM accuracy.

This is not an artefact of the proof but can be observed numerically and is a major problem in the numerical analysis of high-frequency time-harmonic problems. This notorious phenomenon is called **pollution effect**; it is described e.g. in [Ihlenburg98, §4.6][62] It affects all methods based on local approximations of the PDE; see also [Runborg12, §3.2] for a simple analysis of this effect in the case of the finite difference method. High-order methods (e.g. FEM with high-degree piecewise-polynomial discrete spaces) perform better under this respect.

---

[61] The bound suggests a quadratic growth $h_\star \approx k^{-2}$, but $h_\star \approx k^{-3/2}$ is typically enough [Ihlenburg98, eq. (4.7.41)]. Here we are not taking into accounts that C_{stab} depends on k; this dependence is more easily studied for impedance problems and simple geometries (Ω convex or star-shaped).

[62] See also [Babuska, Sauter, Is the pollution effect of the FEM avoidable for the Helmholtz equation considering high wave numbers?, SiRev 2000].

A great deal of research is devoted to the design of Galerkin schemes for time-harmonic problems that are robust and accurate for large wavenumbers.

The BEM can overcome the pollution effect: the error committed by Brakhage–Werner and Burton–Miller formulations, discretised with piecewise-polynomial spaces V_N on quasi-uniform meshes, does not grow with $k \to \infty$ if $h = \mathcal{O}(k^{-1})$, when the scatterer Ω_- is C^∞ and "non-trapping" (e.g. convex or star-shaped)[63]. So the number of DOFs needed to maintain a given accuracy for increasing k is $N = \mathcal{O}(k)$ (more generally, $\mathcal{O}(k^{d-1})$ for $\Omega \subset \mathbb{R}^d$). This is another important advantage of the BEM against the FEM.

Exercise 6.28: (FEM numerical experiments). Use piecewise-linear finite elements on a quasi-uniform mesh to approximate an interior Helmholtz BVP. Choose either a (well-posed) Dirichlet or an impedance problem, in 1D or in 2D.

Plot the norm of (i) the Galerkin error and (ii) the best-approximation error (e.g. computed with the $L^2(\Omega)$ projection) for decreasing mesh sizes h. Repeat the same plot for different values of k. Observe how the best-approximation error starts to converge only for $h \approx k^{-1}$, while the Galerkin method needs even smaller h to start converging. Study numerically the quasi-optimality constant in dependence of k.

You can try to reproduce the example in Figure 30.

6.3.3   BEM ERROR ANALYSIS FOR THE SINGLE-LAYER BIE

We want to apply Theorem 6.23 to the Galerkin-BEM discretisation (§5.2) of the single-layer BIE $S\psi = g_{\mathrm{D}}$, (58). Our goal is to show that the piecewise-constant Galerkin-BEM is well-posed and quasi-optimal if the mesh size h is sufficiently small. We recall the variational formulation (60):

$$\text{find } \psi \in H^{-\frac{1}{2}}(\Gamma) \quad \text{such that} \quad \mathcal{A}(\psi, \xi) := \langle S\psi, \xi \rangle_\Gamma = \langle g_{\mathrm{D}}, \xi \rangle_\Gamma =: \mathcal{F}(\xi) \qquad \forall \xi \in H^{-\frac{1}{2}}(\Gamma).$$

The space in which the variational problem is posed is $H = H^{-\frac{1}{2}}(\Gamma)$. The continuity constant of the sesquilinear form $\mathcal{A}(\cdot, \cdot)$ is $C_\mathcal{A} = \|S\|_{H^{-\frac{1}{2}}(\Gamma) \to H^{\frac{1}{2}}(\Gamma)}$.

One of the ingredients needed in the analysis of §6.3.1 is the study of the approximation properties of the discrete space V_N. We summarise the convergence rates in h of the best-approximation error for the piecewise-constant discrete space in fractional Sobolev norms.

Proposition 6.29: (Piecewise-constant approximation in fractional norms). Let Γ be the boundary of a Lipschitz domain. For any $h > 0$, let $\mathcal{T}_N = \{K\}$ be a mesh on Γ made of N arcs K of length $|K| \le h$, and V_N be the piecewise-constant space on $\mathcal{T}_N$ as in §5.2. Define the $L^2(\Gamma)$-orthogonal projection Π:

$$\begin{aligned}\Pi : L^2(\Gamma) &\to V_N, \\ v &\mapsto \arg\min_{v_N \in V_N} \|v - v_N\|_{L^2(\Gamma)},\end{aligned} \qquad (\Pi v)|_K = \frac{1}{|K|} \int_K v(s)\,\mathrm{d}s \qquad \forall v \in L^2(\Gamma),\ K \in \mathcal{T}_N. \quad (107)$$

Then, for all $-1 \le s \le 0 \le t \le 1$, there is $C_{\mathrm{App}} > 0$ independent of h such that

$$\|v - \Pi v\|_{H^s(\Gamma)} \le C_{\mathrm{App}} h^{t-s} \|v\|_{H^t(\Gamma)} \qquad \forall v \in H^t(\Gamma). \quad (108)$$

Proof. The bound (108) is trivial for $s = t = 0$, with $C_{\mathrm{App}} = 1$. The result for $s = 0, t = 1$ follows (with $C_{\mathrm{App}} = \frac{1}{\pi}$) from the Poincaré–Wirtinger inequality for 0-average functions [Brezis11, p. 312 and Problem 47]:

$$\|v - \Pi v\|_{L^2(\Gamma)}^2 = \sum_{K \in \mathcal{T}_N} \left\| v - \frac{1}{|K|} \int_K v\,\mathrm{d}s \right\|_{L^2(K)}^2 \le \sum_{K \in \mathcal{T}_N} \frac{|K|^2}{\pi^2} \|v'\|_{L^2(K)}^2 \le \frac{h^2}{\pi^2} \|v\|_{H^1(\Gamma)}^2 \qquad \forall v \in H^1(\Gamma),$$

where v' denotes the tangential derivative of v. Then, operator interpolation theory gives a result for the intermediate spaces, with an intermediate power of h:

$$\|v - \Pi v\|_{L^2(\Gamma)} \le C_{\mathrm{App}} h^t \|v\|_{H^t(\Gamma)} \qquad \forall v \in H^t(\Gamma),\ 0 < t < 1$$

(see [McLean00, Thm. B.2] with $A_0 = I - \Pi : L^2(\Gamma) \to L^2(\Gamma)$ and $A_1 = I - \Pi : H^1(\Gamma) \to L^2(\Gamma)$, $\theta = s$, and [McLean00, Thm. B.11] with $s_0 = 0$, $s_1 = 1$). Exploiting the orthogonality of the projection, recalling the duality relation between $H^{\pm s}(\Gamma)$ from §3.3.3, we extend the result to negative norms:

$$\|v - \Pi v\|_{H^s(\Gamma)} = \sup_{0 \ne w \in H^{-s}(\Gamma)} \frac{|\langle v - \Pi v, w \rangle_\Gamma|}{\|w\|_{H^{-s}(\Gamma)}} = \sup_{0 \ne w \in H^{-s}(\Gamma)} \frac{|\langle v - \Pi v, w - \Pi w \rangle_\Gamma|}{\|w\|_{H^{-s}(\Gamma)}}$$

---

[63][Galkowski, Spence, *Does the Helmholtz boundary element method suffer from the pollution effect?*, SiRev 2023]

$$\leq \sup_{0 \neq w \in H^{-s}(\Gamma)} \frac{\|v - \Pi v\|_{L^2(\Gamma)} \|w - \Pi w\|_{L^2(\Gamma)}}{\|w\|_{H^{-s}(\Gamma)}} \leq C_{\mathrm{App}} h^{-s} \|v - \Pi v\|_{L^2(\Gamma)} \qquad \forall v \in L^2(\Gamma), \quad -1 < s < 0.$$

Combining the two results we obtain (108) with a new value of C_{App}.[64] $\hfill\square$

We now verify that the framework of Theorem 6.23 is applicable. We have seen in §6.1 that the operator $S : H^{-\frac{1}{2}}(\Gamma) \to H^{\frac{1}{2}}(\Gamma)$ is Fredholm but we haven't proved a Gårding inequality yet. The Fredholm property of S was proved from the decomposition $S = S_c + (S - S_c)$ for $c \geq 0$, where the first term is coercive and the second compact. Recall from §6.1.2 that S_c is the single-layer operator for the reaction–diffusion or the Laplace equation, for $c > 0$ or $c = 0$, respectively. In the following we choose $c > 0$ for simplicity. To write a Gårding inequality for $\mathcal{A}(\cdot, \cdot)$ we need a space V larger than $H^{-\frac{1}{2}}(\Gamma)$ (recall that $H^{-\frac{1}{2}}(\Gamma)$ is larger than $L^2(\Gamma)$). To identify this space V we need to study the mapping properties of $S - S_c$ and write a Gårding inequality.

We have seen numerically in §6.1.3 (in particular in Figure 28) that, on the circular boundary $\Gamma = \partial B_R$, $S - S_c : H^s(\Gamma) \to H^{s+3}(\Gamma)$ for all $s \in \mathbb{R}$. We assume that Γ is sufficiently regular so that $S - S_c : H^{-1}(\Gamma) \to H^1(\Gamma)$ is a continuous operator. We denote its operator norm by $C_1 := \|S - S_c\|_{H^{-1}(\Gamma) \to H^1(\Gamma)}$, depending only on k, c, Γ. Then the bound

$$|\langle (S - S_c)\psi, \xi \rangle_\Gamma| \leq \|(S - S_c)\psi\|_{H^1(\Gamma)} \|\xi\|_{H^{-1}(\Gamma)} \leq C_1 \|\psi\|_{H^{-1}(\Gamma)} \|\xi\|_{H^{-1}(\Gamma)} \qquad \forall \psi, \xi \in H^{-1}(\Gamma)$$

and the coercivity of S_c shown in §6.1.5 give the Gårding inequality: $\forall \psi \in H^{-\frac{1}{2}}(\Gamma)$,

$$\Re\{\mathcal{A}(\psi, \psi)\} = \Re\{\langle S\psi, \psi \rangle_\Gamma\} = \Re\{\langle S_c\psi, \psi \rangle_\Gamma\} + \Re\{\langle (S - S_c)\psi, \psi \rangle_\Gamma\} \geq \alpha_c \|\psi\|^2_{H^{-\frac{1}{2}}(\Gamma)} - C_1 \|\psi\|^2_{H^{-1}(\Gamma)},$$

where $\alpha_c := \frac{1}{2 C_{\mathrm{tr}} \max\{1, c^2\}}$ and C_{tr} is the continuity constant of the normal trace operator in (90). This Gårding inequality suggests to choose $V = H^{-1}(\Gamma)$.

The adjoint problem (102) is:

given $f \in H^{-1}(\Gamma)$, find $z_f \in H^{-\frac{1}{2}}(\Gamma)$ such that $\mathcal{A}(\xi, z_f) = \langle S\xi, z_f \rangle_\Gamma = (\xi, f)_{H^{-1}(\Gamma)}$ $\forall \xi \in H^{-\frac{1}{2}}(\Gamma)$.

Note the presence of the $H^{-1}(\Gamma)$ scalar product. From $\mathcal{A}(v, w) = \mathcal{A}(\overline{w}, \overline{v})$ (which can be verified by the definitions of $\mathcal{A}(\cdot, \cdot)$ and S) and $(v, w)_{H^{-1}(\Gamma)} = (\overline{w}, \overline{v})_{H^{-1}(\Gamma)}$, we can rewrite the adjoint equation as $\mathcal{A}(\overline{z_f}, \overline{\xi}) = (\overline{f}, \overline{\xi})_{H^{-1}(\Gamma)}$. Dropping the complex conjugates, we obtain $\mathcal{A}(z_f, \xi) = (f, \xi)_{H^{-1}(\Gamma)}$. Since $H^{-1}(\Gamma) \ni \xi \mapsto (f, \xi)_{H^{-1}(\Gamma)}$ defines a continuous antilinear functional on $H^{-1}(\Gamma)$, it can be represented by an element $F \in H^1(\Gamma)$ with $\|F\|_{H^1(\Gamma)} \leq C_* \|f\|_{H^{-1}(\Gamma)}$ (i.e. $(f, \xi)_{H^{-1}(\Gamma)} = \langle F, \xi \rangle_\Gamma$, recall §3.3.3). Thus the adjoint problem is again the single-layer BIE $S z_f = F$ for a "smooth" datum $F \in H^1(\Gamma)$.

Assume that k^2 is not a Dirichlet eigenvalue for Ω_- (which we need to assume for the BIE to be well-posed, as required by the theorem). Then $S : H^{-\frac{1}{2}}(\Gamma) \to H^{\frac{1}{2}}(\Gamma)$ is invertible, as explained in §6.1.1. It is possible to show that the single-layer operator is invertible[65] also as $S : L^2(\Gamma) \to H^1(\Gamma)$. This implies a regularity result for the adjoint problem: $z_f \in L^2(\Gamma)$.

The adjoint problem solution z_f is an element of $L^2(\Gamma)$ which can be approximated by the piecewise-constant space V_N defined in §5.2. Indeed, Proposition 6.29 implies that $v_N = \Pi z_f \in V_N$ approximates z_f with the error bound[66]

$$\|z_f - v_N\|_{H^{-\frac{1}{2}}(\Gamma)} \leq C_{\mathrm{App}} h^{\frac{1}{2}} \|z_f\|_{L^2(\Gamma)} \leq C_{\mathrm{App}} h^{\frac{1}{2}} \|S^{-1}\|_{H^1(\Gamma) \to L^2(\Gamma)} \|F\|_{H^1(\Gamma)}$$

$$\leq C_* C_{\mathrm{App}} h^{\frac{1}{2}} \|S^{-1}\|_{H^1(\Gamma) \to L^2(\Gamma)} \|f\|_{H^{-1}(\Gamma)}.$$

Recall that h is the length of the longest mesh element. This bound corresponds to an estimate on the approximability parameter $\eta(V_N)$ of (103):

$$\eta(V_N) = \sup_{f \in H^{-1}(\Gamma)} \min_{v_N \in V_n} \frac{\|z_f - v_N\|_{H^{-\frac{1}{2}}(\Gamma)}}{\|f\|_{H^{-1}(\Gamma)}} \leq C_* C_{\mathrm{App}} h^{\frac{1}{2}} \|S^{-1}\|_{H^1(\Gamma) \to L^2(\Gamma)}.$$

---

[64]Recall that in §3.3.2 we mentioned that it is possible to define several different equivalent norms on $H^s(\Gamma)$: if we choose norms that give an "exact interpolation scale" we could get $C_{\mathrm{App}} = \pi^{s-t}$ in (108). The Fourier-mode norm on the circle in (28) is such an example. The values of all the bounding constants $C_\bullet$ of the results in this and next section depend on the specific $H^s(\Gamma)$ norms chosen.

[65]We know $S : L^2(\Gamma) \to H^1(\Gamma)$ is injective for this choice of k. We have seen in §6.1.4 that $S - S_0 : L^2(\Gamma) \to H^1(\Gamma)$ is compact, as it corresponds to an integral operator with bounded kernel. It also holds that $S_0 : L^2(\Gamma) \to H^1(\Gamma)$ is invertible. Then Fredholm alternative Theorem 3.17 yields the invertibility of S in the desired spaces.

[66]In order to bound $\eta(V_N)$, both in the FEM and in the BEM cases, we used three main ingredients: (i) the stability of the adjoint problem, (ii) a regularity result for its solution, and (iii) an approximation result. In the FEM case, (i)–(ii)–(iii) correspond to the terms C_{stab}, C_{H^2} and C_{BH}, respectively. In the BEM case, stability and regularity together give $C_* \|S^{-1}\|_{H^1(\Gamma) \to L^2(\Gamma)}$ and the approximation term gives C_{App}.

The threshold condition (104) $\eta(V_N) \leq \frac{1}{C_{\mathcal{A}}} \sqrt{\frac{\alpha}{2C_V}}$ is ensured if $h \leq h_\star$ for

$$h_\star := \left(4 \max\{1, c^2\} C_*^2 C_{\mathrm{App}}^2 C_{\mathrm{tr}} \|S\|_{H^{-\frac{1}{2}}(\Gamma) \to H^{\frac{1}{2}}(\Gamma)}^2 \|S - S_c\|_{H^{-1}(\Gamma) \to H^1(\Gamma)} \|S^{-1}\|_{H^1(\Gamma) \to L^2(\Gamma)}^2 \right)^{-1}. \quad (109)$$

In this case the quasi-optimality estimate (105) follows: if $h \leq h_\star$,

$$\|\psi - \psi_N\|_{H^{-\frac{1}{2}}(\Gamma)} \leq C_{\mathrm{qo}} \inf_{v_N \in V_N} \|\psi - v_N\|_{H^{-\frac{1}{2}}(\Gamma)}, \qquad C_{\mathrm{qo}} := 4C_{\mathrm{tr}} \max\{1, c^2\} \|S\|_{H^{-\frac{1}{2}}(\Gamma) \to H^{\frac{1}{2}}(\Gamma)}. \quad (110)$$

Both $h_\star$ and C_{qo} depend only on Γ, k and c (which can be chosen arbitrarily, e.g. $c = 1$).

Similarly to the FEM case in §6.3.2, we have proved that if h is sufficiently small, then the threshold condition (104) is satisfied and the Galerkin-BEM is well-posed and quasi-optimal.

Table 3 summarises how the FEM and the BEM analysis considered in this section fit the framework of Theorem 6.23. Recall that we are considering the simplest cases: piecewise-linear FEM for interior Dirichlet problem (35), piecewise-constant Galerkin-BEM for the EDP (44) and the single-layer BIE (58).

Abstract framework §6.3.1	FEM §6.3.2	BEM §6.3.3
Helmholtz problem	interior Dirichlet	exterior Dirichlet/single-layer BIE
Energy space H	$H_0^1(\Omega)$	$H^{-\frac{1}{2}}(\Gamma)$
Auxiliary space V	$L^2(\Omega)$	$H^{-1}(\Gamma)$
Sesquilinear form $\mathcal{A}(\cdot, \cdot)$	$\int_\Omega (\nabla u \nabla \overline{w} - k^2 u \overline{w})\, d\mathbf{x}$	$\langle S\psi, \xi \rangle_\Gamma$
Gårding constant α	1	$\alpha_c = \frac{1}{2C_{\mathrm{tr}} \max\{1, c^2\}}$
Gårding constant C_V	$2k^2$	$C_1 = \|S - S_c\|_{H^{-1}(\Gamma) \to H^1(\Gamma)}$
Continuity constant $C_{\mathcal{A}}$	1	$\|S\|_{H^{-\frac{1}{2}}(\Gamma) \to H^{\frac{1}{2}}(\Gamma)}$
Discrete space V_N	piecewise-linears on Ω	piecewise-constants on Γ
Threshold mesh size $h_\star$	(106)	(109)
Quasi-optimality C_{qo}	2	$4C_{\mathrm{tr}} \max\{1, c^2\} \|S\|_{H^{-\frac{1}{2}}(\Gamma) \to H^{\frac{1}{2}}(\Gamma)}$
Valid if	k^2 is not Dirichlet eigenvalue of Ω	k^2 is not Dirichlet eigenvalue of Ω_-

Table 3: How the FEM and BEM considered fit the abstract stability framework of Theorem 6.23.

6.3.4   BIE SOLUTION REGULARITY AND BEM CONVERGENCE RATES

Given the quasi-optimality (110) and the best-approximation estimates (108), we can derive convergence rates for the piecewise-constant BEM. However, convergence rates always depend on the regularity of the solution to be approximated. So, we first want to know for which values of $s \geq -\frac{1}{2}$ the solution ψ of the single-layer BIE $S\psi = g_{\mathrm{D}}$ (58) belongs to $H^s(\Gamma)$.

To this purpose, we assume that k^2 is not a Dirichlet eigenvalue in Ω_-, and that the EDP (44) under consideration is actually an SSSP (45), i.e. $g_{\mathrm{D}} = -\gamma^+ u^{\mathrm{Inc}}$ for some incoming wave u^{Inc}.

By (84), $\psi = -\partial_{\mathbf{n}}^+ u^{\mathrm{Tot}}$. So we need to study the regularity of u^{Tot} and then apply the Neumann trace. Since u^{Tot} is a solution of the homogeneous Helmholtz equation, $u^{\mathrm{Tot}} \in C^\infty(\Omega_+)$, by interior elliptic regularity [McLean00, Thm. 4.16]. However, its smoothness on the boundary Γ depends on the the regularity of Γ itself.

Assume that Ω_- is a polygon. The possible sources of singularities in u^{Tot} are the corners of Ω_-. We first focus on a single corner.

Exercise 6.30: (Laplace solutions in a sector).

Define the non-convex sector $S_\alpha := \{0 < \theta < \alpha : 0 < r < 1\}$ for $\alpha \in (\pi, 2\pi)$.

For $j \in \mathbb{N}$, show that $\phi_{\alpha,j}(\mathbf{x}) := r^{j\frac{\pi}{\alpha}} \sin(j\frac{\pi}{\alpha}\theta) \in C^\infty(S_\alpha)$ solves the Laplace equation $\Delta\phi_{\alpha,j} = 0$ in S_α. (Use the expression (21) of the Laplacian in polar coordinates.)

Use the separation of variables to show that all Laplace solutions u on S_α, with trace 0 on the two segments, can be written as $u(\mathbf{x}) = \sum_{j \in \mathbb{N}} \widehat{u}_j \phi_{\alpha,j}(\mathbf{x})$ for some coefficients $\widehat{u}_j \in \mathbb{C}$.

The corner functions defined in Exercise 6.30 are smooth in the interior of S_α and are singular at the origin. In terms of Sobolev regularity, they satisfy $u_{\alpha,j} \in H^{1+j\frac{\pi}{\alpha}-\epsilon}(S_\alpha) \setminus H^{1+j\frac{\pi}{\alpha}}(S_\alpha)$ for all $\epsilon > 0$ (where we use the fractional-order spaces of Remark 3.12)[67]. This means that the generic Laplace solutions that

---

[67]See Thm. 1.4.5.3 in [Grisvard, Elliptic problems in non-smooth domains, Pitman 1985].

vanish on the two sides of the sector belongs to $H^{1+\frac{\pi}{\alpha}-\epsilon}(S_\alpha) \setminus H^{1+\frac{\pi}{\alpha}}(S_\alpha)$. For larger α, and sharper re-entrant corners, the regularity is lower.

Considering the Helmholtz equation in a small domain is equivalent to considering small wavenumbers, by a scalar change of variables. So we expect that, close to a corner, the Helmholtz equation behaves similarly to the Laplace one. Indeed, repeating the argument of Exercise 6.30 for the Helmholtz equation, we obtain that all the Helmholtz solutions on S_α that are zero on the two sides admit the expansion

$$u(\mathbf{x}) = \sum_{j \in \mathbb{N}} \widehat{u}_j w_{\alpha,j}(\mathbf{x}), \qquad \text{where} \qquad w_{\alpha,j}(\mathbf{x}) := J_{j\frac{\pi}{\alpha}}(kr) \sin\left(j\frac{\pi}{\alpha}\theta\right). \tag{111}$$

The $w_{j,\alpha}$ are called "corner waves" or "fractional Fourier–Bessel function"; see Figure 31. Here we use the Bessel function with non-integer index J_ν, which extends holomorphically the usual Bessel functions to arbitrary complex values of ν, [DLMF, eq. 10.2.2]. The field $w_{\alpha,j}$ is a Helmholtz solutions because J_ν satisfies the Bessel equation (22) with ν in place of ℓ. For small positive arguments, J_ν satisfies the same asymptotics $J_\nu(z) \sim \frac{z^\nu}{\Gamma(\nu+1)2^\nu}$ for $z \searrow 0$ (24), [DLMF, eq. 10.7.3]. Thus $w_{\alpha,j}(\mathbf{x}) \approx Cu_{\alpha,j}(\mathbf{x})$ close to $\mathbf{x} = \mathbf{0}$ for some constant C and are smooth in the rest of S_α. The corner waves inherit the regularity of $u_{\alpha,j}$: $w_{\alpha,j} \in H^{1+j\frac{\pi}{\alpha}-\epsilon}(S_\alpha) \setminus H^{1+j\frac{\pi}{\alpha}}(S_\alpha)$ for all $\epsilon > 0$. The $w_{\alpha,j}$ are bounded but their derivatives blow up at the origin.

Corner waves $J_{\frac{\pi}{\alpha}}(kr)\sin(\frac{\pi}{\alpha}\theta)$, $k = 5$, in $S_\alpha = \{0 < r < 1, 0 < \theta < \alpha\}$

$\alpha = \frac{5}{4}\pi$ $\qquad$ $\alpha = \frac{3}{2}\pi$ $\qquad$ $\alpha = \frac{7}{4}\pi$

Corner waves $J_{\frac{\pi}{\alpha}}(kr)\sin(\frac{\pi}{\alpha}\theta)$, $k = 30$, in $S_\alpha = \{0 < r < 1, 0 < \theta < \alpha\}$

$\alpha = \frac{5}{4}\pi$ $\qquad$ $\alpha = \frac{3}{2}\pi$ $\qquad$ $\alpha = \frac{7}{4}\pi$
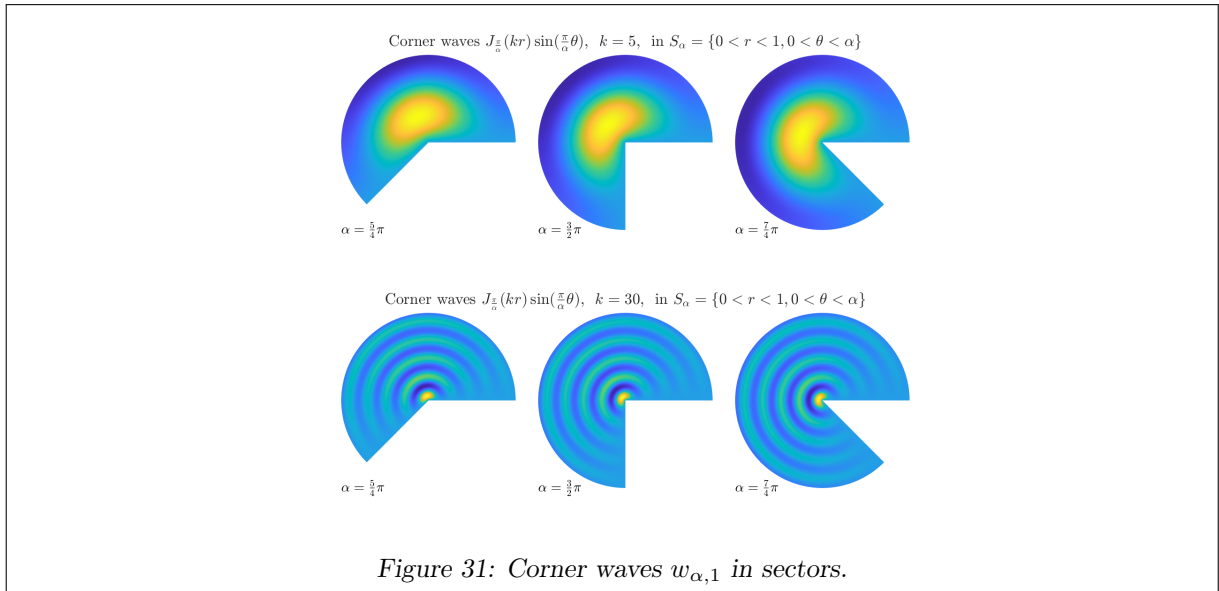
Figure 31: Corner waves $w_{\alpha,1}$ in sectors.

Given a polygonal Ω_-, denote by $\alpha_{\max} \in (\pi, 2\pi)$ the maximal external angle of all its corners (e.g. $\alpha_{\max} = \frac{3}{2}\pi$ for a square, $\alpha_{\max} = \frac{7}{4}\pi$ for the isoceles rectangle triangle $\Omega_- = \{0 < x_1 < x_2 < 1\}$).

Expanding u^{Tot} as in (111) in sectors with small radii around each external angle of Ω_-, and using its smoothness elsewhere, we deduce that

$$u^{\text{Scat}}, u^{\text{Tot}} \in H^{1+\frac{\pi}{\alpha_{\max}}-\epsilon}_{\text{loc}}(\Omega_+) \qquad \forall \epsilon > 0,$$

and that in general they do not belong to $H^{1+\frac{\pi}{\alpha_{\max}}}_{\text{loc}}(\Omega_+)$. Then $\nabla u^{\text{Tot}} \in H^{\frac{\pi}{\alpha_{\max}}-\epsilon}_{\text{loc}}(\Omega_+)$ and $\gamma^+(\frac{\partial u^{\text{Tot}}}{\partial x_j}) \in H^{-\frac{1}{2}+\frac{\pi}{\alpha_{\max}}-\epsilon}(\Gamma)$, $j = 1, 2$, by the trace theorem [McLean00, Thm. 3.37]. The product between an element of $H^t(\Gamma)$ with $|t| < \frac{1}{2}$ and a piecewise-constant belongs to the same $H^t(\Gamma)$. We apply this to $\psi = -\partial^+_{\mathbf{n}} u^{\text{Tot}} = -n_1\gamma^+(\frac{\partial u^{\text{Tot}}}{\partial x_1}) - n_2\gamma^+(\frac{\partial u^{\text{Tot}}}{\partial x_2})$, with $\mathbf{n} = (n_1, n_2)$, which is constant on each side of Γ, and obtain the regularity of the BIE solution:

$$\psi \in H^{-\frac{1}{2}+\frac{\pi}{\alpha_{\max}}-\epsilon}(\Gamma) \qquad \forall \epsilon > 0. \tag{112}$$

In particular, $\psi \in L^2(\Gamma)$.

The approximation result of Proposition 6.29 ensures that, for all piecewise-constant spaces V_N as above, $\inf_{v_N \in V_N} \|\psi - v_N\|_{H^{-\frac{1}{2}}(\Gamma)} \leq Ch^{\frac{\pi}{\alpha_{\max}}}$ (neglecting the arbitrarily small ϵ), for some $C > 0$ depending on u^{Tot} but independent of h and $\mathcal{T}_N$. Combining with the quasi-optimality (110), we have the convergence bound for the BEM

$$\|\psi - \psi_N\|_{H^{-\frac{1}{2}}(\Gamma)} \leq Ch^{\frac{\pi}{\alpha_{\max}}} \qquad \forall h \leq h_\star.$$

Since $\frac{1}{2} < \frac{\pi}{\alpha_{\max}} < 1$, the convergence rate is always at least $1/2$.

However, this rate concerns the convergence of the BEM approximation ψ_N to the BIE density ψ in $H^{-\frac{1}{2}}(\Gamma)$ norm. This is the relevant norm for the variational problem, but is neither practical nor particularly useful to compute. Usually, what we are really interested in is not ψ, but the scattered field u^{Scat} (or the far-field pattern u_∞ (46)). It turns out that the scattered field computed with the BEM converges with *double* velocity, compared to the BIE density ψ. This follows again from a duality argument, which ensures the "superconvergence" of linear functionals J defined by testing against sufficiently smooth distributions φ, [SS11, §4.2.5.1]. In the next lemma and corollary, we first prove this general result, then we apply it to the point evaluation of u^{Scat}.

Lemma 6.31: (Superconvergence of smooth functionals). Let Ω_- be a polygon with maximal external angle $\alpha_{\max}$ and assume k^2 is not a Dirichlet eigenvalue. Given $\varphi \in H^{\frac{1}{2}}(\Gamma)$, define the linear functional

$$J : H^{-\frac{1}{2}}(\Gamma) \to \mathbb{C}, \qquad J : \psi \mapsto \langle \varphi, \overline{\psi} \rangle_\Gamma \qquad \forall \psi \in H^{-\frac{1}{2}}(\Gamma). \qquad (113)$$

Assume that the solution $\zeta \in H^{-\frac{1}{2}}(\Gamma)$ of the variational problem with datum φ

$$\mathcal{A}(\zeta, \xi) = \langle \varphi, \xi \rangle_\Gamma \qquad \forall \xi \in H^{-\frac{1}{2}}(\Gamma) \qquad (114)$$

belongs to $H^{-\frac{1}{2}+t}(\Gamma)$ for some $0 < t \leq \frac{3}{2}$. Let ψ be the solution of the BIE (58) with regularity (112), and ψ_N be its piecewise-constant Galerkin-BEM approximation in V_N with sufficiently small h.
Then, for all $\epsilon > 0$, there is $C > 0$, depending only on Γ and k, independent of h, $\mathcal{T}_N$, ψ, ζ and φ, such that

$$|J(\psi) - J(\psi_N)| \leq C\, h^{\frac{\pi}{\alpha_{\max}}+t-\epsilon}\, \|\psi\|_{-\frac{1}{2}+\frac{\pi}{\alpha_{\max}}-\epsilon}\, \|\zeta\|_{-\frac{1}{2}+t}\,.$$

Proof. We combine many of the tools introduced so far:

$$
\begin{aligned}
&|J(\psi) - J(\psi_N)| \\
&= |\langle \varphi, \overline{\psi - \psi_N} \rangle_\Gamma| && \text{by definition of } J, \\
&= |\mathcal{A}(\zeta, \overline{\psi - \psi_N})| && \text{by definition of } \zeta, \\
&= |\mathcal{A}(\psi - \psi_N, \overline{\zeta})| && \text{by the symmetry properties of } \mathcal{A} \text{ and } S, \\
&= |\mathcal{A}(\psi - \psi_N, \overline{\zeta - \Pi\zeta})| && \text{by Galerkin orthogonality, } \zeta \in L^2(\Gamma), \text{with the projection } \Pi \text{ in (107)}, \\
&= |\langle S(\psi - \psi_N), \overline{\zeta - \Pi\zeta} \rangle_\Gamma| && \text{by definition of } \mathcal{A}, \\
&\leq \|S\|_{H^{-\frac{1}{2}}(\Gamma)\to H^{\frac{1}{2}}(\Gamma)} \|\psi - \psi_N\|_{H^{-\frac{1}{2}}(\Gamma)} \|\zeta - \Pi\zeta\|_{H^{-\frac{1}{2}}(\Gamma)} \\
&\leq C_{\mathrm{qo}} \|S\|_{H^{-\frac{1}{2}}(\Gamma)\to H^{\frac{1}{2}}(\Gamma)} \|\psi - \Pi\psi\|_{H^{-\frac{1}{2}}(\Gamma)} \|\zeta - \Pi\zeta\|_{H^{-\frac{1}{2}}(\Gamma)} && \text{by the BEM quasi-optimality (110)}, \\
&\leq C_{\mathrm{qo}} C_{\mathrm{App}}^2 \|S\|_{H^{-\frac{1}{2}}(\Gamma)\to H^{\frac{1}{2}}(\Gamma)} h^{\frac{\pi}{\alpha_{\max}}+t-\epsilon} \|\psi\|_{-\frac{1}{2}+\frac{\pi}{\alpha_{\max}}-\epsilon} \|\zeta\|_{-\frac{1}{2}+t} && \forall \epsilon > 0, \text{ by the approximation (108)}.
\end{aligned}
$$

$\square$

Corollary 6.32: (Superconvergence of the near-field u^{Scat}). Let u^{Scat} be the solution of the SSSP (45) for a polygonal scatterer Ω_- with maximal external angle $\alpha_{\max}$, where k^2 is not a Dirichlet eigenvalue.
Let $u_N = \mathcal{S}\psi_N$ (64) be the single-layer potential generated by the BEM solution $\psi_N \in V_N$, for a mesh with sufficiently small h.
Then, for any point $\mathbf{x} \in \Omega_+$ and $\epsilon > 0$, there is $C > 0$ independent of h and $\mathcal{T}_N$ such that

$$|u^{\mathrm{Scat}}(\mathbf{x}) - u_N(\mathbf{x})| \leq C\, h^{2\frac{\pi}{\alpha_{\max}}-\epsilon}.$$

Proof. Define $\varphi = \gamma^+ \Phi_k(\mathbf{x}, \cdot) \in H^{\frac{1}{2}}(\Gamma)$, for Φ_k the Helmholtz fundamental solution (53). The corresponding functional J in (113) is $J(\xi) = \langle \gamma^+ \Phi_k(\mathbf{x}, \cdot), \overline{\xi} \rangle_\Gamma = (\mathcal{S}\xi)(\mathbf{x})$, the single-layer potential applied to $\xi \in H^{-\frac{1}{2}}(\Gamma)$ and evaluated in $\mathbf{x}$. In particular, $J(\psi) = u^{\mathrm{Scat}}(\mathbf{x})$ and $J(\psi_N) = u_N(\mathbf{x})$.

By Lemma 6.31, the assertion of the corollary follows if ζ, solution of (114), belongs to $H^{-\frac{1}{2}+\frac{\pi}{\alpha_{\max}}-\epsilon}(\Gamma)$ for all $\epsilon > 0$.

The variational problem (114) is an EDP (44) with boundary datum $g_{\mathrm{D}} = \varphi = \gamma^+ \Phi_k(\mathbf{x}, \cdot)$, which is the trace of a Helmholtz solution that is smooth in a neighbourhood of $\overline{\Omega_-}$. So (114) is simply an SSSP

with $u^{\mathrm{Inc}} = -\Phi(\mathbf{x}, \cdot)$, a point source centred at $\mathbf{x}$. The regularity result (112) applies to its solution ζ and we have precisely the smoothness $\zeta \in H^{-\frac{1}{2}+t}$ with $t = \frac{\pi}{\alpha_{\max}} - \epsilon$ needed to obtain the assertion. $\qquad\square$

From Corollary 6.32 we deduce that $\left\| u^{\mathrm{Scat}} - u_N \right\|_{L^2(D)}$, for a domain $D \subset \Omega_+$, converges with the rate $h^{2\frac{\pi}{\alpha_{\max}}}$. However, this holds only if D lies at a positive distance from the scatterer, as the constant C in the corollary bound blows up when $\mathbf{x}$ approaches Γ. We observe the h-dependence of $\left\| u^{\mathrm{Scat}} - u_N \right\|_{L^2(D)}$ for a simple example in Figure 32.

Figure 32: Convergence plot for the piecewise-constant collocation- and Galerkin-BEM applied to the scattering of a plane wave by the square scatterer $(-0.5, 0.5)^2$. The result obtained from MPSpack available on the course webpage is used as reference solution u^{Ref} (recall the footnote 35). The plot shows the relative error for the scattered field $\left\| u_N - u^{\mathrm{Ref}} \right\|_{L^2(D)} / \left\| u^{\mathrm{Ref}} \right\|_{L^2(D)}$, where u_N is the BEM approximation (64) of u^{Scat}. The set $D = \blacksquare$ is the square $(-1.5, 1.5)^2$ after subtracting the unit disc $B_1(\mathbf{0})$, to avoid near-singularities in the application of the representation formula. The numbers printed inside the plot are the slopes of the corresponding segments. We observe that, after a pre-asymptotic regime, the error converges with rate approximately $h^{\frac{4}{3}}$ (black dashed line), in agreement with Corollary 6.32 and Exercise (6.34). Note also that the Galerkin method is slightly more accurate than collocation.

Uniform meshes with $16, 32, \ldots, 4096$ elements are used. The integrals are approximated with Gauss–Legendre quadrature applied to the formulas in §5.2.1. We used 5 Gauss quadrature nodes for each integral in the off-diagonal entries of the matrix, the Galerkin right-hand side, and in the representation formula, and 30 Gauss nodes for the diagonal terms of the matrix.

Exercise 6.33: (Far-field convergence rates). Show that the BEM approximation of the far-field u_∞ (47) converges in $L^2(\mathbb{S}^1)$ with the superconvergence rate $h^{2\frac{\pi}{\alpha_{\max}}}$. Use the far-field formula (85). What are φ and ζ in the notation of Lemma 6.31?

Exercise 6.34: (Convergence rates in Matlab). Verify that the BEM code you have implemented in §5.2.2 achieves convergence rates in accordance with Corollary 6.32.

For instance, in Figure 32, a BEM code is tested against the MPSpack solution in the .mat file provided. In this example the scatterer is a square, so $\alpha_{\max} = \frac{3}{2}\pi$ and we expect convergence in h with exponent $2\frac{\pi}{\alpha_{\max}} = \frac{4}{3}$, which is what we observe in the plot.

It is not always simple to observe the rate predicted by the theory. This is an *asymptotic* rate in the limit $h \to 0$, while we inevitably work in the pre-asymptotic regime, i.e. with finite values of h. So error sources other than the sharpest corner of Γ can be the dominating effects in the error plots. For instance, the sharpest corner may lie in a shadow region, so its effect can be very weak. More often, at high frequencies many DOFs are needed just to get a qualitatively correct solution, the effect of corner singularities is localised and kicks in only with extremely fine meshes. In general we observe much neater convergence rates at very low frequencies.

7 TIME-HARMONIC WAVES IN HETEROGENEOUS MEDIA

So far we have considered the constant-coefficient Helmholtz equation $\Delta u + k^2 u = 0$, modelling time-harmonic acoustic waves in homogeneous media: the properties of the material are the same everywhere. When a wave propagates in a medium whose physical properties (ρ, c in acoustics, ϵ and μ in electromagnetism, λ, μ and ρ in elastodynamics) vary in space, the wave profile and direction are modified: this is **refraction**. For instance, the study of seismic-wave refraction is the main tool available to investigate the structure of the Earth's interior. In §7.1–7.2 we consider two general cases:

- Only few homogeneous materials are present, giving piecewise-constant material coefficients.

- The properties of the material vary smoothly in space, giving continuous material coefficients.

Of course there are relevant situations involving several heterogeneous materials, where the difficulties of both problems are present. Both cases can be modelled using integral equations, but only the first one with boundary integral equations.

7.1 PIECEWISE-CONSTANT PARAMETERS: TRANSMISSION PROBLEMS

We first consider "transmission problems", i.e. waves propagating through a finite number of homogeneous materials.

7.1.1 TRANSMISSION CONDITIONS

We describe the transmission conditions on the interface between two homogeneous materials for acoustic and electromagnetic waves. Similar arguments can be made for other types of waves, see e.g. [BK00, §2.4] and [CJ77, §20] for waves on strings with different densities, and [BK00, §4.7.1] for water waves (recall Remark 1.28).

As in Remark 3.15, we call Ω_1, Ω_2 two open Lipschitz domains, $\Omega := (\overline{\Omega_1} \cup \overline{\Omega_2})^\circ$ their open union, $\Sigma := (\partial\Omega_1 \cap \partial\Omega_2) \setminus \partial\Omega$ the interface between them, $\mathbf{n}$ a unit normal field on Σ, and $\gamma, \partial_{\mathbf{n}}$ the Dirichlet and Neumann traces from the two domains to Σ.
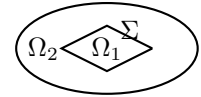
TRANSMISSION CONDITIONS: ACOUSTICS. We first consider the case of an acoustic wave propagating in two different homogeneous fluids, for instance water and air, occupying the regions Ω_1 and Ω_2.

Each fluid has its own static density ρ_1, ρ_2 (which was called ρ_0 in §1.1), and wave speed c_1, c_2. This leads to two copies of the wave equation in each region: $\frac{1}{c_j^2}\frac{\partial^2 p_{j,\approx}}{\partial t^2} - \Delta p_{j,\approx} = 0$ in Ω_j, $j = 1, 2$. How are these two equations coupled? On the interface Σ, the acoustic pressure from the two sides must coincide: $p_{1,\approx} = p_{2,\approx}$. Moreover, the normal component of the particle displacement for the fluids must agree at all times, otherwise they would overlap or leave an empty gap. So also their time derivatives, the normal components of the velocities, must coincide: $\mathbf{n} \cdot \mathbf{v}_{1,\approx} = \mathbf{n} \cdot \mathbf{v}_{2,\approx}$. Recalling the linearised Euler equation (4), this condition can be written in terms of the acoustic pressure as $\frac{1}{\rho_1}\mathbf{n} \cdot \nabla p_{1,\approx} = \frac{1}{\rho_2}\mathbf{n} \cdot \nabla p_{2,\approx}$.

Assuming time-harmonic behaviour (10) (with $p_{j,\approx}$ for U), we obtain two copies of the Helmholtz equation with different wavenumber, coupled by the Dirichlet traces and the Neumann traces weighted by the fluid densities:

$$\Delta u_j + k_j^2 u_j = 0 \quad \text{in } \Omega_j, \; j \in \{1, 2\}, \qquad k_j := \frac{\omega}{c_j},$$

$$\gamma u_1 = \gamma u_2, \quad \frac{1}{\rho_1}\partial_{\mathbf{n}} u_1 = \frac{1}{\rho_2}\partial_{\mathbf{n}} u_2 \quad \text{on } \Sigma. \tag{115}$$

Let u be the field on Ω defined by $u|_{\Omega_j} = u_j$. If $u_j \in H^1_{\text{loc}}(\Omega_j)$, the equality of the Dirichlet traces is equivalent to the condition $u \in H^1_{\text{loc}}(\Omega)$, by Remark 3.15. If $\nabla u_j \in H_{\text{loc}}(\text{div}; \Omega_j)$, see Remark 7.1, the second interface condition ensures that $\frac{1}{\rho}\nabla u \in H_{\text{loc}}(\text{div}; \Omega)$. So (115) can be written as $\nabla \cdot (\frac{1}{\rho}\nabla u) + \frac{\omega^2}{\rho c^2}u = 0$ with $u \in H^1_{\text{loc}}(\Omega)$, in agreement with (11).

Of course, to have a well-defined BVP, together with (115) we also need boundary conditions on $\partial\Omega$ or a radiation condition if Ω is unbounded: this is what we do in the next sections.

TRANSMISSION CONDITIONS: ELECTROMAGNETISM. To describe a similar problem for electromagnetic waves, we first describe some traces of vector fields.

Remark 7.1: (Normal and tangential traces of vector fields). For a Lipschitz domain $\Omega \subset \mathbb{R}^3$, we know that $H^1(\Omega)$ functions v admit Dirichlet traces γv (in $H^{\frac{1}{2}}(\partial\Omega)$, by the trace Theorem 3.10). For vector fields $\mathbf{v} \in H^1(\Omega)^3$ we define normal and tangential traces as

$$\gamma_N \mathbf{v} := \gamma \mathbf{v} \cdot \mathbf{n}, \qquad \gamma_T \mathbf{v} := \gamma \mathbf{v} - (\gamma_N \mathbf{v})\mathbf{n} = (\mathbf{n} \times \gamma \mathbf{v}) \times \mathbf{n} \qquad \text{on } \partial\Omega, \tag{116}$$

where the scalar Dirichlet trace γ is applied componentwise. The normal trace is scalar, while the tangential trace is a vector field. Also $\gamma \mathbf{v} \times \mathbf{n} = \gamma_T \mathbf{v} \times \mathbf{n}$ is tangential on $\partial\Omega$, and is a 90-degree rotation of $\gamma_T \mathbf{v}$. The condition $\mathbf{v} \in H^1(\Omega)^3$ is not necessary: the normal trace is well-defined on $H(\mathrm{div};\Omega)$, while the tangential trace is well-defined on $H(\mathrm{curl};\Omega)$, where

$$H(\mathrm{div};\Omega) := \{\mathbf{v} \in L^2(\Omega)^3 : \mathrm{div}\,\mathbf{v} \in L^2(\Omega)\}, \qquad H(\mathrm{curl};\Omega) := \{\mathbf{v} \in L^2(\Omega)^3 : \mathrm{curl}\,\mathbf{v} \in L^2(\Omega)^3\};$$

see [SBH19, Thm. 6.1 and p. 415]. If Ω is split in two Lipschitz regions Ω_1, Ω_2 as above, then the relevant traces on the interface Σ from the two sides must agree:

$$\begin{aligned} v \in H^1(\Omega) &\implies \big(\gamma(v|_{\Omega_1})\big)|_\Sigma = \big(\gamma(v|_{\Omega_2})\big)|_\Sigma, \\ \mathbf{v} \in H(\mathrm{div};\Omega) &\implies \big(\gamma_N(\mathbf{v}|_{\Omega_1})\big)|_\Sigma = \big(\gamma_N(\mathbf{v}|_{\Omega_2})\big)|_\Sigma, \\ \mathbf{v} \in H(\mathrm{curl};\Omega) &\implies \big(\gamma_T(\mathbf{v}|_{\Omega_1})\big)|_\Sigma = \big(\gamma_T(\mathbf{v}|_{\Omega_2})\big)|_\Sigma. \end{aligned}$$

In words: for the gradient/divergence/curl of a piecewise-defined field to be well-defined and square-integrable, the Dirichlet/normal/tangential traces on the interface taken from the two sides must agree.

In two-dimensions, analogous results hold after replacing the curl operator with its 2D scalar version $\mathrm{curl}_{2D}\,\mathbf{v} := \frac{\partial v_2}{\partial x_1} - \frac{\partial v_1}{\partial x_2}$.

Now consider a time-harmonic electromagnetic wave (13) crossing two homogeneous dielectric materials with electric permittivity ϵ_1, ϵ_2 and magnetic permeability μ_1, μ_2, occupying the regions $\Omega_1, \Omega_2 \subset \mathbb{R}^3$. The transmission conditions for the electric and the magnetic fields require them to have continuous *tangential* trace (defined in (116)):

$$\begin{aligned} \mathrm{curl}\,\mathbf{E}_j - \mathrm{i}\omega\mu_j \mathbf{H}_j = \mathbf{0}, \qquad \mathrm{curl}\,\mathbf{H}_j + \mathrm{i}\omega\epsilon_j \mathbf{E}_j = \mathbf{0}, &\quad \text{in } \Omega_j, \ j \in \{1,2\}, \\ \gamma_T \mathbf{E}_1 = \gamma_T \mathbf{E}_2, \qquad \gamma_T \mathbf{H}_1 = \gamma_T \mathbf{H}_2, &\quad \text{on } \Sigma. \end{aligned} \tag{117}$$

Using that $\gamma_N(\mathrm{curl}\,\mathbf{v}) = \mathbf{n}\cdot\gamma(\mathrm{curl}\,\mathbf{v}) = \mathrm{div}_\Sigma(\gamma_T \mathbf{v} \times \mathbf{n})$ on Σ for all smooth fields $\mathbf{v}$ [Nédélec01, eq. (2.5.190–197)], where div_Σ is the tangential divergence on the (smooth) interface Σ, we obtain that

$$\gamma_N(\epsilon_1 \mathbf{E}_1) = \gamma_N(\epsilon_2 \mathbf{E}_2), \qquad \gamma_N(\mu_1 \mathbf{H}_1) = \gamma_N(\mu_2 \mathbf{H}_2), \qquad \text{on } \Sigma.$$

This means that the *normal* components of $\epsilon\mathbf{E}$ (the "displacement field" $\mathbf{D}$) and $\mu\mathbf{H}$ (sometimes called "magnetic flux density", $\mathbf{B}$) are continuous across material interfaces. So $\epsilon\mathbf{E}, \mu\mathbf{H} \in H(\mathrm{div};\Omega)$ once $\epsilon\mathbf{E}_j, \mu\mathbf{H}_j \in L^2(\Omega_j)^3$ (the divergences in Ω_j vanish by (117) and $\mathrm{div}\,\mathrm{curl} = 0$). See [BK00, §6.7.1] for a justification of the continuity of $\gamma_T\mathbf{E}, \gamma_T\mathbf{H}, \gamma_N(\epsilon\mathbf{E}), \gamma_N(\mu\mathbf{H})$ from Maxwell's equations. Eliminating $\mathbf{H}$ from (117) and passing to second-order equations, we get

$$\begin{aligned} \mathrm{curl}\,\mathrm{curl}\,\mathbf{E}_j - \omega^2\mu_j\epsilon_j\mathbf{E} = \mathbf{0} &\quad \text{in } \Omega_j, \ j \in \{1,2\}, \\ \gamma_T\mathbf{E}_1 = \gamma_T\mathbf{E}_2, \quad \gamma_N(\epsilon_1\mathbf{E}_1) = \gamma_N(\epsilon_2\mathbf{E}_2) &\quad \text{on } \Sigma. \end{aligned}$$

The natural function spaces are $\mathbf{E} \in H_{\mathrm{loc}}(\mathrm{curl};\Omega)$ and $\epsilon\mathbf{E} \in H_{\mathrm{loc}}(\mathrm{div};\Omega)$.

In a TE-mode problem such as that described in Remark 4.33, the electric field takes the form $\mathbf{E}(\mathbf{x}) = (0, 0, u(x_1, x_2))$. We can compute

$$\mathrm{i}\omega\mu\mathbf{H} = \left(\frac{\partial u}{\partial x_2}, -\frac{\partial u}{\partial x_1}, 0\right), \qquad \partial_\mathbf{n} u = \frac{\partial u}{\partial x_1}n_1 + \frac{\partial u}{\partial x_2}n_2 = \mathrm{i}\omega\mu(-H_2 n_1 + H_1 n_2) = \mathrm{i}\omega\mu(\mathbf{H} \times \mathbf{n})_3.$$

Thus, with $u_j = u|_{\Omega_j}$, we have $\frac{1}{\mu_1}\partial_\mathbf{n} u_1 = \mathrm{i}\omega(\mathbf{H} \times \mathbf{n})_3 = \frac{1}{\mu_2}\partial_\mathbf{n} u_2$ on Σ, as $\mathbf{H} \times \mathbf{n}$ is tangential on the interface Σ. So u must satisfy

$$\begin{aligned} \Delta u_j + k_j^2 u_j = 0 &\quad \text{in } \Omega_j, \ j \in \{1,2\}, \qquad k_j := \omega\sqrt{\mu_j\epsilon_j}, \\ \gamma u_1 = \gamma u_2, \quad \frac{1}{\mu_1}\partial_\mathbf{n} u_1 = \frac{1}{\mu_2}\partial_\mathbf{n} u_2 &\quad \text{on } \Sigma. \end{aligned} \tag{118}$$

Note that this is a 2-dimensional problem. Similarly, in a TM-mode the third component of the magnetic field $\mathbf{H}$ satisfies the equations (118) with μ_j replaced by ϵ_j.

TRANSMISSION CONDITIONS: HELMHOLTZ EQUATION. Comparing (115) and (118), a typical homogeneous Helmholtz transmission problem requires

$$\Delta u_j + k_j^2 u_j = 0 \quad \text{in } \Omega_j, \ j \in \{1, 2\},$$
$$\gamma u_1 = \gamma u_2, \quad \partial_{\mathbf{n}} u_1 = A \partial_{\mathbf{n}} u_2 \quad \text{on } \Sigma. \tag{119}$$

Here the normal jump contrast parameter $A > 0$ can represent one of the ratios $\frac{\rho_1}{\rho_2}$, $\frac{\mu_1}{\mu_2}$, $\frac{\epsilon_1}{\epsilon_2}$, or have a different origin. Then, the two transmission conditions in (119) correspond to the continuity of pressure and normal displacement, or the tangential continuity of electric and magnetic fields.

To write a defined scattering problem, the equations in (119) have to be complemented with boundary or radiation conditions. In the following we consider the cases where: (i) each Ω_i is half plane (§7.1.2), (ii) one region is bounded and the other is its complement (§7.1.3).

Remark 7.2: (Refractive index and conventions). In (119) the ratio of the squared wavenumbers $n := \frac{k_2^2}{k_1^2} = \frac{c_1^2}{c_2^2}$ is the **refractive index** of the second material with respect to the first one. For electromagnetic waves, $n = \frac{\epsilon_2 \mu_2}{\epsilon_1 \mu_1}$. In this way, u satisfies $\Delta u + k_1^2 n u = 0$ in Ω_2.

Here we are following the naming convention that is common in mathematics, see e.g. [CK2, p. 306], [Martin06, p. 15]. In physics, particularly in electromagnetism and optics, the refractive index is usually the *square root* of what we call n: $n_{\text{physics}} = \sqrt{n_{\text{maths}}} = \frac{k_2}{k_1} = \frac{c_1}{c_2}$, e.g. [BK00, p. 195] and Wikipedia.

7.1.2 TRANSMISSION HALF PLANE

In §4.1 we described the reflection of a plane wave hitting an impenetrable straight line. We now consider the case where the half line separates two regions with different material parameters, modelling a flat interface between two different fluids. We set some notation:

$$\Omega_\pm := \{x_2 \gtrless 0\}, \qquad \Gamma := \{x_2 = 0\}, \qquad \mathbf{n} := (0, -1), \qquad k_+, k_-, A > 0,$$

$$u^{\text{Inc}}(\mathbf{x}) = e^{ik_+ \mathbf{x} \cdot \mathbf{d}^+}, \qquad \mathbf{d}^+ = (d_1^+, d_2^+) = (\cos \varphi^+, \sin \varphi^+), \qquad -\pi < \varphi^+ < 0, \qquad d_2^+ < 0.$$

We look for a field u^{Tot} that satisfies the Helmholtz equation in $\Omega_\pm$ with wavenumber $k_\pm$ and the transmission conditions:

$$\begin{aligned}
\Delta u^{\text{Tot}} + k_+^2 u^{\text{Tot}} &= 0 && \text{in } \Omega_+, \\
\Delta u^{\text{Tot}} + k_-^2 u^{\text{Tot}} &= 0 && \text{in } \Omega_-, \\
\gamma^+ u^{\text{Tot}} &= \gamma^- u^{\text{Tot}} && \text{on } \Gamma, \\
\partial_{\mathbf{n}}^+ u^{\text{Tot}} &= A \partial_{\mathbf{n}}^- u^{\text{Tot}} && \text{on } \Gamma.
\end{aligned} \tag{120}$$
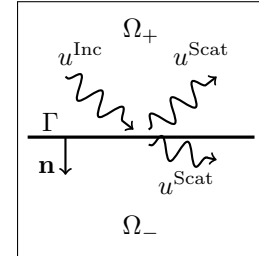
Here $A > 0$ is a parameter as in (119).

We expect that u^{Inc} generates a reflected wave in Ω_+ and a transmitted (refracted) wave in Ω_-, and that both are plane waves:

$$u^{\text{Tot}}(\mathbf{x}) = \begin{cases} u^{\text{Inc}}(\mathbf{x}) + u^{\text{Scat}}(\mathbf{x}) \\ u^{\text{Scat}}(\mathbf{x}) \end{cases} = \begin{cases} e^{ik_+(d_1^+ x_1 + d_2^+ x_2)} + \mathsf{R} e^{ik_+(d_1^+ x_1 - d_2^+ x_2)} & \mathbf{x} \in \Omega_+, \\ \mathsf{T} e^{ik_-(d_1^- x_1 + d_2^- x_2)} & \mathbf{x} \in \Omega_-. \end{cases}$$

The transmission conditions on Γ imply that $u^{\text{Scat}}(x_1, 0) = e^{ik_- d_1^- x_1}$ is proportional to $u^{\text{Inc}}(x_1, 0) = e^{ik_+ d_1^+ x_1}$, thus $d_1^- = \frac{k_+}{k_-} d_1^+$. Define d_2^- such that $|\mathbf{d}^-|^2 = (d_1^-)^2 + (d_2^-)^2 = 1$, to ensure u^{Scat} is Helmholtz solution in Ω_-. The two transmission conditions on Γ become

$$1 + \mathsf{R} = \mathsf{T}, \qquad (1 - \mathsf{R}) k_+ d_2^+ = \mathsf{T} A k_- d_2^-,$$

whose solution is

$$\mathsf{R} = \frac{k_+ d_2^+ - A k_- d_2^-}{k_+ d_2^+ + A k_- d_2^-}, \qquad \mathsf{T} = \frac{2 k_+ d_2^+}{k_+ d_2^+ + A k_- d_2^-}.$$

The reflection coefficient R and the transmission coefficient T determine the phase and the amplitude of u^{Scat} in Ω_+ and Ω_-, respectively.

If $|d_1^-| < 1$, we choose the negative root $d_2^- = -\sqrt{1 - (d_1^-)^2}$, so that u^{Scat} is a downward-propagating plane wave in Ω_- in direction $\mathbf{d}^- = (\cos \varphi_-, \sin \varphi_-)$. We have found **Snell's law of refraction**:

$$k_+ \cos \varphi^+ = k_- \cos \varphi^-.$$

The direction of propagation $\mathbf{d}^-$ of the transmitted wave depends on the ratio $\frac{k_-}{k_+}$ between the wavenumbers. The reflected wave has amplitude smaller than the incoming one: $|\mathsf{R}| < 1$.

If $|d_1^-| > 1$, then d_2^- is an imaginary number and u^{Scat} in Ω_- is an evanescent plane wave (recall §2.2.1). In this case we choose $d_2^- = -\mathrm{i}\sqrt{(d_1^-)^2 - 1}$, to ensure that $|u^{\mathrm{Scat}}| \to 0$ for $x_2 \to -\infty$. We have $|\mathsf{R}| = 1$. This is the case of **total internal reflection** and happens precisely when $k_+ > k_-$ and $\frac{k_+}{k_-}|\cos\varphi_+| > 1$, i.e. when the wavenumber is higher in the first medium than in the second, and the incoming wave is "grazing" (i.e. u^{Inc} hits Γ with a small angle). The incident angle $\varphi^+ = \arccos\frac{k_-}{k_+}$ such that $d_1^- = \pm 1$ is called **critical angle**; see Figures 33–34. We can observe total internal reflection of light when looking a flat water/air interface from the side of the water, e.g. in a calm swimming pool (this is because the light is slower in water than in air, thus $k_{\mathrm{water}} = \frac{\omega}{c_{\mathrm{water}}} > \frac{\omega}{c_{\mathrm{air}}} = k_{\mathrm{air}}$).

$$k_+ < k_- \qquad\qquad k_+ > k_-, \quad |\varphi^+| > \varphi_{\mathrm{crit}} \qquad\qquad k_+ > k_-, \quad |\varphi^+| < \varphi_{\mathrm{crit}}$$
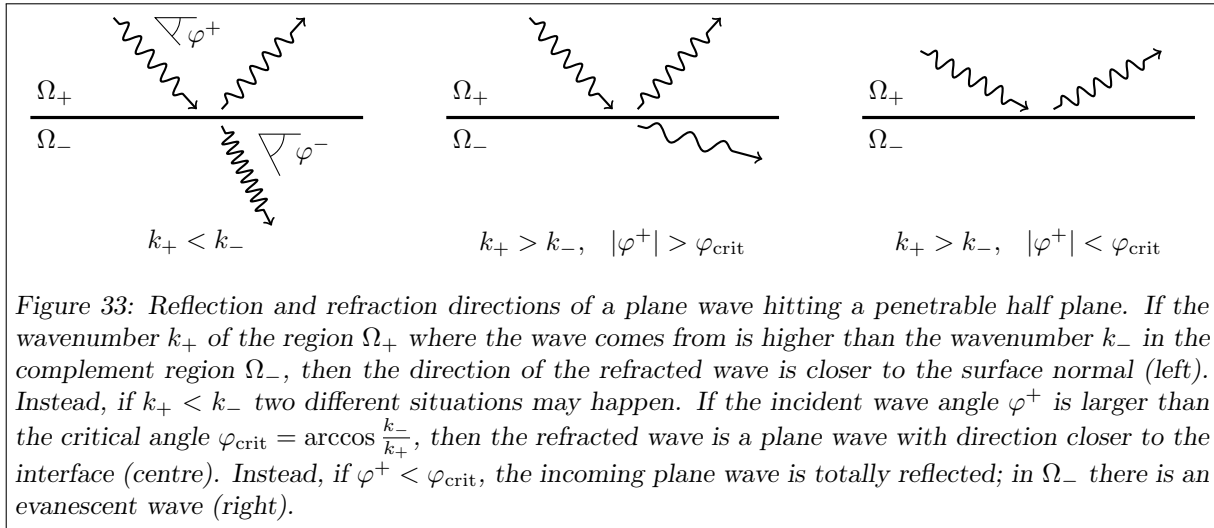
Figure 33: Reflection and refraction directions of a plane wave hitting a penetrable half plane. If the wavenumber k_+ of the region Ω_+ where the wave comes from is higher than the wavenumber k_- in the complement region Ω_-, then the direction of the refracted wave is closer to the surface normal (left). Instead, if $k_+ < k_-$ two different situations may happen. If the incident wave angle φ^+ is larger than the critical angle $\varphi_{\mathrm{crit}} = \arccos\frac{k_-}{k_+}$, then the refracted wave is a plane wave with direction closer to the interface (centre). Instead, if $\varphi^+ < \varphi_{\mathrm{crit}}$, the incoming plane wave is totally reflected; in Ω_- there is an evanescent wave (right).

We derived Snell's law for a plane wave and a flat boundary. It can be written for more general waves and non-straight interfaces, by considering the angles between the "rays" and the interface tangent plane. In this case, Snell's law is not enough to compute the exact solution of a Helmholtz transmission problem but is helpful to construct an approximation, in particular at high frequencies.

The argument in this section can be easily extended to the three-dimensional case, and, with some more work, to electromagnetic [BK00, §6.7.3] and elastic waves. Another classical extension is the case where half space is occupied by a fluid and the other half by a solid, giving the Helmholtz and Navier equations coupled by transmission conditions at the interface.

In acoustics, electromagnetism and optics, real materials have different refractive index $\frac{k_-^2}{k_+^2}$ at different wave frequencies ω. So, when light rays with different colours cross material interfaces, they are deflected by a different angles: this is why we see rainbows. This phenomenon is called **dispersion**.

Exercise 7.3: (Reflection and transmission). Verify all computations made in this section, in particular the calculation of R and T.

Exercise 7.4: (Transmission half plane implementation and general waves). Compute numerically the solution of the transmission problem described in this section and plot the solution. Test your code against Figure 34. Study the dependence on the parameters $k^\pm, A, \varphi^+$.

Extend the code to the case of a downward-propagating Herglotz u^{Inc}, similarly to Remark 4.2.

Remark 7.5: (Impedance matching). If problem (120) models two fluids with densities $\rho_\pm$ and wave speed $c_\pm$ in $\Omega_\pm$, then $A = \frac{\rho_+}{\rho_-}$ and $k_\pm = \frac{\omega}{c_\pm}$. Then the "effective impedances" are defined as $Z_\pm := \frac{\rho_\pm c_\pm}{|\sin\varphi_\pm|}$. The reflection and transmission coefficients are $\mathsf{R} = \frac{Z_- - Z_+}{Z_- + Z_+}$ and $\mathsf{T} = \frac{2Z_-}{Z_- + Z_+}$.

The waves is completely transmitted from Ω_+ to Ω_- with $\mathsf{R} = 0$ when $Z_- = Z_+$: this is called "impedance matching". In many physical settings, avoiding wave reflections important: to make planes or submarines invisible to radar and sonar, on camera lenses, to transmit electrical signals from an antenna to a cable, to transmit ultrasound into a human body during an echography. This is achieved by matching the impedances of the media where the wave propagates, see [BK00, Heller13].

Figure 34: *Field u^{Tot} generated by a plane wave $\mathrm{e}^{\mathrm{i}k_+ \mathbf{d}^+ \cdot \mathbf{x}}$ with $k_+ = 30$ and $\mathbf{d}^+ = (\cos \frac{\pi}{6}, -\sin \frac{\pi}{6})$ hitting a penetrable half space, as in §7.1.2. Top: $k_- = 60$, $A = 1$. Bottom: $k_- = 24$, $A = 1$. In the second case we have total internal reflection: in the lower half plane u^{Tot} is an evanescent wave and $|\mathsf{R}| = 1$.*
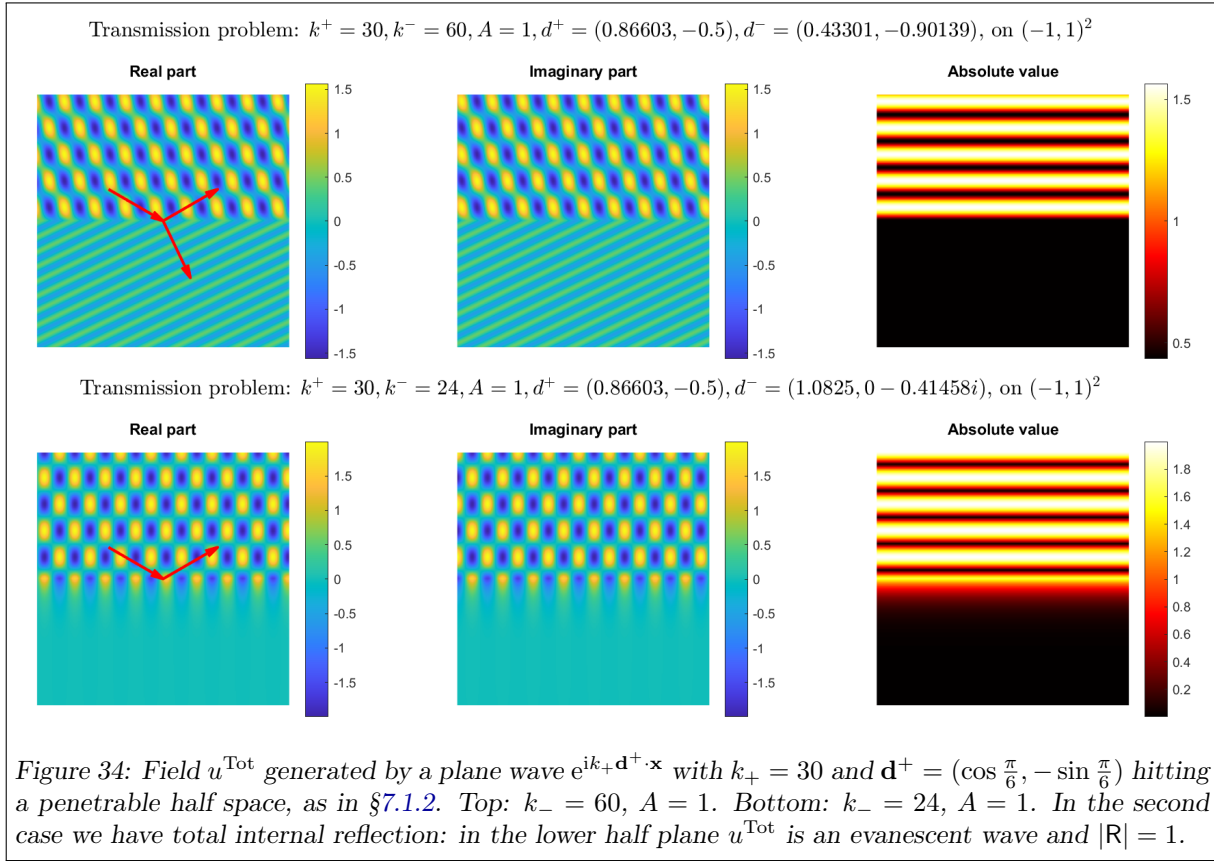
Exercise 7.6: (Many-layer transmission). Extend the analysis to the case of $L \geq 3$ layers, each with constant wavenumber, separated by horizontal lines. In other words, assume that $H_1 < \cdots < H_{L-1}$ are given numbers, and the wavenumber k is constant on the half planes $\Omega_L = \{x_2 > H_{L-1}\}$, $\Omega_1 = \{x_2 < H_1\}$ and on the $L - 2$ strips $\Omega_\ell = \{H_{\ell-1} < x_2 < H_\ell\}$ for $\ell = 2, \dots, L - 1$. Given a downward plane wave u^{Inc} in Ω_L, one has to compute one plane wave in Ω_1 and in Ω_L, and two plane waves (one upward and one downward) in each finite-height strip.

Write a linear system whose solution gives the coefficients of all these waves.

Is the system always invertible?

Exercise 7.7: (Open waveguide). Fix three numbers $k_- > k_+ > 0$ and $H > 0$. Show that the equation

$$x^2 \big(1 + \tan^2(Hx)\big) = k_-^2 - k_+^2$$

has a positive finite number of solutions $x > 0$. (The higher $k_-^2 - k_+^2$, and the higher H, the more solutions exist.) Call one of these solution $k_\star$. Observe that $k_\star^2 \leq k_-^2 - k_+^2$. Define the following field in $\mathbb{R}^2$:

$$u_\star(\mathbf{x}) := \begin{cases} \cos(k_\star H) \, \mathrm{e}^{\mathrm{i}\sqrt{k_-^2 - k_\star^2}\, x_1} \, \mathrm{e}^{-\sqrt{k_-^2 - k_+^2 - k_\star^2}\,(x_2 - H)} & x_2 > H, \\ \mathrm{e}^{\mathrm{i}\sqrt{k_-^2 - k_\star^2}\, x_1} \, \cos(k_\star x_2) & -H \leq x_2 \leq H, \\ \cos(k_\star H) \, \mathrm{e}^{\mathrm{i}\sqrt{k_-^2 - k_\star^2}\, x_1} \, \mathrm{e}^{\sqrt{k_-^2 - k_+^2 - k_\star^2}\,(x_2 + H)} & x_2 < -H \end{cases}$$

Show that $|u_\star|$ decays exponentially for $|x_2| \to \infty$, and that

$$\begin{aligned} \Delta u_\star + k_+^2 u_\star &= 0 & |x_2| &> H, \\ \Delta u_\star + k_-^2 u_\star &= 0 & |x_2| &< H, \\ u_\star &\in C^1(\mathbb{R}^2). \end{aligned}$$

Compute numerically $u_\star$ for some choices of the parameters. You can see two examples in Figure 35.

Exercise 7.7 and Figure 35 show that a wave can be "trapped" by a domain with wavenumber higher than its neighbouring regions. In this case, the domain is the strip $\{|x_2| < H\}$. This is related to total internal reflection: a wave propagating along the strip hits the interface $\{|x_2| = H\}$ with angle smaller

Figure 35: *Two propagation modes in a waveguide. In the notation of Exercise 7.7, the waveguide is* $\{|x_2| < 0.5\}$, *the wavenumbers are* $k_- = 20$ *in the waveguide and* $k_+ = 10$ *in its complement.*
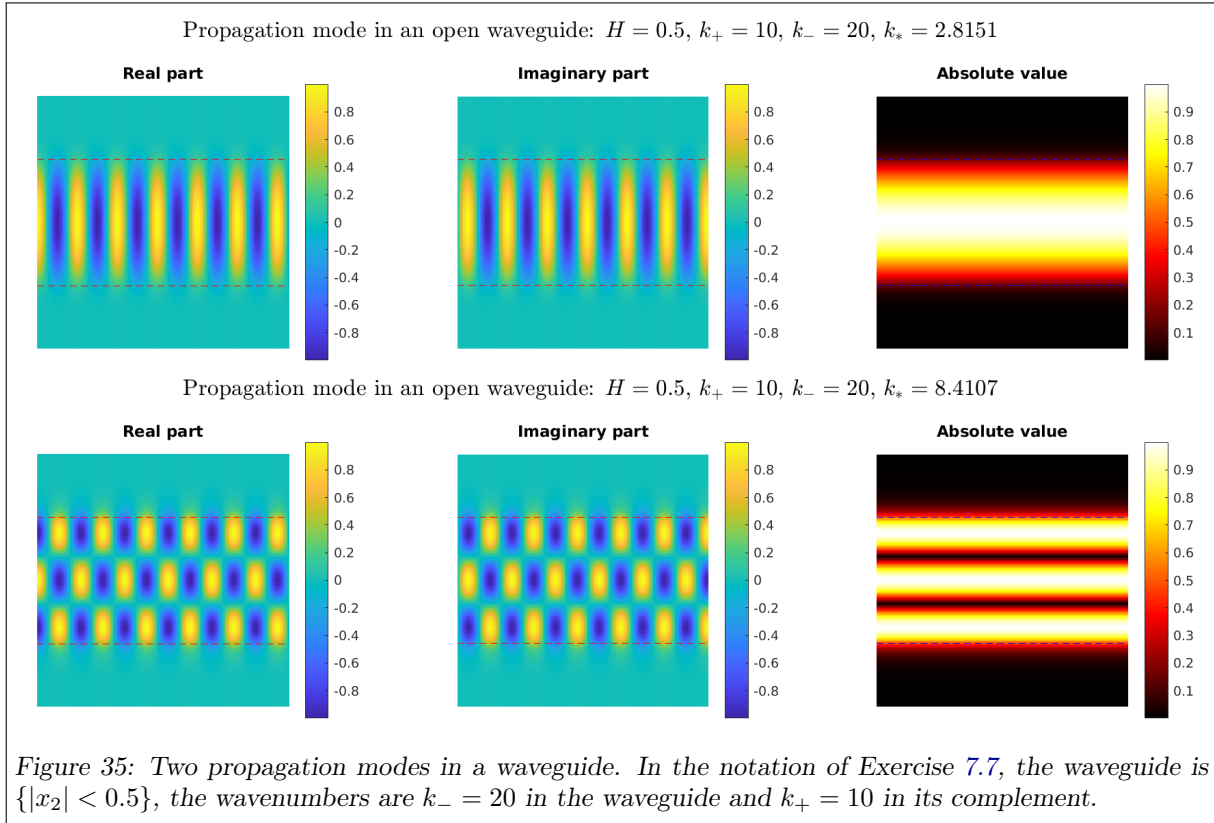
than the critical angle, so it is totally reflected back into the strip. This is the basic working principle of optical fibres [BK00, §6.8.2]. This structure is called **waveguide** and the solution $u_\star$ is a **propagation mode**. At a given frequency ω, a waveguide can support only a finite number of different propagation modes (corresponding to different values of $k_\star$). In particular, this is an "open waveguide" because the wave is contained by the refraction index variations; "closed waveguide" are e.g. those described in Remark 1.22, and satisfy impenetrable boundary conditions such as Dirichlet or Neumann on the sides of the strip.

The existence of propagation modes implies that the well-posedness analysis of transmission problems similar to (120) with more than two regions is delicate.
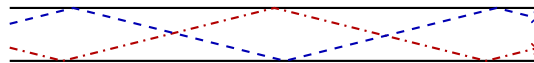
7.1.3 HELMHOLTZ TRANSMISSION PROBLEM

Consider the geometric setting introduced in §4.3 to describe scattering problems: $\Omega_- \subset \mathbb{R}^2$ a bounded, Lipschitz domain, $\Omega_+ = \mathbb{R}^2 \setminus \overline{\Omega_-}$, $\Gamma = \partial\Omega_-$, $\mathbf{n}$ unit normal on Γ pointing into Ω_+, $\gamma^\pm : H^1_{\text{loc}}(\Omega_\pm) \to H^{\frac{1}{2}}(\Gamma)$, $\partial^\pm_{\mathbf{n}} : H^1_{\text{loc}}(\Omega_\pm; \Delta) \to H^{-\frac{1}{2}}(\Gamma)$. We assume that the regions Ω_+ and Ω_- are occupied by two homogeneous fluids with different mechanical properties. Some physical examples are air bubbles in water and fog droplets in air. Fix three positive parameters: k_o, k_i denoting the wavenumbers in Ω_+ and Ω_- respectively (with the subscripts $_{o/i}$ for outer/inner), and the normal jump parameter A introduced in (119).

Assume that a wave u^{Inc} satisfying $\Delta u^{\text{Inc}} + k_o^2 u^{\text{Inc}} = 0$ in $\mathbb{R}^2$ hits the obstacle Ω_-. This generates a scattered wave u^{Scat} in Ω_+ that solves $\Delta u^{\text{Scat}} + k_o^2 u^{\text{Scat}} = 0$ and is outgoing, as in the Dirichlet case of §4.3.2. We denote the total field $u^{\text{Tot}} = u^{\text{Inc}} + u^{\text{Scat}}$ in Ω_+. However, another wave is generated inside the obstacle Ω_-: in this region we do not split it in two terms but we just consider the total field u^{Tot}, which satisfies $\Delta u^{\text{Tot}} + k_i^2 u^{\text{Tot}} = 0$ in Ω_-. Since u^{Tot} is the "physical field", e.g. the acoustic pressure or a component of the electric or magnetic field, it satisfies the transmission conditions (119): $\gamma^+ u^{\text{Tot}} = \gamma^- u^{\text{Tot}}$

and $\partial_{\mathbf{n}}^+ u^{\mathrm{Tot}} = A\partial_{\mathbf{n}}^- u^{\mathrm{Tot}}$ on Γ. Collecting the conditions on u^{Tot} we obtain

$$
\begin{aligned}
\Delta u^{\mathrm{Tot}} + k_o^2 u^{\mathrm{Tot}} = 0 && \text{in } \Omega_+, \\
\Delta u^{\mathrm{Tot}} + k_i^2 u^{\mathrm{Tot}} = 0 && \text{in } \Omega_-, \\
\gamma^+ u^{\mathrm{Tot}} - \gamma^- u^{\mathrm{Tot}} = 0 && \text{on } \Gamma, \\
\partial_{\mathbf{n}}^+ u^{\mathrm{Tot}} - A\partial_{\mathbf{n}}^- u^{\mathrm{Tot}} = 0 && \text{on } \Gamma, \\
u^{\mathrm{Tot}} - u^{\mathrm{Inc}} \text{ is radiating.}
\end{aligned}
\tag{121}
$$

This problem corresponds to (119), where one of the region is bounded and the other is its complement, with in addition the Sommerfeld radiation condition on $u^{\mathrm{Tot}} - u^{\mathrm{Inc}}$ to ensure the uniqueness of the solution. However, in view of the use of boundary integral equations, it is convenient to use as unknown a field that satisfies the radiation conditions. We set

$$
u = \begin{cases} u^{\mathrm{Scat}} = u^{\mathrm{Tot}} - u^{\mathrm{Inc}} & \text{on } \Omega_+ \\ u^{\mathrm{Tot}} & \text{on } \Omega_-. \end{cases}
\tag{122}
$$

In particular, u is radiating and satisfies the two copies of the Helmholtz equation in (121) exactly as u^{Tot}. On the other hand, u is discontinuous across the interface Γ. Substituting (122) in (121), we obtain a **Helmholtz transmission problem** (HTP, [Martin06, §1.3.3]) for u:

$$
\boxed{
\begin{aligned}
\Delta u + k_o^2 u = 0 && \text{in } \Omega_+, \\
\Delta u + k_i^2 u = 0 && \text{in } \Omega_-, \\
\gamma^+ u - \gamma^- u = g_{\mathrm{D}} && \text{on } \Gamma, \\
\partial_{\mathbf{n}}^+ u - A\partial_{\mathbf{n}}^- u = g_{\mathrm{N}} && \text{on } \Gamma, \\
u \text{ is radiating,}
\end{aligned}
}
\tag{123}
$$

where the data are

$$
g_{\mathrm{D}} = -\gamma u^{\mathrm{Inc}} \qquad \text{and} \qquad g_{\mathrm{N}} = -\partial_{\mathbf{n}} u^{\mathrm{Inc}}.
$$

These are two copies of the Helmholtz equation, with different wavenumbers, coupled to one another by imposing the values of the jumps of their Dirichlet and Neumann traces. The boundary data can also be taken to be some general $g_{\mathrm{D}} \in H^{\frac{1}{2}}(\Gamma)$, $g_{\mathrm{N}} \in H^{-\frac{1}{2}}(\Gamma)$ (recall the relation between the SSSP (45) and the EDP (44)). Problem (123) is well-posed, but the proof of this fact is not simple.
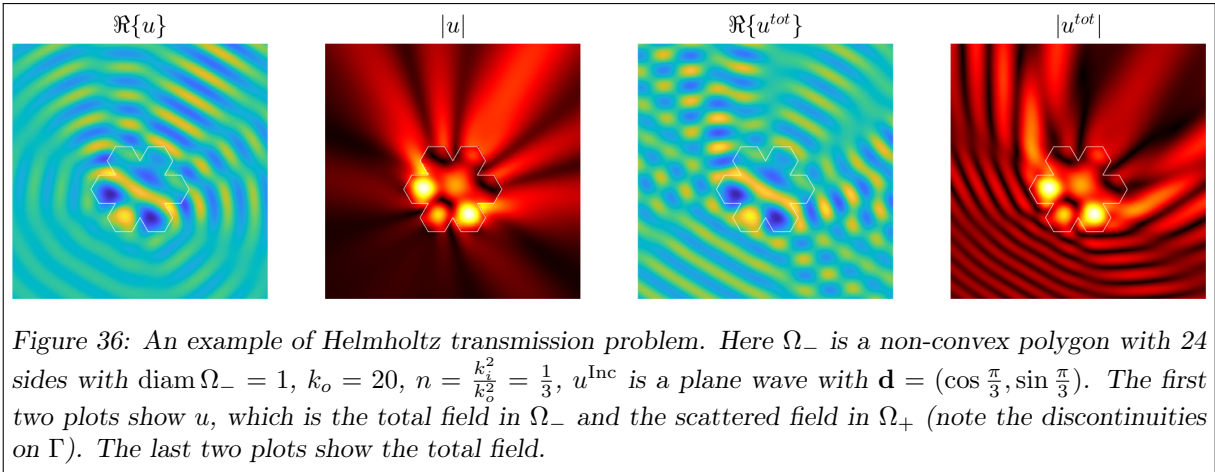
Figure 36: An example of Helmholtz transmission problem. Here Ω_- is a non-convex polygon with 24 sides with $\operatorname{diam}\Omega_- = 1$, $k_o = 20$, $n = \frac{k_i^2}{k_o^2} = \frac{1}{3}$, u^{Inc} is a plane wave with $\mathbf{d} = (\cos\frac{\pi}{3}, \sin\frac{\pi}{3})$. The first two plots show u, which is the total field in Ω_- and the scattered field in Ω_+ (note the discontinuities on Γ). The last two plots show the total field.

Exercise 7.8: (Transmission problem for the disc). Consider the transmission problem (123) when Ω_- is the disc B_R, and the source terms $g_{\mathrm{D}}, g_{\mathrm{N}}$ are the traces of an incoming plane wave u^{Inc}.

Compute the solution u analytically by separation of variables, similarly to §4.3.1.

Plot the field for different values of $k_o > k_i$ and $k_o < k_i$, see e.g. Figure 37.

In Ω_+, u has the usual Fourier–Hankel expansion, while in Ω_- it has to be expanded in a sum of smooth Fourier–Bessel functions:

$$
u(\mathbf{x}) = \begin{cases} \displaystyle\sum_{\ell \in \mathbb{Z}} a_\ell^+ H_\ell^{(1)}(k_o r) \mathrm{e}^{\mathrm{i}\ell\theta} & \text{in } \Omega_+, \\ \displaystyle\sum_{\ell \in \mathbb{Z}} a_\ell^- J_\ell(k_i r) \mathrm{e}^{\mathrm{i}\ell\theta} & \text{in } \Omega_-. \end{cases}
$$

The same-index coefficients a_ℓ^+ and a_ℓ^- of the two expansions are coupled by the two jump conditions on Γ. You need to compute the first derivatives of Bessel and Hankel functions, using e.g. [DLMF, eq. 10.6.1].
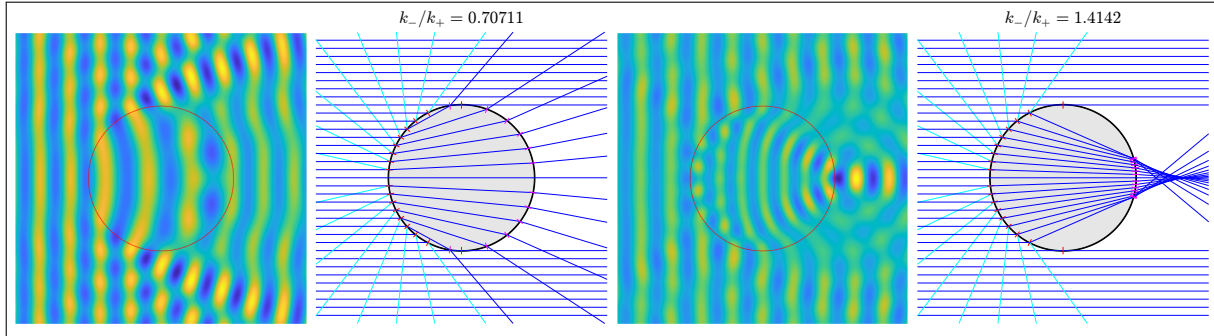
Figure 37: *Helmholtz transmission problems for a disc. A plane wave with $k_o = 15$ hits a penetrable unit disc from the left. The refractive index in the disc is $n = \frac{k_i^2}{k_o^2} = \frac{1}{2}$ (left) and $n = 2$ (right). We show the real part of the total field u^{Tot} and some rays refracted according to Snell's law. The light blue lines are the reflected rays. We do not show the reflection of the refracted rays when they hit Γ from Ω_-. The little red segments are normal to the disc boundary. Note that for $n = \frac{1}{2}$ some rays do not refract: this is an example of total reflection.*
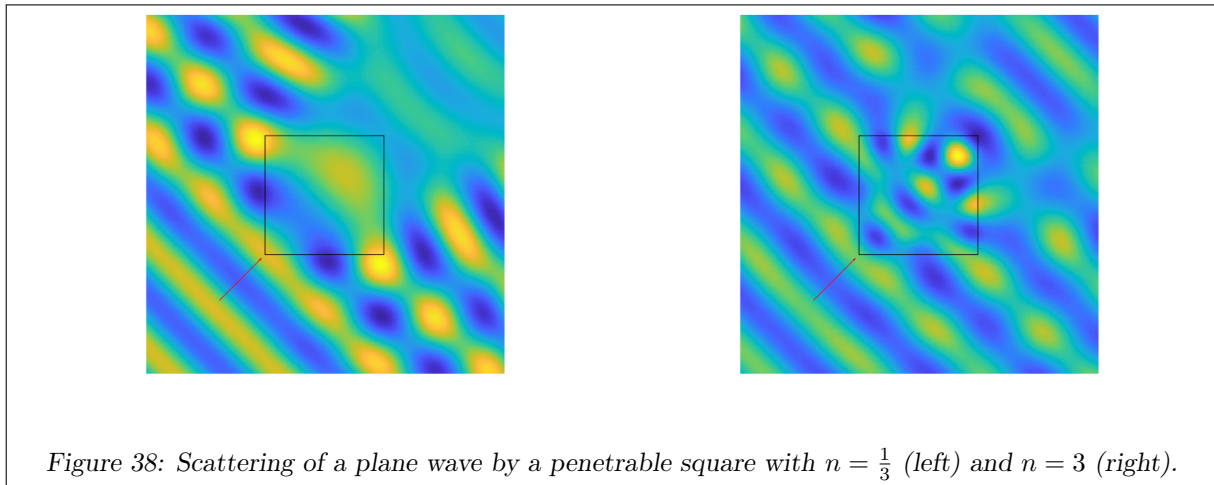
Figure 38: *Scattering of a plane wave by a penetrable square with $n = \frac{1}{3}$ (left) and $n = 3$ (right).*

Observing Figures 37 and 38, we see that if $k_i > k_o$ (i.e. $n > 1$) the obstacle can focus the wave in a region: this is how lenses work. Indeed, glass has higher refractive index than air. We can understand this by tracing rays and applying Snell's law when they cross Γ.

Exercise 7.9: (Transmission quasi-resonances). Compute and plot the solutions of the Helmholtz transmission problems for the unit disc $\Omega_- = B_1$, refractive index $n = 100$ (so $k_i = 10k_o$), and wavenumbers $k_o = 1.77945199481921$ and $k_o = 1.779451994815$. Use the Fourier expansion developed in Exercise 7.8.

The two wavenumbers differ by a relative factor of about $2.4 \cdot 10^{-12}$, but the solutions u are completely different (see in particular the magnitude of u). Can you explain why?

7.1.4 BIEs for the Helmholtz transmission problem

The HTP (123) can be written as an integral equation. Since two wavenumbers are involved we need to use two copies of each BIO: we write $S_o, S_i, D_o, D_i, D'_o, D'_i, H_o, H_i$ for the four BIOs with $k = k_o$ and $k = k_i$. We recall the Cauchy traces and the Calderón projectors of Exercise 5.33

$$\gamma_C^\pm := (\gamma^\pm, \partial_{\mathbf{n}}^\pm) \ : \ H_{\mathrm{loc}}^1(\Omega_\pm; \Delta) \to \mathcal{H}, \qquad \text{where } \mathcal{H} := H^{\frac{1}{2}}(\Gamma) \times H^{-\frac{1}{2}}(\Gamma),$$

$$P_{o/i}^\pm : \mathcal{H} \to \mathcal{H}, \qquad P_{o/i}^\pm := \frac{1}{2}I \pm \begin{pmatrix} D_{o/i} & -S_{o/i} \\ H_{o/i} & -D'_{o/i} \end{pmatrix}.$$

The key property of Calderón projectors is (82): their kernels characterize the traces of outer and inner Helmholtz solutions. In particular, for u solution of (123),

$$P_i^+ \boldsymbol{\gamma}_C^- u = P_o^- \boldsymbol{\gamma}_C^+ u = \mathbf{0}. \tag{124}$$

Introduce $M := \begin{pmatrix} 1 & 0 \\ 0 & A \end{pmatrix} \in \mathbb{R}^{2 \times 2}$ and $\mathbf{g} := \begin{pmatrix} g_{\mathrm{D}} \\ g_{\mathrm{N}} \end{pmatrix} \in \mathcal{H}$, so that the transmission condition in (123) reads

$$\boldsymbol{\gamma}_C^+ u - M \boldsymbol{\gamma}_C^- u = \mathbf{g}.$$

Applying P_o^- to this condition, (124) gives

$$-P_o^- M \boldsymbol{\gamma}_C^- u = P_o^- (\boldsymbol{\gamma}_C^+ u - M \boldsymbol{\gamma}_C^- u) = P_o^- \mathbf{g}. \tag{125}$$

Define the two operators $B_{\mathrm{I}}, B_{\mathrm{II}} : \mathcal{H} \to \mathcal{H}$

$$B_{\mathrm{I}} := P_o^- M - M P_i^+ = \begin{pmatrix} -D_o - D_i & A S_o + S_i \\ -H_o - A H_i & A D_o' + A D_i' \end{pmatrix},$$

$$B_{\mathrm{II}} := P_o^- M + M P_i^+ = M + \begin{pmatrix} -D_o + D_i & A S_o - S_i \\ -H_o + A H_i & A D_o' - A D_i' \end{pmatrix}.$$

Applying these two operators to $\boldsymbol{\gamma}_C^- u$ and using (124)–(125) we have

$$\boxed{B_{\mathrm{I}} \boldsymbol{\gamma}_C^- u = -P_o^- \mathbf{g}, \qquad B_{\mathrm{II}} \boldsymbol{\gamma}_C^- u = -P_o^- \mathbf{g}.} \tag{126}$$

These are two BIEs for the transmission problem (123). They are direct BIEs, because the unknown is $\boldsymbol{\gamma}_C^- u$, which is a trace of the HTP solution. The operators B_{I} and B_{II} are of the first and second kind, respectively, as only the second has the M term summed to the layer potentials. These two BIEs are called PMCHWT (Poggio–Miller–Chang–Harrington–Wu–Tsai) and Müller formulations, respectively. Both operators $B_{\mathrm{I}}, B_{\mathrm{II}} : \mathcal{H} \to \mathcal{H}$ are bounded and invertible; B_{II} is also a Fredholm operator[68]. Many other BIEs are possible for the HTP (123), [Martin06, §6.2] [69].

If the data come from an incoming wave, i.e. $\mathbf{g} = -\boldsymbol{\gamma}_C u^{\mathrm{Inc}}$, or equivalently $g_{\mathrm{D}} = -\gamma u^{\mathrm{Inc}}$ and $g_{\mathrm{N}} = -\partial_{\mathbf{n}} u^{\mathrm{Inc}}$, then $P_o^- \mathbf{g} = \mathbf{g}$ and the right-hand side of both BIEs in (126) further simplifies.

Once the BIE solution $\boldsymbol{\gamma}_C^- u$ is known, then $\boldsymbol{\gamma}_C^+ u$ can be computed by the transmission condition, and u can be computed in $\Omega_\pm$ by Green's representation formulas (73), using k_o and k_i appropriately.

An important difference between (126) and the BIEs for the exterior problems in §6.2 (including (58)) is that the unknown of (126) is composed of two scalar fields on Γ: $\boldsymbol{\gamma}_C^- u = (\gamma^- u, \partial_{\mathbf{n}}^- u) \in \mathcal{H}$. Since $\mathcal{H} = H^{\frac{1}{2}}(\Gamma) \times H^{-\frac{1}{2}}(\Gamma)$, a typical low-order BEM discretisation of (126) uses piecewise-constant functions for the first variable and continuous piecewise-linear for the second one, or continuous piecewise-linear for both.

Remark 7.10: (Variational form of the transmission BIEs). Recall that in §3.3.3 we introduced the duality product $\langle v, w \rangle_\Gamma$ that extends the $L^2(\Gamma)$ scalar product $\int_\Gamma v \overline{w} \, \mathrm{d}s$ to $v \in H^{\frac{1}{2}}(\Gamma), w \in H^{-\frac{1}{2}}(\Gamma)$ or to $v \in H^{-\frac{1}{2}}(\Gamma), w \in H^{\frac{1}{2}}(\Gamma)$. For $\psi = (\psi_1, \psi_2), \xi = (\xi_1, \xi_2) \in \mathcal{H} = H^{\frac{1}{2}}(\Gamma) \times H^{-\frac{1}{2}}(\Gamma)$, we define the duality $\langle \psi, \xi \rangle_{\mathcal{H} \times \mathcal{H}} := \langle \psi_1, \xi_2 \rangle + \langle \psi_2, \xi_1 \rangle$, which extends the $L^2(\Gamma)^2$ scalar product $\int_\Gamma (\psi_1 \overline{\xi}_2 + \psi_2 \overline{\xi}_1) \, \mathrm{d}s$. Note that the (possibly) singular distributions $\psi_2, \xi_2 \in H^{-\frac{1}{2}}(\Gamma)$ are paired with the more regular ones in $\xi_1, \psi_1 \in H^{\frac{1}{2}}(\Gamma)$.

The variational formulation of the first-kind BIE in (126) with $\mathbf{g} = -\boldsymbol{\gamma}_C u^{\mathrm{Inc}}$ consists in finding $\psi = (\psi_1, \psi_2) \in \mathcal{H}$ such that

$$\langle B_{\mathrm{I}} \psi, \xi \rangle_{\mathcal{H} \times \mathcal{H}} = \langle -D_o \psi_1 - D_i \psi_1 + A S_o \psi_2 + S_i \psi_2, \, \xi_2 \rangle_\Gamma + \langle -H_o \psi_1 - A H_i \psi_1 + A D_o' \psi_2 + A D_i' \psi_2, \, \xi_1 \rangle_\Gamma$$
$$= -\langle \gamma u^{\mathrm{Inc}}, \xi_2 \rangle_\Gamma - \langle \partial_{\mathbf{n}} u^{\mathrm{Inc}}, \xi_1 \rangle_\Gamma = \langle \mathbf{g}, \xi \rangle_{\mathcal{H} \times \mathcal{H}} \qquad \forall \xi = (\xi_1, \xi_2) \in \mathcal{H}.$$

The similar formula for the second-kind BIE is $\langle B_{\mathrm{II}} \psi, \xi \rangle_{\mathcal{H} \times \mathcal{H}} = \langle \mathbf{g}, \xi \rangle_{\mathcal{H} \times \mathcal{H}} \, \forall \xi \in \mathcal{H}$, or equivalently

$$\langle \psi_1 - D_o \psi_1 + D_i \psi_1 + A S_o \psi_2 - S_i \psi_2, \, \xi_2 \rangle_\Gamma + \langle -H_o \psi_1 + A H_i \psi_1 + A \psi_2 + A D_o' \psi_2 - A D_i' \psi_2, \, \xi_1 \rangle_\Gamma$$
$$= -\langle \gamma u^{\mathrm{Inc}}, \xi_2 \rangle_\Gamma - \langle \partial_{\mathbf{n}} u^{\mathrm{Inc}}, \xi_1 \rangle_\Gamma \qquad \forall \xi = (\xi_1, \xi_2) \in \mathcal{H}.$$

---

[68] [Hiptmair, Moiola, Spence, Spurious quasi-resonances in boundary integral equations for the Helmholtz transmission problem, SIAM 2022]

[69] [van't Wout, Haqshenas, Gélat, Betcke, Saffari, Boundary integral formulations for acoustic modelling of high-contrast media, CAMWA 2022; Benchmarking preconditioned boundary integral formulations for acoustics, IJNME 2021]

We can pose both problems in the smoother space $H^1(\Gamma) \times L^2(\Gamma)$: this allows to avoid fractional-exponent spaces and write duality products as integrals. We look for $\boldsymbol{\psi} = (\psi_1, \psi_2)$ in this space such that one of the following holds:

$$\int_\Gamma \left[(-D_o\psi_1 - D_i\psi_1 + AS_o\psi_2 + S_i\psi_2)\overline{\xi}_2 + (-H_o\psi_1 - AH_i\psi_1 + AD_o'\psi_2 + AD_i'\psi_2)\overline{\xi}_1 \right] \mathrm{d}s$$

$$= \int_\Gamma \left[-\gamma u^{\mathrm{Inc}}\overline{\xi}_2 - \partial_\mathbf{n} u^{\mathrm{Inc}}\overline{\xi}_1 \right] \mathrm{d}s \qquad \forall \boldsymbol{\xi} = (\xi_1, \xi_2) \in H^1(\Gamma) \times L^2(\Gamma),$$

$$\int_\Gamma \left[(\psi_1 - D_o\psi_1 + D_i\psi_1 + AS_o\psi_2 - S_i\psi_2)\overline{\xi}_2 + (-H_o\psi_1 + AH_i\psi_1 + A\psi_2 + AD_o'\psi_2 - AD_i'\psi_2)\overline{\xi}_1 \right] \mathrm{d}s$$

$$= \int_\Gamma \left[-\gamma u^{\mathrm{Inc}}\overline{\xi}_2 - \partial_\mathbf{n} u^{\mathrm{Inc}}\overline{\xi}_1 \right] \mathrm{d}s \qquad \forall \boldsymbol{\xi} = (\xi_1, \xi_2) \in H^1(\Gamma) \times L^2(\Gamma).$$

The Galerkin approximation of the BIEs (126) with a discrete space $V_N \subset H^1(\Gamma) \times L^2(\Gamma)$ relies on these formulations.

7.2 NON-PIECEWISE-CONSTANT MATERIALS

In §7.1 we have considered waves propagating in two different homogeneous media. This can be extended to a finite number of materials. However, often the properties of the material where the wave propagates change continuously. Examples are acoustic waves in the atmosphere, where air density and pressure vary with height and temperature, or in the oceans, where water density depends on salinity, temperature and depth[70].

As mentioned in Remark 1.15, time-harmonic acoustic waves in heterogeneous media satisfy the Bergmann equation [Martin06, eq. (1.27)]:

$$\mathrm{div}\left(\frac{1}{\rho_0(\mathbf{x})} \nabla u(\mathbf{x}) \right) + \frac{k^2 n(\mathbf{x})}{\rho_0(\mathbf{x})} u(\mathbf{x}) = 0, \qquad n(\mathbf{x}) = \frac{c_0^2}{c^2(\mathbf{x})}. \tag{127}$$

Here ρ_0 is the fluid static density (i.e. when the fluid is not acoustically perturbed), c_0 a constant reference wave speed, c the local wave speed, $k = \frac{\omega}{c_0}$ the reference wavenumber, n the refractive index, and the unknown u is the acoustic pressure.[71]

In the following we consider the Bergmann equation (127), and, for simplicity, we assume that ρ_0 is constant. The heterogeneity in the material, which determines refraction and scattering, is completely described by the refractive index n. We assume that

$$n \in L^\infty(\mathbb{R}^2), \qquad n > 0, \qquad \mathrm{supp}(n-1) \text{ is compact.}$$

The last condition means that the medium is homogeneous with $n = 1$ outside of a sufficiently large ball. The datum is u^{Inc}, which is solution of the constant-coefficient Helmholtz equation $\Delta u^{\mathrm{Inc}} + k^2 u^{\mathrm{Inc}} = 0$. Then we seek u^{Tot} such that

$$\Delta u^{\mathrm{Tot}} + k^2 n\, u^{\mathrm{Tot}} = 0 \qquad \text{in } \mathbb{R}^2,$$

$$u^{\mathrm{Tot}} - u^{\mathrm{Inc}} \text{ is radiating.}$$

This problem is studied in detail in [CK2, Ch. 8].[72] Defining, as usual, $u^{\mathrm{Scat}} = u^{\mathrm{Tot}} - u^{\mathrm{Inc}}$, this field satisfies the Helmholtz equation with a source term and the Sommerfeld radiation condition:

$$\boxed{\begin{aligned} \Delta u^{\mathrm{Scat}} + k^2 n\, u^{\mathrm{Scat}} &= -f \qquad \text{in } \mathbb{R}^2, \qquad \text{with } f := k^2(n-1)u^{\mathrm{Inc}}, \\ u^{\mathrm{Scat}} &\text{ is radiating.} \end{aligned}} \tag{128}$$

Proceeding as in §4.4.2, a variational formulation of this problem is:
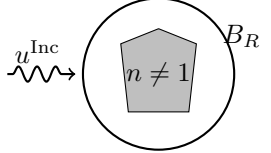
find $\quad u^{\mathrm{Scat}} \in H^1(B_R) \quad$ such that $\quad \mathcal{A}_n(u^{\mathrm{Scat}}, w) = \mathcal{F}_n(w) \quad \forall w \in H^1(B_R), \quad$ where $\qquad$ (129)

---

[70][Jensen, Kuperman, Porter, Schmidt, Computational ocean acoustics, Springer 2011]

[71]Analogously, from (13), time-harmonic electromagnetic waves in media with variable electric permittivity ϵ, magnetic permeability μ and conductivity σ, satisfy

$$\mathrm{curl}\left(\mu^{-1} \mathrm{curl}\,\mathbf{E} \right) - (\omega^2\epsilon + \mathrm{i}\omega\sigma)\mathbf{E} = \mathbf{0}, \qquad \text{or, equivalently,} \qquad \mathrm{curl}\left((\epsilon - \mathrm{i}\sigma/\omega)^{-1} \mathrm{curl}\,\mathbf{H} \right) - \omega^2\mu\mathbf{H} = \mathbf{0}.$$

[72]See also Chapter 7 of [Kirsch, An introduction to the mathematical theory of inverse problems, Springer 2021].

$$\mathcal{A}_n(u^{\text{Scat}}, w) := \int_{B_R} (\nabla u^{\text{Scat}} \nabla \overline{w} - k^2 n\, u^{\text{Scat}} \overline{w})\, d\mathbf{x} - \int_{\partial B_R} (\text{DtN}\gamma u^{\text{Scat}})(\gamma \overline{w})\, ds,$$

$$\mathcal{F}_n(w) := \int_{B_R} f \overline{w}\, d\mathbf{x}.$$

Here B_R is a ball of radius $R > 0$ centred at the origin such that $\text{supp}(n-1) \subset B_R$, and the DtN map is defined in (50).

Exercise 7.11: (The variable-index problem is well-posed). Using §4.4.3, show the Gårding inequality

$$\Re\{\mathcal{A}_n(w,w)\} \geq \|w\|^2_{L^2(B_R)^2} - k^2 \|n\|_{L^\infty(\mathbb{R}^2)} \|w\|^2_{L^2(B_R)} \qquad \forall w \in H^1(B_R).$$

Following §4.4, deduce that the problem (129) is well-posed.

We observe that the problem is well-posed also if n is complex with non-negative imaginary part, i.e. when some part of the domain is occupied by absorbing materials; recall Exercise 1.14.

Exercise 7.12: (Relation with the transmission problem). Write the HTP (123), with $A = 1$, $g_D = -\gamma u^{\text{Inc}}$ and $g_N = -\partial_{\mathbf{n}} u^{\text{Inc}}$, in the form of problem (128).

7.2.1 The Lippmann–Schwinger equation

Recall the volume (or Newton) potential operator (71) $(\mathcal{V}f)(\mathbf{y}) = \int_{\mathbb{R}^2} \Phi_k(\mathbf{x}, \mathbf{y}) f(\mathbf{x})\, d\mathbf{x}$, and that, for all compactly supported f, $\mathcal{V}f$ is radiating and $(\Delta + k^2)\mathcal{V}f = -f$.

Since $\Delta u^{\text{Scat}} + k^2 u^{\text{Scat}} = k^2(1-n)u^{\text{Tot}}$ and u^{Scat} is radiating, we have

$$u^{\text{Scat}} = k^2 \mathcal{V}\big((n-1)u^{\text{Tot}}\big).$$

Expanding $u^{\text{Tot}} = u^{\text{Inc}} + u^{\text{Scat}}$, we obtain

$$u^{\text{Scat}} + k^2 \mathcal{V}\big((1-n)u^{\text{Scat}}\big) = k^2 \mathcal{V}\big((n-1)u^{\text{Inc}}\big). \tag{130}$$

Summing u^{Inc} to both sides in one of these identities, we have

$$\boxed{u^{\text{Tot}} + k^2 \mathcal{V}\big((1-n)u^{\text{Tot}}\big) = u^{\text{Inc}}.} \tag{131}$$

Equations (130) and (131) are two versions of the **Lippmann–Schwinger equation**; [CK2, eq. (8.13)], [Martin06, §6.3.3]. In both (130) and (131) the argument of $\mathcal{V}$ is compactly supported, because $n = 1$ outside of a compact region.

The Lippmann–Schwinger equation is again an integral equation, but it is not a BIE, as it is not posed on a boundary. It is an example of **volume integral equation (VIE)**. Equations (130) and (131) are weakly-singular, second-kind VIEs.

Exercise 7.13: (Far-field pattern for heterogeneous media). Recall the definition (46) of the far-field pattern u_∞ of a radiating Helmholtz solution u. Recall that it can be computed from formula (47) for any Lipschitz boundary Γ such that u is a homogeneous Helmholtz solution in the region exterior to Γ.

Show that the far-field pattern of the solution u^{Scat} of problem (128) can be computed as

$$u_\infty(\theta) = \frac{e^{i\frac{\pi}{4}}}{\sqrt{8\pi k}} \int_\Omega k^2\big(n(\mathbf{x}) - 1\big) u^{\text{Tot}}(\mathbf{x}) e^{-ik\mathbf{x}\cdot\mathbf{d}}\, d\mathbf{x} \qquad \mathbf{d} = (\cos\theta, \sin\theta).$$

See [CK2, eq. (8.28)] for the corresponding formula in 3D.

7.2.2 Numerical approximation of the Lippmann–Schwinger equation

Either version of the Lippmann–Schwinger equation can be approximated with a collocation or a Galerkin scheme. Here we only consider the equation (131) for the total field. Let $\Omega \subset \mathbb{R}^2$ be a bounded domain that contains $\text{supp}(n-1)$, for instance a rectangle. Let V_N be a finite-dimensional subspace of $L^2(\Omega)$ with basis $\{\varphi_1, \ldots, \varphi_N\}$. Fix N points $\mathbf{x}_1, \ldots, \mathbf{x}_N$ in Ω. Then the collocation method applied to (131) consists in finding

$$\psi_N \in V_N \qquad \text{such that} \qquad \psi_N(\mathbf{x}_j) + k^2 \mathcal{V}\big((1-n)\psi_N\big)(\mathbf{x}_j) = u^{\text{Inc}}(\mathbf{x}_j) \qquad \forall j = 1, \ldots, N.$$

As in §5.2, expanding $\psi_N = \sum_{m=1}^{N} \Psi_m \varphi_m$, the vector $\boldsymbol{\Psi} = (\Psi_1, \ldots, \Psi_N) \in \mathbb{C}^N$ solves the $N \times N$ linear system $\underline{\underline{\mathbf{A}}}^{\mathrm{Col}} \boldsymbol{\Psi} = \mathbf{F}^{\mathrm{Col}}$, where

$$A_{j,m}^{\mathrm{Col}} = \varphi_m(\mathbf{x}_j) + \mathcal{V}\big((1-n)\varphi_m\big)(\mathbf{x}_j) = \varphi_m(\mathbf{x}_j) + \int_{\mathbb{R}^2} \Phi_k(\mathbf{x}_j, \mathbf{y})\big(1 - n(\mathbf{y})\big)\varphi_m(\mathbf{y})\,\mathrm{d}\mathbf{y}, \qquad F_j^{\mathrm{Col}} = u^{\mathrm{Inc}}(\mathbf{x}_j).$$

The integral has to be computed only on the intersection between the support of $(1-n)$ and that of φ_m. If V_N is chosen as the space of piecewise-constant functions on a mesh $\mathcal{T}_N = \{K_1, \ldots, K_N\}$ that partitions Ω, with the obvious basis ($\varphi_m = 1$ on K_m and 0 elsewhere), then the collocation matrix reduces to

$$A_{j,m}^{\mathrm{Col}} = \delta_{j,m} + \int_{K_m} \Phi_k(\mathbf{x}_j, \mathbf{y})\big(1 - n(\mathbf{y})\big)\,\mathrm{d}\mathbf{y}. \tag{132}$$

As for the BEM, for stability purposes it is often preferable to take more collocation points than basis functions, and solve the resulting overdetermined system in the least squares sense (oversampling).

To write a Galerkin discretisation of the Lippmann–Schwinger equation (131), we first write a variational formulation:

$$\text{find} \quad u^{\mathrm{Tot}} \in L^2(\Omega) \quad \text{such that} \quad \mathcal{A}_{\mathrm{LS}}(u^{\mathrm{Tot}}, w) = \mathcal{F}_{\mathrm{LS}}(w) \quad \forall w \in L^2(\Omega) \quad \text{where} \tag{133}$$

$$\mathcal{A}_{\mathrm{LS}}(u, w) := \int_\Omega \left(u\overline{w} + k^2 \mathcal{V}\big((1-n)u\big)\overline{w} \right) \mathrm{d}\mathbf{x}$$
$$= \int_\Omega \left(u(\mathbf{x})\overline{w}(\mathbf{x}) + k^2 \int_\Omega \Phi_k(\mathbf{x}, \mathbf{y})\big(1 - n(\mathbf{y})\big)u(\mathbf{y})\,\mathrm{d}\mathbf{y}\,\overline{w}(\mathbf{x}) \right) \mathrm{d}\mathbf{x},$$
$$\mathcal{F}_{\mathrm{LS}}(w) := \int_\Omega u^{\mathrm{Inc}}\overline{w}\,\mathrm{d}\mathbf{x}.$$

The Galerkin approximation of (133) consists in finding $\psi_N \in V_N$ such that $\mathcal{A}_{\mathrm{LS}}(\psi_N, \xi_N) = \mathcal{F}_{\mathrm{LS}}(\xi_N)$ for all $\xi_N \in V_N$. In matrix form, the coefficient vector $\boldsymbol{\Psi} \in \mathbb{C}^N$ of ψ_N satisfies the linear system $\underline{\underline{\mathbf{A}}}^{\mathrm{Gal}} \boldsymbol{\Psi} = \mathbf{F}^{\mathrm{Gal}}$, where

$$A_{j,m}^{\mathrm{Gal}} = \int_\Omega \left(\varphi_m(\mathbf{x})\overline{\varphi}_j(\mathbf{x}) + k^2 \int_\Omega \Phi_k(\mathbf{x}, \mathbf{y})\big(1 - n(\mathbf{y})\big)\varphi_m(\mathbf{y})\,\mathrm{d}\mathbf{y}\,\overline{\varphi}_j(\mathbf{x}) \right) \mathrm{d}\mathbf{x}, \qquad F_j^{\mathrm{Gal}} = \int_\Omega u^{\mathrm{Inc}}\overline{\varphi}_j\,\mathrm{d}\mathbf{x}.$$

Choosing a piecewise-constant discrete space, with the same basis and notation above, this reduces to

$$A_{j,m}^{\mathrm{Gal}} = |K_j|\delta_{j,m} + k^2 \int_{K_j} \int_{K_m} \Phi_k(\mathbf{x}, \mathbf{y})\big(1 - n(\mathbf{y})\big)\,\mathrm{d}\mathbf{y}\,\mathrm{d}\mathbf{x}, \qquad F_j^{\mathrm{Gal}} = \int_{K_j} u^{\mathrm{Inc}}\,\mathrm{d}\mathbf{x}. \tag{134}$$

The collocation and the Galerkin methods for the VIEs lead to dense matrices. However, VIEs do not enjoy the dimensional reduction of BIEs: to solve a 2D problem we need to discretise a 2D domain. So we have disadvantages compared to both FEM and BEM. On the other hand, VIEs can be used for arbitrary (non-piecewise-constant) heterogeneous materials, differently from BIEs and BEMs, and their solutions automatically satisfy the radiation condition, differently from FEM.

Similarly to the BEM described in §5.2, a crucial part of the method consists in computing the weakly singular integrals entering the matrices. For the Lippmann–Schwinger equation (131) in two dimensions, collocation requires 2D integrals and Galerkin requires 4D integrals: the dimension is higher than for the BEM. Techniques similar to those seen in §5.2.1 to deal with the singularities of the fundamental solution apply also in this case.

Once one has computed an approximation ψ_N of u^{Tot} in Ω, then one can evaluate u^{Tot} or u^{Scat} in the unbounded complement $\mathbb{R}^2 \setminus \Omega$ using again (131), and recalling that $\mathcal{V}$ acts on a function supported in Ω. So there is no need for another representation formula (such as (59) for (58)).

A different strategy to approximate (128) consists in coupling a finite element method on the bounded region Ω and a method to approximate a BIE on $\partial\Omega$, [CK2, §8.7].

In this section we have considered the Bergmann equation (127) with constant density ρ_0, i.e. $\Delta u + k^2 n u = 0$. The Lippmann–Schwinger equation can be extended to the more general case $\mathrm{div}(a\nabla u) + k^2 n u = 0$ for variable a, n. In this case we obtain integro-differential equations.[73]

VIEs for the scattering of electromagnetic waves by heterogeneous materials are considerably more complicated than for acoustic waves. In particular, the volume potential operator relative to the Maxwell equations has a stronger singularity than $\mathcal{V}$. The approximation of $\mathrm{curl}\,\mu^{-1}\,\mathrm{curl}\,\mathbf{E} - (\omega^2\epsilon + \mathrm{i}\omega\sigma)\mathbf{E} = \mathbf{0}$ with

---

[73][Costabel, On the spectrum of volume integral operators in acoustic scattering, 2015]
[Martin, Acoustic scattering by inhomogeneous obstacles, SIAM 2003]

a collocation method, piecewise-constant basis functions, a single-point quadrature rule for off-diagonal matrix terms, and a special recipe for diagonal terms is called "discrete dipole approximation" (DDA)[74], and is very popular in optics, atmospheric sciences, and astrophysics.

Remark 7.14: (Born approximation and series). For any linear operator T on a Banach space, such that its **Neumann series** $\sum_{j=0}^\infty T^j$ converges in the operator norm, we have

$$(I - T) \sum_{j=0}^n T^j = \sum_{j=0}^n T^j - \sum_{j=0}^n T^{j+1} = I - T^{n+1} \xrightarrow{n \to \infty} I \qquad \Longrightarrow \qquad (I - T)^{-1} = \sum_{j=0}^\infty T^j.$$

The convergence of the Neumann series is guaranteed if $\|T\| < 1$, or more generally if $\sum_{j=0}^\infty \|T^j\| < \infty$.

The VIE (131) can be written in operator form as

$$u^{\text{Tot}} - A u^{\text{Tot}} = u^{\text{Inc}}, \quad \text{where} \quad A : w \mapsto -k^2 \mathcal{V}((1-n)w).$$

Consider the sequence

$$u_0 = u^{\text{Inc}}, \qquad u_j = u^{\text{Inc}} + A u_{j-1} = \sum_{j=0}^n A^j u^{\text{Inc}} \qquad j \in \mathbb{N}.$$

If the Neumann series $\sum_{j=0}^\infty A^j$ converges, then the sequence u_j approximates the BIE solution u^{Tot}:

$$\lim_{j \to \infty} u_j = \sum_{j=0}^\infty A^j u^{\text{Inc}} = (I - A)^{-1} u^{\text{Inc}} = u^{\text{Tot}}.$$

This is called **Born series**. When only the 0th and the 1st terms are kept, this is the (first) **Born approximation** or **Rayleigh–Gans** approximation: $u^{\text{Tot}} \approx u^{\text{Inc}} + A u^{\text{Inc}}$. The Born series allows to approximate the total field without solving a VIE, but simply by repeatedly applying the volume integral operator. At the discrete level, the solution of a linear system is replaced by matrix-vector products. For the Born series to converge, the operator A has to be small in norm: this is true for "weak scatterers" such that $k^2 D^2 (n-1)$, with $D = \text{diam}(\text{supp}(n-1))$, is sufficiently small (see eq. (7.31) in the book of footnote 72). In particular, the wave speed in the obstacle can not be very different from outside. Iterative methods that approximate u^{Tot} under more general assumptions and with faster convergence have been developed improving on the Born series.[75]

If the mesh elements are identical and regularly distributed, the matrix of the corresponding VIE piecewise-constant discretisation has a special structure that allow low storage and efficient computations. In Exercise 7.15 we describe a very simple example, and in Exercise 7.16 a more complex one.

Exercise 7.15: (Strip domain: Toeplitz matrix).
For $h > 0$ and $N \in \mathbb{N}$, let $\Omega \subset \mathbb{R}^2$ be the strip $(0, Nh) \times (0, h)$, partitioned in the N square elements $\mathcal{T}_N = \{K_1, \dots, K_N\}$, with $K_m = (h(m-1), hm) \times (0, h)$ for $m = 1, \dots, N$:
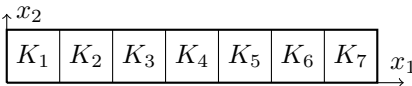
Let the refractive index n be constant in Ω and $n \neq 1$.

Show that the collocation or Galerkin matrix $\underline{\underline{\mathbf{A}}}$ in (132)–(134) is a **Toeplitz matrix**: all entries on each diagonal parallel to the main one are identical. In particular, only $2N - 1$ complex values are needed to store $\underline{\underline{\mathbf{A}}} \in \mathbb{C}^{N \times N}$. A Toeplitz linear system can be solved efficiently with specialised algorithms.

Recall that $\Phi_k(\mathbf{x}, \mathbf{y})$ only depends on the distance $|\mathbf{x} - \mathbf{y}|$.

$$\underline{\underline{\mathbf{A}}} = \begin{array}{|c|c|c|c|c|c|c|}
\hline
A_0 & A_1 & A_2 & A_3 & A_4 & A_5 & A_6 \\
\hline
A_{-1} & A_0 & A_1 & A_2 & A_3 & A_4 & A_5 \\
\hline
A_{-2} & A_{-1} & A_0 & A_1 & A_2 & A_3 & A_4 \\
\hline
A_{-3} & A_{-2} & A_{-1} & A_0 & A_1 & A_2 & A_3 \\
\hline
A_{-4} & A_{-3} & A_{-2} & A_{-1} & A_0 & A_1 & A_2 \\
\hline
A_{-5} & A_{-4} & A_{-3} & A_{-2} & A_{-1} & A_0 & A_1 \\
\hline
A_{-6} & A_{-5} & A_{-4} & A_{-3} & A_{-2} & A_{-1} & A_0 \\
\hline
\end{array}$$

Exercise 7.16: (Regular 2D mesh: BTTB matrix). Let Ω be the rectangle $(0, L_x) \times (0, L_y)$, and $\mathcal{T}_N$ its partition in $N = N_x N_y$ identical rectangular elements:

$$\mathcal{T}_N = \{K_{m_x, m_y} : \ m_x = 1, \dots, N_x, \ m_y = 1, \dots, N_y\},$$
$$K_{m_x, m_y} = (x_{m_x - 1}, x_{m_x}) \times (y_{m_y - 1}, y_{m_y}),$$
$$x_m = \frac{L_x}{N_x} m \quad m = 0, \dots, N_x, \qquad y_m = \frac{L_y}{N_y} m \quad m = 0, \dots, N_y.$$
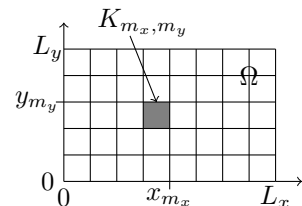
[74][Yurkin, Hoekstra, The discrete dipole approximation: An overview and recent developments, JQSRT 2007]
[75][Kleinman, Roach, van den Berg, Convergent Born series for large refractive indices, JOSA 1990]

Order the elements first along the horizontal and then along the vertical direction: $K_{N_x(m_y-1)+m_x} = K_{m_x,m_y}$, so we can write $\mathcal{T}_N = \{K_1, \ldots, K_N\}$. Consider the space V_N of piecewise-constant functions on $\mathcal{T}_N$, with mth basis element φ_m the characteristic function of K_m.

To start with, assume that n is constant and different from 1 in Ω.

The (collocation or Galerkin) matrix $\underline{\underline{\mathbf{A}}}$ in (132)–(134) has a special block structure. It is composed of $N_y \times N_y$ square blocks of size $N_x \times N_x$: the block with row indices from $N_x(m_y-1)+1$ to $N_x m_y$ and column indices from $N_x(m'_y - 1) + 1$ to $N_x m'_y$ corresponds to the interaction of the elements in the m_y-th and the m'_y-th horizontal rows of the mesh. We name this block $B_{m_y,m'_y} \in \mathbb{C}^{N_x \times N_x}$.

Show that $\underline{\underline{\mathbf{A}}}$ is a **block-Toeplitz-with-Toeplitz-blocks (BTTB)** matrix (or 2-level Toeplitz matrix). This means that *(i)* each block B_{m_y,m'_y} is a Toeplitz matrix, and *(ii)* all blocks along the same diagonal, i.e. with the same value of $m_y - m'_y$, are identical. See Figure 39 for an example of a small BTTB matrix.

To be able to work with the matrix $\underline{\underline{\mathbf{A}}}$, it is enough to compute and store the first row and the first column of the blocks in the first row and in the first column, for a total of $(2N_x - 1)(2N_y - 1) \le 4N \ll N^2$ different entries. This allows the efficient computation of matrix–vector products, and thus the implementation of iterative solvers such as GMRES. Moreover, an $N \times N$ BTTB matrix can be embedded in a $2N \times 2N$ block-circulant-with-circulant-blocks matrix, whose product with a vector is a discrete convolution and can be done with $\mathcal{O}(N \log N)$ effort using the fast Fourier transform (FFT). See e.g. Sections 4.3–4.4 in the reference of Footnote 74.

If the refractive index n is not constant in the rectangle Ω, it can be approximated by an elementwise-constant function $\widetilde{n}$. This leads to VIE matrices in the form $\underline{\underline{\mathbf{A}}} = \underline{\underline{\mathbf{I}}} + \underline{\underline{\mathbf{T}}}\,\underline{\underline{\mathbf{D}}}$, where $\underline{\underline{\mathbf{I}}}$ is the identity matrix, $\underline{\underline{\mathbf{T}}}$ a BTTB matrix, $\underline{\underline{\mathbf{D}}}$ a diagonal scaling matrix depending on n with $\overline{\overline{D}}_{j,j} = 1 - \widetilde{n}|_{K_j}$ (up to a scalar factor $|\overline{K}_j|$ in the Galerkin case). This includes also the case where some elements of the rectangle Ω are not part of the obstacle, so that $n = 1$ on these elements.

Similar ideas can be applied to other regular grids, e.g. made of triangles or hexagons, and even to higher-order piecewise-polynomial spaces.

Figure 39: Entries of a 24×24 block-Toeplitz-with-Toeplitz-blocks (BTTB) matrix corresponding to a regular mesh with $N_x = 6$ elements in the horizontal direction and $N_y = 4$ in the vertical direction. Equal numbers correspond to equal entries. There are $(2N_x - 1)(2N_y - 1) = 77$ different entries (shaded squares).

A VECTOR CALCULUS FORMULAS AND NOTATION

$B_R(\mathbf{x}) := \{\mathbf{y} \in \mathbb{R}^n : |\mathbf{y} - \mathbf{x}| < R\}, \qquad B_R := B_R(\mathbf{0}), \qquad \mathbb{S}^1 := \{\mathbf{d} \in \mathbb{R}^2 : |\mathbf{d}| = 1\},$

polar coordinates: $\mathbf{x} = (x_1, x_2) = (r\cos\theta, r\sin\theta), \qquad r = |\mathbf{x}| \geq 0,\ 0 \leq \theta < 2\pi, \qquad \mathrm{d}x_1\,\mathrm{d}x_2 = r\,\mathrm{d}r\,\mathrm{d}\theta,$

$e^{\mathrm{i}z} = \cos z + \mathrm{i}\sin z, \quad \cos z = \dfrac{e^{\mathrm{i}z} + e^{-\mathrm{i}z}}{2}, \quad \sin z = \dfrac{e^{\mathrm{i}z} - e^{-\mathrm{i}z}}{2\mathrm{i}}, \qquad \Re = \text{real part}, \quad \Im = \text{imaginary part},$

$\mathbf{v} \times \mathbf{w} := (v_2 w_3 - v_3 w_2,\ v_3 w_1 - v_1 w_3,\ v_1 w_2 - v_2 w_1), \qquad\qquad \mathbf{u} \times (\mathbf{v} \times \mathbf{w}) = \mathbf{v}(\mathbf{u} \cdot \mathbf{w}) - \mathbf{w}(\mathbf{u} \cdot \mathbf{v}),$

$\nabla u := \left(\dfrac{\partial u}{\partial x_1},\ \dots,\ \dfrac{\partial u}{\partial x_n}\right), \qquad\qquad\qquad\qquad \mathrm{div}\,\mathbf{v} := \nabla \cdot \mathbf{v} := \dfrac{\partial v_1}{\partial x_1} + \cdots + \dfrac{\partial v_n}{\partial x_n},$

$\Delta u := \nabla^2 u := \mathrm{div}(\nabla u) \quad = \dfrac{\partial^2 u}{\partial x_1^2} + \cdots + \dfrac{\partial^2 u}{\partial x_n^2} \quad \overset{\text{if } n=2}{=} \dfrac{1}{r}\dfrac{\partial}{\partial r}\left(r\dfrac{\partial u}{\partial r}\right) + \dfrac{1}{r^2}\dfrac{\partial^2 u}{\partial\theta^2} \quad = \dfrac{\partial^2 u}{\partial r^2} + \dfrac{1}{r}\dfrac{\partial u}{\partial r} + \dfrac{1}{r^2}\dfrac{\partial^2 u}{\partial\theta^2},$

$\mathrm{curl}\,\mathbf{v} := \nabla \times \mathbf{v} := \left(\dfrac{\partial v_3}{\partial x_2} - \dfrac{\partial v_2}{\partial x_3},\ \dfrac{\partial v_1}{\partial x_3} - \dfrac{\partial v_3}{\partial x_1},\ \dfrac{\partial v_2}{\partial x_1} - \dfrac{\partial v_1}{\partial x_2}\right),$

$\mathrm{curl}\,\nabla u = \mathbf{0}, \qquad \mathrm{div}\,\mathrm{curl}\,\mathbf{v} = 0,$

$\mathrm{curl}\,\mathrm{curl}\,\mathbf{v} = \nabla\,\mathrm{div}\,\mathbf{v} - \boldsymbol{\Delta}\mathbf{v}$

$= \left(\frac{\partial^2 v_2}{\partial x_1 \partial x_2} + \frac{\partial^2 v_3}{\partial x_1 \partial x_3} - \frac{\partial^2 v_1}{\partial x_2^2} - \frac{\partial^2 v_1}{\partial x_3^2},\quad \frac{\partial^2 v_1}{\partial x_1 \partial x_2} + \frac{\partial^2 v_3}{\partial x_2 \partial x_3} - \frac{\partial^2 v_2}{\partial x_1^2} - \frac{\partial^2 v_2}{\partial x_3^2},\quad \frac{\partial^2 v_1}{\partial x_1 \partial x_3} + \frac{\partial^2 v_2}{\partial x_2 \partial x_3} - \frac{\partial^2 v_3}{\partial x_1^2} - \frac{\partial^2 v_3}{\partial x_2^2}\right).$

B BESSEL FUNCTION FORMULAS

All these formulas can be found in [DLMF, §10] and [CK2, §3.5]. Here $r > 0$ and $\ell \in \mathbb{Z}$.

$r^2 f''(r) + r f'(r) + (r^2 - \ell^2) f(r) = 0 \qquad$ Bessel differential equation, $f \in \{J_\ell, Y_\ell, H_\ell^{(1)}, H_\ell^{(2)}\},$

$J_\ell(r) = \left(\dfrac{r}{2}\right)^\ell \sum_{j=0}^{\infty} (-1)^j \dfrac{(\frac{1}{4}r^2)^j}{j!(\ell+j)!} \quad \ell \in \mathbb{N}_0,$

$J_{-\ell} = (-1)^\ell J_\ell, \qquad Y_{-\ell} = (-1)^\ell Y_\ell, \qquad J_\ell' = \dfrac{J_{\ell-1} - J_{\ell+1}}{2}, \qquad Y_\ell' = \dfrac{Y_{\ell-1} - Y_{\ell+1}}{2},$

$H_\ell^{(1)} := J_\ell + \mathrm{i}Y_\ell, \qquad H_\ell^{(2)} := J_\ell - \mathrm{i}Y_\ell = \overline{H_\ell^{(1)}}, \qquad \dfrac{\partial}{\partial r}|H_\ell^{(1)}(r)| < 0,$

$e^{\mathrm{i}r\cos\alpha} = \sum_{\ell \in \mathbb{Z}} \mathrm{i}^\ell J_\ell(r) e^{\mathrm{i}\ell\alpha} \quad$ Jacobi–Anger formula, $\qquad J_\ell(r) Y_\ell'(r) - Y_\ell(r) J_\ell'(r) = \dfrac{2}{\pi r} \quad$ Wronskian identity,

$J_\ell(r) = \sqrt{\dfrac{2}{\pi r}}\cos\left(r - \dfrac{\ell\pi}{2} - \dfrac{\pi}{4}\right)\left(1 + \mathcal{O}_{r\to\infty}\left(\dfrac{1}{r}\right)\right), \quad Y_\ell(r) = \sqrt{\dfrac{2}{\pi r}}\sin\left(r - \dfrac{\ell\pi}{2} - \dfrac{\pi}{4}\right)\left(1 + \mathcal{O}_{r\to\infty}\left(\dfrac{1}{r}\right)\right),$

$J_\ell(r) \sim \dfrac{1}{\sqrt{2\pi}}\left(\dfrac{er}{2}\right)^\ell \ell^{-\ell-\frac{1}{2}}, \qquad H_\ell^{(1)}(r) \sim -\mathrm{i}\sqrt{\dfrac{2}{\pi}}\left(\dfrac{2}{er}\right)^\ell \ell^{-\frac{1}{2}} \qquad \text{for } \ell \to \infty,$

$J_\ell(r) \sim \dfrac{r^\ell}{\ell!\,2^\ell} \quad \ell \in \mathbb{N}_0, \qquad H_0^{(1)}(r) \sim \dfrac{2\mathrm{i}}{\pi}\log r, \qquad H_\ell^{(1)}(r) \sim -\dfrac{\mathrm{i}}{\pi}(\ell-1)!\dfrac{2^\ell}{r^\ell} \quad \ell \in \mathbb{N} \qquad \text{for } r \searrow 0.$

Here $a(x) \sim b(x)$ for $x \to X$ means that $\lim_{x \to X} \frac{a(x)}{b(x)} = 1.$

C ACRONYMS

- **BCs**: boundary conditions.
- **BEM**: boundary element method.
- **BIE**: boundary integral equation.
- **BIO**: boundary integral operator.
- **BVP**: boundary value problem.
- **CFIE**: combined-field integral equation.
- **DOFs**: degrees of freedom.
- **DtN**: Dirichlet-to-Neumann map.
- **EDP**: exterior Dirichlet problem.
- **FEM**: finite element method.
- **HTP**: Helmholtz transmission problem.
- **PDE**: partial differential equation.
- **PEC**: perfect electric conductor.
- **SSSP**: sound-soft scattering problem.
- **TE**: transverse-electric.
- **TEM**: transverse-electric and magnetic.
- **TM**: transverse-magnetic.
- **VIE**: volume integral equation.

D UNITS OF MEASUREMENT

We summarise the SI units of measure of the physical quantities introduced in §1.

§1.1			
	Mass density	ρ	$\frac{\text{kg}}{\text{m}^3}$
	Pressure	p	$\text{Pa} = \frac{\text{N}}{\text{m}^2} = \frac{\text{kg}}{\text{m}\cdot\text{s}^2}$
	Fluid velocity, wave speed	$\mathbf{v}, c$	$\frac{\text{m}}{\text{s}}$
	Acoustic velocity potential	ϕ	$\frac{\text{kg}}{\text{m}\cdot\text{s}}$
	Damping parameter	γ	$\frac{1}{\text{s}}$
	Acoustic intensity	$\mathbf{I}$	$\frac{\text{kg}}{\text{s}^3}$
	Sound power		$\text{W} = \frac{\text{kg}\cdot\text{m}^2}{\text{s}^3}$
	Sound pressure level	SPL	dB
	Force density	$\mathbf{F}$	$\frac{\text{N}}{\text{m}^3} = \frac{\text{kg}}{\text{m}^2\cdot\text{s}^2}$
	Impedance parameter	ϑ	1
§1.2	Angular frequency	ω	$\frac{\text{rad}}{\text{s}}$
	Time frequency	f	$\text{Hz} = \frac{1}{\text{s}}$
	Wavenumber	k	$\frac{1}{\text{m}}$
	Wavelength	λ	m
§1.3	Electric field	$\mathcal{E}, \mathbf{E}$	$\frac{\text{V}}{\text{m}} = \frac{\text{kg}\cdot\text{m}}{\text{s}^3\cdot\text{A}}$
	Magnetic field	$\mathcal{H}, \mathbf{H}$	$\frac{\text{A}}{\text{m}}$
	Electric permittivity	ϵ	$\frac{\text{s}^4\cdot\text{A}^2}{\text{kg}\cdot\text{m}^3}$
	Magnetic permeability	μ	$\frac{\text{N}}{\text{A}^2} = \frac{\text{kg}\cdot\text{m}}{\text{s}^2\cdot\text{A}^2}$
	Conductivity	σ	$\frac{\text{s}^3\cdot\text{A}^2\cdot\text{rad}}{\text{kg}\cdot\text{m}^3}$
	Current density	$\mathcal{J}, \mathbf{J}$	$\frac{\text{A}}{\text{m}^2}$
§1.4	Displacement	$\mathbf{U}, \mathbf{u}$	m
	Lamé constants, Young modulus	λ, μ, E	$\text{Pa} = \frac{\text{kg}}{\text{m}\cdot\text{s}^2}$
	Poisson ratio	ν	1
	Elastic potentials	$\chi, \boldsymbol{\psi}$	m^2
	Traction, stress and stiffness tensor	$\mathbf{T}, \underline{\underline{\sigma}}, \mathsf{C}$	$\text{Pa} = \frac{\text{kg}}{\text{m}\cdot\text{s}^2}$
	Strain tensor	$\underline{\underline{\varepsilon}}$	1
	Somigliana potential	$\mathbf{g}$	m^3

s	second
m	metre
kg	kilogram
A	ampere
N	newton
Pa	pascal
W	watt
Hz	hertz
V	volt
rad	radian

Four of these (s, m, kg, A) are SI base units, the others are derived units. We also used the decibel (dB), which is not a SI unit.

E Summary

In this course we studied the boundary element method (BEM) for the numerical approximation of sound-soft scattering problems for the homogeneous Helmholtz equation in two dimensions.

The Helmholtz equation $\Delta u + k^2 u = 0$ is relevant because it characterizes the space dependence $u(\mathbf{x})$ of time-harmonic solutions $U(\mathbf{x}, t) = \Re\{u(\mathbf{x})e^{-i\omega t}\}$ of the wave equation $\frac{1}{c^2}\frac{\partial^2 U}{\partial t^2} - \Delta U = 0$, where $k = \omega/c > 0$ is the wavenumber, ω the time frequency and c the wave speed (§1.2). The wave equation models the propagation and the scattering of acoustic waves (§1.1). The Helmholtz equation arises also in the modelling of electromagnetic (§1.3) and elastic (§1.4) waves.

The solutions of the Helmholtz equation that are separable in Cartesian coordinates are the plane waves (§2.2), which are either propagative or evanescent (§2.2.1). The solutions that are separable in polar coordinates are the circular waves, which are products of Bessel (J_ℓ, Y_ℓ) and Hankel ($H_\ell^{(1)}$, $H_\ell^{(2)}$) functions (§2.3) in the radial variable r (times k) and circular harmonics $e^{i\ell\theta}$ in the angular variable.

We can easily compute by hand the reflection of a plane wave hitting an infinite straight line equipped with Dirichlet, Neumann, or impedance conditions (§4.1). In order to study the wave scattering by bounded obstacles we need to deal with Lipschitz domains (§3.1), function spaces defined on them (§3.2) and on their boundaries (§3.3) and Green's identities (§3.4). With these tools we can formulate the exterior Dirichlet problems, and in particular the sound-soft scattering problems (§4.3.2). The simplest example is given by a circular scatterer (§4.3.1), for which we can write the solution explicitly. The key condition "at infinity", used to select the correct solution, is the Sommerfeld radiation condition $|\partial_r u - iku| = o_{r\to\infty}(r^{-1/2})$.

Using the fundamental solution Φ_k of the Helmholtz equation, we define the single-layer potential $\mathcal{S}$ and the single-layer operator S. These allow to write the boundary integral equation (BIE) $S\psi = g_D$ and the representation formula $u = \mathcal{S}\psi$. Solving the BIE and applying the representation formula we obtain the solution of the exterior Dirichlet problem (§5.1). The BIE can be discretised with a collocation-BEM or a Galerkin-BEM (§5.2). The implementation of the BEM requires a careful use of quadrature formulas (§5.2.1). Several variations and extensions of the BEM are possible (§5.2.2).

The analysis of the Helmholtz equation (either in the form of a BVP or a BIE) relies on Fredholm theory and involves non-coercive variational problems that admit Gårding inequalities (§3.5). This allows to study BVPs posed both in bounded domains (§4.2), which are closely related to Laplace eigenvalue problems, and in exterior domains (§4.3). An important formula is Green's representation, which allows to write all (radiating) Helmholtz solutions in terms of their traces (§5.3). One can also define the double-layer potential $\mathcal{D}$ and operator D (§5.4), the adjoint double-layer operator D' and the hypersingular operator H (§5.5). The two potentials and the four operators are related to one another by the Dirichlet and Neumann trace operators (79), which determine the jump relations (80).

The well-posedness of the single-layer BIE (§6.1) follows from the injectivity and the Fredholm property of S. The injectivity holds only when k^2 is not a Laplace eigenvalue (§6.1.1). The Fredholm property (§6.1.2) is obtained by decomposing S in the sum of a coercive part related to the reaction-diffusion equation (§6.1.5) and a compact part corresponding to a bounded kernel function (§6.1.4).

Many other integral equations are possible for the same exterior Dirichlet problem (§6.2), some of which are well-posed for all values of k (§6.2.3, §6.2.4).

Galerkin discretisations of non-coercive problems that satisfy a Gårding inequality are well-posed and quasi-optimal if the discrete space is "sufficiently fine" (§6.3.1). This applies to both the finite element method (§6.3.2) and the BEM (§6.3.3) approximations of Helmholtz problems. The proof of convergence rates for the BEM requires studying the BIE solution regularity in fractional Sobolev norms (§6.3.4).

A wave is refracted when it propagates in a heterogeneous medium (§7). When two homogeneous materials are in contact, transmission conditions must be imposed on their interface (§7.1.1). If the interface is flat, we can compute exactly the reflection and the refraction of a plane wave, in agreement with Snell's law (§7.1.2). Instead, if the interface is bounded we have a Helmholtz transmission problem (HTP) (§7.1.3), which can be written as a BIE (§7.1.4). A more general setting is when the medium is truly heterogeneous, and its properties vary continuously (§7.2). This problem is modelled by the Lippmann–Schwinger volume integral equation (VIE) (§7.2.1), which can be approximated with collocation or Galerkin schemes (§7.2.2).

F WHAT ELSE?

In these notes we have mostly considered exterior Dirichlet BVPs for the 2D Helmholtz equation. However BIEs and BEMs have a much broader range of applicability. They may be used to model, analyse and approximate Helmholtz BVPs posed on bounded domains, and on domains with unbounded or non-Lipschitz boundaries. BIEs can be used for much more general linear PDEs (of all kinds: elliptic, parabolic and hyperbolic) in any dimension, including systems of PDEs such as those of elasticity[76] and electromagnetism (e.g. [CK1, Ch. 4], [Nédélec01, §5.6]) described in §1.3–1.4. In computational electromagnetism, the BEM is often called "method of moments" (MoM). The main requirement for implementing a BEM is that the fundamental solution of the differential operator is known, either in exact or approximate form.

A BEM can be coupled with a FEM (or another volume-based method) for approximating problems with different physical models in different subdomains. Typically, FEMs are used in small regions of high geometric complexity, variable coefficients or non-linearities, and BEMs are used to deal with unbounded regions where coefficients are constant.

The use of BEM in applications requires the solution of large dense linear systems. Often their solution with direct methods (such as Gauss elimination) is too expensive and requires iterative (Krylov) methods such as GMRES, usually with preconditioning, [SS11, Ch. 6]. For large systems, even assembling the matrix may be unfeasible. Several techniques to compute matrix–vector multiplications, which are the key steps in Krylov methods, without explicitly assembling the matrix have been developed. These techniques exploit the structure of the BEM matrix and the properties of the fundamental solution. Important realisations of this idea are the fast multipole method (FMM) by Greengard and Rokhlin [Martin06, §6.14], the panel clustering [SS11, Ch. 7], and the hierarchical matrices ($\mathcal{H}$-matrices) by Hackbusch.

Several open-source BEM codes addressing the Helmholtz equation are available online:

- *Bempp* is a high-performance Galerkin-BEM code with a Python interface.   `https://bempp.com/`

- *Bembel* is a C++ isogeometric Galerkin BEM library.   `https://temf.github.io/bembel/`

- *DeltaBEM* is a Matlab suite for 2D BEM on smooth curves, focused on frequency-domain and time-domain wave problems.   `https://github.com/team-pancho/deltaBEM`

- *Gypsilab* is a Matlab toolbox for fast Galerkin BEM and FEM computations, including acoustics.
    `https://github.com/matthieuaussal/gypsilab`

- *IGABEM2D* is a Matlab library implementing adaptive isogeometric BEM in 2D.
    `https://zenodo.org/records/6282998`

Another important numerical method for the discretisation of BIEs is the Nyström method, which can converge extremely fast for smooth scatterers; see e.g. [CK2, §3.6] for the application to 2D Brakhage–Werner equation or [Sayas15, pp. 33 and 36] for the Laplace case.

Besides integral equations, volume-based discretisations of the Helmholtz equation are very popular. Important examples are *hp*-finite element[77] and discontinuous Galerkin (DG)[78] methods, also with non-polynomial basis functions[79] (such as plane waves or Fourier–Bessel functions). A considerable portion of current research on these methods studies their wavenumber dependence and the design of schemes that scale well for large k. The solution of the linear systems associated to these methods is particularly challenging because of the indefiniteness of the variational form used and the propagative nature of the solution[80]; the domain decomposition (DD)[81] method is a commonly used technique to solve or precondition these large linear systems.

A considerable amount of research is currently devoted to the modelling and the mathematical analysis of wave propagation problems, and to the design and the analysis of numerical methods for their approximation. To get an idea of the most active research topics, take a look at the books of abstract of recent conferences[82].

---

[76][Darbas, Le Louër, Well-conditioned boundary integral formulations for high-frequency elastic scattering problems in three dimensions, MMAS 2014]

[77][Melenk, Sauter, Wavenumber explicit convergence analysis for Galerkin discretizations of the Helmholtz eq., SiNum 2011]

[78][Melenk, Parsania, Sauter, General DG-methods for highly indefinite Helmholtz problems, JSC 2013]

[79][Hiptmair, Moiola, Perugia, A survey of Trefftz methods for the Helmholtz equation, LNCSE 2016]

[80][Ernst, Gander, Why it is difficult to solve Helmholtz problems with classical iterative methods, LNCSE 2010]
[Gander, Zhang, A class of iterative solvers for the Helmholtz equation: factorizations, sweeping preconditioners, source transfer, single layer potentials, polarized traces, and optimized Schwarz methods, SiRev 2019]

[81][Graham, Spence, Vainikko, Recent results on domain decomposition preconditioning for the high-frequency Helmholtz equation using absorption, GSMA 2017], [Bootland, Dolean, Jolivet, Tournier, A comparison of coarse spaces for Helmholtz problems in the high frequency regime, CAMWA 2021]

[82]Berlin, 2024: `https://doi.org/10.17617/3.MBE4AA`
Karlsruhe, 2025: `https://conference25.waves.kit.edu/wp-content/uploads/2025/02/BoA.pdf`

G References

[BK00] J. Billingham, A.C. King, *Wave motion*, Cambridge University Press, 2000.

[Brezis11] H. Brezis, *Functional analysis, Sobolev spaces and PDEs*, Springer, 2011.

[CGLS12] S.N. Chandler-Wilde, I.G. Graham, S. Langdon, E.A. Spence, *Numerical-asymptotic boundary integral methods in high-frequency acoustic scattering*, Acta Numerica, 21:89–305, 2012.

[CJ77] C.A. Coulson, A. Jeffrey, *Waves: a mathematical approach to the common types of wave motion*, Longman, 1977.

[CK1] D. Colton, R. Kress, *Integral equation methods in scattering theory*, SIAM, 2013, reprint of 1983 original.

[CK2] D. Colton, R. Kress, *Inverse acoustic & electromagnetic scattering theory*, Springer, 2019, 4th ed.

[Costabel87] M. Costabel, *Principles of boundary element methods*, North-Holland 1987. Available on https://perso.univ-rennes1.fr/martin.costabel/publis/Co_PrinciplesBEM.pdf

[DLMF] *NIST Digital Library of Mathematical Functions*, https://dlmf.nist.gov/

[Heller13] E.J. Heller, *Why you hear what you hear*, Princeton University Press, 2013. Online supplement material: https://www.whyyouhearwhatyouhear.com/

[Ihlenburg98] F. Ihlenburg, *Finite element analysis of acoustic scattering*, Springer, 1998.

[Martin06] P.A. Martin, *Multiple scattering: interaction of time-harmonic waves with N obstacles*, Cambridge University Press, 2006.

[McLean00] W. McLean, *Strongly elliptic systems and boundary integral equations*, Cambridge University Press, 2000.

[Nédélec01] J.-C. Nédélec, *Acoustics and electromagnetic equations. Integral representations for harmonic problems*, Springer, 2001.

[Runborg12] O. Runborg, *Helmholtz equation and high frequency approximations*, notes 2012. Available on https://www.csc.kth.se/utbildning/kth/kurser/DN2255/ndiff12/Lecture5.pdf

[Sayas06] F.-J. Sayas, *Introduction to the boundary element method. A case study: the Helmholtz equation*, notes 2006. Available on https://team-pancho.github.io/classnotes.html

[Sayas15] F.-J. Sayas, *First steps in boundary element method*, notes 2015. Available on https://team-pancho.github.io/classnotes.html

[SBH19] F.-J. Sayas, T.S. Brown, M.E. Hassell, *Variational techniques for elliptic partial differential equations*, CRC Press, 2019.

[Spence14] E.A. Spence, *"When all else fails, integrate by parts" – an overview of new and old variational formulations for linear elliptic PDEs*, report 2014. Available on https://people.bath.ac.uk/eas25/ibps.pdf

[SS11] S.A. Sauter, C. Schwab, *Boundary element methods*, Springer, 2011.

References on wave phenomena. [CJ77] is classical book that describes clearly and succinctly many kinds of wave phenomena, developing both physical intuition and mathematical formalism; [BK00] is similar in spirit but more advanced and up to date. [Heller13] is a very clear and instructive non-mathematical book to gain an intuitive understanding of acoustic phenomena. [Martin06] describes analytical and numerical methods for the scattering of different kinds of time-harmonic waves by multiple obstacles, including BIEs for the Helmholtz equation; it also has a rich bibliography and many historical comments.

References on the Helmholtz equation. [Ihlenburg98] describes in detail the Helmholtz BVPs and their discretisation with the finite element method. Several Helmholtz (and Maxwell) BVPs and the corresponding boundary integral equations (BIEs) are analysed in mathematically rigorous way in [CK1, §3], [CK2, §1–3], [Nédélec01, §2–3]. [Spence14] is a survey of several variational formulations for Helmholtz and Laplace BVPs, the corresponding BIEs and the numerical methods for their discretisation; it is an accessible introduction to Helmholtz problems and the related literature. The lecture notes [Runborg12] consider analytical and numerical methods for interior and scattering Helmholtz BVPs, with a special focus on high-frequency problems.

References on PDEs. The book [SBH19] is an excellent PDE textbook: it is written with applications to numerical methods in mind and it includes a detailed analysis of the Helmholtz equation. [McLean00] is a book on elliptic PDEs and integral equations; in particular, Chapter 1 summarises the (pre)history of BIEs, Chapter 3 is a very clear and rich introduction to Sobolev spaces, and Chapter 9 focuses on the Helmholtz equation. [Brezis11] is a classical reference on functional analysis with application to PDEs.

References on the BEM. The lecture notes [Sayas15] and [Sayas06] are good introductions to BIEs for Laplace and Helmholtz equations, respectively, and their discretisations with the boundary element method (BEM). [Costabel87] is a brief and clear introduction to the BEM for several PDEs. [SS11] is a comprehensive and mathematically-oriented textbook on the BEM for elliptic PDEs, including Helmholtz. Section 2 of [CGLS12] is devoted to the BIE formulation of 2D Dirichlet–Helmholtz problems (precisely those we mostly focus on in these notes); the rest of the article analyses in detail a special class of BEM for the same problems.

[DLMF] is the main online resource for special functions and related topics. It is the "successor" of the famous book by Abramowitz and Stegun.

H INDEX OF PERSONS

I INDEX

J Contents

— — —